UNDERSTANDING AUTOTAXIN-INDUCED MIRNA EXPRESSION IN CANCER TO GAIN INSIGHT INTO TUMORIGENESIS AND DISEASE PROGRESSION

by

SUDEEPTI SAI KUPPA

(Under the Direction of MANDI M. MURPH)

ABSTRACT

Early diagnoses and targeted therapies are the crux of successful patient care for almost every cancer. Within this work, we explore various facets of this by studying tumorigenesis and therapeutic development in a variety of cancer models.

First, we explored the potential cytotoxicity of compounds previously used for their anti-microbial purposes in order to repurpose them in cancer. We successfully tested two candidate compounds in *in vivo* xenograft models, which resulted in successful tumor inhibition and characterization of some adverse events associated with treatment. Second, we sought to understand the development and progression of cancer, particularly ovarian cancer, through autotaxin-induced miRNA changes. Using an autotaxin transgenic mouse model, we were able to mimic the progression of a healthy patient to one that had elevated autotaxin that later developed tumors. Changes in serum miRNA expression in these mice were crucial in understanding the functional role of miR-489-3p as not only an indicator of autotaxin elevation and tumorigenesis, but also as an inhibitor of the prominent oncogene MEK1 in malignant cells *in vivo* and *in vitro*. Finally, we developed a novel bioengineered particle named antibody-labeled exosomes (Abi-

exosomes) that are capable of being fully customized with a surface antibody and loaded miRNA of choice to specifically target cancer cells. Abi-exosomes are capable of achieving significantly higher miRNA delivery efficiency compared to miRNA transfection and exosomes without the antibody-label on the surface. This invention is currently under patent consideration and being explored in the lab as a possible carrier for therapeutics beyond miRNA such as small molecules, proteins, and currently approved therapeutics to further improve target reachability upon delivery.

Overall, we have investigated the repurposing of anti-microbial compounds for cancer, sought to understand the underlying biology of miRNA expression driven by autotaxin, and developed a novel therapeutic delivery system in Abi-exosomes to benefit future drug delivery. This will help us better understand the complexity of cancer, and combat it with powerful tools that can improve patient survival in the clinic.

INDEX WORDS: autotaxin, lysophosphatidic acid, ovarian cancer, melanoma, antibody-labeled exosomes, miRNA, autotaxin transgenic mouse

UNDERSTANDING AUTOTAXIN-INDUCED MIRNA EXPRESSION IN CANCER TO GAIN INSIGHT INTO TUMORIGENESIS AND DISEASE PROGRESSION

by

SUDEEPTI SAI KUPPA

B.S. University of Georgia, 2014

A Dissertation Submitted to the Graduate Faculty of The University of Georgia in Partial Fulfillment of the Requirements for the Degree

DOCTOR OF PHILOSOPHY

ATHENS, GEORGIA

2019

UNDERSTANDING AUTOTAXIN-INDUCED MIRNA EXPRESSION IN CANCER TO GAIN INSIGHT INTO TUMORIGENESIS AND DISEASE PROGRESSION

by

SUDEEPTI SAI KUPPA

Major Professor:	Mandi M. Murph
Committee:	Arthur G. Roberts
	Aaron M. Beedle
	Houjian Cai

Electronic Version Approved:

Suzanne Barbour
Dean of the Graduate School
The University of Georgia
August 2019

DEDICATION

My persistence through the trials and tribulations of graduate school could not have been possible without the constant love and support I received from family and friends that stood by me on this journey.

To my parents, who have been there to pick me up at my lowest lows and celebrate my highest highs, and wholeheartedly supported my decisions throughout graduate school and life. Without your push to help me be dedicated, optimistic and patient with this process, I would not have made it here. Your unconditional love and understanding have motivated me more than you know, and I'm so honored to have made you proud with this accomplishment.

To Sid, who I have gotten to know over and over again through the years and for always helping me see the light of things. I'm glad we're getting to know each other all over again after you started college, and although I'm sad to be moving right as we connect more, know you'll always have a big sister and mentor to count on.

To my grandparents, who have patiently let me pursue this "long" degree and celebrating my accomplishments along the way from halfway across the world. I will always be thankful for the time and investment you put into my upbringing through the years and am excited to share this with you.

To Chetan, who came back into my life when I least expected it again and has only picked me up more and more along the way. I feel blessed beyond my wildest dreams to have you as my future husband, and I can't put into words how much you've taught me about life. Your ability to always make me laugh and see the bright side when I'm feeling down, and celebrate my dreams and accomplishments as if they were your

own will always amaze me. I'm beyond excited to share this thing called life with you and so excited for our move to D.C. (and beyond) together.

This isn't quite customary, but a huge heartfelt gratitude to my sweet Fessy, who I adopted almost impulsively, knowing nothing about rabbit care. You've been such a huge source of happiness to come home to everyday, and I'm so thankful for your cute face and antics to laugh about as I've seen you grow up. You've stolen literally everybody's heart in the family and if there was one thing I wouldn't change about the last five years, it would be adopting you.

And finally, to my friends and extended family, who have been there for countless wine nights on the day experiments failed, and uplifting coffee breaks at Jittery Joes, encouraging me to never give up. I will never do anything as rewarding as this experience, and I'm honored to share this with all of you. Your support and reassurance have been beyond valuable over the years.

ACKNOWLEDGEMENTS

In graduate school, I have had the incredible opportunity to conduct my thesis work under the advisement of Dr. Mandi Murph in the Department of Pharmaceutical & Biomedical Sciences at University of Georgia. Her scientific brilliance, strong support and motivation of young scientists, and dedication to my success have made this experience greatly valuable. As part of her laboratory, I have worked on a diverse array of projects which have exposed me the creative and varied nature of scientific research. I have also had the opportunity to develop and foster collaborations that opened new avenues to succeed in my research endeavors. I'm greatly appreciative of her patience, advice and supporting my scientific independence.

My graduate committee, consisting of Dr. Audie G. Roberts, Dr. Aaron M. Beedle and Dr. Houjian Cai, are also owed immense thanks for their critical eye to help make my projects and endeavors as thorough and complete as possible. Your encouragement and constant push for me to raise my standards for myself have helped me developed the confidence and grit needed to be a successful scientist. A special thank you to Dr. Roberts for exposing me to an entirely new set of techniques and entrusting me to implement his creative ideas in the laboratory leading to a patent, which is an incredibly unique opportunity for any graduate student to be a part of. The committee's advisement and support through the years have been a foundational pillar to my scientific success.

Lastly, I would like to thank the multiple collaborators I have had the chance to work with during my time at UGA. Dr. Balazs Rada, your generous donation of PBMCs and the additional training I received from you in handling human blood donations were invaluable to the success of the Abi-exosomes project leading to a patent application.

Another special thanks to a senior graduate student and now Ph.D., Dr. Nhat Quach, who has been essential to not only my scientific success but also to my personal growth and well-being in graduate school through his advice that made graduate school an even more rewarding experience. I truly believe I am going into the world with the core foundational skills that have set me up for success regardless of my future goals, and I owe it all to the relationships I have built here that I leave UGA with more than I could have imagined.

TABLE OF CONTENTS

LIST OF TABLES

Page

LIST OF FIGURES

Page

CHAPTER I

INTRODUCTION

The complexity of cancer as a disease poses an immense clinical challenge for patients who have been diagnosed too late to achieve a cure. Since the development and metastatic capability of cancer is influenced by various hallmarks of cancer, such as angiogenesis, evasion of the immune system, and proliferative potential in the tumor microenvironment, the work herein attempts to decode the role of microRNAs and exosomes as potential mediators of signaling in the cancer cell. Further, we have explored the importance of miRNAs as biomarkers, as well as the novel capability of exosomes and miRNAs to serve as an enhanced therapeutic option for patients with targetable markers predominantly responsible for cancer growth, possibly helping to address the heterogeneity of this disease. Melanoma and ovarian cancer are both especially difficult to cure at later stages of diagnosis and have therefore been part of a high throughput novel compounds study to measure potential cytotoxicity, which may further contribute to the drug formulary in these cancer types. Overall, this work serves to contribute a part to understanding the highly complex nature of cancer, and uncovering a small segment of the larger picture required to improve understanding of tumorigenesis and contributing factors to disease progression and metastasis.

MicroRNA Expression and Functionality

MiRNA Discovery

microRNAs (miRNAs) are a class of small RNAs approximately 18-29 nucleotides in length that were first discovered in 1993 in *Caenorhabditis elegans* (1). In this study, they initially explored the gene *lin-4* and its functionality in the postembryonic development of *C. elegans*, but instead found that *lin-4* is a short nucleotide transcript with sequence complementarity to the gene *lin-14*, which is considered a temporal developmental switch (2). It was found earlier that *lin-4* and *lin-28* both regulate *lin-14* expression during *C. elegans* development, and that *lin-4* interacts with the 3'-UTR region of *lin-14* to control translation of the gene (3). These studies were essential to establishing the first discovery of endogenous small RNAs that can modulate post-transcriptional mRNA expression.

Further, two groups concurrently discovered the miRNA let-7 in the year 2000, also in *C. elegans*, as a regulator of multiple developmental genes through sequence complementarity and binding at the 3'UTR region (4, 5). This was essential to expanding the relevance of miRNA from its original breakthrough in a nematode model to other organisms, since soon after it was also discovered that let-7 was conserved across a multitude of species (6). In fact, this did not apply solely to vertebrates, but also to arthropods, mollusk, and other marine invertebrate phyla or classes such as Hemichordate and Ascidia. Around this time, studies had also begun to report that a single miRNA could regulate the expression of multiple mRNAs, while one single mRNA strand could be regulated at multiple locations by different miRNAs (7). Since then, over 1900 human miRNAs have been discovered that regulate a multitude of genes and are conserved

across many species (8, 9). The initial finding of miRNAs in *C. elegans* has now resulted in a distinct field of research focused not only on the discovery of new miRNAs, but also the intensive exploration into their diverse roles in controlling endogenous physiological processes and gene expression as well as their influence on disease state and progression.

MiRNA Synthesis

Transcription of miRNAs happens much like that of mRNA from DNA. Earlier studies found that while some miRNAs were within the introns of the genes they later repressed the translation of, others were also found in intron-exon junctions of genes that were meant to serve as alternative splicing variants for the corresponding mRNA transcript (7, 10). Depending on their intronic or exonic source, miRNAs are synthesized to a mature nucleotide quite differently. Around 80% of miRNAs reside in noncoding intronic regions of DNA, and are transcribed along with the primary mRNA under the same promoter by RNA polymerase II, which is considered the catalytic subunit of machinery that can transcribe mRNA from DNA (11, 12). On the other hand, exonic or intergenic miRNAs that arise from exons in the genome can be processed by both RNA polymerase II and RNA polymerase III, which is partially responsible for RNA synthesis (13). After being transcribed into what is considered a stem-loop primary miRNA (pri-miRNA) structure, further processing machinery is required for mature miRNA synthesis.

For intronic pri-miRNAs, spliceosome machinery is required for cleavage and removal of exons before export out of the nucleus to form a fully mature miRNA duplex (14). Conversely, intergenic pri-miRNAs undergo processing by Drosha and DCGR8 prior to nuclear export, which make up what is known as the miRNA microprocessor

complex (15). Drosha is essentially an RNase III nuclease that processes the stem-loop structure of pri-miRNA to precursor miRNA (pre-miRNA) by cleaving the hairpin loop required for maturation in complex with DCGR8, which acts as an RNA binding element (16, 17). Additionally, Drosha and DCGR8 are able to post-transcriptionally regulate each other through DCGR8 stabilizing Drosha to function as a microprocessor complex and Drosha destabilizing DCGR8 mRNA to control protein translation (18). While most intergenic miRNAs are processed through this microprocessor complex, some intronic miRNAs can also undergo this process, while other 'mirtrons' bypass cleavage by Drosha/DCGR8 and are directly exported to the cytoplasm for processing (19).

Export to the cytoplasm is mediated by pre-miRNAs forming a complex with Exportin5 and RanGTP, two nucleocytoplasmic transport factors (20, 21). Once the pre-miRNA has left the nucleus, it is loaded onto another complex known as RISC that involves Dicer, TRBP and Ago2 proteins. The role of TRBP is to interact with and recruit Dicer to Ago2 to form the catalytic complex of RISC that can then carry out processing to a mature miRNA duplex (22, 23). Dicer, similar to Drosha, is an RNase III endonuclease, that cleaves the terminal end of the pre-miRNA stem-loop structure and has been found to be conserved in all organisms except for budding yeast (24). Ago2, alias eIF2C2, is also responsible for another cleavage intermediate to form the miRNA duplex that can then be loaded onto RISC for subsequent RNA inference activity (25, 26). The final step of converting the miRNA duplex into a functional guide strand that can inhibit its mRNA target is separating the miRNA passenger strand. This has been speculated to occur one of many ways, with a majority of data revealing that Ago2 cleaves the duplex between the two strands thereby separating them (27, 28). Therefore,

Ago2 might be involved both in processing of the pre-miRNA into the duplex form as well as cleavage of the passenger strand from the guide strand (26). Another theory also suggests that duplex unwinding might be the result of conformational changes in the RISC complex itself that allows the strands to simply dissociate from each other (29). Once the guide strand is free from its complementary passenger strand, it is now able to find its mRNA target and bind through sequence complementarity to inhibit translation.

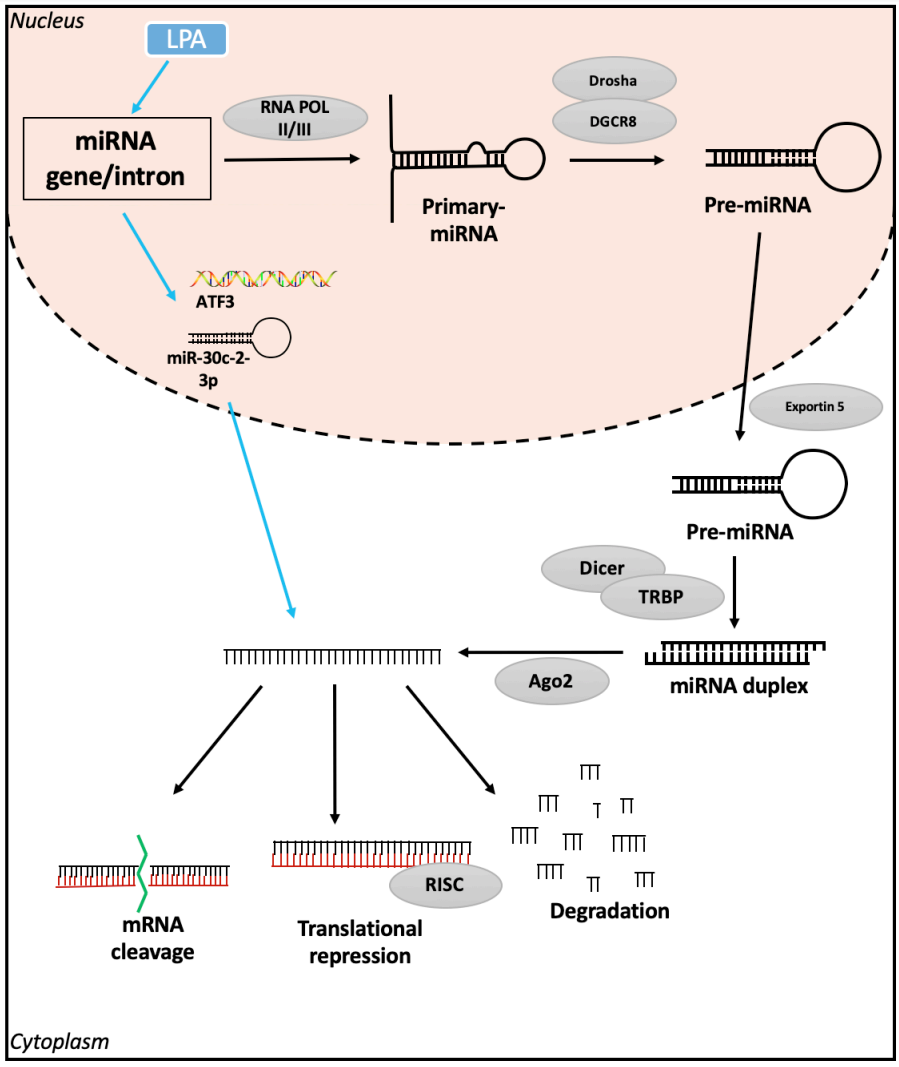

Figure 1.1: miRNA synthesis and function. miRNA is synthesized in the nucleus either through intronic transcription with another gene or exclusively along with related regulatory genes. Once exported into the cytoplasm, miRNA can inhibit its target through cleavage or translational repression. Adapted from a previous publication (30).

Functionality

The miRNA duplex exists as a guide strand, which is capable of binding mRNA and inhibiting translation into protein, and a passenger strand, which stabilizes the guide strand until it finds its mRNA target, and is cleaved by Ago2 to liberate the guide strand in the cytoplasm (27, 28, 31). The guide strand is annotated as the "5p" strand, whereas the passenger is the "3p" strand, annotated as miR-21-5p and miR-21-3p for example. Over time, the hypothesis that the passenger strand has no role has been challenged due to growing evidence that they persist even after the guide strand has been released to inhibit its target. For example, miR-30c-2-3p, discovered in our laboratory, is shown to inhibit its own target, oncogene BCL9, and results in apoptosis in OVCAR-3 cells (32).

Target recognition by the guide strand is highly dependent on base complementarity to mRNA, especially at the 5' end (33). While base-pair complementarity need not be 100% to bind and inhibit a target, the first 2-8 base pairs in the 5' region of the miRNA are crucial to determining the stability of the interaction and subsequently, strength of mRNA translation inhibition (34). In fact, while the first 8 base pairs bind based on sequence and free energy, the rest of the miRNA strand can bind mRNA based on the thermodynamic stability and wobble base paring between guanine and uracil nucleotides (35). It has also been shown that a single miRNA can have an average of 100 target sites across multiple mRNA transcripts, and one mRNA can also be targeted by multiple miRNAs, further explaining the lack of full sequence complementarity needed for binding and inhibition (35, 36).

Once bound, mRNA silencing can occur in one of two reported ways. The RISC complex, which is essential for miRNA synthesis and maturation, is also involved in

loading the mature guide miRNA onto the mRNA transcript and stabilizing the interaction between the two strands (37). Previous studies have shown that following the interaction, Ago2 in the RISC complex is then responsible for cleaving the mRNA and thus making it irreversibly untranslatable (38). There have been four discovered Argonaute proteins, numbered Ago1-4, involved in the RISC complex, but no evidence has been found to distinguish the activity of each one from the others as they all have the same cleavage capabilities (39). Following cleavage, mRNA is deadelynated to remove the poly(A) tail and can be fully degraded by exonuclease activity from the 3' to 5' end or enzymatic de-capping followed by exonuclease activity from the 5' to 3' end (40-42).

Another mechanism for mRNA translation inhibition can be attributed to a simple repression of translation of the targeted mRNA transcript, which is reversible. This occurs through redirection of the mRNA-miRNA loaded into the RISC complex to what are known as processing bodies, or P-bodies, which can inhibit translation (43, 44). Specifically, a protein known as GW182 has been shown to interact with Ago2 inside P-bodies to repress translation by assisting in mRNA silencing (45, 46). If needed, the mRNA-miRNA complex can be rescued from P-bodies to reinitiate translation if the cell experiences stressful conditions, allowing the mRNA to be translated into protein through the usual process of initiation, elongation and termination (47).

miRNAs in Cancer

The relevance of miRNAs has exponentially grown in both physiological and pathological processes as more miRNAs and their counterpart mRNA targets are discovered. Cancer cells are known to harbor a plethora of genetic, morphological and

metabolic changes compared to normal cells, which are considered the "hallmarks of cancer". They are able to evade immune detection and destruction while still maintaining inflammatory signaling beneficial to their survival, initiate constitutive proliferative signaling, and also access and process nutrients and energy differently (48). DNA replication stress has also recently been considered a hallmark of cancer due to mutations in proteins that can repair DNA damage and regulate the cell cycle (49). Oncogene activation or overexpression can contribute to tumor growth and help the cells overcome inhibitory signals, and mutation in a tumor suppressor gene can debilitate the cell's ability to rescue itself from stressful conditions that would normally result in apoptosis instead of uncontrolled growth (50-52). The most famous tumor suppressor, p53, is mutated in almost all incidences of cancer and interacts with hundreds of regulators that control processes spanning from epigenetics and cell cycle to stress response and the tumor microenvironment (53).

As the field of miRNAs has grown, it has come to light that although miRNAs have a generally inhibitory function, they can have a dual role in cancer as both tumor suppressors and oncogenes depending on the specific miRNA and its corresponding target (54, 55). For example, miR-125b can act as an oncogene by inhibiting translation of proapoptotic genes such as p53 resulting in cell survival, or as a tumor suppressor by inhibiting anti-apopototic genes such as BCL2 resulting in cell death (56, 57). In fact, mutations and changes in functionality of miRNA synthesis and maturation machinery can also serve an oncogenic or tumor suppressor role (58).

There are several families of miRNAs that are considered to have a prominent role in cancer, due to their strong association with disease state or their ability to target

prominent players involved in tumorigenesis and metastasis. The first of these families to be discovered was the 'let' family, particularly let-7, which contains over 10 members in humans alone, has been shown to be highly conserved across various species (4, 59). Previous studies on let-7 reveal that it can promote cell proliferation in lung cancer cells and target Ras, a prominent oncogene. Therefore, due to its ability to regulate such important players in cancer, it is understandable that the loss of let-7, as observed in many cancers provides a proliferative advantage to sustain cell growth (60). Another prominent miRNA family highly conserved in humans is the miR-17~92 cluster, which contains 6 members namely miR-17, miR-18a, miR-19a, miR-19b-1, miR-20a and miR-92-1 (61). These miRNAs are clustered together on the genome and transcribed together to cooperate with the oncoprotein Myc and exacerbate cancer cell proliferation (62).

The most well-known single miRNA in cancer is likely miR-21, which was originally published simply as an anti-apoptotic factor under homeostatic conditions (63). It was first discovered to be overexpressed in various cancers such as breast, colon, and lung cancer, and characterized as an inhibitor of tumor suppressors, thereby promoting cell growth, invasion and proliferative properties (64-66). MiR-21 has been widely studied in breast cancer in context of the Programmed Cell Death 4 (PDC4) tumor suppressor protein, whose inhibition has been linked to poor prognosis and higher rates of metastasis (67-69). The most well-known target of miR-21 across many cancers, however, is phosphatase and tensin homolog or PTEN. This tumor suppressor controls the switch between PIP_3, a stimulator of the Akt pathway, and PIP_2 by dephosphorylating the former to generate the latter; the reverse process of phosphorylating PIP_2 is controlled by phosphoinositide 3-kinase (PI3K) (70). The activity of miR-21 in this regard has been

established in hepatocellular carcinoma, cervical cancer, gastric cancer, colorectal cancer and breast cancer, among many others (71-74). More importantly, miR-21 can modulate chemoresistance by the same mechanism in various cancer models, extending its relevance beyond cancer biology to a possible therapeutic target in the future (75, 76).

Beyond their endogenous role as regulators of gene expression, miRNAs have also been considered potential indicators of changing disease states and important players in the tumor microenvironment. Comparison of normal fibroblasts with cancer-associated fibroblasts (CAFs), which play a role in tumor progression through upregulated growth factor supply and angiogenesis, has shown that the miRNA signature in CAFs is significantly different, suggesting that miRNAs could be involved in programming normal fibroblasts to CAFs (77, 78). Inflammation and immunosuppression are two hallmarks of cancer previously established as crucial for the cancer-friendly tumor microenvironment, and miRNAs, especially miR-155, have also been shown to modulate cytokine and inflammatory signaling to support tumor growth (79, 80). Once in systemic circulation encapsulated in exosomes, miRNAs can not only be indicators of disease state, but also can be taken up by other cells in the tumor microenvironment and exert pro-tumorigenic effects to support tumor growth (81).

MiRNAs, as endogenous regulators of gene expression, have become a highly relevant sector of cancer biology and lend another layer of regulation to what is an already complex and heterogeneous disease. Due to their sensitivity to changing homeostatic or disease state and ability to effectively communicate with surrounding cells in the tumor microenvironment, they should not only be considered highly accurate biomarker candidates, but possibly also new therapeutics in various cancer models.

Exosomes

Extracellular Vesicle Discovery and Biogenesis

Extracellular vesicles are released by almost all cell types, especially immune cells, and found in all biological fluids isolated across various species (82). They were first discovered over 50 years ago as 'particle dust' from platelets that could be isolated by ultracentrifugation and were largely composed of phospholipids (83). Over the years, research across many fields has shown that they are not only an essential facet of homeostatic maintenance, but also that there are different varieties of extracellular vesicles that each serve a distinct purpose. Apoptotic bodies are the largest class of extracellular vesicles, with a size ranging from 400-5,000 nm, while microvesicles are the medium-sized class ranging from 50-1,000 nm in diameter (82). Exosomes are the smallest, but possibly the most important, class of extracellular vesicles that range in size from 40-150 nm. Exosomes were first discovered as particles emerging from the late endosome in rat reticulocytes and sheep reticulocytes, and assumed to be exported encapsulating cellular waste (84-86). However, as studies have shown over the last 2-3 decades, exosomes are essential purveyors of cell-to-cell communication and can modulate cell signaling in their target cell to control both pathological and physiological processes (87).

Exosomes, and other extracellular vesicles, are formed within each cell type through the endosomal and Golgi apparatus in what are known as multivesicular bodies (MVBs) before being exported out of the cell. This process begins in the early endosome which then matures into the late endosome and fuses with MVBs which contain intraluminal vesicles (88). This process is mediated by a complex of proteins known as

ESCRTs that aid MVB maturation and subsequent vesicle export by plasma membrane fusion (89). While most extracellular vesicles are formed through this pathway, not all are fit to be released from the cell. Previous studies in B-lymphocytes have shown that only cholesterol-rich MVBs can fuse with the plasma membrane to release vesicles into the extracellular space (90). Exosomes have been found to be enriched in cholesterol, which likely aids their export out of the cell and lends to their importance as the forefront of cell-to-cell communication as carriers of diverse cargo (91).

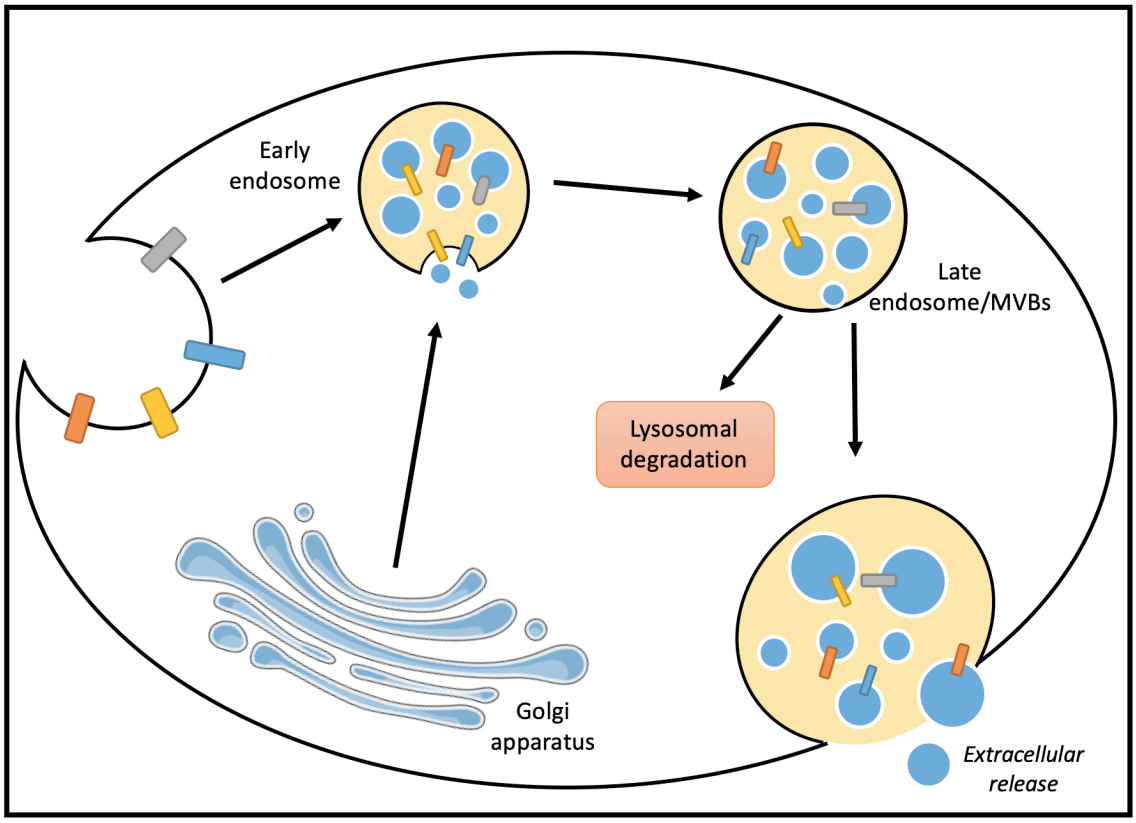

Figure 1.2: Exosome packing and export. Exosomes originate from the Golgi apparatus and bud into early endosomes, which then form multivesicular bodies and fuse with the plasma membrane to release vesicular content, such as exosomes into the extracellular space. Adapted from a previous publication (92).

Exosomes in Cancer

While the physiological release of exosomes as mediators of cell-to-cell communication was established early, exosomes are even more crucial in cancer signaling due to their ability to robustly influence the surrounding tumor microenvironment and systemically circulate in the body. There are various facets to exosome involvement in cancer that have only exponentially grown over time, including their ability to carry diverse types of cargo, confer metastatic or malignant properties to otherwise healthy cells, or be a harbor for potential biomarkers indicative of disease state.

The primary and most well-studied cargo in extracellular vesicles, specifically exosomes is miRNA, which can be utilized by both malignant and non-malignant cells to exert distinct effects on their target cells type and therefore are crucial facilitators in oncogenic signaling (93). Most importantly, miRNAs can be exported in exosomes and circulate stably throughout the body (94). Systemically circulating exosomes carrying miRNA have shown to be indicators of breast, lung and colorectal cancer (95-97). In a renal cell carcinoma model involving SCID mice, an animal model with a severely deficient immune system lacking both T- and B-cells, exosomal miRNAs were able to infiltrate endothelial cells to initiate angiogenesis and tumor cell attachment to the endothelium (98). In another study, breast cancer cells received miRNA-embedded exosomes from surrounding macrophages that were then able to significantly mitigate the invasive properties of the breast cancer cells (99). Even beyond the cancer field, circulating miRNAs have been studied as possible predictors of aging and Alzheimer's disease (100, 101). This suggests that is there is notable miRNA-mediated crosstalk in the tumor microenvironment that can help decipher disease state and signaling occurring in

both cancer cells and the surrounding healthy cells, immune system players, and other stromal components.

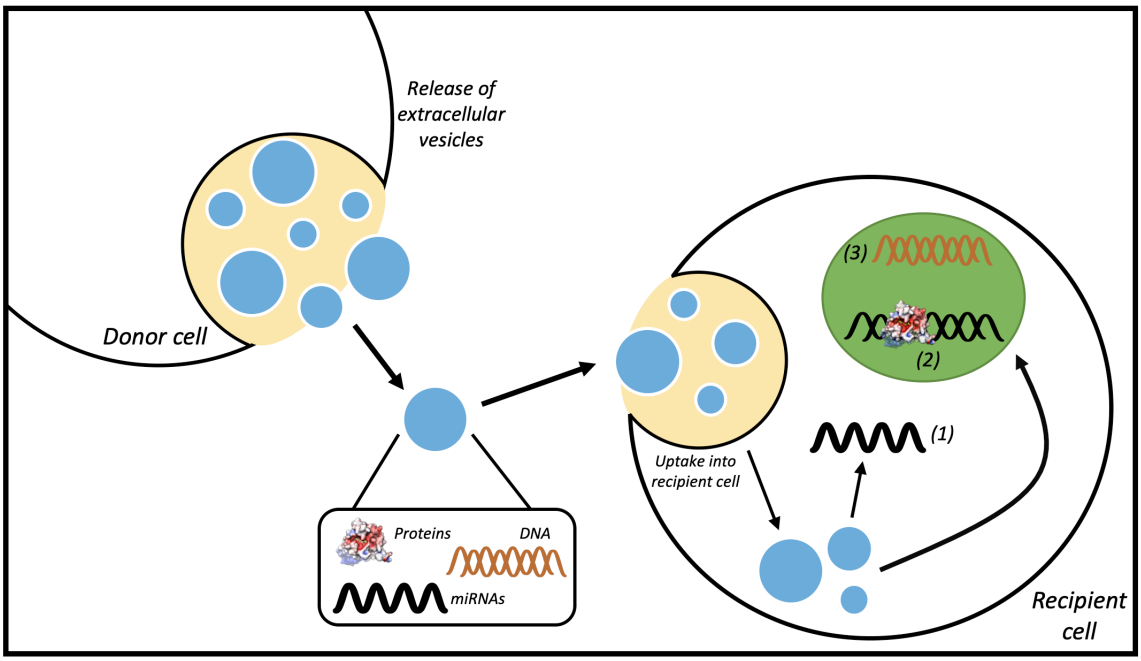

Figure 1.3: Exosomes in cell-to-cell communication. Once released from the originating donor cell, exosomes can enter recipient cells to deliver cargo such as miRNA and protein which are then able to modulate signaling in that target cell, a common process in the tumor microenvironment. Adapted from a previous publication (92).

A database known as ExoCarta, created a few years ago, is a comprehensive resource detailing all known exosomal cargo across various species (102). While exosomal cargo can greatly vary depending on the cell type, intracellular conditions and also any influencing signals the cell has received from its surroundings, the three general cargo categories are miRNA, proteins and lipids (82). Lipid rafts and proteins such as KRAS can influence miRNA loading into exosomes, but not much is known about exactly how cargo insertion occurs (103-105). Exosomes derived from cancer cells can be enriched with a host of immunosuppressive proteins such as the inhibitory cytokines IL-10 and TGF-ß, or death receptor ligands, which are designed to induce apoptosis in T-

cells overseeing an anti-tumor response (106, 107). However, they can also stimulate basal levels of inflammatory signals in their surrounding environment that are essential to tumor growth (108). Exosomes can also carry lipids, although the lipids coating their surface are more exciting to explore since they help the exosome adhere to and enter the recipient cell after export out of the originating cell (109). While it is yet unknown whether cancer cells can produce exosomes capable of targeting specific cells in the tumor microenvironment, it is known that the cargo they carry can manipulate their surroundings for optimal growth and survival.

Most extracellular vesicles, but especially exosomes, carry cargo that can change intracellular signaling in the target cell. Previous studies have revealed that vesicles released from cancer cells carrying diverse cargo can be selectively taken up my non-metastatic cells that can then result in higher rates of migration and metastatic behavior (110). More specifically, exosomal miRNAs released by cancer cells have been shown to promote brain metastasis through loss of the tumor suppressor PTEN (111). Most interestingly, cancer cells that are on the verge of death due to hypoxia can stimulate exosome release containing factors that enhance angiogenesis to quickly salvage their suboptimal conditions (112, 113). Another study in mouse and human models detailed the release of exosomes from melanoma cells and their ability to educate distant bone marrow progenitor cells to exhibit pro-metastatic behavior, proving that the effects of exosomes can extend far beyond the immediate surrounding cell types (114). However, this exchange of information is not unilateral; immune mediators and other cells in the tumor microenvironment can also secrete exosomes containing cytokines, miRNAs and bioactive phospholipids in an attempt to influence signaling within the cancer cells (115).

Outside the context of cancer, immune cells naturally release exosomes to communicate with each other to effectively neutralize a foreign threat within the body (116). In fact, mature dendritic cells can infiltrate lymphoid tissue to 'train' T-cells to present certain antigens required for an adequate immune response, as can be observed in the context of allograft rejection (117). Additionally, as mentioned before, exosomes can carry FasL or TRAIL proteins capable of suppressing or inhibiting T-cell function (118, 119). Since the prevalence of exosomes is abundant even without any malignant presence, the utilization of these carriers by cancer cells to manipulate their neighboring cells and create a favorable environment for incessant survival and growth is a fascinating area of study.

Exosomes as Biomarker and Therapeutic Carriers

An increase in exosome secretion from cancer cells could be a highly disadvantageous process for other, healthy cells in the tumor microenvironment, but it is also an opportunity to study the circulation of factors released from cancer cells to discover a potential biomarker. Exosome circulation is an established physiological process in a number of organisms, and has been extensively studied in the context of miRNAs in cancer (120). Studies in both melanoma and ovarian cancer have detailed the relevance of circulating miRNAs, or certain miRNA signatures, that can be utilized as biomarkers for early detection or disease progression (121, 122). Circulating exosomes have also been shown to carry miRNAs that can assess the effectiveness of radiotherapy or chemotherapy in patients with prostate or non-small cell lung cancer (120, 123). A more established biomarker in ovarian cancer, known as the cancer antigen 125 (CA-

125), is elevated in the presence of malignant growth, and is routinely monitored in patients with ovarian cancer. However, there has been some debate on the specificity and accuracy of CA-125 levels predicting early-stage or recurrent ovarian cancer, since it has also been shown to be increased in women with endometriosis or inflammatory bowel disease (124, 125). More recent evidence suggests that CA-125 in conjunction with exosomal miRNA expression, such as miR-1307 and -375, can result in more accurate detection of malignant ovarian cancer (126). There are also currently several clinical trials in the recruitment phase aiming to study the components of circulating exosomes in lung, prostate and pancreatic cancer patients. These studies hope to either improve the accuracy of current biomarkers, such as the prostate specific antigen (PSA) in prostate cancer, or characterize the changes in expression of exosomal components such as protein or tumor cell-derived RNA with or without therapeutic intervention.

The theory behind circulating exosomes carrying miRNAs or other molecules indicative of disease state comes from the established understanding that cancer cells release exosomes that reflect their intracellular environment or to expel cargo that may be disadvantageous for their survival. Since the latter implies that circulating exosomes carry tumor suppressor miRNAs that inhibit oncogene expression, and therefore may inhibit tumor growth, it is vital that exosomes can be used as carriers of anti-tumor therapeutics. Thus far, preliminary studies have shown that doxorubicin and paclitaxel, both chemotherapeutic compounds, can both be successfully loaded into nanoparticles and delivered to the target site, even crossing the blood-brain barrier, and result in tumor growth reduction with lower adverse effects (127, 128). Additionally, since exosomes naturally carry inhibitory miRNAs, a clinical trial, which is due to begin recruiting

shortly, is set to explore the efficacy of KRAS siRNA loaded into mesenchymal cell-derived exosomes in pancreatic cancer patients with mutated KRAS protein (NCT03608631). The role of mesenchymal stem cells as mass producers of exosomes well suited for drug delivery purposes has been extensively explored, but our laboratory has also seen success with exosomes derived from peripheral blood mononuclear cells (PBMCs), both of which could have immunosuppressive effects as well (129).

In addition to exosomes endogenously derived from a patient or donor, artificially created liposomes or nanoparticle encapsulation can also be utilized as drug carriers. Liposomes are advantageous due to their ability to encapsulate therapeutics of various sizes by simply constructing larger liposomal particles around them, and their ability to be readily taken up into cell and tissues (130). In fact, liposomal irinotecan has already been explored in a phase I clinical trials for solid refractory tumors, revealing that the formulation improves irinotecan's half-life and absorption into tissues (131). Nanoparticles, on the other hand, are also artificially constructed and can contain therapeutics embedded inside clusters of nanoparticles that can then be delivered to target tissues (132). However, safety and quality of nanoparticle and liposomal drug delivery systems has been questioned due to their artificial nature and high dependency on the composition of the particles themselves, which can affect large-scale manufacturing (130, 132). To overcome this, researchers have also begun to discuss the validity and usability of hybrid lipid-polymer nano-carriers that incorporate both liposomal and nanoparticle components with a loaded therapeutic inside the molecule (133). However, there are several advantages to using exosomes over liposomal or nanoparticle drug delivery. Firstly, since exosomes are naturally derived, there is a lower chance of immunogenicity

and therefore a much longer half-life in the body (134). Secondly, studies have shown the ability of exosomes to cross the blood-brain barrier to deliver anti-cancer drugs to brain tumors, making them a particularly attractive option for previously inaccessible drug target areas such as brain metastasis (128). Further, they are capable of carrying diverse nucleic acids such as DNA, RNA, miRNA and siRNA, as well as proteins and small molecule therapeutics (135).

Exosome utilization as therapeutic carriers does pose some concerns, however. First, while their endogenous sourcing does confer an advantage, it also restricts the scalability of the product since a large volume of blood or tissue is required for ultracentrifugation, which ultimately results in a relatively low exosome yield (136). Additionally, while exosomes can avoid immunogenicity, they must be further engineered for therapy to successfully and accurately find their target cell type for therapeutic delivery. This requires attachment of antigens corresponding to the target cell or tissue that can aid exosome navigation once delivered into the body. The impact and applicability of exosomes as drug carriers in cancer can range far and wide with sufficient personalization and accurate engineering paired with a drug capable of high cytotoxicity in the cancer of interest.

The Autotaxin and Lysophosphatidic Acid Signaling Axis

Autotaxin Discovery and Function

The ecto-nucleotide pyro-phosphatase/phosphodiesterase (ENPP) family are broadly responsible for hydrolyzing phosphodiester bonds on their substrates within their structure's catalytic domains. Substrates in the ENPP family can vary greatly, including nucleotides and their derivatives, choline phosphate esters and lysophospholipids (137). Autotaxin, or ENPP2, is the second, and most prominent, of seven the members belonging to the ENPP2 family due to its motility-stimulating activity. It is largely responsible for the conversion of lysophosphatidylcholine (LPC) to bioactive lysophosphatidic acid (LPA), which is able to initiate various pathophysiological processes through receptor signaling. The ENPP2 gene encoding for autotaxin is present on chromosome 8 on a 116-kbp DNA segment and is possibly regulated by the nuclear factor of activated T-cells (NFAT) family or c-Jun transcription factors through a promotor residing 254 nucleotides upstream of the start codon (138-140). Further, autotaxin gene expression has also been shown to be controlled by LPA and sphingosine-1-phosphate through an inhibitory feedback loop regulated by the PI3K signaling (141). Once transcribed and translated by intracellular machinery, the pre-pro-enzyme form of autotaxin localizes to the Golgi apparatus, where it is cleaved by pro-protein convertases and glycosylated before the mature protein is secreted out of the cell (142).

It was found in 2002 that autotaxin is the same 125 kDa lysophospholipase-D (lysoPLD) that was previously discovered by the same group in 1986 in rat plasma with the ability to produce LPA (143, 144). Full-length autotaxin protein is known to have five isoforms, with the first being cloned from a melanoma cell line in 1992 with a length of

915 amino acids (145). Shortly after discovery of this first autotaxin isoform in melanoma, it was found that the protein shared homology with phosphodiesterases such as PC-1, thereby implying its role in motility regulation (146). Research over the next ten years recognized other isoforms of the protein, which varied from 859 to 915 amino acids in length and differed in their nuclear and catalytic domains (147-150). Although the various isoforms have not yet been found to have distinct catalytic activities, there have been variations in the expression patterns between them to distinguish the specific roles some play in cancer.

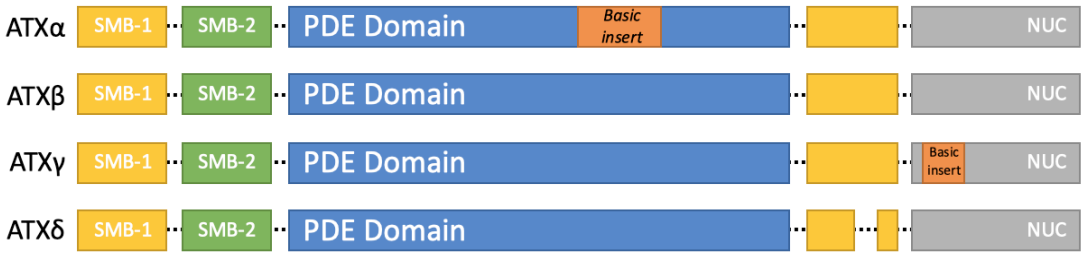

Figure 1.4: Autotaxin isoforms. The four isoforms of autotaxin have varied tissue expression in humans with ATXß being the most common in plasma and therefore being the most relevant as a possible biomarker. Adapted from a previous publication (151).

There are a variety of tissues that express autotaxin, of which the brain, ovaries, lung, kidneys and lymph nodes contain the highest levels of autotaxin mRNA. The three major isoforms, denoted as autotaxin alpha, beta, or gamma are all present in varying levels in humans. The beta isoform is most abundant in plasma, whereas the alpha isoform has been found to be unstable in plasma and therefore is largely present in surface proteoglycan-bound form near the cell surface where it cannot be cleaved by proteases in circulation (144, 152). Further, all three isoforms are widely present in adipose tissue, where later studies have shown autotaxin's strong involvement in adipogenesis and link to obesity (153, 154). In fact, up to 50% of plasma autotaxin has

been shown to be produced by adipose tissue (155). Autotaxin gamma has also been shown to exclusively have the highest expression in the brain, while other isoforms dominated expression in organs such as the lungs or kidneys as detected by PCR analysis (156). The same study also found that autotaxin isoforms beta and gamma were more catalytically active compared to the alpha isoform, which may be susceptible to protease cleavage more easily due to a 52-amino acid insertion in the catalytic domain (152).

In fact, variations in the isoforms have led to the discovery of specific structure-function roles for the enzyme's activity. All isoforms share the same basic components in their structure, which contains a signal peptide, somatomedin type ß (SMB) 1 and 2 domains, a phosphodiesterase (PDE) catalytic domain, connecting loop structures and a nuclease domain (157). The signal peptide on the N-terminus is responsible for regulating the extracellular release of autotaxin through interaction with the plasma membrane (158). Since autotaxin is an extracellular enzyme, but produces LPA, which initiates downstream signaling through membrane receptors, the SMB domains on the enzyme interact with integrins on the cell surface (159). While the mechanism of integrin binding has not yet been elucidated, studies have shown that strong binding results in higher catalytic activity, possibly due to efficient LPA signaling since production occurs close to the cell surface (160). The PDE catalytic domain is crucial for enzyme function as it is responsible for the hydrolyzing activity that converts LPC to bioactive LPA, which is capable of then initiating downstream signaling. This domain is connected to the nuclease domain by two disulfide bridges and by a loop structure to both the SMB and nuclease domains (157). This same study also found that the hydrophobic active pocket of autotaxin contains threonine (Thr) residues highly conserved across all but one ENPP

members, and a hydrophilic binding groove, both of which together can accommodate the LPC structure for successful hydrolysis. The structure also contains an open tunnel formed between the SMB1 and PDE domains, that may serve as an LPA binding and release site near the cell surface. However, the exact binding of LPC and LPA in the autotaxin structure is still being explored, as varied saturated isoforms of LPC or LPA may bind in different conformations, possible impacting enzyme activity.

Lysophosphatidic Acid and Downstream Signaling Mechanisms

Lysophosphatidic acid is the primary product of ATX activity, and is produced when lysophosphatidylcholine is hydrolyzed to remove of the choline head group, thereby forming LPA. Interestingly, LPA, a water-soluble phospholipid, was discovered prior to autotaxin or any of its receptors, and originally thought to be a passive membrane lipid (161). After being established as the primary product of mitogenic autotaxin, it then gained interest as a mediator of signaling. In the body, LPA exists as serum albumin-bound molecule, and can accumulate in pathophysiological fluids such as serum, plasma or also ascites fluid formed by growing ovarian tumors (162, 163). Plasma LPA levels in humans generally ranges between 0.1 to 10 μM, while serum concentrations, especially in ascites fluid often observed in ovarian cancer patients, can often exceed those parameters (164).

Once produced at the plasma membrane surface, LPA is then able to signal through G-protein coupled receptors (GPCRs) known as LPA receptors (LPARs) to initiate downstream signaling (165, 166). There are currently six established LPA receptors that originate from two distinct sets of gene families. The first three belong to

the endothelial differentiation gene (EDG) family, denoted as EDG2/$LPAR_1$, EDG4/$LPAR_2$, and EDG7/$LPAR_3$ (167). The first of these was discovered in cortical neurons and initiates downstream signaling through the G_i protein coupling (168). However, $LPAR_2$ and $LPAR_3$ primarily utilize the $G_{q/11}$ protein to initiate signaling and were discovered by sequence similarity shortly after $LPAR_1$ (169, 170). Over time, it was found that not all LPA activity was attributable to $LPARs_{1-3}$, eventually leading to the discovery of non-EDG family of LPAR receptors (171). The first non-EDG discovered was named $LPAR_4$, and being a purinergic receptor, it can bind purine and pyrimidine nucleotides, but still functions as a GPCR (172). Soon after, $LPAR_5$ and $LPAR_6$ were also discovered, which also bind and regulate LPA signaling with varied downstream effects (173-175).

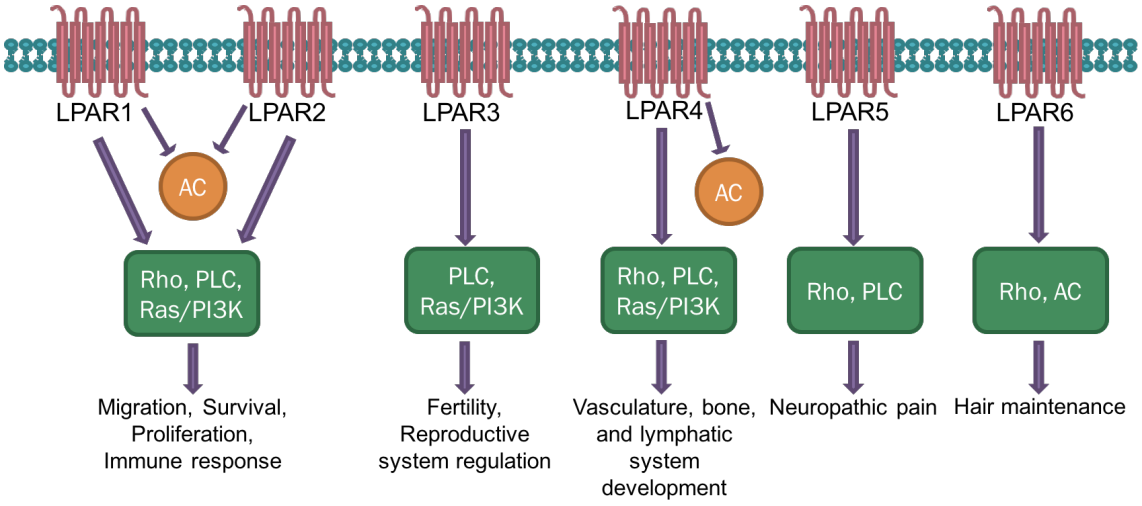

Figure 1.5: LPA and its receptor-specific signaling outcomes. LPA receptors are responsible for a wide array of pathophysiological signaling outcomes, depending on the specific receptor activated. Oncogenic signaling is largely the result of $LPAR_{1-3}$ activation, which control migration, proliferation, and immune response. Own creation.

The diversity in LPARs is largely present to accommodate for the varied signaling outcomes associated with LPA production and binding to these receptors, not to mention the multiple LPA species that differ in saturation content of their fatty acid chain (167).

Previous analysis has detected unsaturated LPA species such as oleoyl LPA (18:1), linoleoyl LPA (18:2) or arachidonoyl LPA (20:4) that can contain carbon double bonds at various parts of their fatty acid chain as well as saturated forms such stearoyl (18:0) and palmitoyl LPA (16:0) (176). The abundance of these LPA species also varies, with LPA 18:2 and 18:1 being the first and second most abundant, respectively (177). Since various LPAR receptors have varying affinities to each LPA species and sub-form, the signaling outcomes associated with LPA can be widely diverse as well.

$LPARs_{1-3}$ are largely responsible for maintaining proliferation, survival, inflammation and angiogenic potential of the cell, and are activated by LPA in physiological processes such as wound repair and maintenance and other immune signals such as cytokine production (178-181). In conditions like cancer, which often exhibit much higher concentrations of circulating LPA and autotaxin, signaling outcomes can be amplified, resulting in the oncogenic properties that can drive growth, invasiveness, and immune mediation (182). On the other hand, $LPARs_{4-6}$ play a more general physiological role by mediating signaling associated with neuropathic pain and hair maintenance, while $LPAR_4$ is still partially involved in controlling cell adhesion and aggregation, which can be important in cancer cell migration and tumor growth (182-185). Aside from receptor-specific effects, LPA in general is involved in several oncogenic processes through its influence, particularly its angiogenic potential (164). For example, LPA has been shown to increase VEGF expression in ovarian cancer cells specifically through the HIF1-alpha transcription factor downstream of $LPAR_2$ (186).

Endogenously, LPA levels are controlled by lipid phosphate phosphohydrolase type 1 (LPP1), which is able to degrade LPA extracellularly and in the bloodstream

(187). However, as an extracellular target, increased circulating LPA in cancer is particularly challenging to inhibit. Therefore, a majority of LPA inhibitor investigations are focused on mitigating amplified signaling conferred to LPARs. Most LPAR inhibitors are designed to target $LPARs_{1-3}$ since those receptors are responsible for the bulk of oncogenic signaling. For example, Ki16425, which is an $LPAR_{1/3}$ inhibitor has shown immense success both *in vitro* and *in vivo* with a breast cancer model (188). Another $LPAR_{1/3}$ inhibitor, VPC12249, has also shown promising results *in vivo*, but in a renal ischemia model, where inhibition of both LPAR receptors has a protective effect (189). The most successful LPAR inhibitors are those that target $LPAR_1$ alone, such as BMS-986020 reached phase II trials for efficacy in pulmonary fibrosis where it showed a significant reduction in decline in patients, but was terminated early due to cholecystitis in some patients (190). SAR-100842, which inhibits $LPAR_1$, also reached a phase IIa clinical trial for diffuse cutaneous systemic sclerosis where it was well tolerated, but did not produce any significant outcome (191). Selective inhibitors for the remaining LPARs are still being investigated, although since they play a lesser role in oncogenic signaling the focus of research thus far has been on $LPARs_{1-3}$. Future preclinical and clinical work in the LPAR inhibitors is sure to involve cancer models, especially given the significant role these receptors play in promoting oncogenic signaling in cells.

Autotaxin in Cancer and Relevant Model Systems

Since it was originally cloned from a melanoma cell line, the correlation of autotaxin to cancer has been well-established for decades. The enzyme sequence and structure are widely conserved at all crucial sites on its structures across multiple species,

and is considered essential for embryonic development, since autotaxin homozygous null-mice are embryonic lethal (192, 193). In fact, a single nucleotide substitution at T210A in the PDE catalytic domain can obliterate autotaxin function completely and also results in embryonic lethality (194). While it is actively and consistently involved in crucial physiological and pathological processes through LPA production and signaling, autotaxin can also be rapidly cleared from the blood once produced by localizing to liver sinusoidal endothelial cells (195). Given its short-half life in the blood, the overexpression of autotaxin in cancer is even more clinically relevant as it suggests that increased circulating levels are not indicative of a defective clearance mechanism.

The first indication of autotaxin being overexpressed in cancer was a study involving neuroblastoma patients and their tissue samples (139). Since then there have been multiple studies stating the role of autotaxin in renal cell carcinoma and bladder carcinoma progression, (196), progression of hepatitis C to hepatocellular carcinoma (197), thyroid carcinoma progression (198), non-small-cell lung cancer motility stimulation (199) and promoting glioblastoma invasion (200). Most notably, as per the Cancer Genome Atlas and other research studies, autotaxin is most frequently overexpressed in ovarian and breast cancer, where it is known to promote aggressiveness and angiogenic processes to exacerbate growth and metastasis (201-205).

In addition to the well-established hallmarks of cancer such as increased angiogenesis, invasion, metastasis and evasion of growth suppressors or cell death, both inflammation and immune signaling have emerged as additional key hallmarks in the last decade (48, 206). The connection of cancer and inflammation is now well established, with the involvement of pro-inflammatory cytokine upregulation, changes in T-cell

response and also changes in macrophage and white blood cell responses (207-209). Specifically with respect to autotaxin, which is already known to control immune response through various LPARs, the immune system undergoes several changes with upregulation of this enzyme in cancer (210). For example, autotaxin has been shown to initiate lymphocyte migration and homing to the tumor site, causing inflammation and exacerbating tumor progression (211, 212). Further, adipose tissue has been found to significantly contribute to autotaxin production in breast cancer cells directly increasing inflammatory signaling through $LPARs_{1-3}$ (213). A similar effect is observed in ovarian cancer where increased interleukin and VEGF production promote invasive properties of the cancer cells (214). The involvement of autotaxin in promoting pertussis toxin-mediated motility has also long been established, as pertussis toxin has been shown to inhibit early inflammatory response such as neutrophil and macrophage recruitment, which in turn promote cell migration (145, 215).

To study the varied and highly impactful effects of autotaxin in cancer, inflammation and conditions unrelated to cancer, several *in vivo* and *in vitro* models of autotaxin have been developed over the years. Specifically, in our laboratory, we have developed *in vitro* models of autotaxin for cancer by creating cell lines stably overexpressing functional (ATX wildtype or ATXwt), or nonfunctional (ATX mutant or ATXmut) autotaxin which can be utilized to explore its effects in OVCAR-3 cells (216). In other literature, *in vivo* models of autotaxin are fairly common, as are patient-derived samples with corresponding autotaxin levels characterized for analysis. For example, a group exploring the involvement of autotaxin in renal cell and bladder carcinoma utilized tumor tissue and adjacent normal tissue from a patient for analysis (196). Another group

utilized $LPAR_3$-overexpressing transgenic mice to mimic the effects of autotaxin through that specific receptor, which controls survival and proliferation signaling upon activation (201). This shows the abundance of possible models to better study autotaxin's diverse influence on tumor cells, and utilization of multiple models to build a cohesive picture of autotaxin function may be crucial to understanding how to target its effects in cancer.

There are two autotaxin mouse models that are available to study the enzyme's effects *in vivo*. Both of these models were developed around the same time, but for different purposes. One mouse model of autotaxin used the transgenic $LPARs_{1-3}$ genes placed under the MMTV promotor (204). In this study, it was shown that a portion of the multiparous female transgenic mice developed mammary tumors with overexpression of autotaxin or $LPARs_{1-3}$ directly attributable to the transgene insertion, as non-transgenic littermates and transgenic males did not develop tumors. A second model, in which the autotaxin transgene was expressed under the alpha-1-antitrypsin promotor in the liver was used to study adipogenesis related to autotaxin overexpression, specifically the distinction between brown and white adipose tissue (217, 218). In our studies, we utilized the latter alpha-1-antitrypsin promotor driven mouse model, which had previously not been utilized to study cancer. As we aged the female mice, a portion of them developed spontaneous tumors, while non-transgenic littermates did not (216). In fact, male transgenic mice exhibited aggressive behavior and required extensive cage separations, resulting in their eventual termination before they were fully aged (219). Therefore, both mouse models have now been initially explored for their utility in studying cancer, in addition to patient samples providing more relevant into the involvement of autotaxin in specific cancers.

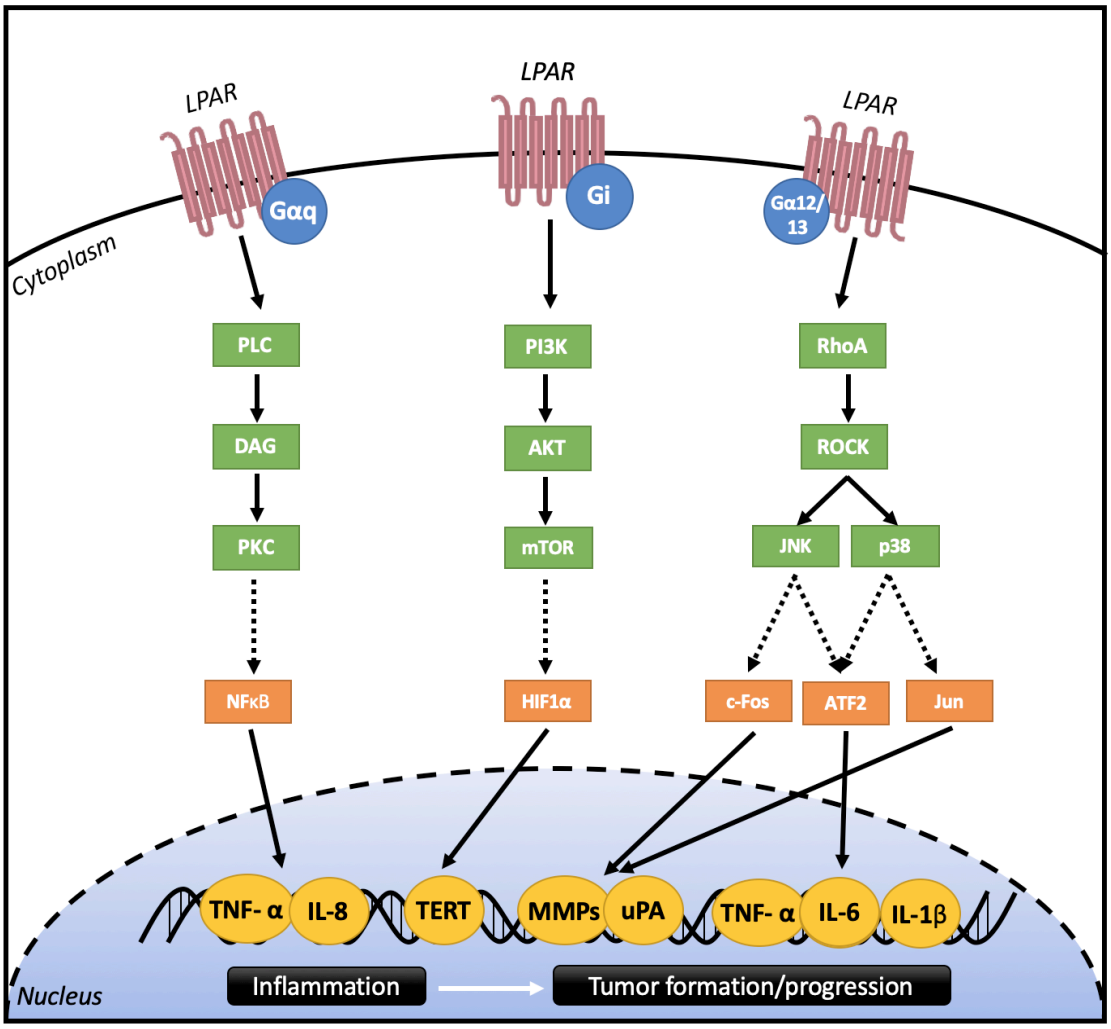

Figure 1.6: Inflammatory signaling as a result of LPAR activation. Depending on the G-protein related second messenger located after LPAR activation, this pathway can contribute to inflammation through the increased transcription of various cytokines, interleukins and other proteins. This process further contributes to oncogenic signaling, allowing cancer cells to grow and survive. Adapted from a previous publication (220).

Autotaxin as a Potential Target

Due the diverse outcomes of autotaxin and LPA/LPAR signaling, the field has consistently explored the possibility of inhibitors that target these prominent players in cancer. Studies in melanoma xenografts with novel inhibitors for autotaxin has shown that the enzyme's expression levels directly correlate with tumor stage and grade, and chemical screens with autotaxin inhibitors showed decreased migration and invasion

(221). In terms of inhibitors, there have been boronic acid-based and tyrosine-based inhibitors as well as those that have an aromatic sulfonamide motif that interacts with the hydrophobic pocket of autotaxin (222-225). One specific inhibitor that has made it past the *in vitro* testing stage in cancer is ONO-8540506, which has been tested in rats through oral administration to successfully reduce plasma autotaxin and LPA levels in a study focused on reducing urethral tension in conditions such as prostatic hyperplasia (226). This same compound has also been studied in mouse models of breast cancer to show successful inhibition of lung metastasis and primary tumor growth, and in a SCID model for thyroid cancer where it reduced inflammatory mediators and significantly lower tumor volume (227, 228). Finally, there has also been an LPA analog in preclinical testing named BrP-LPA, which has shown to have pan-activity against autotaxin as well as all the LPARs except $LPAR_6$, which is involved most commonly in hair maintenance. BrP-LPA has found to be effective in radio-sensitization of glioblastoma *in vivo*, and demonstrate tumor regression and reduced tumor burden in xenografts created with MDA-MB-231 triple-negative breast cancer cells (229, 230) One of the most potent autotaxin inhibitors to date, CVS-16, was previously investigated in our laboratory, and is a vinyl sulfone analog of lysophosphatidylcholine that irreversibly inhibits autotaxin activity after binding its hydrophobic pocket. This compound was also able to show significant reduction in angiogenic and mitogenic potential of melanoma xenografts *in vivo*, and was more potent *in vitro* and *in vivo* than HA-130 and PF-8380, which are well-established autotaxin inhibitors and currently under preclinical testing (231).

HA-130 is currently being investigated for its effectiveness melanoma, while PF-8380 is being studied in glioblastoma preclinical trials, but some autotaxin inhibitors

have also made it into the clinical trials stage, albeit not all in the context of cancer (224, 232, 233). GLPG-1690 that has been evaluated in clinical trials for idiopathic pulmonary fibrosis. Bioavailability was assessed in the Phase I trial of this compound, and in the Phase 2a trial, results showed that the inhibitor was able to exhibit sustained decreased levels of LPA in patient plasma and did not cause any significant adverse events in patients (234, 235). Therefore, the compound has now moved on to an additional Phase 2 trial investigating its safety and efficacy in systemic sclerosis, as well as two Phase 3 studies involving a combination treatment of GLPG-1690 with standard medical treatment ISABELA1 or ISABELA2, all of which are in the recruitment phase.

For the future of autotaxin inhibitors, the structure of autotaxin has begun to provide some insight and tools into the development of more targeted inhibitors, or inhibitors that are more potent than those available current, such as CVS-16 investigated in our laboratory. Additionally, as depicted in a recent study, using fluorescent probes or docking-based experiments to design inhibitors can specifically inhibit the catalytic site of autotaxin to stop it from producing LPA (236, 237). This approach might also ensure more specific binding and inhibition of the enzyme as well as mitigate some off-target effects that may be present when nonspecific targeted inhibitors are developed using high-throughput chemical screening.

Cancer Therapeutics

Melanoma in the Clinic

According to the 2019 Cancer Statistics, melanoma is the 5th most diagnosed cancer in both men and women in the United States (238). Melanoma also accounts for 4% of all adolescent cancer cases, partially attributable to increased UV exposure and environmental or lifestyle hazards such as tanning beds. While most melanoma cases are diagnosed at localized stages through regular mole checkups, discovery of malignant disease that has spread to metastatic sites reduces the 5-year survival rate from over 90% to just above 20% across all races (238). Additionally, only 1% of melanoma cases are considered to be cutaneous malignant melanoma, which is an aggressive, potentially fatal disease when metastasized and is responsible for the greatest percentage of melanoma-related deaths (239). Other subtypes of melanoma also exist with varying degrees of prevalence such as lentigo maligna melanoma (4-15% incidence), superficial spreading melanoma (up to 70% incidence), nodular melanoma (10-15% incidence) and to a lesser extent, acral lentiginous, mucosal and desmoplastic melanoma which are much rarer (240). However, due to the high mortality rates observed in cutaneous malignant melanoma, although its incidence is very low, most therapeutics research has been focused on combating this disease.

Comprehensive analysis of DNA, RNA and protein from primary melanoma tumors and their metastatic sites through the years have revealed several genetic abnormalities that can be exploited in the clinic. Much of the research and approved therapies for melanoma are focused on targeting a specific protein and mutation, namely B-RAF particularly at the V600E position, which is mutated in up to 50% of diagnosed

melanoma cases (241). Other mutations in melanoma were also discovered through similar studies and include RAS, NF-1, CDKN2A, and TP53, among others (242, 243). While some of these are involved in the MAPK signaling cascade, others, such as CDKN2A are responsible for cell cycle control and proliferation (244). Additionally, MITF, a transcription factor that has been shown to be dysregulated in up to 10% of cutaneous melanoma cases, controls the transcription of genes related to cell survival and growth (244).

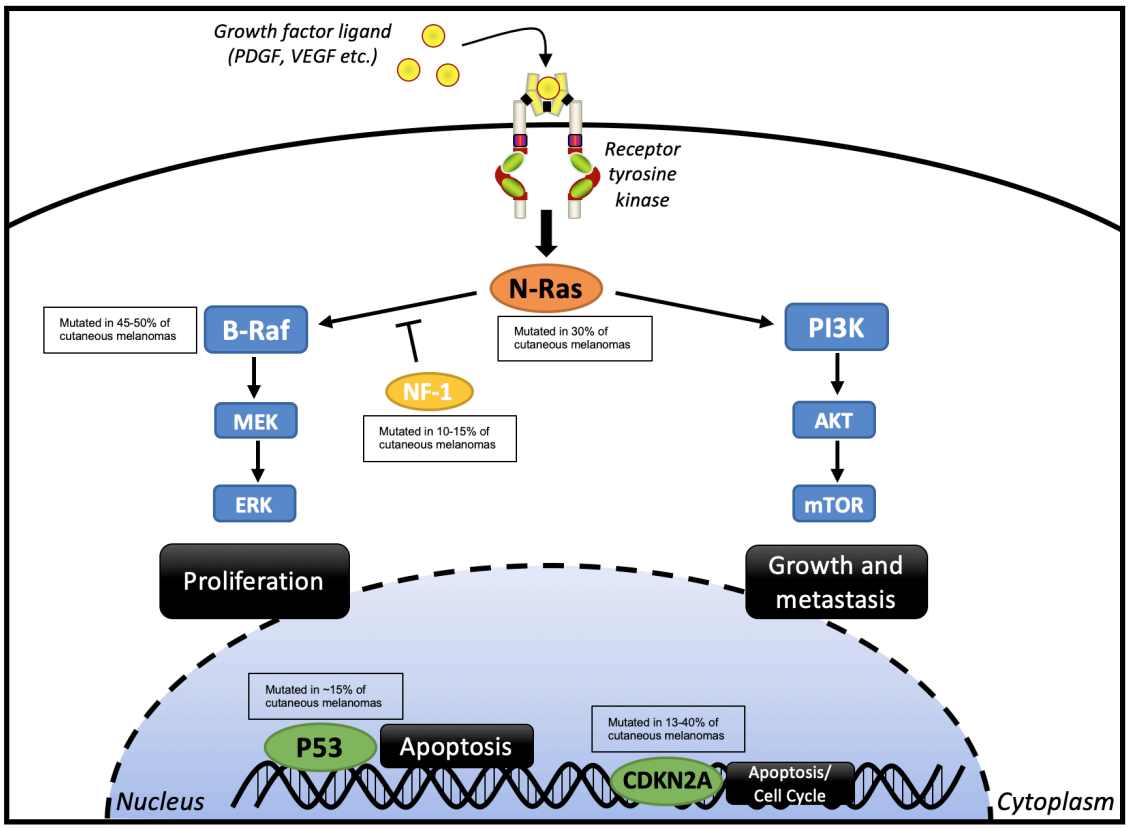

Figure 1.7: Common mutations in proliferative pathways contributing to melanoma progression. N-Ras, B-Raf, p53, NF-1 and CDKN2a are commonly misregulated in melanoma, contributing to growth and progression through their involvement in proliferation, cell cycle control and apoptosis. Adapted from a previous publication (240).

Based on tumor staging through imaging and pathology after a sentinel node biopsy, the genetic features, abnormalities and location of disease, melanoma is treated

differently in the clinic (245). Targeted inhibitors are widely used in this disease, especially against the V600E B-RAF mutation, while other targeted inhibitors are also available. In addition to this, surgery, radiation, immunotherapy and photodynamic therapy can also be used in a patient, although earlier stages of the disease can be successfully treated with minimally invasive therapy such as surgery (246). On the other hand, later stages of melanoma requiring mostly palliative care have recently begun to depend on laser or light-based therapies (247).

The first therapeutic ever to be approved for use in melanoma was dacarbazine, which is a chemotherapeutic agent, and still stands as one of the only options in this class of drugs, despite showing unimpressive patient response rates (248). Temzolomide, which is more commonly used in glioblastoma, is another chemotherapy option in melanoma, but still does not result in a large difference in overall survival compared to placebo or dacarbazine alone (249). In fact, immunotherapy and targeted inhibitors are the two classes of drugs that have shown immense potential and success in melanoma. B-RAF inhibitors, as stated above, are widely used in this disease and include several options based on patient disease status. Vemurafenib was approved in 2011 by the FDA to treat unresectable or metastatic melanoma with the V600E B-RAF mutation, and showed an incredible 90% regression in disease in clinical trials (250). Dabrafenib was also approved in 2013 under the same indications, and both these B-RAF inhibitors have consistently been in clinical trials since their approval as combination treatments with immunotherapy, chemotherapy or with other targeted inhibitors for metastatic disease (251). However, melanoma cells with mutated B-RAF are so dependent on the protein's proliferative signaling capacity that targeted inhibition eventually leads to resistant

disease, with upregulation of other oncoproteins such as MEK1, N-RAS and AKT1 (252). Therefore, combination therapy of B-RAF inhibitors with MEK1 inhibitors were shown to be more effective around the same time as the approval of vemurafenib.

Targeted inhibitors against MEK1 such as tramatenib, which was approved in 2012 against metastatic and unresectable melanoma, have shown a remarkable increase progression-free and overall survival in combination with vemurafenib or compared to chemotherapy (253, 254). Tramatenib was also combined with dabrafenib in 2014 at full monotherapy doses under the same indications, resulting in a 3.6-month increase in progression free survival compared to monotherapy of either drug (255). A combination of vemurafenib with cobimetinib, another MEK1 inhibitor, also resulted in increased overall survival, although did require dose adjustments to reduce high-grade adverse events during the clinical trial (256). This was approved for use in 2015 for advanced melanoma (257). Finally, encorafenib, a third MEK1 inhibitor is approved in combination with binimetinib, a B-RAF inhibitor, albeit with adverse effects (258-261).

There are also other targeted inhibitors in melanoma that downregulate VEGF and related receptors, players in the PI3K, AKT, and mTOR pathway, as well as CKIT that all lead to resistant disease after B-RAF inhibitor therapy. VEGF and its receptors are targeted with bevacizumab in clinical trials as a combination treatment with temozolomide, resulting in increased overall survival in patients, but this regimen has not yet received FDA approval (262). Since melanoma is highly vascularized, a VEGF inhibitor would be beneficial since it blocks angiogenic processes that are crucial for metastatic spread, although adverse events with bevacizumab can be dose-limiting (263, 264). While CKIT inhibitors such as imatinib and sunitinib or PI3K-AKT-mTOR

pathway inhibitors such as rapamycin have been in clinical trials for melanoma, there have been no approvals as yet for these indications either (246).

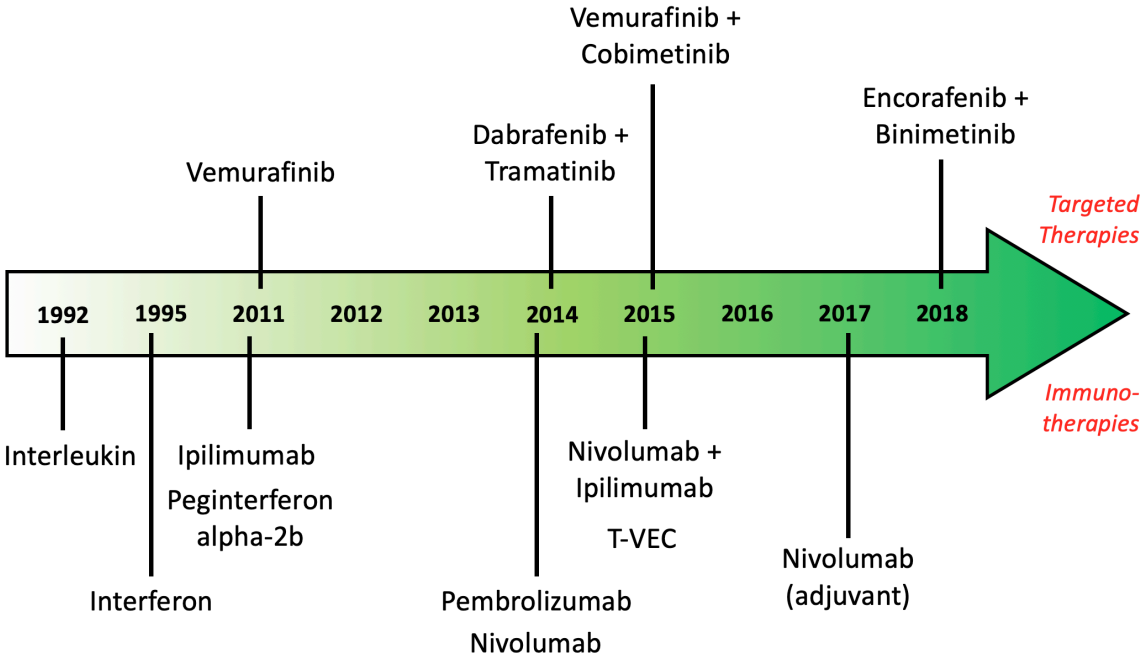

Fig 1.8: Timeline of therapeutic approvals for melanoma. The drug formulary for melanoma consists of both targeted therapies and immunotherapies, which together have continued improve overall and progression-free survival in patients through various combinations and adaptations. Adapted from a previous publication (265).

Melanoma also exhibits high immunosuppressive properties, which have given way to the development and approval of several immunotherapies (266). In 1995, the approval of interferon (IFN) alpha 2b, which stimulates the immune system to have a pro-apoptotic effect on cancer cells, for resected stage II and III melanoma resulted in decreased recurrence and paved the way for further immunotherapy development (267, 268). A PEGylated version of IFN alpha-2b (PEG-interferon alpha-2b) was then approved for stage III melanoma in 2011 and showed longer recurrence-free survival due to its increased half-life in the blood and bioavailability (269). In the same year, ipilimumab, an anti-CTLA-4 antibody, was approved for advanced melanoma (270). CTLA-4 is a receptor that is responsible for regulation of T-cell function, and inhibition

results in a more robust immune response, leading to increased tumor cell death (271). The PD-1 receptor and its ligands, PD-L1 and PD-L2, are also responsible for suppressing T-cell activation and are commonly expressed on tumor cells and cells in the surrounding tumor microenvironment (272, 273). In 2014 and 2015, two inhibitors of this process were approved for use in melanoma, namely nivolumab and pembrolizumab (272). While nivolumab inhibits binding of the PD-1 receptor and PD-L1 ligand and pembrolizumab only inhibits PD-1 receptor activation, pembrolizumab exhibited longer progression-free and overall survival in patients along with lower-grade adverse events (274, 275). In an effort to combine immunotherapies and further improve survival in metastatic melanoma, clinical trials testing a combination of nivolumab and ipilimumab were successful, leading to the approval of this regimen in 2015 (276). Nivolumab was also approved as adjuvant therapy in 2017 for late-stage melanoma, resulting in a significant improvement in recurrence-free survival and milder adverse events compared to adjuvant ipilimumab (277).

In addition to immunotherapy and targeted therapies in melanoma, oncolytic virus therapy and the BCG vaccine have also been evaluated. The first and only oncolytic viral therapy named T-VEC was approved for injectable, but non-resectable melanoma in 2015 (278). The success behind this concept lies in the ability of the virus to replicate in the tumor cell and result in cell lysis, which can then generate an immune response for an additive cytotoxic effect (279). Additionally, the BCG vaccine, which is a weakened formulation of *Mycobacterium bovis*, was tested in clinical trials in late-stage melanoma, resulting in 90% regression in patients, but was unable to prevent disease recurrence and therefore was not approved (280). Looking into the future, adjuvant immunotherapy and

targeted-inhibitor therapy is becoming more popular for high risk-of-recurrence cases in melanoma to improve patient outcomes (281).

Finally, light-based therapy can be considered as a palliative option for patients requiring end-of-life support. This involves injecting a photosensitizer that is selectively taken up by cancer cells due to their high metabolic state, after which light can activate reactive oxygen species production, eventually resulting in cell death (247). In conclusion, melanoma has several approved therapeutics, but the focus of future research must be focused on successfully controlling metastatic spread and resistance in patients.

Ovarian Cancer in the Clinic

Although not the most common gynecological malignancy, ovarian cancer is the 5th leading cause of cancer-related deaths among women in the United States (238). Since it is diagnosed at later stages in approximately 60% of cases when distant metastasis is already present, 5-year survival rates are only around 25% (238). There are multiple subtypes of ovarian cancer, with some originating from the epithelium, and others of non-epithelial nature that originate from the sex chord or germ cell lining (282). Epithelial tumors occur more frequently and make up 90% of all diagnosed cases, with high-grade serous ovarian carcinoma being the most common, with less common subtypes being endometrioid, clear cell, mucinous, and low-grade serous ovarian carcinoma (283, 284). These subtypes have recently been further divided into Type I tumors, which consist of all epithelial ovarian cancer subtypes except high-grade serous ovarian carcinoma and Type II, which is high-grade serous ovarian carcinoma alone, based on their histopathological characteristics and genetic mutations or alterations (283, 285). Type I

tumors generally have a predictable genetic profile, with mutations in several common oncogenes such as K-RAS, B-RAF, PI3K, ARID1A and PTEN, while Type II tumors, or high-grade serous ovarian carcinoma, are highly heterogeneous and aggressive, with TP53 being the only common mutation (284, 286, 287). Further, high-grade serous ovarian carcinoma can also harbor BRCA mutations in up to 50% of cases, which can be a driver for carcinogenesis (288). While there is not enough evidence detailing how these tumors originate, there is postulation that high-grade serous ovarian carcinoma tumors originate from the fallopian tube, as their genetic profile closely resembles that of the fallopian tube rather than the ovarian surface epithelium (289, 290). High-grade serous ovarian carcinoma that originates from the fimbria of the fallopian tube are now known as serous tubal intraepithelial carcinoma lesions which are highly invasive and more often carry BRCA mutations (291-293).

Ovarian cancer presents clinical challenges due to many reasons: 1) late-stage diagnoses significantly reduce the chance of a cure, 2) there is a lack of reliable biomarkers that rapidly detect disease development or progression and 3) high heterogeneity of the most common subtype, high-grade serous ovarian carcinoma, is perplexing to treat with effective targeted inhibitors. Since BRCA mutations are implicated in at least half of high-grade serous ovarian carcinoma cases, ovarian cancer prevention partially begins with genetic testing for those with a family history of female gynecological cancers. While there are events in the reproductive life of a female that can decrease the risk of developing ovarian cancer, such as the use of oral contraceptives for at least 5 years, longer time breastfeeding, more full-term pregnancies, fewer miscarriages, and healthy weight, once the tumor develops, detection methods are fairly

conventional (294). Procedures can involve tests as simple as a pelvic exam or ultrasound imaging to more complicated imaging such as computed scans, positron emission tomography scan or magnetic resonance imaging (295, 296). Other tests such as laparoscopy to look at the ovaries and surrounding organs internally, colonoscopy to check for metastasis and a biopsy to remove a tumor specimen for histopathological analysis can also be performed (295).

There is an urgent need for the development and approval of reliable biomarkers that cater to both low- and high-risk populations. To achieve cure, these should be tailored to high-grade serous ovarian carcinoma detection, since it is more common and a majority of diagnoses occur with metastatic disease already present (297). Two methods that have been developed for this purpose are the large (~5 MDa) CA-125 protein biomarker, and a transvaginal sonography, which both underwent prolonged clinical trials resulting in no overall survival benefit and the occurrence of false-positive results (298, 299). Specifically, results revealed that CA-125 needs to be detected much earlier than after disease has already developed in order to obtain a personalized baseline for each patient. In addition, benign ovarian tumors do not elevate the biomarker candidate as previously expected (300, 301). However, the initial study was followed up with another clinical trial including women at average-risk for developing ovarian cancer and resulted in a 20% reduction in mortality with lower false-positive results (302). Regardless, definitive and specific results have yet to determined and the use of CA-125 as a biomarker remains to be elucidated.

Therapy for patients with ovarian cancer can vary by stage at diagnosis, but includes platinum-based chemotherapy (cisplatin or carboplatin), taxanes (paclitaxel or

docetaxel), surgery or targeted inhibitors aimed at PARP or angiogenesis. Typically, a patient that has been diagnosed with the disease will undergo surgery for tumor debulking, which can also be used to assess the disease stage and remove a section for histopathological analysis to obtain tumor subtype (303). If the patient has early-stage disease, watchful waiting is generally recommended instead of prophylactic chemotherapy. However, if the tumor has progressed to the tail end of stage II or later, patients typically receive a combination treatment of platinum chemotherapy and taxanes.

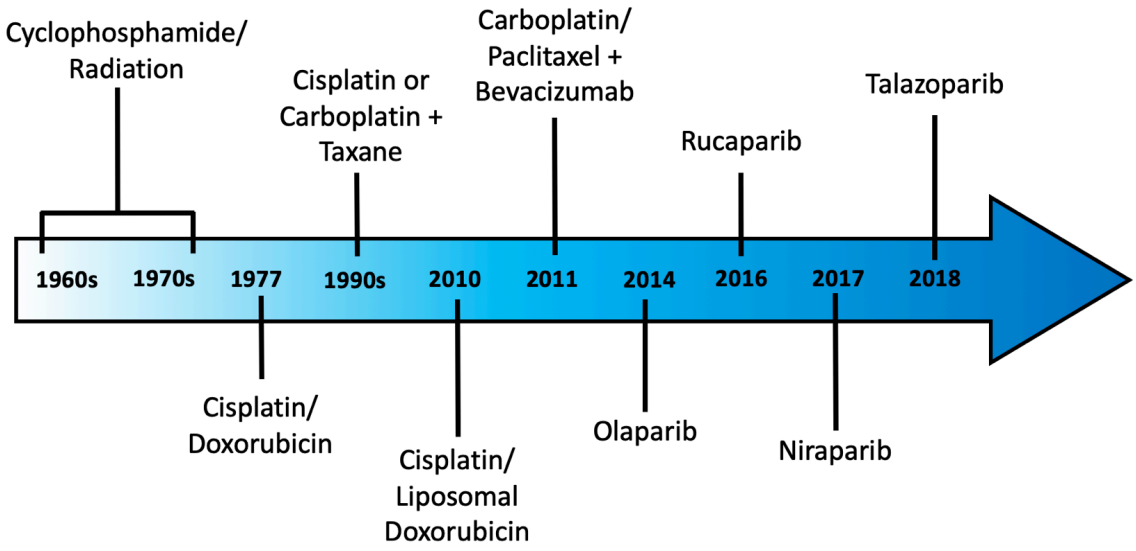

Fig 1.8: Timeline of therapeutic approvals for ovarian cancer. Due to the heterogeneity and inherent chemoresistant phenotype of ovarian cancer, chemotherapy is still the staple of the drug formulary. With the recent addition of targeted inhibitors against PARP, there has been notable improving survival in a subset of patients, although a large number still succumb to the disease. Adapted from a previous publication (304).

Originally, for patients requiring adjuvant chemotherapy, cisplatin and paclitaxel were administered intraperitoneally and indicated improved progression-free survival, overall survival as well as higher quality of life (305). Neoadjuvant chemotherapy for ovarian cancer has shown no survival benefit as per previous clinical trials in later-stage ovarian cancer diagnoses (306). However, due to the dose-limiting nephrotoxicity and

possibly untreatable ototoxicity associated with cisplatin, carboplatin later replaced its use in this combination regimen with paclitaxel (307, 308). Bevacizumab, an inhibitor targeting angiogenesis through inhibition of VEGF and VEGF receptors, was added to first-line ovarian cancer treatment in combination with carboplatin and paclitaxel in 2013 (309, 310). Patients experiencing extreme adverse events with this regimen can also be administered lower-dose cisplatin and docetaxel to achieve possible remission (311).

Following first-line chemotherapy/taxane regimens, a patient with relapsed disease is characterized as platinum-sensitive (recurrence within 6-18 months), platinum-refractory (recurrence during first-line treatment or weeks after) or platinum-resistant (recurrence within 6 months), which provides a guide for future treatment (312). For platinum-sensitive disease, second-line therapy involving different platinum-chemotherapy and taxanes are used, however, most patients present with platinum-resistant or –refractory disease, which typically does not have a good prognosis (313), While surgical debulking can add another 12 months to progression-free survival after recurrence, not all patients are eligible to receive this procedure depending on disease spread (313). Another option for relapsed patients is dose-dense taxane therapy with paclitaxel and carboplatin plus bevacizumab, which consists of weekly paclitaxel to increase its effects, resulting in increased progression-free survival with no additional adverse events (314). However, even after first- and second-line therapy, up to 85% of patients will develop recurrent and possibly resistant disease within 12-18 months, resulting in shorter and shorter disease-free intervals for each subsequent line of treatment, eventually leading to death (315).

Targeted therapies have been slowly emerging in the ovarian cancer drug formulary, and there have been multiple options that can be added to already established platinum-based chemotherapy and taxane regimens. RAS/RAF/MEK/ERK inhibitors are now commonly used in low-grade serous ovarian carcinoma since these genes are frequently overexpressed in this subtype, while PI3K/mTOR inhibitors such as rapamycin can be used in clear cell or endometrioid ovarian carcinoma (316, 317). For high grade ovarian serous carcinoma, PARP inhibitors have become a very popular option as well. Especially in BRCA-mutated patients who already have a homology directed repair deficiency for double stranded breaks, inhibiting PARP results in synthetic lethality in the cancer cells since the PARP enzyme is responsible for repairing single-stranded DNA breaks (318).

Olaparib was the first PARP inhibitor to be approved against both PARP1 and PARP2 in 2014 through an accelerated clinical trial for patients who have undergone at least three chemotherapy lines and also have a BRCA mutation (319). Soon afterwards, it was also approved as single-agent maintenance therapy for relapsed ovarian cancer patients that have platinum-sensitive disease and for those patients with a germline-BRCA mutation in 2016, both showing a significant increase in overall survival for this particular group (320, 321). Olaparib was also approved as combination therapy for relapsed platinum-sensitive patients with carboplatin and paclitaxel followed by olaparib monotherapy, resulting in a significant increase in overall survival and manageable toxicity (322). Another PARP1/2 inhibitor, Niraparib, received approval in 2017 for ovarian cancer patients with relapsed, platinum-sensitive disease regardless of BRCA status and increased progression-free survival under these indications (323, 324).

Although niraparib resulted in many high-grade adverse events in the clinical trials, it is considered a more effective PARP inhibitor than olaparib due to a lower IC_{50} value, and has also been approved as a single-agent maintenance therapy for recurrent disease (325). Finally, the third PARP inhibitor currently on the market is rucaparib, which is a pan PARP1, PARP2 and PARP3 inhibitor and was approved in 2016 as monotherapy for patients with a BRCA mutation and recurrent disease after at least 2 lines of chemotherapy (326, 327). Veliparib and talazoparib are two other existing PARP inhibitors that are still being evaluated for their potential to improve disease progression or survival in patients (328).

As stated above, bevacizumab has been frequently used as an addition to first-line chemotherapy in ovarian cancer, and it is also approved for use in platinum-sensitive and platinum-resistant recurrent ovarian cancer to provide significant progression-free survival advantage (329, 330). Other anti-angiogenic therapies, mainly aimed towards inhibiting Zeste homolog 2 (EZH2) and the Notch/Delta-like ligand 4 (Dll4) have also been pursued, since their involvement in ovarian cancer progression and prognosis has been well-established *in vitro* (331, 332).

Future therapies for ovarian cancer are mainly focused on the involvement of the immune system in promoting disease progression as well as tackling the highly heterogeneous nature of the high grade serous ovarian carcinoma itself. The ascites fluid that develops in the abdomen of ovarian cancer patients is known to be a hotbed of immune cells promoting inflammatory conditions advantageous to tumor growth, while the presence of infiltrating T-cells have shown significant tumor shrinkage (333, 334). Pembrolizumab is currently being tested in clinical trials as first-line therapy in

combination with carboplatin and paclitaxel (NCT02520154), while ipilimumab is being explored as a second-line agent for recurrent disease in platinum-sensitive patients (NCT01611558) (335). Additionally, variations of existing drug formulations in the ovarian cancer formulary may improve the agent's bioavailability and targeting ability. Nab-paclitaxel, packaged into a Cremophore-free nanoparticle capable of being albumin bound to increase circulation half-life exhibited significant progression-free and overall survival with tolerable adverse events in platinum-refractory ovarian cancer patients (336). Liposomal doxorubicin now has superiority over the carboplatin/paclitaxel regimen in platinum-sensitive disease as well as in combination with PARP inhibitors in BRCA mutated patients with recurrent disease (337-339). These new formulations of paclitaxel and doxorubicin are now widely used in therapeutic combinations for platinum-sensitive disease. Future drug development, or formulations of existing drugs to achieve better bioavailability, in ovarian cancer require a multifactorial approach to target the immunogenicity, heterogeneity, and aggressiveness of this disease together to successfully achieve a cure and reduce mortality in patients.

CHAPTER II

AUTOTAXIN EXACERBATES TUMOR PROGRESSION BY ENHANCING MEK1 AND OVERRIDING THE FUNCTION OF MIR-489-3P

Sudeepti S. Kuppa, Wei Jia, Shuying Liu, Ha Nguyen, Susan S. Smyth, Gordon B. Mills, Kevin K. Dobbin, William J. Hardman, and Mandi M. Murph

Published in Cancer Letters (2018).

Abstract

Upregulated expression of autotaxin, a secreted phospholipase and phosphodiesterase enzyme, appears in malignant disease. The identification of a circulating miRNA signature should distinguish autotaxin-mediated disease and also elucidate unknown molecular mechanisms that rationalize its malignant potential. Using female transgenic 'AT-ATX' mice, whereby human wild-type autotaxin is expressed in liver under the control of the alpha-1 antitrypsin promoter, transgenic animals express augmented autotaxin in circulation and a percentage develop tumors. Serum collected at necropsy had circulating miRNAs analyzed for statistical significance. The ensuing autotaxin-mediated miRNome differentiated between groups: healthy FVB/N mice versus AT-ATX mice with and without tumors. Intriguingly, miR-489-3p was sharply increased in AT-ATX tumor-bearing mice. Tissue analysis showed a correlation between miR-489-3p expression in tumors and surrounding milieu with autotaxin concentration in circulation. Sequence alignment suggested miR-489-3p targets MEK1, which was confirmed through *in vitro* studies. Exogenously added miR-489-3p, which decreases MEK1 in normal cells, dramatically increased MEK1 expression in cells stably expressing autotaxin. Taken together, this suggests that autotaxin overrides the normal regulatory function of miR-489-3p to inhibit MEK1 via coordinately increased miR-489-3p appearing in serum.

Introduction

Cancer is the leading cause of mortality in the United States for those between the ages of 40-79 years, surpassing heart diseases by more than 100,000 deaths (340). The

cause of most cancer subtypes remains idiopathic and may arise out of 'bad luck' among otherwise seemingly healthy individuals (341). Less than 10% of all cancers have known heritable germline alterations that contribute to increased predisposition for cancer development. For a number of other cancers, a comprehensive molecular explanation does not exist to elucidate why they spontaneously occur.

Autotaxin is a secreted ectonucleotide enzyme found in circulation and tissues throughout the body, where it metabolizes lysophosphatidyl choline to yield lysophosphatidic acid. In addition to its phospholipase functions, autotaxin is a phosphodiesterase involved in inflammation and cancer progression (145, 204, 210, 342). The most critical role of autotaxin occurs in the developing embryo, whereby autotaxin-null mice suffer embryonic lethality from defects in vasculature system formation (192, 343). Even a single point mutation within autotaxin's enzymatic catalytic site, a substitution of threonine 210 for alanine, recapitulates this lethality (194).

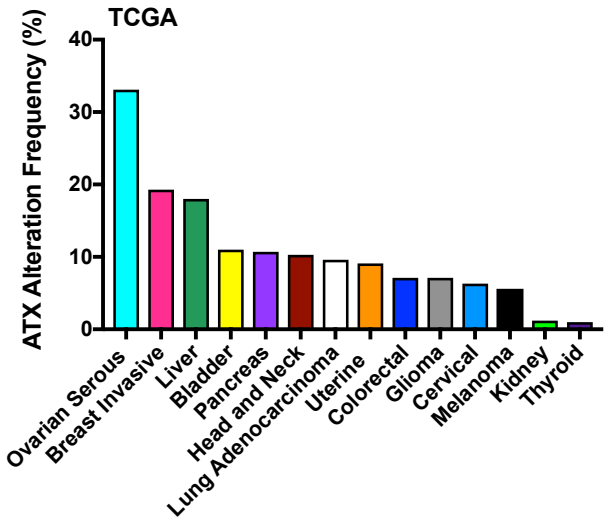

Supplementary Figure 2.1 (2.S1). Data from The Cancer Genome Atlas (TCGA) displays cancer subtypes with autotaxin amplification. Publically-available human data was mined for autotaxin amplification among cancer specimens. Serous epithelial ovarian carcinoma showed the highest percentage of alterations, at 30%, followed by invasive breast carcinoma (~19%) and hepatocellular carcinoma (~17%).

Alterations in autotaxin expression are correlated with numerous human diseases. For example, among patient specimens, autotaxin is overexpressed in renal cell carcinoma, bladder carcinoma, thyroid carcinoma and glioblastoma multiforme(196, 198, 344). The Cancer Genome Atlas reveals additional cancer types with altered levels of autotaxin (195, 345, 346) (**Fig. 2.S1**). Experimentally, the overexpression of autotaxin in mice promotes late-onset metastatic breast carcinoma, an elevation of circulating lysophosphatidic acid, bleeding diathesis, thrombosis attenuation, hepatocellular carcinoma and chronic liver disease (204, 217, 347). These observations coincide with autotaxin's regulation of the vasculature and angiogenesis (231, 348, 349).

Tumor cells release DNA, RNA, protein and microRNA (miRNA) into the circulation, suggesting the application of 'liquid' biopsies to eventually become clinically possible as more evidence about specific molecules and their interpretation are revealed (350). A recent study tested CancerSEEK, which measures a combination of circulating DNA and protein, and positively detected ~70% of eight cancer types, with 43% of stage I cancers detected (351). As the ability to accurately measure small molecules advances, the potential impact of liquid biopsies increases.

MicroRNAs are nucleotides ~22 in length that regulate mRNA, non-coding RNAs, pseudogenes and other types of transcripts through complementary binding interactions with 3′ or 5′ untranslated regions and other elements. There are approximately 3,000 defined miRNAs in the human genome, but at least 3,707 more novel ones likely exist and it is unclear how many could ultimately be discovered (352). Since miRNAs have the ability to silence transcriptional gene expression across a number of targets, this suggests a much broader role for these entities than what is currently appreciated (9). Previously,

miRNAs have shown superior biomarker ability to delineate cancer tissue classification, progression and prognostic outcomes (353, 354). In addition, miRNAs possess a high degree of stability in circulation (355), suggesting the possibility that these molecules are ideal biomarkers for liquid biopsies.

In this report, we employ a transgenic mouse model of autotaxin overexpression that formed tumors in various organs among aging (>12-month-old) female mice with low penetration, similar to what is observed in the general human population. Using this mouse model, we isolated circulating miRNAs among littermates to determine whether these animals could be distinguished based on profiles of the miRNAs detected. Indeed, we observed that miR-489-3p shows a dramatic increase in circulation in the presence of the autotaxin-induced tumors.

Materials and Methods

Animal Models

All protocols for the use of vertebrate animals were approved by the University's Institutional Animal Care and Use Committee. Transgenic mice expressing the wild-type, full length human autotaxin gene, *ENPP2*, under the control of the alpha-1 antitrypsin promoter were the kind gift of Drs. Gordon B. Mills and Susan S. Smyth and generated as previously described, on an FVB/N genetic background (217). Pups were weaned after 21 days and fed standard rodent chow and water *ad libitum* prior to aging experiments for the subsequent 18-24 months. PCR analysis was used to confirm the genotyping and expression of autotaxin from ear clips with Agilent 2100 Bioanalyzer (Agilent, Santa Clara, CA, USA) with the Forward 5′-GATCCCAGCCAGTGGACTTA-3′ and Reverse

5′-TCTGACACGACTGGAACGAG-3′ primers. Mice were palpated weekly after reaching 12 months of age to monitor spontaneous tumor formation and tumors were harvested after sacrificing the mice. Most tumors were flash-frozen in liquid nitrogen and stored in RNA*Later* Stabilization Solution (Thermo Fisher Scientific, Waltham, MA, USA) for subsequent analysis.

Histology

All tumors were stored in 10% formalin obtained for 24-48 hours immediately after removal from the mice and later transferred into 70% ethanol for another 24-48 hours. Paraffin embedding and slide sectioning was performed at the Histology Laboratory, Department of Pathology at UGA's College of Veterinary Medicine per standard protocol. Slides were cut at 4µm and stained for the following markers: Hematoxylin and Eosin, Mucicarmine, Cytokeratin AE1-3, CD-31, CD3 (T-cells), CD20 (B-cells), E-cadherin, Ki-67, HAS (hepatic tissue), Caspase 3, S-100 and MEK1. Images were taken using the Olympus BX41 microscope with Olympus DP71 high resolution digital camera (Tokyo, Japan) or the Carl Zeiss Axio Observer A1 microscope (Oberkochen, Germany) at 20x magnification.

Autotaxin enzyme-linked immunosorbent assay (ELISA)

To perform ELISA for ATX expression determination, the blood samples of mice were collected from the heart immediately following sacrifice and the serum was separated by centrifugation at 4000 rpm for 3 min. ATX concentration in the serum was

measured using an ATX sandwich ELISA kit (Echelon Biosciences, Salt Lake City, UT, USA) as per the manufacturer's instructions. Each sample was measured in duplicate.

Serum profiling for miRNA

Blood samples collected from mice were centrifuged at 4000 rpm for 3 min, followed by collection of serum, which was stored at -80˚C. Three wild-type FVB/N female mice, seven female AT-ATX non-tumor mice and seven female AT-ATX tumor mice were randomly selected for serum miRNA profiling. Exiqon's RNA Isolation Kit for Biofluids (Woburn, MA) was used for 50µL of serum RNA as per the rodent protocol provided by the company. An RNA Spike-In Mix also obtained from Exiqon was added for quality control of samples at the RNA extraction stage. All samples were eluted in 50µL of RNase-free dH_2O. The cDNA synthesis for the extracted RNA was carried out as per protocol of the Exiqon Universal cDNA Synthesis Kit II, along with a cDNA Spike-in Mix provided in the kit. The cDNA was stored at -20˚C before the serum profiling was performed. Data was obtained from loading Exiqon Ready-to-use Serum microRNA PCR Panels I and II V4.M plates with pre-loaded miRNA primers in each of the 384-wells and performing qPCR analysis using Applied Biosystems ABI7900HT machine (Foster City, CA).

There were a total of 752 miRNAs on the Exiqon panels, and other wells contained spike-in primers and inter-plate calibration primers. The PCR reaction was set up using 2mL of Exiqon ExiLENT SYBR Green Master Mix, 1.896mL nuclease-free H_2O provided in the kit, ROX passive reference dye (400nM) and 40µL of cDNA. Master mix was loaded into each 384-well plate at 10µL per well. All solutions and the qPCR plate

were kept on ice and away from excess bright light while preparing and loading. The plate was centrifuged at 4˚C and 1500rpm for 1 min. The qRT-PCR was performed as per the following protocol: one cycle of 2:00 minutes at 50˚C and 10:00 minutes at 95˚C; 40 cycles of 0:15 minutes at 95˚C and 1:00 minute at 60˚C; 1 cycle (melt curve analysis) of 0:15 minutes at 95˚C, 0:15 minutes at 60˚C, and 0:15 minutes at 95˚C.

miRNome data analysis

Preliminary data analysis was carried out using Exiqon GenEx qPCR Analysis Software. Raw data files were loaded into GenEx along with the plate layouts for Panel I and II obtained from the Exiqon website under "Resources". First, both Panel I and II were calibrated as per the expression of the interplate calibrator present on both plates for each sample. Samples were grouped and named corresponding to the genotype of each transgenic mouse. Expression of RNA and cDNA spike-ins, as well as U6 was checked using the appropriate commands on the software to eliminate any samples with inconsistent spike-in expression. The software was also used to detect outliers (none were discovered), and remove miRNAs with a low call rate (greater than 50% missing data or undetermined values) to accurately establish significance. All data was normalized to miR-16-5p, a miRNA widely regarded as an endogenous control. Normalization, relative quantification to the Wildtype group and conversion to Log2 values were subsequently performed in the same software. miRNAs were filtered to include only significant (p-value <0.05) candidates that also shared greater than 85% homology to human miRNAs through miRViewer, a multispecies miRNA homology database. GraphPad Prism 7 (La Jolla, CA) was utilized to create a volcano plot comparing Wild-type and AT-ATX Non-

tumor as well as AT-ATX Non-tumor and AT-ATX Tumor serum samples using the Log2 values previously created in GenEx. Fold change in expression and box plot graphs were generated with significant miRNAs between groups.

Hierarchical clustering

Hierarchical clustering analysis was performed as previously described (356). Using Cluster, the genes were mean centered prior to clustering both genes and arrays. The data was then automatically processed by Cluster, which created average linkages between the genes and arrays (357). To visualize the resulting hierarchical clustering Graphs, TreeView was also used.

Generation of autotaxin stable cell lines

Functional ATX with enzymatic activity and mutant pSecTag vectors expressing human ATX (pSecTag-hATX) or enzymatically inactive mutant ATX (pSecTag-hATX(T210A)) were purchased from Addgene (Cambridge, MA). OVCAR-3 cells were plated in a 24-well plate at a density of 2×10^4 cells per well and grown overnight in a humidified atmosphere of 5% CO_2, followed by transfection with 0.75 μg pSecTag-hATX or pSecTag-hATX(T210A) in each well using Lipofectamine 2000 (Invitrogen, Thermo Fisher Scientific, Waltham, MA, USA). The stable transfectants of OVCAR-3 cells were prepared with selection in 500 μg/ml of zeocin (Invitrogen, Thermo Fisher Scientific). The expression of ATX was determined with qRT-PCR using two sets of primers, ATX-222: 5'-TCGCTGTGACAACTTGTGTAAG -3' (forward) and 5'-CCAATGCGACTCTC CTTTGC-3' (reverse); and ATX-583: 5'-

TGTGGCACACACTCTCCCTA -3' (forward) and 5'-TCGCCCTCGCAGATGAAAAG-3' (reverse).

miRNA extractions

Total RNA was extracted from tissue or cells using Trizol reagent (Invitrogen, Thermo Fisher Scientific) followed by reverse transcription for cDNA synthesis from mRNA or miRNA using iScript™ cDNA Synthesis Kit (Bio-Rad, Hercules, CA, USA) and TaqMan® MicroRNA Reverse Transcription Kit (Thermo Fisher Scientific), respectively. The miRNA levels were determined with TaqMan® primers (Integrated DNA Technologies, Coralville, IA, USA) as indicated by quantitative real-time PCR using TaqMan® Fast Universal PCR Master Mix (Thermo Fisher Scientific). All qPCR reactions were run using the Applied Biosystems ABI7900HT PCR machine.

Protein extraction and SDS-PAGE electrophoresis

Approximately 40mg of tissue sample was obtained from each tumor tissue sample or organ sample for protein extraction. In vitro samples were set up in a 6-well format and all cells were used from the well for protein extraction. Tissues were washed with 1x PBS twice and shaken on ice with occasional vortexing with RIPA Lysis and Extraction Buffer containing Protease/Phosphatase Inhibitor Cocktail (100x) (Thermo Fisher Scientific), and supernatant was collected after centrifuging. Samples were boiled with 6x Laemelli sample buffer at 95ºC for 5-10 minutes prior to loading on an SDS-PAGE gel. The BioRad SDS-PAGE System and protocol were used to probe for ERK1/2, phospho-ERK1/2, MEK1, phospho-MEK1 and GAPDH antibodies at 1:1000 dilution

overnight and HRP-conjugated anti-rabbit secondary antibodies at 1:10000 dilutions (BioRad). Flourchem Imager System (Protein Simple, San Jose, CA, USA) was used to detect bands on the PVDF membrane and band quantification was performed using the ImageJ Software (National Institutes of Health, Rockville, MD, USA).

Treatment with miR-489-3p mimic and PARP inhibitors

OVCAR-3, ATXwt and ATXmut cell lines were plated in a 6-well format at 300,000 cells per well. The following day, each cell line was treated with Dharmafect control or 50nM of miR-489-mimic (Dharmacon, Lafayette, CA, USA). The transfection was allowed to proceed for approximately 48-60 hours and protein or RNA was extracted from wells as previously described. OVCAR-3 cells were plated 5000 cells/well in a 96-well format and treated with 50nM of miR-489-3p mimic, and 25µM or 50µM of Olaparib or Niraparib, the following day (SelleckChem, Houston, TX, USA). The combination treatment was allowed to proceed for an additional 24 hours before addition of Cell Titer Blue Cell Viability Assay (Promega, Madison, WI, USA) for 3 hours before using SpectraMax M2 Plate Reader (Molecular Devices, Sunnyvale, CA, USA) to detect florescence as a measurement of cell viability.

Statistics

All data was subject to statistical analyses with a standard confidence interval of 95% with all p-values under 0.05 considered to be indicative of a significant result, specifically $*p < 0.05$, $**p < 0.01$ and $***p < 0.001$ indicate the level. The data was evaluated through comparison of the means of three or more groups using an analysis of

variance (ANOVA) and then subsequent post tests to determine the significance using Bonferroni's Multiple Comparison. If there were comparisons between two groups, the Student's t-test was used. Both GraphPad Prism and Microsoft Excel were used to perform these calculations.

Results

To assess whether circulating miRNA could distinguish between inbred littermates that developed tumors, as a result of autotaxin expression, from those that did not develop tumors, heterozygous mice with autotaxin under the control of the alpha-1 antitrypsin promoter primarily expressed in liver were utilized. These "AT-ATX" transgenic mice were developed on an FVB/N background and females were aged to determine whether spontaneous tumors would form (217, 358). The heterozygous autotaxin genotype was used because homozygous autotaxin overexpression and/or homozygous knockout leads to embryonic lethality from defects in the vasculature system (192, 343, 359). Importantly, tumors developed in 21% of transgenic mice, but not in wild-type FVB/N females (**Fig. 2.1A**). The earliest appearance of tumors occurred at 12 months and the latest at 24 months, with an average onset at 18 months (**Fig. 2.1B**). This would be roughly equivalent to cancer presenting in a patient between 60 – 70 years of age. In transgenic animals, autotaxin expression was relatively increased in serum (*$p<0.05$, **Fig. 2.1C**). Tumors appeared in disparate regions, including the mammary glands, chest cavity, liver, abdomen, uterus and head (**Fig. 2.1D**). Although many tumors could be classified, approximately 20% were unclassified and considered cancers of unknown primary origin. Histology was unable to determine the characteristics indicative

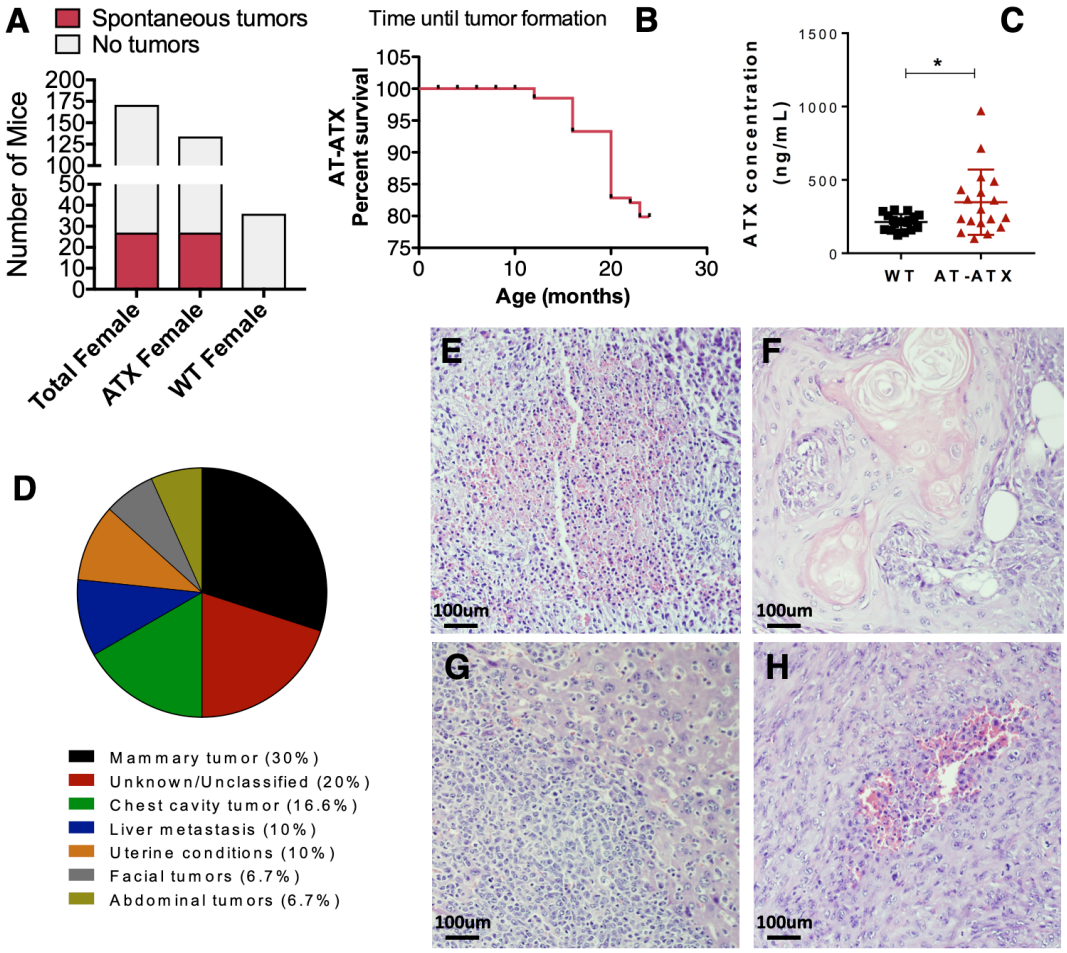

Figure 2.1. Autotaxin generates cancer formation in female mice. (A) One hundred and sixty-four female mice were genotyped, which yielded 128 AT-ATX transgenic females, 27 of which developed tumors. None of the 36 wild-type (WT) females had identifiable lesions. (B) Tumors first appeared at 12 months and the incidences peaked between 18- 20 months, with ~21% of transgenic mice displaying identifiable tumors overall. (C) Serum from wild-type and transgenic animals was measured for the concentration (ng/mL) of autotaxin (*$p<0.05$). (D) Tumors were categorized based on their primary origin and pathological findings. (E) Immunohistochemistry shows a mouse with an unclassified tumor with signs of diffuse carcinoma and necrosis in the center. The large nuclei are indicative of malignant cells, however, histological analysis was unable to pinpoint the origin of the neoplasm. (F) Immunohistochemistry from a mouse with a fluid-filled uterine horn, the histology of which shows evidence of infiltrating squamous cell carcinoma of epithelial origin with spread into the surrounding adipose tissue. (G) Liver histology from a mouse with a tumor in the chest cavity shows metastatic spread in the liver, as evidenced by malignant cells. Surrounding lightly-colored cells may be non-malignant hepatocytes reacting to an inflammatory response. (H) Tumor histology of a mouse with a mammary tumor shows spindle cell carcinoma with a region of necrosis in the center, with spread into the surrounding adipose and muscle fibers, and therefore is considered to be aggressive.

of a tissue of origin in these cases, although typical pathological features of central necrosis, large nuclei and diffuse carcinoma confirmed malignancy (**Fig. 2.1E-H**).

The earliest appearance of tumors occurred at 12 months and the latest at 24 months, with an average onset at 18 months (**Fig. 2.1B**). This would be roughly equivalent to cancer presenting in a patient between 60 – 70 years of age. In transgenic animals, autotaxin expression was relatively increased in serum (*p<0.05, **Fig. 2.1C**). Tumors appeared in disparate regions, including the mammary glands, chest cavity, liver, abdomen, uterus and head (**Fig. 2.1D**). Although many tumors could be classified, approximately 20% were unclassified and considered cancers of unknown primary origin. Histological analysis was unable to determine the characteristics indicative of a tissue of origin in these cases, although typical pathological features of central necrosis, large nuclei and diffuse carcinoma confirmed malignancy (**Fig. 2.1E-H**).

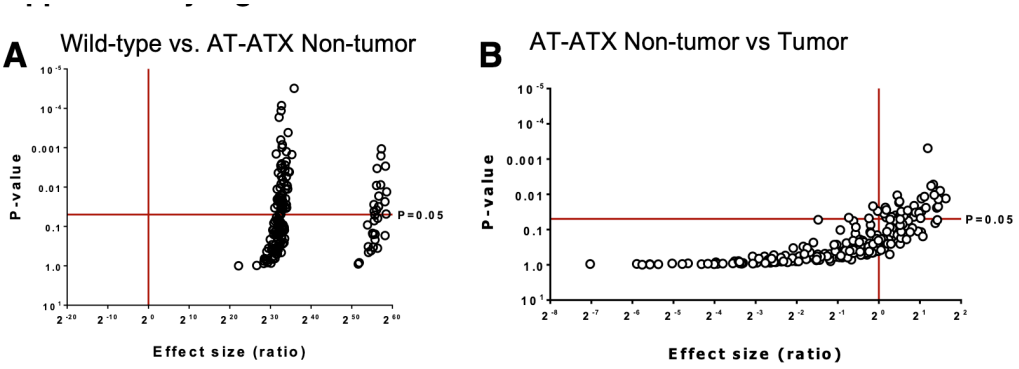

Supplementary Figure 2 (2.S2). Volcano plot showing the p-values of miRNAs detected in the serum. The endogenous control, miR-16-5p, was used to normalize raw miRNA values using GenEx Software. Normalized tumor miRNA values were then made relative to non-tumor mice and converted to Log2 values. A) Shows the difference between Wild-type and AT-ATX Non-tumor mice whereas B) shows the difference between AT-ATX non-tumor and AT-ATX tumor samples. GraphPad Prism 7 and Log2 values were used to create the volcano plot, which provided the p-values and effect size of the data. Confidence intervals were set to 95% and all miRNAs with a significant change in expression (p<0.05) were selected for further analysis.

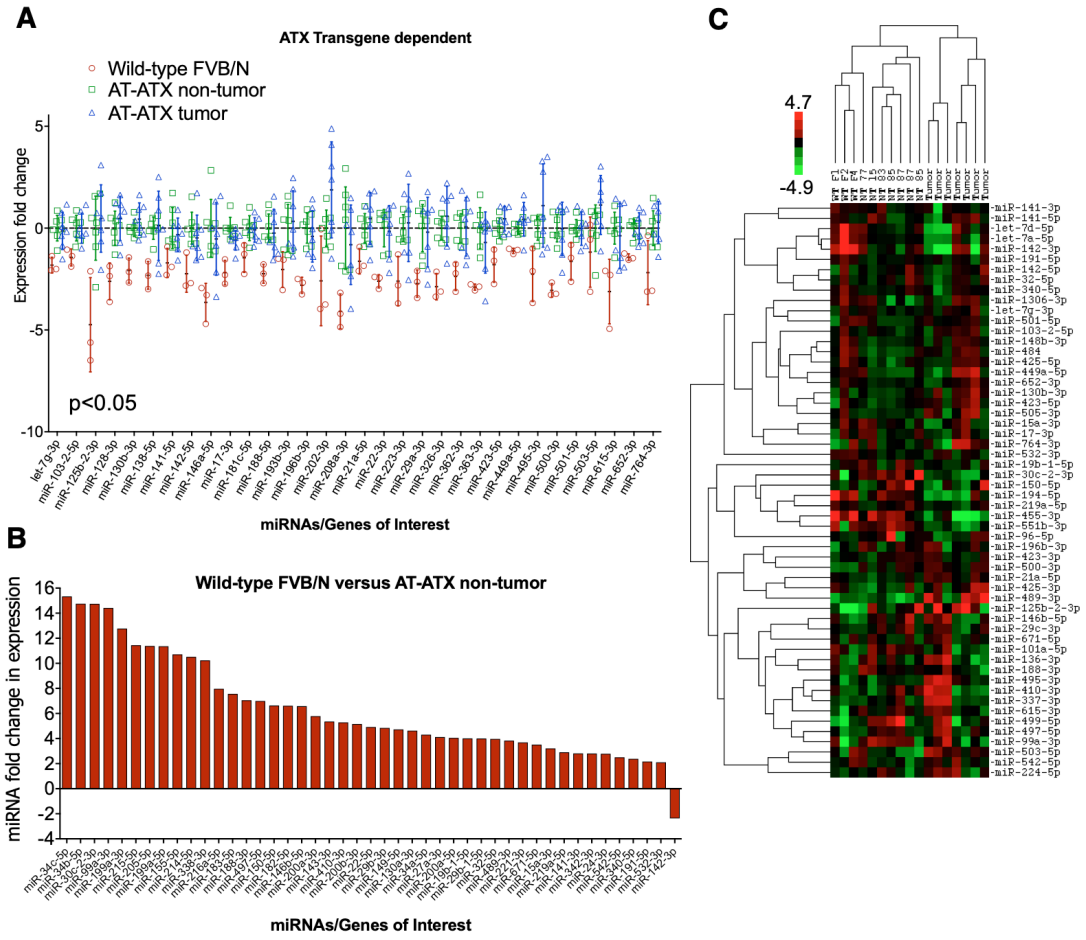

Figure 2.2. The autotaxin-mediated miRNome signature differentiates between wild-type, AT-ATX tumor and AT-ATX non-tumor mice based on miRNA changes. Seven serum samples from tumor and seven from non-tumor-bearing AT-ATX transgenic mice as well as three serum samples from wildtype mice were randomly selected for analysis. The circulating exosomes and their miRNA cargo were isolated prior to measuring the miRNA and identifying the molecular signature. (A) Log2 values of the changes in serum miRNA between wildtype, AT-ATX tumor and AT-ATX non-tumor mice display a subset of miRNAs that are increased due to transgene presence alone. (B) The average raw fold change for significant serum miRNAs from wild-type versus AT-ATX non-tumor mice are displayed. All miRNAs with >2-fold change and had cancer-related targets in a Pubmed and DIANA TarBase database for target prediction were included. Data was generated in the GenEx software and used to create graphs in GraphPad Prism 7. Only data that was significant (*p < 0.05) was used. (C) Unsupervised hierarchical clustering was performed on the logarithmic data collected from the microarray. Average linkages resulted in a dendogram that classified the wild-type, AT-ATX non-tumor and AT-ATX tumor mice into their respective groups.

Biofluids were collected at necropsy and RNA was isolated for serum microRNA PCR panels that probe the expression of 752 miRNAs in circulation (see **Methods**). GenEx qPCR Analysis Software (Exiqon/Qiagen) calculated the p-value significance of the data between groups versus the ratio of the effect size (**Fig. 2.S2**). Intriguingly, the autotaxin-mediated miRNome signature distinguished between wild-type FVB/N, AT-ATX tumor-bearing and AT-ATX non-tumor-bearing mice. Significant ($p<0.05$) increases in miRNA correlated with an autotaxin-mediated signature and clearly identified wild-type mice, but not *necessarily* the presence or absence of tumors in AT-ATX mice (**Fig. 2.2A**). Fold changes in miRNA expression comparing circulating miRNA in wild-type versus AT-ATX mice without tumors, further supported this observation, with increases up to 15-fold (**Fig. 2.2B)**. Overall, patterns of circulating miRNA differentiated mice based on genotype status after hierarchical clustering algorithms computationally organized related groups with a miRNA signature (**Fig. 2.2C)**.

. Analysis of the autotaxin-mediated miRNome signature through the DIANA TarBase database classified the miRNAs into various groups of oncogenic processes and signaling pathways. Autotaxin-dependent miRNAs show significant involvement in nearly all categories (**Table I**). This suggests an impact of autotaxin on miRNA expression and its 'high-risk' influence on neoplastic disease. Subsequent aberrant miRNA regulation in signaling is a likely mechanism required for progression to a disease state, with the involvement of MAPK and other pathways. Comparing AT-ATX tumor-bearing versus non-tumor-bearing mice, miR-489-3p showed a significant ($p<0.05$) and consistent increase with autotaxin expression and subsequent tumor presence (**Fig. 2.3A**).

Table I. Signature analysis of the serum miRNome shows significant correlation of classified miRNAs with diverse processes involved in oncogenic signaling. miRNAs (*p<0.05) were categorized into relevant pathways using DIANA Tools miRPath v.3 database with target prediction based on sequence alignment. The involvement of at least one miRNA in a given pathway, process or cancer type was marked in red.

	High-risk individuals	Disease progression
Oncogenic processes		
Cell cycle		
Inositol phosphate metabolism		
N-Glycan biosynthesis		
Pathways in cancer		
Protein processing in the ER		
Proteoglycans in cancer		
RNA transport		
Transcriptional dysregulation in cancer		
Oncogenic signaling pathways		
ErbB signaling pathway		
Estrogen signaling pathway		
FoxO signaling pathway		
HIF-1 signaling pathway		
Hippo signaling pathway		
MAPK signaling pathway		
mTOR signaling pathway		
Phosphatidylinositol signaling system		
PI3K-Akt signaling pathway		
Ras signaling pathway		
TGF-beta signaling pathway		
Malignant Neoplasms		
Colorectal cancer		
Endometrial cancer		
Melanoma		
Non-small cell lung cancer		
Pancreatic cancer		
Renal cell carcinoma		
Small cell lung cancer		
Thyroid cancer		

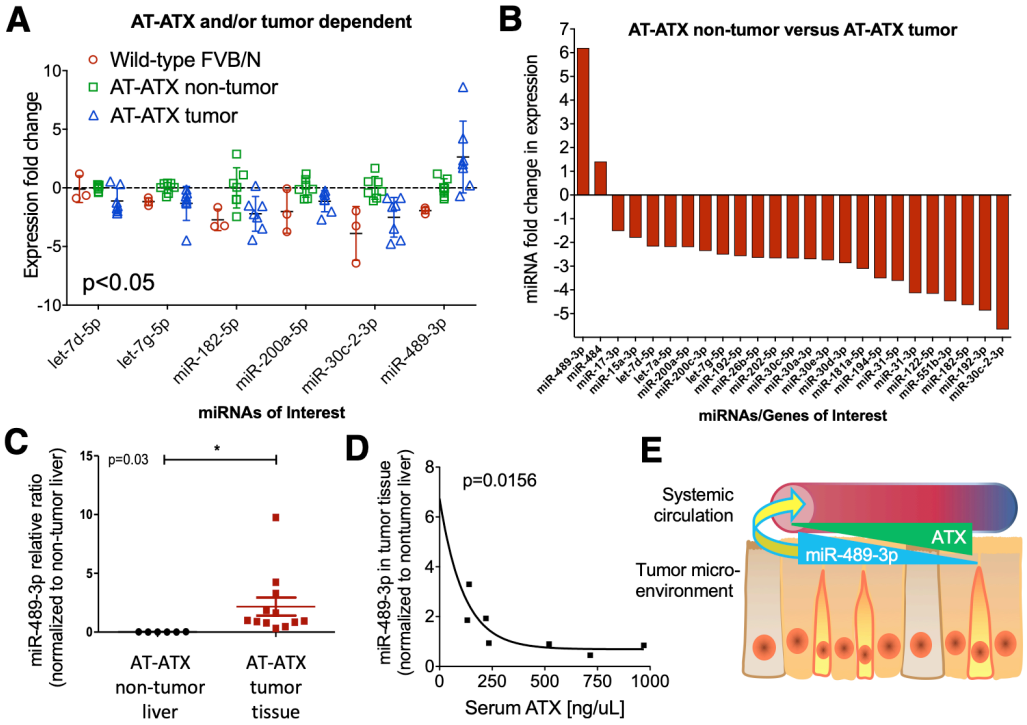

Figure 2.3. MiR-489-3p is significantly increased in the circulation of AT-ATX animals with tumors. (A) Log2 values of the changes in serum miRNA between the three groups previously stated depict that certain miRNAs change based on transgene presence in AT-ATX non-tumor mice, and also upon tumor development in AT-ATX tumor mice. All data was generated in the GenEx software and used to create a scatterplot of the data in GraphPad Prism 7. Only data that was significant (*p < 0.05) was used in this graph. (B) The average miRNA raw fold change for significant values between serum from tumor versus non-tumor transgenic mice were automatically generated by GenEx Software. MiR-489-3p shows the greatest fold increase in expression at 6.2-fold (p=0.047) and miR-30c-2-3p has the greatest decrease in expression at 5.6-fold (p=0.005). (C) AT-ATX non-tumor livers and AT-ATX tumor tissue was assessed for miR-489-3p levels by qRT-PCR. Results show that miR-489-3p has comparatively higher expression in tumor tissue and the associated microenvironment, supporting its increased appearance and export in AT-ATX tumor mice. Student's t-test was conducted to determine statistical significance with a p-value of 0.03. (D) Serum autotaxin was plotted on the x-axis relative to miR-489-3p expression in tumor tissue and a curve was generated by a nonlinear fit model and determined to be significant (p=0.0156) by an exact Wilcoxon Signed Rank test. (E) Working model showing that as autotaxin increases in serum, miR-489-3p in the local tumor tissue and surrounding milieu decreases, with a coordinated allocation appearing in the serum.

The logarithmic scale differentiations were largely due to dramatic decreases in miRNA expression detected, with few exceptions, like miR-489-3p and miR-484 (**Fig.**

2.3B). Many significant miRNAs were decreased between AT-ATX tumor and non-tumor mice, with miR-30c-2-3p (p-value=0.005) displaying the largest decrease, along with miR-192-3p (p-value=0.0005) and miR-182-5p (p-value=0.023). Interestingly, miR-489-3p shows an almost 4-fold increase in expression between the wild-type and non-tumor groups, and a further 6-fold increase with the presence of a tumor

Among AT-ATX mice that developed tumors, their pulverized tissues displayed generally more miR-489-3p than non-tumor AT-ATX mice (**Fig. 2.3C**, p=0.03). Intriguingly, there was a correlation between the concentration of serum autotaxin with miR-489-3p expression in the tumor tissue and associated milieu (**Fig. 2.3D**, p=0.0156). This suggests that with enhanced serum autotaxin concentration there is a coordinated displacement of miR-489-3p from cells to the milieu and serum (**Fig. 2.3E**). There was no relationship between the observed, primary, solid tumor volume with autotaxin concentration (data not shown).

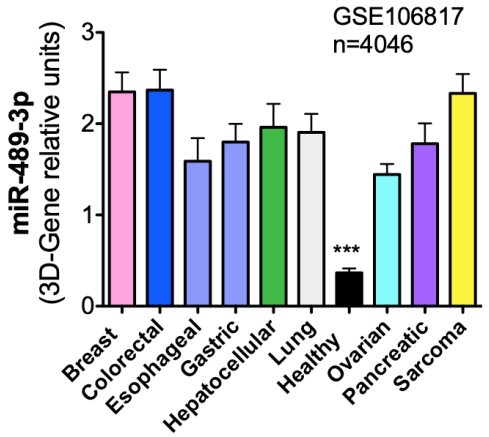

Supplementary Figure 3 (2.S3). Serum miR-489-3p is significantly increased among human cancers. The human dataset GSE106817 (n=4046) was downloaded from the NCBI's Gene Expression Omnibus and mined for miRNA. The raw data (3D-Gene units) is presented as an average number in bar graphs organized by cancer type and colored accordingly. Healthy, non-cancer individuals (black bar; n=2759) show comparatively low expression (***p<0.001) of miR-489-3p.

To determine whether changing miR-489-3p in mouse circulation has relevancy to human disease, we assessed human data. GSE106817 from Yokoi A. and colleagues contains over four-thousand serum samples from healthy, non-cancer controls (n=2759) and patients with various cancers from nine major types (n=1,287). Circulating miR-489-3p was significantly increased among all cancer types (**Fig. 2.S3**, ***p<0.001).

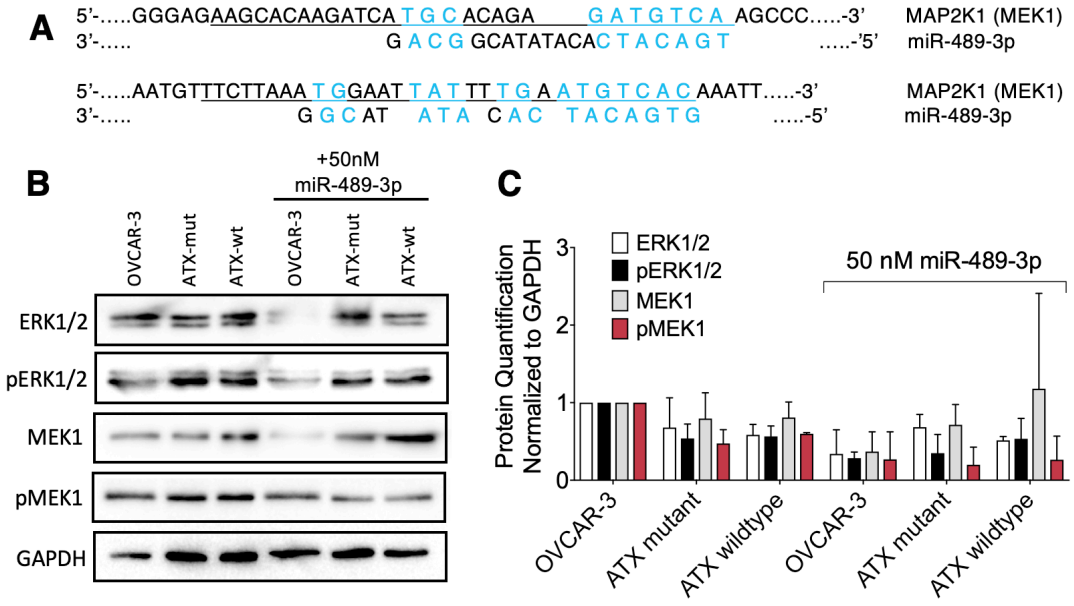

Figure 2.4. MiR-489-3p increased in AT-ATX tumors regulates MEK1 expression. (A) Database analysis through DIANA TarBase miRPath v.3 shows sequence alignment between MAP2K1 and miR-489-3p at two locations of the MAP2K1 sequence, the gene product of oncogene MEK1. Both sequences are in the 3'-UTR region of the MAP2K1 gene and considered to have strong miRNA binding at 10-14 base pair complementarity. (B) Transfecting OVCAR-3 parental cells with 50 nM of miR-489-3p for 48 h shows a marked reduction in protein levels of MEK1 and phosphorylated MEK1 (pMEK1), as well as the downstream target ERK1/2 and phosphorylated ERK1/2 (pERK1/2). In contrast, among the ATX-wt (wild-type, overexpressing) cells, and to a lesser extent ATX-mut (mutation) cells, MEK1 is increased with miR-489-3p treatment. (C) Combined immunoblotting results are plotted as a bar graph to reflect the band quantification, normalized to GAPDH.

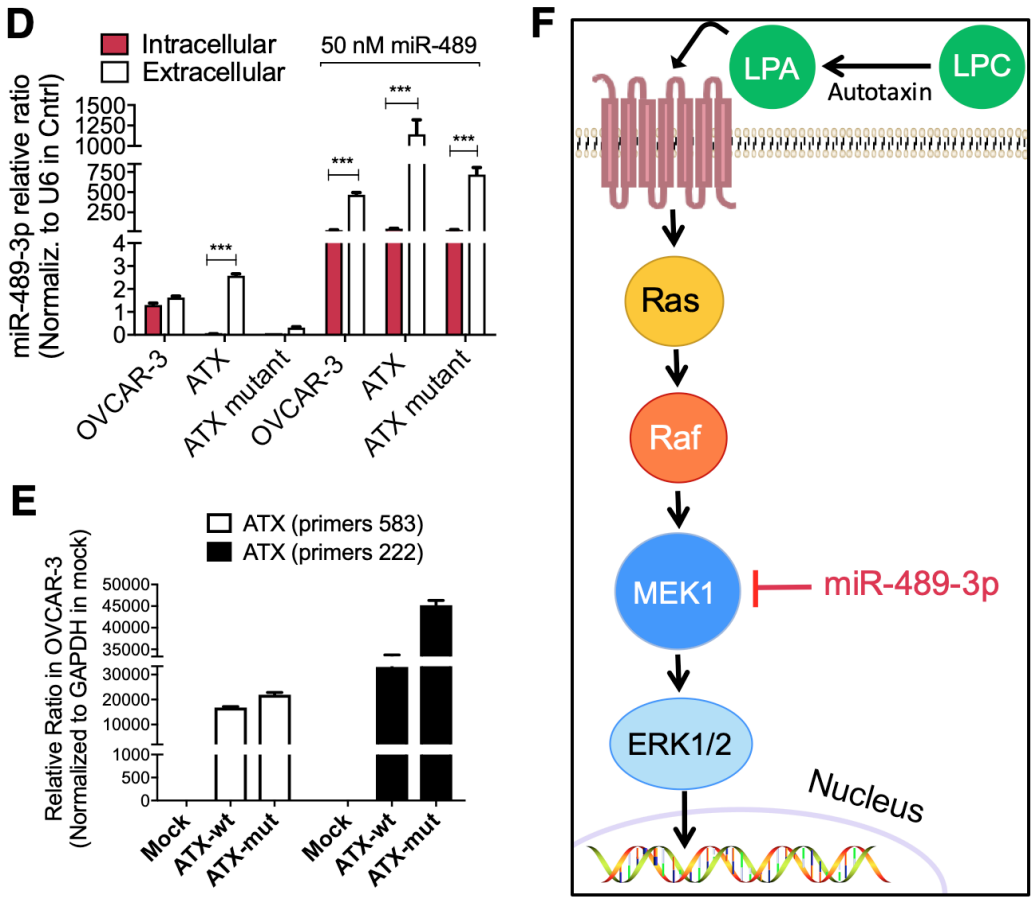

Figure 2.4. MiR-489-3p increased in AT-ATX tumors regulates MEK1 expression. (D) Expression of miR-489-3p in the ATX-wt cells shows a significant increase in exosomes versus intracellular pools by qRT-PCR, even when the mimic is exogenously introduced. (E) Stable expression of wild-type (wt) and mutant (mut) autotaxin (ATX) in OVCAR-3 cells. Two independent sets of primers were used, (583 and 222), to validate expression. Mock was normalized to 1.0, but the value is not visible due to the large y-axes. (F) The working model shows autotaxin-dependent production of lysophosphatidic acid (LPA) results in MAPK pathway activation. Though miR-489-3p inhibits MEK1, enhanced autotaxin expression overrides this effect and may suggest an active feedback loop.

Further analysis sought to understand the mechanism associated with the autotaxin-mediated increase of miR-489-3p in circulation. Based upon sequence complementarity, DIANA TarBase predicted miR-489-3p targets MAPK2K1, or MEK1, an oncogene widely dysregulated in cancer (**Fig 2.4A**). To test this relationship, exogenous addition of

a miR-489-3p mimic to parental OVCAR-3 resulted in a marked reduction in total MEK1, ERK1/2, pMEK1 and pERK1/2 (**Fig. 2.4B, C**).

Although OVCAR-3-ATX-wt and OVCAR-3-ATX-mut cell lines displayed decreases in pMEK1, a notable increase in total MEK1 was observed when OVCAR-3-ATX-wt cells were treated with miR-489-3p with limited changes to ERK1/2 or pERK1/2. We further confirmed that miR-489-3p is secreted from cells *in vitro* (**Fig. 2.4D, E**). Taken together, these data confirm the prediction of TarBase in that miR-489-3p targets MEK1 (**Fig. 2.4F**) and also that upregulated autotaxin overrides the function of miR-489-3p and increases MEK1.

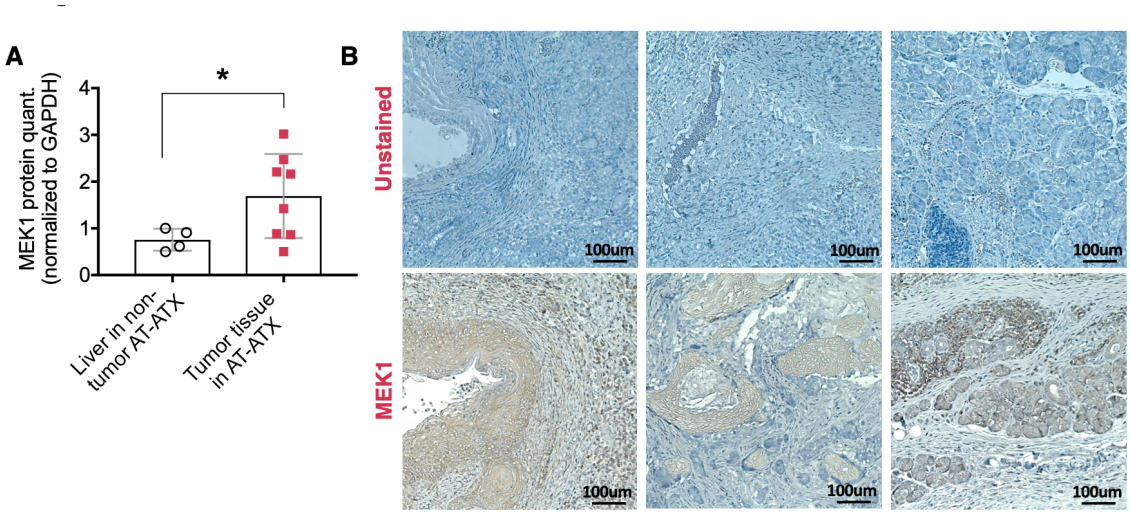

Figure 2.5. MEK1 is enhanced in tumor tissue of AT-ATX mice. Tissue specimens collected at necropsy were pulverized for protein extraction and analyzed by SDS-PAGE analysis for MEK1 or paraffin-embedded and sectioned for immunohistochemistry. (A) Tumor tissues contain significantly (*$p<0.05$) higher levels of MEK1 compared to liver tissues of AT-ATX nontumor female mice. (B) Immunohistochemical staining using MEK1 antibody confirmed expression in tumor tissue compared to unstained sections of corresponding tissue samples.

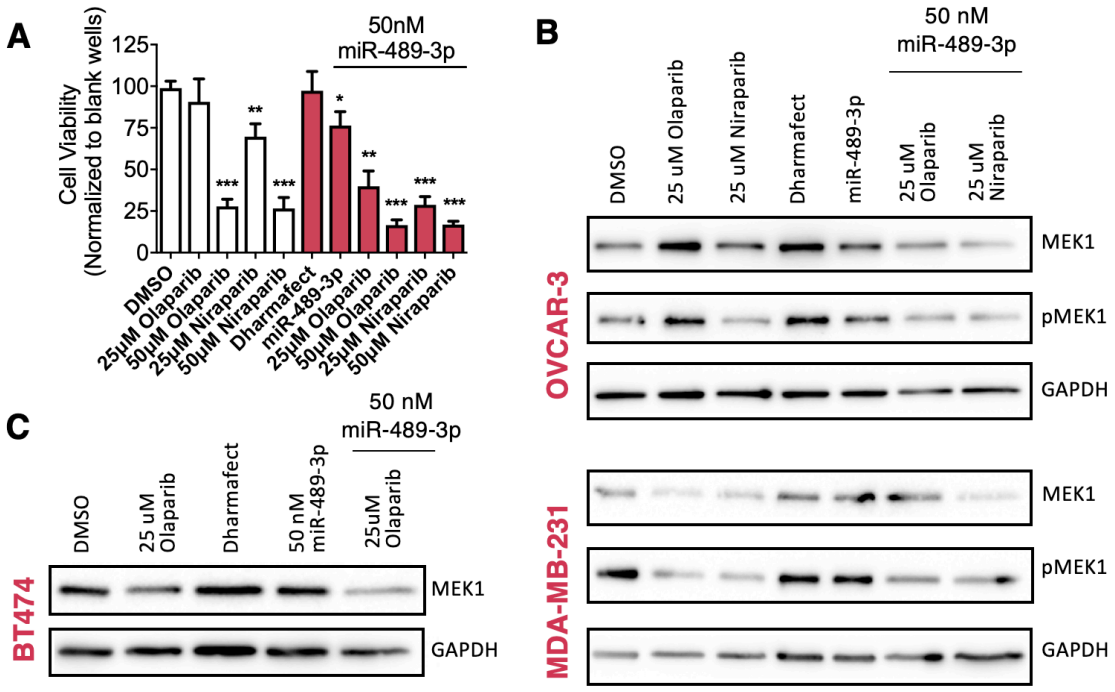

Figure 2.6. Co-treatment of miR-489-3p with either PARP inhibitor, olaparib or niraparib, reduces the viability of OVCAR-3 and MDA-MB-231 cells and augments inhibition of MEK1. (A) OVCAR-3 cells were transfected with 50 M miR-489-3p for 24 hours before additional treatment with olaparib and niraparib, at 25 M or 50 M per well in a 96-well format for 48 h. Results show that while olaparib or niraparib alone have a dose dependent effect on viability, they have an additive effect when combined with miR-489-3p. *p<0.05, **p<0.01 or ***p<0.001 vs. DMSO. (B) Co-treatment of miR-489-3p with olaparib or niraparib followed by SDS-PAGE analysis to detect MEK1 expression shows that MEK1 and pMEK1 are reduced with 25 M olaparib or niraparib treatment alone. Since miR-489-3p targets MEK1, this phenomenon is amplified in co-treatment conditions for both PARP inhibitors in OVCAR-3 and MDA-MB-231. (C) However, BT474 breast cancer cells, which are HER2-positive, ER/PR-negative, only show a marked decreased in MEK1 with co-treatment of miR-489-3p and Olaparib, with the miRNA or Olaparib alone having negligible effects on MEK1 expression.

To verify that MEK1 was increased in tumor tissue as a result of miR-489-3p export, we assessed the protein levels in specimens. Comparing tumor tissue to liver tissue of non-tumor AT-ATX animals, there was a significant increase in MEK1 (*p<0.05) in the tumors (**Fig. 2.5A**). Further, immunohistochemistry data confirms

MEK1 expression in tumor tissues compared to corresponding unstained sections **(Fig. 2.5B)**. Localization of MEK1 staining to certain regions of the tissue may be attributable to the exportation of miR-489-3p from the tumors into circulation, resulting in the lack of MEK1 inhibition in those areas.

We next determined the effects of miR-489-3p on the activity of an emerging class of inhibitors in ovarian cancer. OVCAR-3 cells transiently transfected with 50nM miR-489-3p followed by 48 hours of treatment with the PARP inhibitors Olaparib and Niraparib at 25μM and 50μM resulted in a significant decrease in cell viability, particularly in the presence of miR-489-3p, either alone or in combination with either PARP inhibitor (**Fig. 2.6A**). This indicates that miR-489-3p may have an additive affect with Olaparib or Niraparib to further reduce cell viability. SDS-PAGE analysis displays a similar effect of miR-489-3p and PARP inhibitors at the protein level on the inhibition of MEK1 in OVCAR-3 (**Fig 2.6B**). Since Olaparib is FDA-approved for use in triple-negative breast cancer, MDA-MB-231 cells were also subjected to miR-489-3p and PARP inhibitor co-treatment, resulting in a marked decrease in MEK1 expression (**Fig. 2.6B**). However, in HER2-positive, ER/PR-negative BT474 breast cancer cells, miR-489-3p had negligible effects on MEK1 alone, but synergized together with Olaparib to inhibit MEK1 (**Fig. 2.6C**). Niraparib treatment on BT474 cells was highly toxic and therefore excluded from analysis (data not shown).

Discussion

Herein, an autotaxin mouse model illuminated unknown molecular mechanisms to explain how autotaxin influences malignant potential. Indeed, the results suggest that

there are significant changes in serum miRNA expression between wild-type and non-tumor transgenic mice, as well as tumor-bearing and non-tumor-bearing transgenic mice. Our data shows that one miRNA, miR-489-3p, consistently increases in expression with the presence of autotaxin and increases further with subsequent tumor appearance.

MiR-489-3p has been shown to target several oncogenes and largely appears to have a tumor suppressive role across various cancer types. For example, studies in pancreatic cancer show a repression of miR-489-3p expression driven by KRAS and inflammatory NF-kB signaling (360). Similarly, miR-489-3p has been found to be significantly decreased in hepatocellular carcinoma patients with late recurrence compared to early recurrence, suggesting its role in tumor suppression and possibly, progression free survival (358).

Our data shows that exogenous miR-489-3p addition inhibits MEK1, which is a target for miR-489-3p predicted by DIANA TarBase miRPath v.3. Interestingly, a substantial increase in MEK1 among OVCAR-3-ATX-wt cells treated with miR-489-3p (**Fig. 2.4B, 2.4C**) indicates the likely presence of an override mechanism or feedback loop triggered by autotaxin. Indeed, autotaxin reverses the effects of miR-489-3p from inhibiting MEK levels to increasing MEK levels. Other studies have demonstrated that a feedback loop encompassing HER2, SHP2 and MAPK is inhibited by miR-489-3p to control breast cancer cell proliferation, further lending significance to the role of miR-489-3p in our results (359).

Additionally, in a previous transgenic model with autotaxin under the control of the MMTV-LTR promoter, aberrant expression of human autotaxin caused late-onset, metastatic breast cancer (204). The AT-ATX transgenic model is analogous to the

previous one because ~ 30% of all spontaneous tumors appeared in the mammary glands of mice. Overall, approximately 21% of transgenic animals developed tumors. Although this is a smaller percentage than we predicted, it is comparable to the percentage of patients presenting with HER2-positive breast cancer, which tends to be more aggressive than ER-positive disease. It also correlates with the data we retrieved from The Cancer Genome Atlas showing that ~19% of invasive breast cancers have an autotaxin alteration (345, 346).

Autotaxin has a well-known role in mediating tumorigenesis (361, 362). The autotaxin-mediated miRNome signature derived from our model shows upregulation of miR-34c-5p, miR-34b-5p, and miR-30c-2-3p. The former two miRNAs have been found to play protective roles for cancer cells in lung cancer and thyroid carcinoma, respectively. This lends importance to their overexpression in the presence of elevated autotaxin as a precursor to tumorigenesis here (363, 364).

Limitations of this study arose while delineating the miRNA signature and conducting homology verification to segregate clinically relevant human miRNAs. Among the 126 miRNAs verified, several miRNAs showed significant and interesting trends, but did not have strong homology to corresponding human miRNA. For example, miR-2137 had a similar sequential increase in expression similar to miR-489-3p, however, it is not present in humans and therefore clinically irrelevant. Other miRNAs did not appear in the DIANA TarBase database as having any potential targets based on sequence alignment. Thus, we can interpret the *known* components appearing in our serum miRNome, but are technically limited and unable to interpret 100% of the information, due to currently nonexistent scientific knowledge.

Intriguingly, all detected mouse tumors arose between the ages of 12-24 months. The average age of tumor identification or "diagnosis" was 18 months. Converting this mouse age, 18 months, into human age, 60-70 years, coincides with the median age of breast cancer diagnosis among U.S. women, > 60 years. Taken together with the Cancer Genome Atlas correlation of autotaxin alteration and the percentage of tumors which developed, this suggests the AT-ATX transgenic model is a suitable prototype of aggressive female cancer.

Overall, our study suggests that autotaxin and autotaxin-induced neoplasms influence miR-489-3p function in tumor cells as well as secretion into circulation. It further suggests that even though miR-489-3p appears to have a tumor suppressive role inhibiting MEK1 in normal cells and in some tumor lineages, autotaxin triggers a mechanism to override this inhibition of MEK1 by miR-489-3p. Due to the increase of miR-489-3p in serum resultant from autotaxin overexpression and further with subsequent tumor development, it could be clinically relevant for a liquid biopsy. Further, its ability to inhibit translation of the key oncogene MAP2K1 coding for MEK1 protein further enhances its clinical utility, particularly in neoplasms with MEK1 overexpression, or in combination with PARP inhibitors to enhance cytotoxicity. Future studies will confirm the suitability of miR-489-3p for a liquid biopsy development using human serum.

CHAPTER III

BIOENGINEERING NOVEL ANTIBODY-LABELED EXOSOMES CARRYING MICRORNA FOR CANCER CELL TARGETING.

Sudeepti S. Kuppa, Wei Jia, Balázs Rada, Arthur G. Roberts, and Mandi M. Murph

Under review at Scientific Reports.

Abstract

Exosomes have recently been of growing clinical relevance as potential carriers of therapeutics, as have microRNAs due to their ability to inhibit gene expression. Both exosomes and microRNA (miR) are endogenous entities capable of manipulating cell signaling and highly involved in cell-to-cell communication. Herein, we utilize peripheral blood mononuclear cell-derived (PBMC) exosomes bioengineered with antibody-labels (Abi-exosomes) to deliver miR to cells. To engineer Abi-exosomes, an antibody covalently linked to a fatty acid is passively integrated into the exosomal membrane and the miR is then internalized through electroporation. Abi-exosomes provide 700,000-fold higher miRNA levels compared to un-electroporated exosomes and higher cell-targeting specificity with antibody attachment optimization. Consequently, miR-21-5p, which targets the phosphatase and tensin homolog (PTEN) gene, delivered to triple negative breast cancer (TNBC) MDA-MB-231 cells significantly inhibits PTEN expression. Triple-negative breast cancer (TNBC) cells were utilized here to address the desperate need for novel therapeutic approaches to combat this aggressive tumor type and reduce mortality. The customizable bioengineering of Abi-exosomes makes them a highly versatile tool to optimize miR or other therapeutic cargo delivery and uncover an innovative and targeted approach to drug delivery. This approach may also be utilized in other cancers or conditions requiring efficient miR delivery.

Introduction

Since their discovery in 1983 by two distinct research groups (84, 365), exosomes have been widely investigated in both cancer and other fields of research. Studies have

shown that they are key regulators of cell-to-cell communication, biomarker vehicles in conditions such as Alzheimer's disease and cancer (355, 366), or as carriers for therapeutics (367). While exosomes require extensive purification before being utilized as carriers, they can hold diverse cargo such as microRNA (miR), protein and mRNA, and widely access all cell types through circulation, including crossing the blood-brain barrier (368). Due to this, exosomes are increasingly being utilized for drug delivery, such as paclitaxel loaded into exosomes showing increased accumulation in both drug-sensitive and -resistant lung cancer cells (369). Endogenously, cancer cell-derived exosomes play a major role in cancer through conferring immunosuppressive effects (370), while immune cell-derived exosomes attempt to mount an anti-tumor response on rapidly proliferating cells (371). MiRs, small 20-22 nucleotide RNAs, have also been at the forefront of therapeutics research, especially in cancer, due to their ability to effectively inhibit gene expression in cancer cells. For example, miR-26a-containing exosomes delivered to hepatocellular carcinoma cells were shown to significantly slow cell migration and proliferation due to increased miR levels (372). In this study, we have utilized these powerful players in the development of Abi-exosomes, which has given us the ability to manipulate endogenous processes to target cancer cells using microRNAs (miRs), thereby reducing risk of a possible immunogenic response.

Herein, we explore the development of a method where exosomes are bioengineered as a tool for miR delivery using a targetable molecular cell surface marker to increase cargo uptake. We describe the successful construction of antibody-labeled exosomes (Abi-exosomes) through dialysis, where we covalently bonded an antibody to a fatty acid, and upon removal of the stabilizing n-dodecyl-β-D-maltoside (DDM)

detergent, the tail of the fatty acid was inserted into the exosomal membrane to maintain its hydrophobicity. We have developed this tool using purified exosomes from peripheral blood mononuclear cells (PBMCs) obtained from a human blood donor, and attached a specific antibody-label to the exterior of the exosomal membrane to create Abi-exosomes. The addition of an antibody attachment allows for the exosomes loaded with miR cargo to target specific cell surface proteins corresponding to the antibody used for construction, thereby increasing the likelihood of exosomal uptake.

We have utilized triple negative breast cancer (TNBC) as our model for this study, as breast cancer is the most commonly diagnosed malignancy in women, accounting for up to 30% of all diagnosed cancers annually (373). While a majority of breast tumors overexpress the targetable hormone receptors and can be treated with inhibitors, resulting in low mortality rates, 15-20% of new diagnoses are classified as TNBC (374). This refers to the lack of targetable hormone receptors that results in aggressive tumors that are unresponsive to chemotherapy (375, 376). In the enclosed study, we have explored the possibility of using customized Abi-exosomes as carriers for miR delivery to aggressive, triple-negative breast cancer cells and shown high miR delivery MDA-MB-231 cells. Because our study is focused on TNBC cells, we anticipate our results will lead to more effective therapeutic options and will provide an exciting avenue of research to develop unique strategies for specifically targeting TNBC cells.

The overall goal of this study was to bioengineer versatile and customizable antibody-labeled exosomes (Abi-exosomes) that are effective at specifically targeting cells and delivering miR with higher efficiency than the standard delivery method of transfection. As the relevance of exosomes and miRs in therapeutics grows, this method

forms the stepping stone to improving cell-specific therapeutics delivery in a variety of cells, possibly mitigating off-target effects.

Materials and methods

Harvesting of human peripheral blood mononuclear cells (PBMCs)

Human donors were enrolled for blood collection in compliance with the guidelines of the World Medical Association's Declaration of Helsinki and the Human Research Protection Program and Institutional Review Board (IRB) for human subject research at the University of Georgia (UGA) after necessary protocols were approved by the same entities. Enrolled healthy volunteers signed informed consent forms after being educated on the study. The human blood protocol (University of Georgia protocol no. 2012-10769) and the consent forms were reviewed and approved by the IRB at UGA. Peripheral blood mononuclear cells (PBMCs) were isolated from heparinized blood samples using the Histopaque 1077 Reagent (Sigma Aldrich, St. Louis, MO, USA) as per manufacturer instructions and as previously described (377) and resuspended in RPMI without glutamine and phenol red (Corning, Corning, NY, USA) supplemented with 1M HEPES buffer (Sigma Aldrich). Cells were counted and plated at a density of 1 million cells per 25 cm^2 in a 75 cm^2 flask in RPMI (Corning) supplemented with 10% fetal bovine serum (FBS) (Atlanta Biologicals, Flowery Branch, GA, USA) and penicillin/streptomycin (Thermo Fisher, Waltham, MA, USA).

Preparation of fatty acids, antibody and exosomes

Two fatty acids, namely 1,2-distearoyl-sn-glycero-3-phosphoethanolamine-N-

[maleimide(polyethylene glycol)-2000] (DSPE-PEG(2000) maleimide), and fluorescent 1,2-distearoyl-sn-glycero-3-phosphoethanolamine-N-(7-nitro-2-1,3-benzoxadiazol-4-yl) (NBD-DSPE) (Avanti Polar Lipids, Alabaster, AL, USA), were obtained and dissolved in DMSO to yield a 1 mg/mL solution. N-dodecyl-β-D-maltoside (DDM) detergent (Sigma Aldrich) was resuspended in 1x PBS to yield 100 mg/mL and 0.1% w/v solutions. DSPE-PEG 2000 Maleimide and NBD-DSPE were dissolved in 1 mL of 0.1% DDM at a concentration of 100 μM each. This solution was used to verify excitation (445-460 nm) and emission (540 nm) of the fluorescent NBD-DSPE using the SpectraMax M2 Plate Reader (Molecular Devices, Sunnyvale, CA, USA) (data not shown). Equivalent concentrations of the two fatty acids were used for Abi-exosomes construction, which were chosen due to the fatty acid maleimide functional group's ability to covalently bond to amines, as present on an antibody tail.

PBMCs were plated in RPMI (Corning) supplemented with 10% fetal bovine serum (FBS) (Atlanta Biologicals) and penicillin/streptomycin (Thermo Fisher) and incubated in a humidified atmosphere of 5% CO_2 at 37ºC for 24-48 h. Exosomes were isolated using the Exiqon Exosome Isolation Kit (Exiqon, Woburn, MA, USA) and stored at -80ºC prior to use. Invitrogen ENPP2/autotaxin antibody (Thermo Fisher) and CD44 or CD29 antibodies were purchased (Cell Signaling Technologies, Danvers, MA, USA).

Construction of fatty acid-antibody anchored exosomes

The fatty acid solution in 0.1% DDM was dialyzed using Slide-A-Lyzer MINI Dialysis units with a 10 kDa molecular weight cut-off (Thermo Fisher) against 2L of 1x PBS for 2 h in a 4ºC cold room to remove excess detergent. Following dialysis, the

presence of the fatty acid was confirmed by fluorescence emission at 540 nm after exciting between 445 and 460 nm on a SpectraMax M2 Plate Reader (data not shown). The remaining sample was combined with antibody at a 2:1 ratio and incubated at room temperature for 1 h to generate the antibody-label and subsequently combined with 100 µL of purified PBMC exosomes. This solution was mixed by pipetting, briefly centrifuged, and incubated at room temperature for an additional 1 h. Then, the sample once again underwent dialysis using the 10 kDa dialysis units against 2L of 1x PBS for 2 h in a 4ºC cold room to integrate the fatty acid-attached antibody into the exosomal membrane and remove all DDM from solution.

The dialyzed product, containing the exosomally integrated antibody-label or Abi-exosomes, was incubated overnight with Exosome Precipitation Buffer from the Exosome Isolation Kit per manufacturer instructions (Exiqon), and centrifuged at 104,000 xg for 1 h at 20ºC to pellet the Abi-exosomes. The supernatant was removed and Abi-exosomes were resuspended in 1x PBS to prepare for miR electroporation.

Electroporation of exosomes with miR

Exosomes were quantified using the Pierce BCA Protein Assay Kit (Thermo Fisher) as per manufacturer's protocol. Under a sterile hood, 1 µg each of exosomes and miR (Thermo Fisher) were combined in 400 µL of serum-free DMEM medium in a Gene Pulser Cuvette (Bio-Rad, Hercules, CA, USA). The Bio-Rad Gene Pulser X-Cell CE was used to electroporate miR into exosomes at the following parameters: 150 Volts and 125µF capacitance for 10-15 microseconds in a 4mm cuvette using an exponential decay protocol as available in the machine. The electroporated Abi-exosomes were incubated at

room temperature for 30 min prior to treating cells.

Treatment of cell lines

MDA-MB-231 cells were grown and maintained in Dulbecco's Modified Eagle Medium (DMEM) (Corning), while OVCAR-3, MeWo and BT-474 cells were grown in Roswell Park Memorial Institute (RPMI) medium (Corning). Both were supplemented with 10% fetal bovine serum (FBS) (Atlanta Biologicals) and 5% penicillin/streptomycin (Thermo Fisher) and incubated in a humidified atmosphere of 5% CO_2 at 37ºC., Cell lines were plated at 200,000 cells per well in a 6-well format and incubated overnight. Media was refreshed the following day with 2.6mL of fresh 10% DMEM or RPMI (complete medium) and treated with 400 uL of Abi-exosomes electroporated with miR. The plate was incubated for 48 or 72 h before protein or intracellular/exosomal RNA, respectively, were extracted.

Intracellular and exosomal RNA extraction and Quantitative Real-Time PCR

TRIzol Reagent (Invitrogen, Carlsbad, CA, USA) was used to isolate intracellular RNA as per the manufacturer's protocol. Exosomal RNA extraction was performed using the Exosome Isolation Kit followed by the miRCURY RNA Isolation Kit – Cell & Plant (Exiqon). All RNA was stored at -80ºC.

Complementary DNA (cDNA) was prepared from intracellular and exosomal RNA using the Taqman microRNA Reverse Transcription Kit (Thermo Fisher). cDNA was run in a 384-well format in a quantitative real-time PCR (qRT-PCR) assay using Taqman Universal PCR MasterMix (Thermo Fisher) and the ABI 7900HT machine

(Applied Biosystems, Foster City, CA, USA). Microsoft Excel and GraphPad Prism 7 (GraphPad, San Diego, CA, USA) were used for data analysis and statistics.

Protein Extraction and SDS-PAGE gel electrophoresis

Cells were washed with 1x PBS twice and centrifuged at 1,500 xg for 5 min to collect cell pellet before addition of RIPA Lysis and Extraction Buffer containing Protease/Phosphatase Inhibitor Cocktail (100x) (Thermo Fisher). They were shaken on ice with occasional vortexing for 30 min, sonicated, and centrifuged at 15,000 xg for 10 min to collect the protein supernatant. Protein was stored at -80ºC before quantification using the Pierce BCA Protein Assay Kit (Thermo Fisher) as per manufacturer's protocol.

Protein samples (30 µg) were boiled with 6x Laemelli sample buffer at 95ºC for 5-10 minutes prior to loading on an SDS-PAGE gel. The BioRad SDS-PAGE System and protocol were used to probe for CD44, CD29, and GAPDH antibodies at 1:1,000 dilution overnight and HRP-conjugated anti-rabbit secondary antibodies at 1:10,000 dilution (BioRad; Cell Signaling Technologies). All antibodies have been produced and characterized by Cell Signaling Technologies. The LI-COR Imager (LI-COR Biosciences, Lincoln, NE, USA) was used to detect bands on the PVDF membranes with the following exposure times: GAPDH (1 min), CD44 and CD29 (4 min) at room temperature. All images were inverted to display black bands on a white background, and slightly darkened using the software automation to make lighter bands visible, as evident on the CD29 blot. The white background is typical in images rendered using the LI-COR machinery; a grey background cannot be achieved without excessive manipulation of the images. Band quantification was performed using the ImageJ Software (National

Institutes of Health, Rockville, MD, USA).

Dynamic Light Scattering (DLS)

To determine whether antibodies were successfully anchored into the exosomal membrane to form Abi-exosomes, dynamic light scattering (DLS) was used to determine particle size in solution compared to each individual component required for the final product. At 25ºC, purified water has a viscosity of 0.8872 cP, and a refractive index of 1.330, compared to vesicles such as exosomes, which have a refractive index of 1.447 (378). This allowed for successful distinction between the "blank" water solution, Abi-exosomes, or its individual components. A generic, undiluted IgG antibody has a hydrodynamic diameter of 11.3 nm (379), while the PEG(2000) group has a hydrodynamic radius between 1.6 and 3.2 nm, averaging to 3 nm (380). These two components would result in an approximately 14.3 nm size increase upon exosomal integration. PEG(2000) fatty acid was prepared at or below critical micelle concentration (0.0087% DDM). The Zetasizer Nano ZS was used to perform DLS and configured with a protein protocol to determine exosomes and Abi-exosomes size (Malvern Panalytical, Malvern, United Kingdom). The Zetasizer software (Malvern Panalytical) was used to obtain and analyze data. Graphs were created using GraphClick (Arizona Software) and Microsoft Excel.

Statistics

One-way analysis of variance (ANOVA) test was used to determine statistical significance between groups comparing miR uptake into cells and Student's T-Test was

used to compare two groups to one another. A confidence interval of 95% with p-values less than 0.05 (*), 0.01 (**) and 0.001 (***) were considered significant under both statistical tests. All experiments were run in triplicate non-concurrently, resulting in an n=3. Microsoft Excel (Microsoft) and GraphPad Prism 7 (GraphPad) were used to analyze the data.

Results

Construction and confirmation of antibody-labeled exosomes

Fig. 1 shows the steps required to produce customized antibody-labeled exosomes (Abi-exosomes) with miR from human PBMCs. For exosome isolation, PBMCs were purified from a human blood donor and cultured for 24-48 hours before exosomes were extracted **(Fig. 3.1A)**. The antibody and fatty acid were incubated together in 0.1% DDM detergent to covalently bond the maleimide functional group on the PEG(2000) fatty acid to the amine groups on the antibody tail, resulting in the antibody-label. This was then incubated with exosomes and dialyzed to remove the DDM stabilizing the hydrophobic fatty acid tail, resulting in passive insertion of the antibody-label into the exosomal membrane to maintain its hydrophobicity, forming Abi-exosomes. **(Fig. 3.1B)**. Following electroporation of miR (R) into Abi-exosomes, we expect that the antibody on Abi-exosomes would target a marker at or near the cell surface and be endocytosed, and subsequently degraded to release miR, which may then have functional outcomes on its target mRNA within the cell **(Fig. 1C)**. We hypothesize that using an antibody for Abi-exosome construction with a protein target on the cell surface increases their proximity to the cells and therefore increased cellular uptake efficiency and miR levels in the cells.

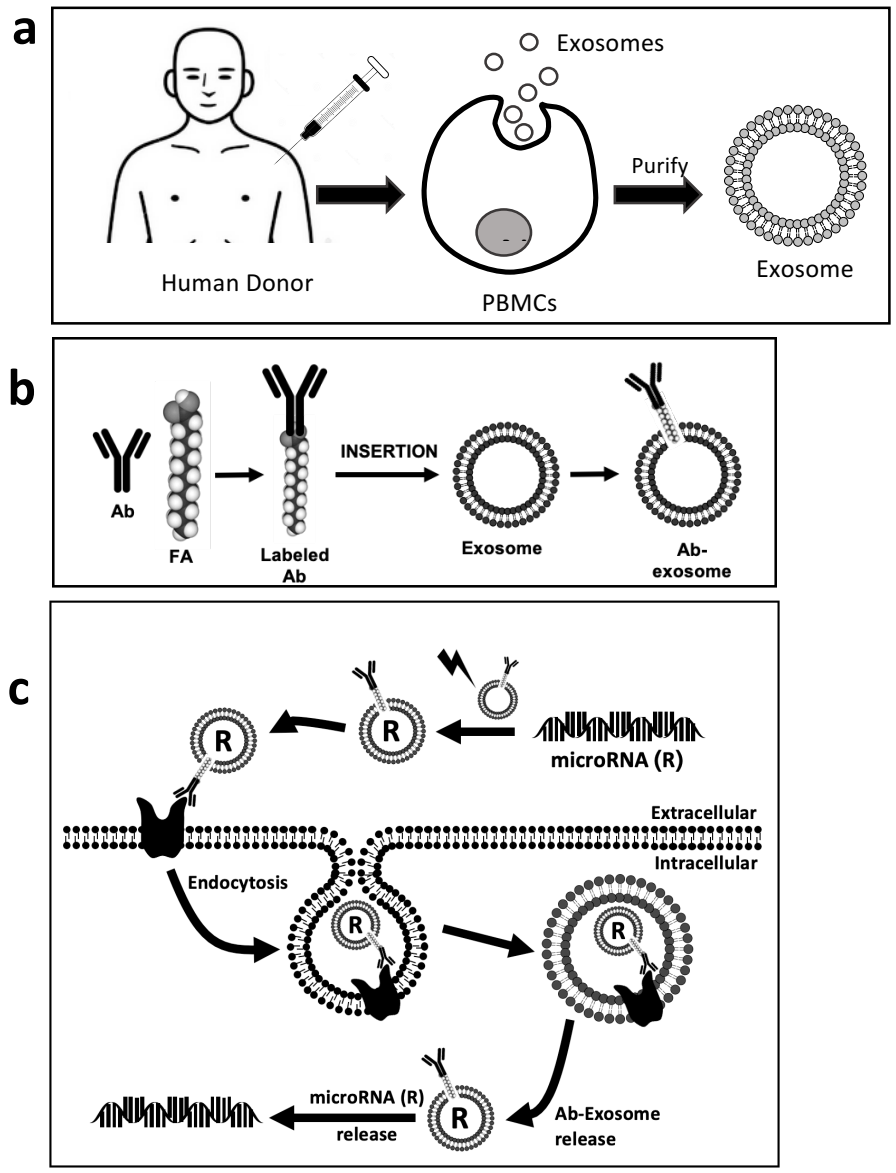

Fig 3.1. Construction and model of Abi-exosomes for cellular delivery.
a) PBMCs extracted from blood obtained from a human donor are cultured for 24-48 hours before PBMC-derived exosomes are extracted and purified. b) Antibody is covalently attached to a fatty acid before passive insertion into exosomal membrane by removing hydrophobicity-stabilizing detergent through dialysis, forming antibody-labeled exosomes (Abi-exosomes). This passive integration of the antibody-label into the exosomal membrane ensures that there is no disruption in the exosomal membrane, creating a stable final particle. c) Following electroporation of miR (R) into Abi-exosomes, they are delivered to cells, allowing for the antibody to bind a protein target on the or near the cell surface, resulting in Abi-exosome internalization and intracellular miR release from the particle.

Dynamic light scattering was used to confirm the formation of Abi-exosomes (381, 382). Due to the size of the antibody-label adding up to 14.5 nm (see Methods and Materials), the possibility that there are multiple attachments on the exosomal surface, and that some length is lost with insertion of the fatty acid tail into the exosome, we expected a 10-20 nm size increase corresponding to a rightward peak shift comparing exosomes alone and Abi-exosomes. Our data revealed that this was indeed the case; Abi-exosomes (54 nm) had a particle size approximately 14 nm larger in size on average compared to purified exosomes without antibody-label (40 nm), and was therefore determined to be successfully constructed **(Fig. 3.2)**. Autotaxin antibody, used to optimize the method as a neutral antibody that targets an enzyme close to the cell surface, was also consistent with the 10-15 nm size expected in a generic IgG antibody. However, fatty acid molecules formed micelles that were unable to be broken up, therefore generating large, inaccurate particle size measurements (data not shown).

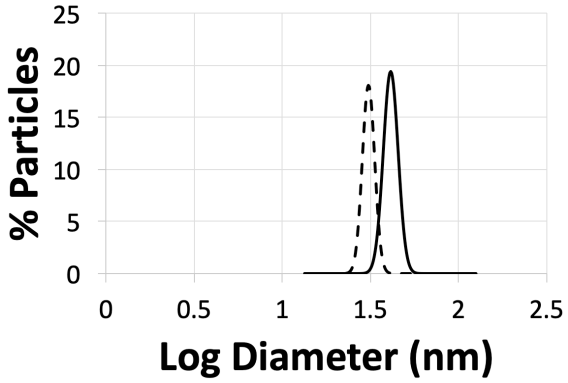

Figure 3.2. Particle size of exosomes and Abi-exosomes investigated by dynamic light scattering. Dynamic light scattering provides a means to measure particle size in solution, allowing us to deduce whether Abi-exosomes were successfully formed. Attachment of the antibody-label to exosomes causes a size peak shift to the right, indicating a larger particle size compared to exosomes without the antibody-label, confirming the attachment. Abi-exosomes were approximately 14 nm larger than purified exosomes as expected due to the size of the individual components required to build Abi-exosomes.

Cellular delivery of miR with Abi-exosomes

We first wanted to assess whether miR delivery efficiency into cells could be increased by encapsulating the miR into purified PBMC-derived exosomes compared to standard miR transfection. For this, cells were treated with 1 μg of exosomes electroporated with equivalent miR for 72 h or transfected with miR. Then, RNA was extracted from cells and exosomes in cultured media, and miR levels were assessed by qRT-PCR to measure miR transfer efficiency to MDA-MB-231 cells by different approaches.

Fig. 3.3A shows the efficiency of miR internalization by electroporation into exosomes or transfection by comparison of intracellular and exosomal miR expression levels. The "untreated" and "exosomes only" conditions contained similarly low levels of miR, possibly due to the lower quantities of endogenous miR that would not result in a spike in expression. Electroporation increased intracellular miR expression by 4-fold compared to both transfection ($*p<0.05$) and exosome-miR delivery without electroporation ($**p<0.01$). In fact, electroporated exosomes contained up to 700,000-fold higher levels of miR compared to purified exosomes, that were then successfully taken up by cells to result in higher miR concentrations **(Fig. 3.3A)**. Since it is possible that presence of an antibody-label on the exosomal membrane may result in structural hindrances for exosomal uptake into cells, we assessed miR uptake efficiency through transfection and miR electroporated into purified exosomes or Abi-exosomes. The autotaxin antibody was used for this purpose to ensure that it enhances cellular proximity of Abi-exosomes due to the autotaxin enzyme residing close to the cell surface. We found that electroporation of miR into Abi-exosomes was able to significantly increase miR

uptake efficiency into the cells compared to electroporation into both unlabeled exosomes and miR transfection (***p<0.001) **(Fig 3.3B)**.

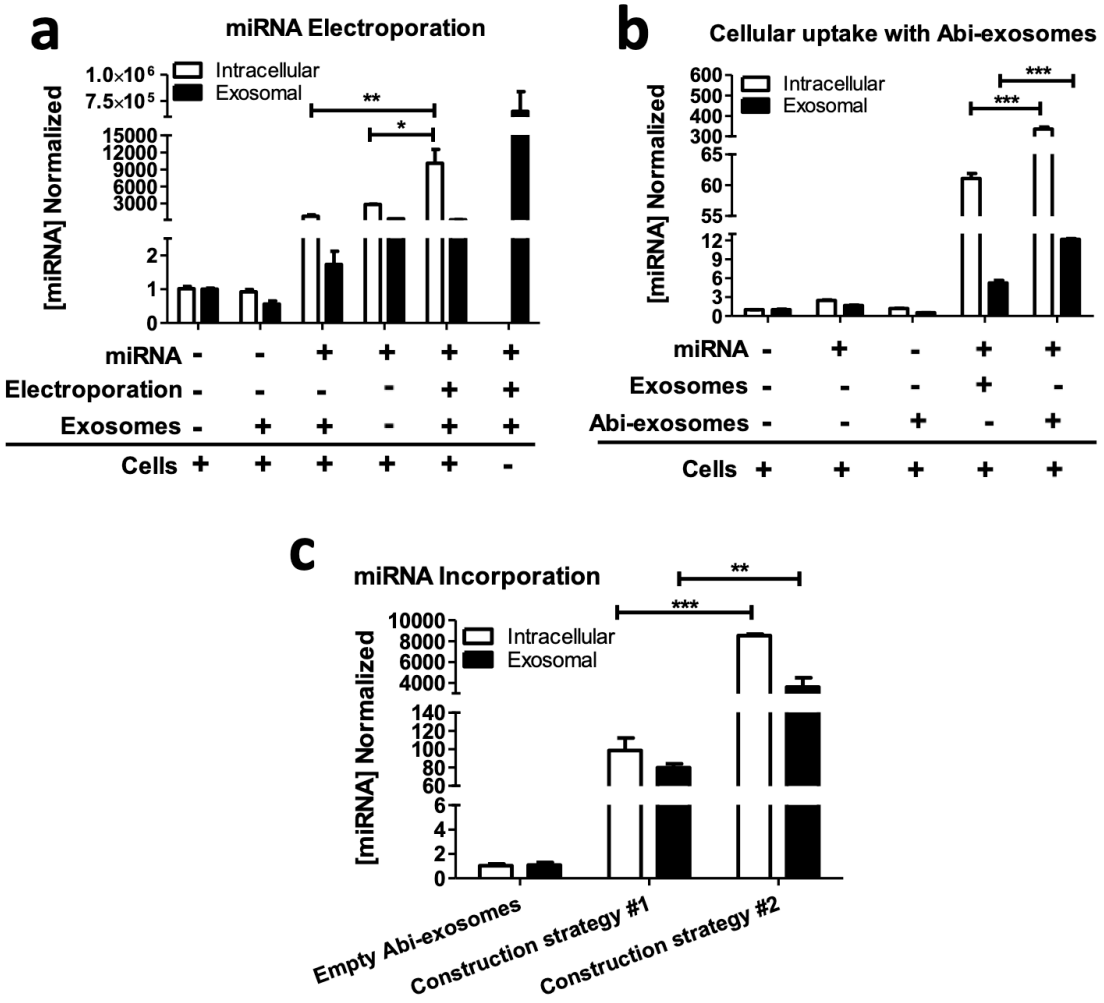

Figure 3.3. Abi-exosome electroporation with miR and delivery efficiency in MDA-MB-231 cells. a) Electroporation significantly increases miR levels up to 700,000-fold in exosomes as well as delivery into cells compared to standard protocol of transfection (*p<0.05), or incubation of miR with exosomes without electroporation (**p<0.01). Purified exosomes contain low amounts of this miR, which is comparable to exosomes emerging from untreated cells. b) Abi-exosomes are able to deliver miR to cells in significantly higher concentrations (***p<0.001) compared to exosomes without the antibody-label, highlighting the advantage of the antibody-label. c) Electroporation of miR into completed Abi-exosomes significantly increases (**p<0.01) miR delivery into cells compared to miR electroporation into purified exosomes before particle construction. All miR expression was normalized to U6 endogenous control expression.

Thus far, miR was electroporated into fully constructed Abi-exosomes, or in other words, after the attachment of the autotaxin antibody-label to purified exosomes. However, we wanted to explore whether miR electroporation before the antibody-label attachment would be more stable, since electroporation may result in minor membrane disruption possibly affecting the antibody-label attachment. Therefore, we devised two construction strategies that involved electroporating miR into purified exosomes before Abi-exosome construction (Strategy #1) or electroporating miR into fully constructed Abi-exosomes (Strategy #2) **(Fig. 3.S1)**. Using qRT-PCR, we confirmed that miR electroporation after Abi-exosome construction resulted in higher exosomal miR levels (**p<0.01) and subsequently, higher intracellular concentrations as well (***p<0.001) compared to exosome electroporation before Abi-exosome construction **(Fig. 3.3C)**. This could be due to miR leaking out of the exosomal membrane during antibody-label attachment, resulting in overall lower levels in completed Abi-exosomes.

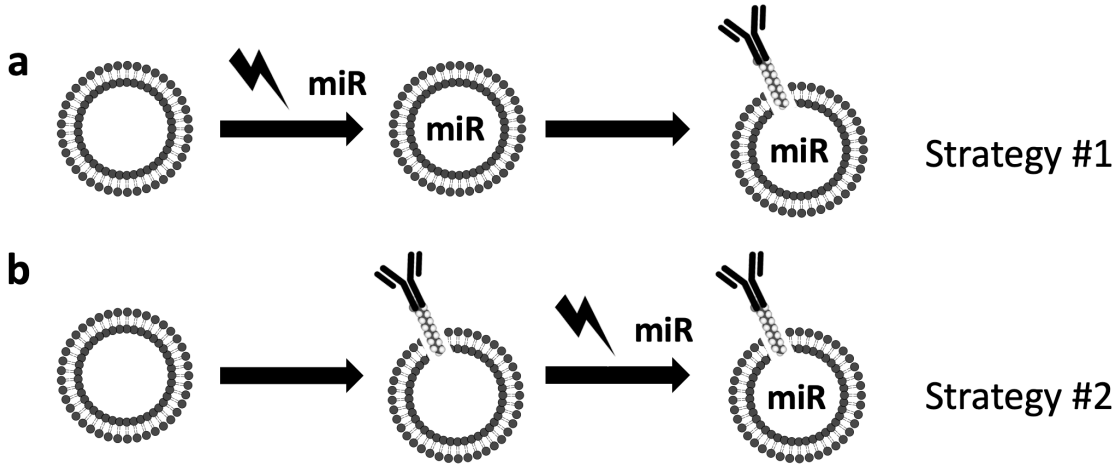

Supplementary Figure 3.1 (3.S1). Various construction strategies were developed to determine the miR electroporation protocol that results in highest miR uptake into Abi-exosomes and subsequent delivery into cells. A) Construction strategy #1 involves electroporating miR into purified exosomes before antibody-label attachment to build the final Abi-exosome particle. B) Construction strategy #2 requires that Abi-exosomes be fully constructed before miR electroporation, and subsequent treatment to cells.

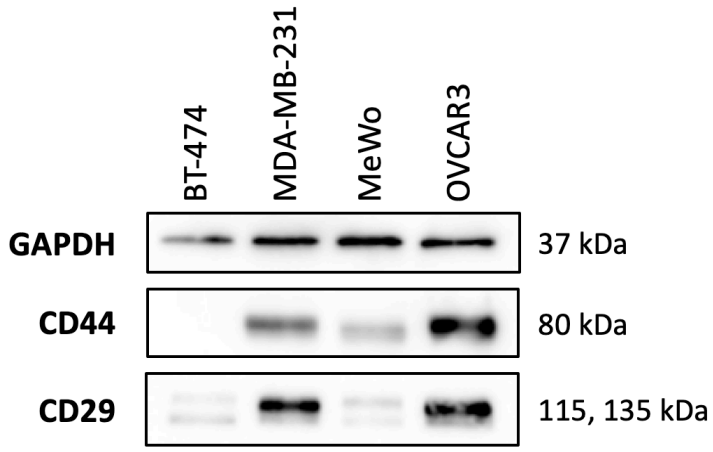

Supplementary Figure 3.2 (3.S2). Immunoblot analysis shows increased CD44 and CD29 expression in MDA-MB-231 (TNBC) cells. This is also observed in OVCAR-3 (ovarian cancer) cells, compared to lower expression in BT474 (triple-positive breast cancer) and MeWo (melanoma) cells. All samples were derived from the same experiment and processed together at the same time although they are on separate gels due to size of the bands, and the possibility of unclear band separation during imaging. All membranes were exposed for 4 min with the exception of GAPDH which was exposed for 1 min. Loading controls were all run on the same blot and full gel images, inverted to display dark bands on a light background, are attached below.

Optimization of antibody-label attachment

Previous studies have shown that certain proteins, such as CD44 and CD29, are overexpressed on the MDA-MB-231 cell surface (383, 384). We hypothesized that targeting these proteins might allow for higher proximity of Abi-exosomes to the cell surface and subsequently higher uptake efficiency. We first measured the expression of these markers on TNBC MDA-MB-231 cells to confirm overexpression of CD44 and CD29 in MDA-MB-231 **(Fig. 3.S2)**. OVCAR-3 (ovarian cancer) cells, also of gynecological origin, showed a similar level of expression for both targets, while MeWo (melanoma) cells and BT474 (triple-positive breast cancer) cells had low expression for both. Further, when CD44 and CD29 antibodies were used for Abi-exosome construction,

miR expression after treatment in MDA-MB-231 cells showed that CD44-labeled-exosomes had the highest miR delivery efficiency into cells compared to Abi-exosomes constructed with autotaxin antibody (*p<0.05) **(Fig. 3.4)**. This confirms that while Abi-exosomes targeting an extracellular enzyme close to the cell surface can be slightly more efficient than miR transfection, directly targeting a marker on the cell surface can result in significantly higher miR uptake into cells. CD29-labeled-exosomes achieved significantly less efficient miR delivery (*p<0.05), possibly due to inefficient targeting by the antibody to this surface marker.

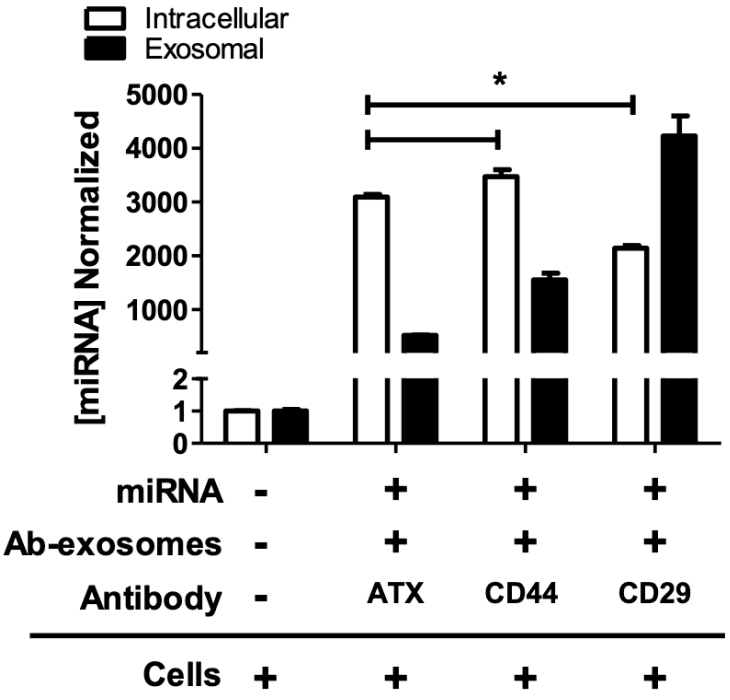

Figure 3.4. Modifying antibody incorporation in Abi-exosomes.
Various antibodies were utilized for Abi-exosome construction based on their target expression on the MDA-MB-231 cell surface. Compared to the autotaxin (ATX) antibody used for the Abi-exosomes construction optimization, CD44 has significantly higher miR delivery into MDA-MB-231 cells (*p<0.05). CD29 was not efficient at miR delivery (*p<0.05) and ATX antibody for Abi-exosome construction was slightly higher than miR transfection. miR expression levels were normalized to U6 endogenous control expression in cells and exosomes.

Functionality of miR delivery into TNBC cells

Due to the high miR uptake efficiency through Abi-exosomes, we wanted to assess whether miR delivered into cells is fully functional and able to successfully inhibit its target mRNA. PTEN has been previously reported in various studies to be a miR-21-5p target in MDA-MB-231 cells and is also implicated in cancers other than TNBC such as gastric or colorectal cancer (73, 74, 385). Therefore, to test the functionality of miR in cells, we measured the expression of PTEN in MDA-MB-231 cells treated with miR-21-5p-containing Abi-exosomes. Results showed that Abi-exosomes could deliver miR-21-5p up to a significant 2.4-fold higher levels into cells (**p<0.01) and result in significant and remarkable inhibition of PTEN in the same experiment (*p<0.05) **(Fig. 3.5B).**

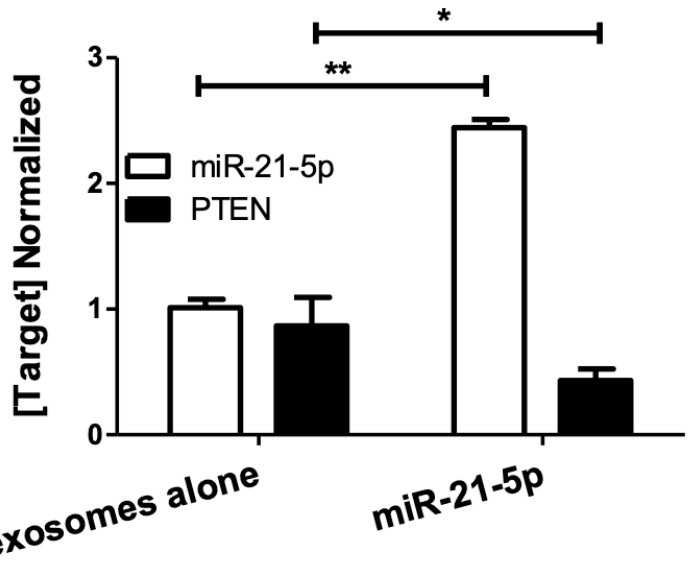

Figure 3.5. miR-21-5 targets and inhibits PTEN expression in MDA-MB-231 cells. MiR-21-5p was electroporated into Abi-exosomes and incubated with MDA-MB-231 cells for 48 hours for uptake. miR-21 expression increased 2.4-fold upon Abi-exosome treatment compared to empty Abi-exosomes (**p<0.01). Treatment with miR-21-5p in Abi-exosomes then resulted in significant inhibition of PTEN expression (*p<0.05), confirming that the miR delivered through this method is functional. miR and PTEN expression were normalized to U6 and 18S endogenous control, respectively.

Discussion

In this study, we aimed to bioengineer novel and customizable antibody-labeled exosomes (Abi-exosomes) that can be used as a vehicle to deliver miR cargo to cells utilizing exosomes derived from peripheral blood mononuclear cells. MiR was electroporated into the completed particle and incubated with cells to characterize uptake of the Abi-exosomes and miR release into the cells **(Fig. 3.1)**. We then used dynamic light scattering, a method often employed to determine particle sizes in solution (382), to confirm successful formation of Abi-exosomes by observing an increase in particle size with the addition of the antibody-label to exosomes as expected **(Fig. 3.2)**. Further, experiments comparing efficiency of Abi-exosomes to transfection, the standard miR delivery method, and unlabeled exosomes showed that antibody-label attachment results in more efficient uptake and miR delivery into cells **(Fig. 3.3A, B)**. Additionally, electroporation of miR *after* Abi-exosomes construction was confirmed to be more efficient for miR delivery into cells **(Fig. 3.3C)**. This could be due to the miR leaking out of exosomes during antibody-label attachment through dialysis if electroporated prior to construction, therefore decreasing miR concentration in the final particle. When the Abi-exosomes were bioengineered with antibodies targeting markers overexpressed on the MDA-MB-231 cell surface such as CD44, and CD29 **(Fig. 3.S2),** we found that CD44-labeled-exosomes were most efficient at uptake and miR delivery into cells compared to ATX or CD29 antibody-labels **(Fig. 3.4B)**. In fact, CD44 is highly overexpressed in various cancer cells and named a prominent regulator of metastasis, especially in breast cancer cells (386). Utilizing this target for cargo delivery with CD44-labeled-exosomes allows us to hijack an inherent survival tactic in cancer cells and target them with lethal

miR cargo in the bioengineered exosomes. Finally, functionality of this method was confirmed by treating MDA-MB-231 cells with miR-21-5p which resulted in successful inhibition of PTEN as observed in previous studies involving the same cell line **(Fig. 3.5)** (385, 387).

This study has several limitations that must be addressed prior to considering this method for clinical relevance. First, long-term stability of the completed Abi-exosome at -80ºC has shown to significantly reduce the ability of the constructed particle to deliver miR into cells. It is possible that the Abi-exosomes themselves are stable when stored at low temperatures, but that the miR is unable to be electroporated in or is subsequently exported out of the particle. In this case, electroporating higher concentrations of the miR into the Abi-exosome before treatment to cells may increase uptake efficiency. If the Abi-exosome itself is unstable upon storage at -80ºC, storage at -20ºC or 4ºC may also be considered. Secondly, while literature outlines increased CD44 expression in MDA-MB-231 cells, CD44 expression is also relatively high in healthy peripheral blood mononuclear cells (384). Since the exosomes used in study are derived from peripheral blood mononuclear cells, it is possible that they also contain higher expression of CD44, but due to their small size and low concentration for protein analysis, expression could not be assessed. High CD44 expression on exosomal surfaces could result in the CD44-label targeting the surface of exosomes themselves instead of successfully integrating into the exosomal membrane to form Abi-exosomes. However, dynamic light scattering has allowed us to confirm that the antibody-label is in fact inserted into the exosome correctly, and not targeting CD44 on the surface due to the size distribution of Abi-exosomes compared to exosomes alone. In other words, if the antibody-label was not

inserted into the membrane, the particle size increase would be ~2-fold higher based on the component sizes.

MiRs are recently becoming more applicable as a class of therapeutics due to their ability to control expression of target mRNA by binding them and inhibiting protein translation (9). Loading miRs as cargo into the exosomal cavity after particle construction makes Abi-exosomes a highly versatile tool since there are thousands of diverse miRs that target genes relevant to countless conditions, lending to its applicability in personalized medicine. Specifically, in cancer, miRs have been considered as key candidates for circulating biomarkers indicative of disease state and, in some cases, tumor staging and progression (353, 354). For example, a recent study published in our laboratory revealed the significance of miR-489-3p in ovarian cancer development and its ability to target and repress MEK1, a prominent oncogene relevant in several malignancies (216). On the therapeutic end, miR-34 has been well classified as a tumor suppressor in several cancers in the past, and reached phase 1 clinical trials in 2017 (388, 389) and Miraversin, which is an anti-sense miR inhibitor that targets overexpression of miR-122, reached phase 2 clinical trials for Hepatitis C virus infections (390). Exosomes are also therapeutically relevant as drug carriers, as evidenced by studies involving exosomally delivered miR-9 in breast cancer fibroblasts and miR-122 as a chemo-sensitizer in hepatocellular carcinoma (391, 392). The bioengineered Abi-exosomes outlined in this study are a powerful utilization each of its components, with the possibility of antibody and miR and more efficient therapeutic delivery into cells.

Future studies involving the bioengineered Abi-exosomes may include electroporating various miRs into Abi-exosomes to result in additive target inhibition and

subsequent cytotoxic effects of the miR in different cell types. Multiple antibody attachments on the Abi-exosomes can also be investigated to assist the particle in navigating the tumor microenvironment to specifically target a cell type overexpressing multiple surface proteins. Finally, as obtaining exosomes from human blood might enhance the opportunity for personalizing Abi-exosomes with a patient's own exosomes, we can also examine whether exosomes purified from other immune cells or stromal cells can be relevant to make this method more efficient. To fully pursue the clinical relevancy of Abi-exosomes, an *in vivo* tumor xenograft study could also be conducted using athymic nude mice and xenograft tumors sensitive to oncogene inhibition achievable by higher miR levels delivered by Abi-exosomes. The diversity and customization ability of Abi-exosomes outlined in this study make it relevant not only to cancer, but a variety of other conditions that might require more efficient miR delivery to effectively achieve target inhibition.

CHAPTER IV

DEFINING THE CYTOTOXIC EFFECTS AND STRUCTURE-ACTIVITY RELATIONSHIP OF NOVEL ORGANIC COMPOUNDS.

Introduction

The goal of this study was to elucidate the cytotoxic effects of 34 compounds provided to us by a collaborator at Augusta University. We aimed to test the cell lines in a variety of cell lines of melanoma, ovarian cancer and pancreatic cancer origin. These cancer types were chosen for two reasons: 1) Our laboratory largely focuses on the biology of melanoma and ovarian cancer; thus, we are familiar with many of the cell lines and their mutational statuses, and 2) melanoma, ovarian and pancreatic cancer are all difficult to treat when diagnosed after regional spread of disease, and therefore the need for novel compounds with notable cytotoxic effects may be higher. Several therapeutics available to melanoma patients are small molecule inhibitors of B-Raf (393). This oncoprotein is mutated in up to 50% of melanoma patients, and is easily targetable by administering B-Raf inhibitors to patients (394). On the other hand, the ovarian and pancreatic cancer drug formulary is generally made up of DNA targeting agents such as gemcitabine or platinum-based therapy such as cisplatin (395, 396). Especially in ovarian cancer, patients respond well to first line therapy initially, but up to 80% quickly relapse within 18-24 months following the prior treatment with resistant disease (397).

Our study strives to determine the cytotoxic effects of 34 compounds grouped into subsets based on structural similarity and determine if there is a preliminary structure-activity relationship to be defined based on functional group modifications. The synthesis of several compounds in their respective subsets have been previously published or their efficacy as an anti-microbial compound has been measured. The largest subset of this study contains 14 compounds in total which are generally derived from diamidines such as pentamidine. Pentamidine has been shown to have anti-microbial effects against African trypanosomiasis, pneumonia and other parasites, and aromatic diamidines have also shown to play a role as anti-parasitic candidate therapeutics for a variety of diseases (398-400). Furamidine, also known as DB75, is a well-known aromatic diamidine that has not only been studied for its relevance as an anti-parasitic, but also for its ability to be cytotoxic to cancer cells. Five compounds in this study, namely DB1855, DB1856, DB1943, DB1931 and DB1908 have all been synthesized as variations of DB766, which is a furamidine analogue (401). Assuming that they carry the core characteristics of their parent furamidine compound, we hypothesized that they may have cytotoxic effects in some measure on melanoma, ovarian cancer, and pancreatic cancer cells. Further, preliminary target analysis of tumor tissue treated with DB1856 may provide insight into possible mechanism of action of this compound, outlined in Chapter IV.

Arylimidamides are essentially aromatic diamidine analogues, which include compounds such as furamidine and DB766 (400, 402). Previous studies have shown that arylimidamides are able to bind DNA, specifically in the minor groove (400, 403). If this holds true, we expect that all DB766 derivatives explored in this study are able at least partially retain their DNA-binding activity. This would make any successful compounds

highly relevant in the ovarian and pancreatic cancer field, which already contains DNA targeting agents, but may need a unique way to bind inhibit DNA replication. DNA minor groove binders have been studied in many fields outside cancer biology, however, and are known to bind DNA to subsequently inhibit chromosome condensation, a process required for mitosis to occur (403, 404). In fact, furamidine, previously established as a DNA minor groove binder, has already been shown to have cytotoxic effects in cancer cells. Further, it can bind both mitochondrial and nuclear DNA to inhibit the mitotic process as well as inhibit epithelial mesenchymal transition, often required for cancer to metastasize (405).

Interestingly, compounds within this subset of furamidine analogues have also shown other unique properties. For example, CES-IX-49 has been tested *in vivo* for its anti-parasitic activity against *Neospora caninum* and resulted in significantly lower parasite load in the brain, indicating that it is able to cross the blood-brain barrier (406). This is further relevant in melanoma, as between 12-20% of distant metastatic sites are in the brain, and a compound that is able to reach a metastatic site could be utilized for patients with advanced disease (407). Additionally, CES-IX-38 has been compared to chemotherapeutic intervention to treat infection by *Leishmania infantum* parasites with an IC_{50} in the low nanomolar range (408).

However, the hypothesis that furamidine and DB766 derivatives are DNA minor groove binders and have anti-parasitic activity only applies to 14 of the 34 compounds included in this study. Of the remaining 20 compounds investigated for their cytotoxic effects, only 2 have been previously published for their synthesis. RAH-A-2 and ZAM-II-41, both of which have a dihydropyrrole-quinazoline backbone, have been evaluated

purely for their chemical reactivity and ability to be formed by oxygenation, or exposure to oxygen (409).

We believe this study sheds light on the potential of crossover between anti-microbial and anti-cancer therapeutics and opens a new avenue for exploring the multidimensionality of compounds already established for a different purpose. Since we only briefly investigated the target of DB1856, future work with these compounds will help solidify their possible targets in the cancer types explored here, namely melanoma, ovarian and pancreatic cancer. Most importantly, our study has shown that changes in functional groups can directly affect cytotoxicity in cells, a feature that can be further utilize to optimize structure-activity relationships.

Materials and Methods

Cell Lines and Compounds

Cell lines for this study were obtained from ATCC (Manassas, VA, USA), grown in the appropriate medium, such as RPMI or DMEM (Corning, Corning, NY, USA) supplemented with 10% fetal bovine serum (FBS) (Atlanta Biologicals, Flowery Branch, GA, USA) and Penicillin/Streptomycin (Thermo Fisher, Waltham, MA, USA) in a humidified atmosphere of 5% CO_2 at 37ºC. Cell lines were of pancreatic cancer (MIA PaCa-2 and Panc-1), ovarian cancer (OVCAR-3, OVCAR-5 and OVCAR-8) and melanoma (HEMA-LP (melanocytes), SB-2, MeWo, A-375, SK-Mel-5, SK-Mel-2, SK-Mel-2 LPAR3wt, SK-Mel-2 2aa-mutant) origin. The last two cell lines, SK-Mel-2 LPAR3wt and SK-Mel-2 2aa mutant, were generated from SK-Mel-2 parental cells in the laboratory as previously described (410).

All compounds were received in powder form from Dr. Chad E. Stephens at Augusta University (Medical College of Georgia) and resuspended in dimethyl sulfoxide (DMSO) (Corning) to yield a 100 μM solution, and stored at -20ºC in glass vials wrapped with parafilm and with aluminum foil to avoid light exposure. A total of 34 compounds were tested in 13 cell lines and those with the highest efficacy, determined by the lowest IC_{50} concentration, were considered as candidates for *in vivo* studies.

Compound Synthesis

The 34 compounds tested have been segregated into sets based on structural similarity to others in the study. The synthesis of some compounds have been previously published and certain have been explored for their broad anti-microbial activity. The compounds with published synthesis are CES-IX-49, CES-IX-38, CES-II-50, DB1908, RAH-A-2, ZAM-II-41 (406, 408, 409, 411-413). Derivatives of the furamidine analog DB766, namely DB1855, DB1943, DB1931 and DB1856 have also been previously published on their synthesis and anti-parasitic activity (401).

***In vitro* treatment with compounds and cell viability assay**

Cell lines were plated in 96-well plates at a density of 4,000-7,000 cells per well (~50% confluency) depending on cell size. The following day, the cells were serum starved overnight with either RPMI or DMEM containing penicillin-streptomycin, but lacking FBS. Following serum starvation, cells were treated with varying concentrations of the compounds as follows, with 0.2% DMSO as the control condition: 0, 0.8, 1.6, 3.1, 6.25, 12, 25, 50, 100, 200μM. Treated plates were placed back in the incubator at 5%

CO_2 at 37ºC for 48 hours. Following the incubation, cells were treated with Cell Titer Blue Cell Viability Assay (Promega, Madison, WI, USA) for 4-6 hours. A change in color of the Cell Titer Blue solution from blue to pink indicates the presence of viable cells and their ability to metabolize Resazurin to Resorufin, a fluorescent dye. The SpectraMax M2 Plate Reader (Molecular Devices, Sunnyvale, CA, USA) was then used to detect florescence as a measurement of cell viability.

Absorbance values for compound-treated groups were compared to the DMSO-treated control group and cell viability was calculated as a percentage of control group cells using Microsoft Excel. Then, GraphPad Prism 7/8 was used to transform the values to log-based dose response in cells, and a non-linear regression line was drawn to determine IC_{50} values for each compound treatment. Based on comprehensive *in vitro* compound testing, it was determined that DB1856 and CES-IX-49 had the highest efficacy (lowest IC_{50}) compared to all other compounds tested and were therefore chosen for further *in vivo* studies.

***In vivo* xenograft studies**

Animals for the xenograft study were ordered from Jackson Laboratories (Bar Harbor, ME, USA). The mouse strain selected was Nu/J or athymic nude mice. These mice have a defective thymus epithelium and therefore cannot produce T-cell responses and lack immunity, but have a partial B-cell response, creating an ideal environment for tumor xenograft growth. Mice were 7-8 weeks old on injection day.

To create tumor xenografts in mice, MeWo cells were revived from liquid nitrogen storage and cultured in 10% RPMI with 10% fetal bovine serum (FBS) (Atlanta

Biologicals) and Penicillin/Streptomycin (Thermo Fisher). Cells were grown in 15cm dishes and harvested and counted for injection. To embed the cells into the collagen matrix required for xenograft development, HyStem-C Hydrogel matrix was ordered (ESI Bio, Alameda, California) and the cell-hydrogel matrix was prepared per supplied protocol.

Animals receiving injections were anesthetized using 2-4% isoflurane in a nose cone and allowed to naturally revive following injection and monitored for discomfort. For animals receiving the MeWo injections, 1 million cells embedded in hydrogel were injected in the back flank subcutaneously, in a total volume of 125-150uL. Animals were monitored over the course of the study for tumor development at or near the injection site and maintenance of healthy appearance and weight in case of tumor metastasis, causing rapid decline in health.

Animal dosing and tumor growth

For the CES-IX-49 study, MeWo (melanoma) xenograft tumors appeared around 2.5 weeks following injection and dosing was commenced at the same time. Mice were heavier than is typically observed at 30-35 grams throughout the study, and dosing at 5, 12.5 and 25 mg/kg of CES-IX-49 was determined based on mouse weight each week. The vehicle-treated control group (5% DMSO, 95% sterile, UltraPure DNase/RNase-free Distilled Water (Invitrogen, Carlsbad, CA, USA)) and the 12.5 and 25 mg/kg group was dosed subcutaneously, while the 5 mg/kg was dosed intraperitoneally. Adverse events in the CES-IX-49 treated mice throughout the study included injection site swelling, excess eye discharge resembling rheum, and shivering and disorientation after recovering from

anesthesia. Mice were euthanized 8 weeks following the first CES-IX-49 dose due to tumors in the control group being extremely large and oozing at injection sites. Serum, organs and tumors were collected for all mice and stored in liquid nitrogen for future RNA and protein analysis.

Statistics

In vitro data was statistically determined to be significant using the Students T-Test comparing the control, DMSO-treated group to each treated concentration. One-way ANOVA statistical test was used to analyze and determine significance of *in vivo* results involving change in mouse weight and tumor volume over time. A confidence interval of 95% with p-values under 0.05 were considered significant. GraphPad Prism 7/8 and Microsoft Excel were used for data calculations and determination of statistical significance.

Results

***In Vitro* Cytotoxicity Studies**

Over the course of this project, we tested 34 compounds in 13 cancer cell lines of melanoma, ovarian cancer and pancreatic cancer origin. We found 14 compounds of the total 34 were structurally similar, the largest group in this study, and derived from non-aromatic and aromatic diamidines and their analogues. These compounds were grouped by structural similarity to determine the structure-activity relationship of changing functional groups and subsequent cytotoxicity in cancer cells. We found that certain

functional groups in related compounds resulted in a more prominent reduction in cell viability that was sometimes specific to the cancer type.

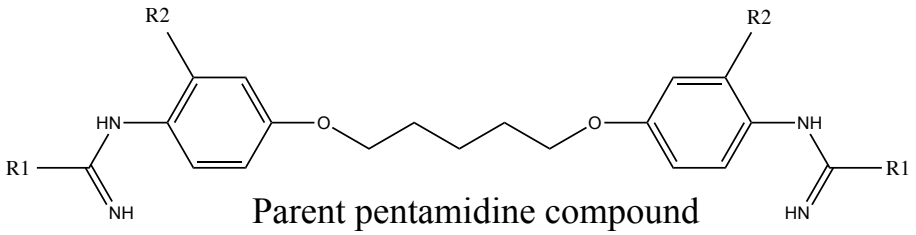

Figure 4.1. Parent pentamidine compound. Of the 34 compounds in this study, 14 are derived from this parent pentamidine structure.

A general pentamidine structure was the precursor to some of the 14 structurally similar compounds, containing two benzene rings with attached imidamide groups and variable R_1 and R_2 groups. Pentamidines are part of the diamidine class of compounds, and have symmetrical structures with high functional group variability. In our study, CES-V-19 was pentamidine-related compound with terminal pyridine rings (R_1) and a benzene-attached O-methyl group (R_2). Our results show that CES-V-19 had selective, but moderate cytotoxicity in melanoma cell lines MeWo (IC_{50}: 22.08 μM, 95%CI: 18.06 to 27.00) and SKMEL-2 (IC_{50}: 27.59 μM, 95%CI: 21.91 to 34.74). Cell viability in ovarian and pancreatic cancer cell lines was not largely affected, with IC_{50} values ranging from 75 to approximately 21,000 μM.

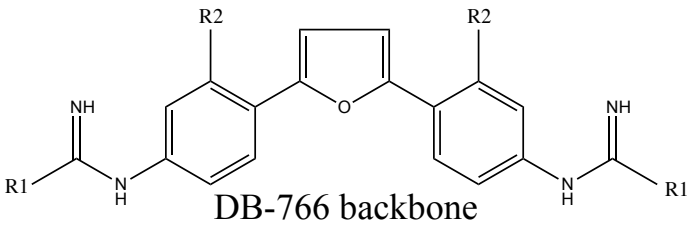

Figure 4.2. DB-766 backbone. Db-766 is an arylamidamide, which is a furamine-related analog, and also derived from pentamidine that 14 of the compounds in this study are derived from.

Aromatic diamidines are another class of compounds that contain a central furan ring flanked by benzene rings and imidamide groups, which are the basis for arylamidamides (AIAs). Many of the 14 structurally similar compounds in this study have been derived from DB766, a prominent AIA with anti-parasitic activity (401). The compounds related to DB766 were synthesized with modified functional groups to define a structure-cytotoxicity relationship. The first set of compound contained a terminal pyridine ring (R_1) but changing functional groups at the R_2 position

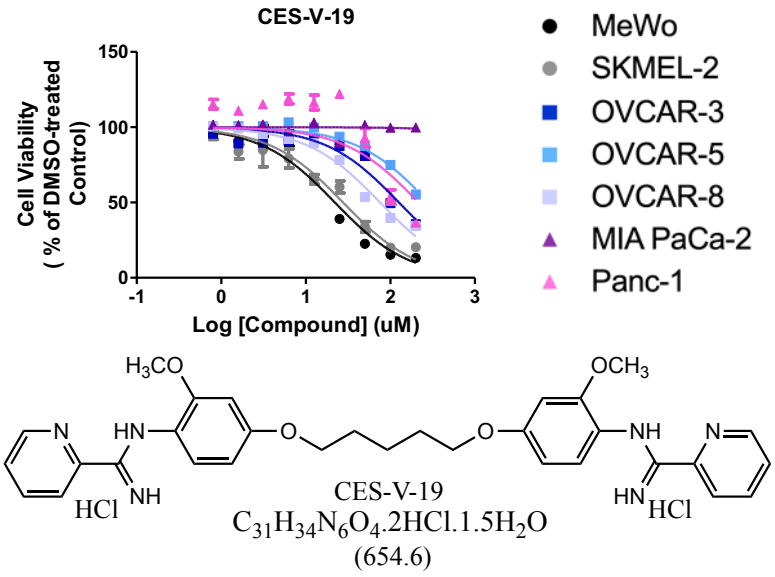

Figure 4.3. CES-V-19 cytotoxicity in various cell lines.

First, we looked at the cytotoxic effects of CES-IX-38 and CES-IX-49, which contained an O-ethyl group and hydroxyl group at the R_2 position, respectively. Initially, both compounds were tested in a variety of melanoma cell lines and HEMA-LP, a human epidermal melanocyte cell line. Results showed that CES-IX-49 had significantly higher cytotoxicity in every cell line tested compared to CES-IX-38. Therefore, the cytotoxicity

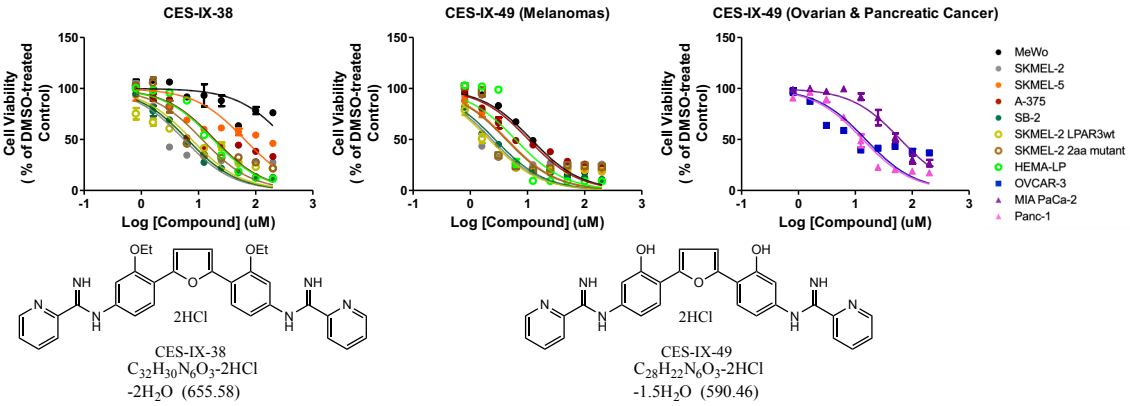

Figure 4.4. CES-IX-38 and CES-IV-49 cytotoxicity in various cell lines.

of CES-IX-49 was also measured in OVCAR-3 and two pancreatic cancer cell lines, MIA PaCa-2 and Panc-1, which showed that its efficacy was not as pronounced in these cells compared to the melanoma cell lines. Therefore, we could conclude that in comparing CES-IX-38 and CES-IX-49, the hydroxyl group in the R_2 position of the structure was responsible for the higher cytotoxicity in melanoma cells.

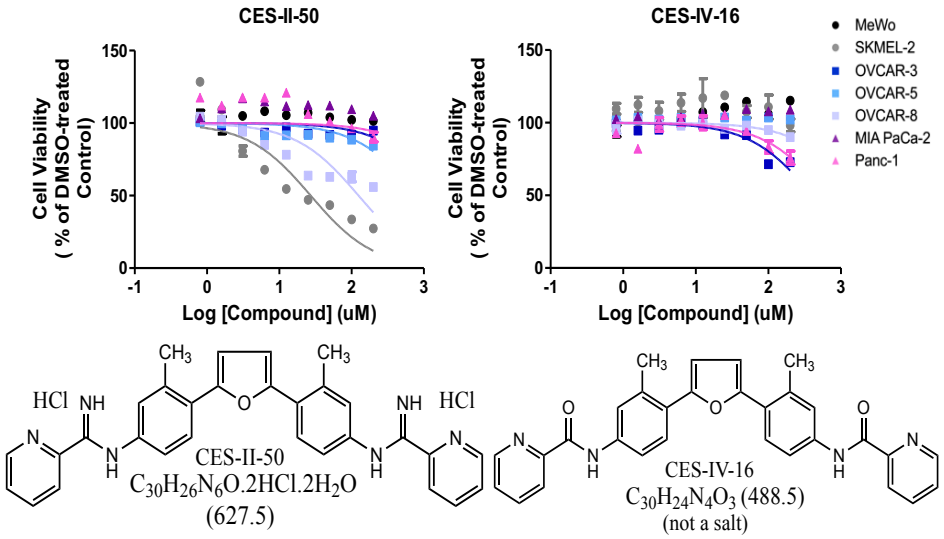

Figure 4.5. CES-II-50 and CES-IV-16 cytotoxicity in various cell lines.

Next, the R_2 position was modified to a methyl (CH_3) group to result in CES-II-50. This compound did not show remarkable cytotoxicity in any cell line except SKMEL-2 (IC_{50}: 27.22 µM, 95%CI: 18.44 to 40.17). In fact, MeWo and MIA PaCa-2 cells did not show any change in cell viability, while other cell lines had IC_{50} values ranging from 124.8 to over 3000 µM. To determine if the imidamine group between the benzene rings in the backbone and the terminal pyridine rings was negatively affecting cytotoxicity, this was modified to an amide group in CES-IV-16. However, this compound did not result in any changes in cell viability in MeWo, SKMEL-2, OVCAR-5 and MIA PaCa-2, while IC_{50} values for the other cells ranged from 406.8 to 1802 µM. Therefore, we concluded that the imidamide group originally present in the DB766 backbone is more effective at reducing cell viability than an amide group.

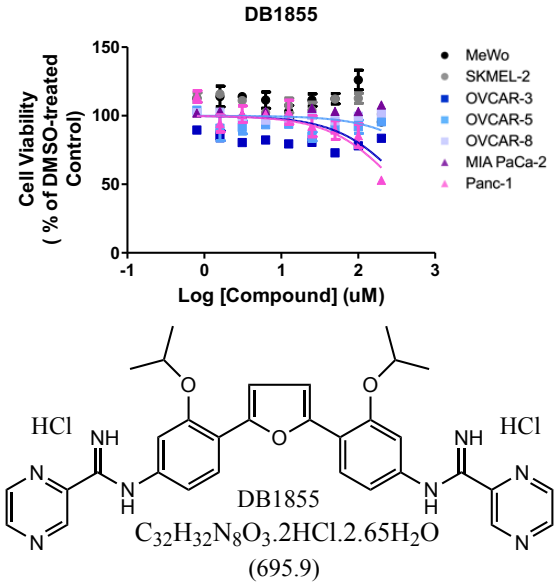

Figure 4.6. DB1855 cytotoxicity in various cell lines.

Next, we tested a group of compounds with isopropyl groups at the R_2 position, but with varying R_1 terminal functional groups. First, we looked at DB1855, which

maintained the terminal pyridine rings from CES-II-50 but replaced the methyl groups at the R_2 position with O-isopropyl groups. However, this resulted in much lower cytotoxicity with MeWo, SKMEL-2, OVCAR-8 and MIA PaCa-2 cells showing no change in cell viability at all. While OVCAR-3 and Panc-1 did show better cytotoxicity compared to CES-II-50, IC_{50} values still ranged from 327.4 to 408.7 µM, suggesting no promising changes in cell viability.

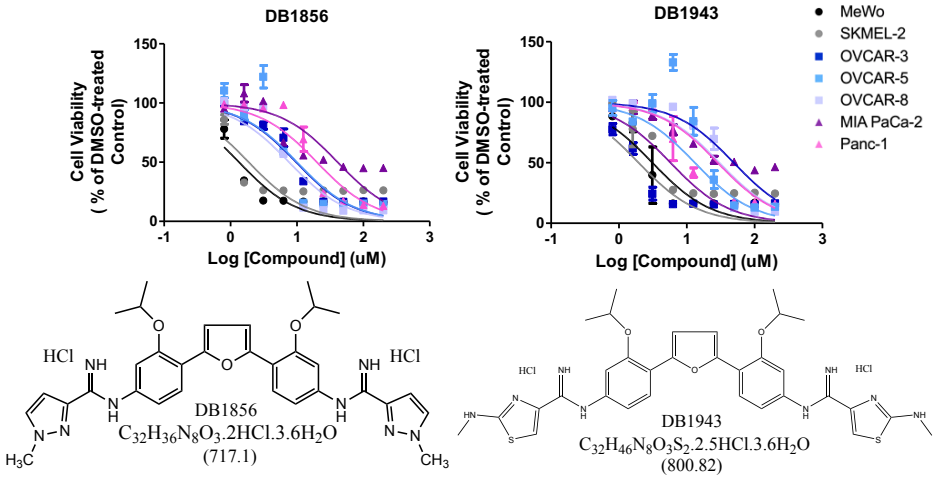

Figure 4.7. DB1856 and DB1943 cytotoxicity in various cell lines.

We then tested compounds that maintained the O-isopropyl, or isopropoxy, groups at the R_2 position, but contained terminal functional groups that was based on 5-membered rings compared to the 6-membered ring groups investigated thus far. DB1856 is a closely related to DB1855 shown above, and contains a terminal pyrazole ring with a methyl group. Further, DB1943 also has the same functional group at R_2, but contains a methylamine-attached thaizole rings. DB1856 and DB1943 both had remarkable cytotoxic effects in most cell lines tested here. DB1943 showed high cytotoxic effects in MeWo (IC_{50}: 3.118 µM, 95%CI: 2.039 to 4.769), SKMEL-2 (IC_{50}: 1.954 µM, 95%CI: 1.452 to 2.628) and Panc-1 (IC_{50}: 5.766 µM, 95%CI: 3.908 to 8.509) cells, but only

moderate changes in cell viability in the remaining cell lines with IC_{50} values ranging from 13.19 to 49.42 µM.

DB1856 had the lowest cytotoxicity observed in our study overall in MeWo (IC_{50}: 1.341 µM, 95%CI: 0.9397 to 1.915) and SKMEL-2 (IC_{50}: 1.887 µM, 95%CI: 1.148 to 3.069) and also showed high cytotoxicity in OVCAR-3 (IC_{50}: 9.74 µM, 95%CI: 7.757 to 12.23), OVCAR-5 (IC_{50}: 10.04 µM, 95%CI: 5.998 to 16.81) and OVCAR-8 (IC_{50}: 7.602 µM, 95%CI: 5.276 to 10.95). However, the compound was unable to successfully reduce cell viability in MIA PaCa-2 and Panc-1 cells as effectively compared to melanoma and ovarian cancer cell lines, with IC_{50} values ranging from 19.96 to 41.00 µM. Therefore, this suggests that the methyl-attached pyrazole rings could be more responsible for the cytotoxic effects in these cells rather than the methylamine-attached thiazole rings on DB1943's structure.

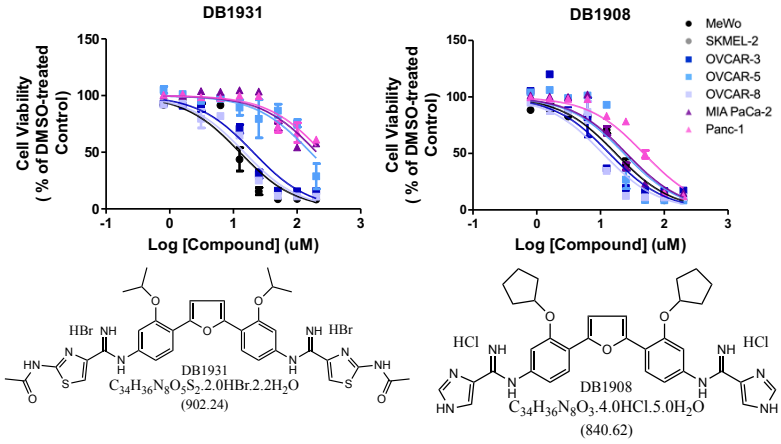

Figure 4.8. DB1931 and DB1908 cytotoxicity in various cell lines.

A further modification of DB1943 comes with terminal methylamine-attached thaizole replaced with a carboxyamine-attached thiazole to result in DB1931. This resulted in very little cytotoxicity in pancreatic cancer cell lines (IC_{50} ranging from 203.7 to 249.8 µM) and moderate cytotoxicity in OVCAR-3 (IC_{50}: 20.51 µM, 95%CI: 15.62 to

26.92) and OVCAR-8 (IC_{50}: 14.79 µM, 95%CI: 11.82 to 18.52), but not OVCAR-5 (IC_{50}: 162.8 µM). MeWo cells also showed somewhat high cytotoxicity with an IC_{50} value of 12.61and 95% CI of 9.126 to 17.42. Therefore, we then tested DB1908 which had a more simplistic terminal end with imidazole rings at the R_1 position and O-pentyl groups at the R_2 position. This resulted in improved cytotoxicity in all the ovarian cancer and pancreatic cell lines with IC_{50} values as follows: OVCAR-3 (IC_{50}: 13.78 µM, 95%CI: 9.066 to 20.94); OVCAR-5 (IC_{50}: 23.29 µM, 95%CI: 14.98 to 36.51); OVCAR-8 (IC_{50}: 10.92 µM, 95%CI: 7.993 to 14.91); MIA PaCa-2 (IC_{50}: 25.61 µM, 95%CI: 19.72 to 33.26); and Panc-1 (IC_{50}: 47.78 µM, 95%CI: 38.33 to 59.54). MeWo and SKMEL-2 did not experience as much cytotoxicity with IC_{50} values at 17.4 µM.

The final set of compounds with a backbone similar to DB766 were provided to us for cytotoxicity testing. They differed from the DB-766 backbone in that the imidamide

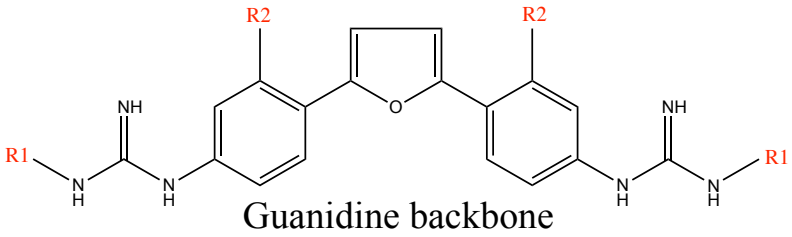

Guanidine backbone

Figure 4.9. Guanidine backbone. A subset of the DB-766 derived compounds contained a slightly different backbone structure as depicted here, made up of a guanidine group.

group was repalced with a guanidine group. Terminal groups were modified at the R_1 and R_2 positions similar to the other compounds tested above and cell viability was measure as a function of changing functional groups. First, we tested CES-VI-14, which has no functional group at the R_2 position, but has a pyridine ring at the R_1 position. This

compound had very little effect on cell viability in pancreatic cancer cell lines MIA PaCa-2 and Panc-1 with IC_{50} values at approximately 290 µM for both, and had moderate

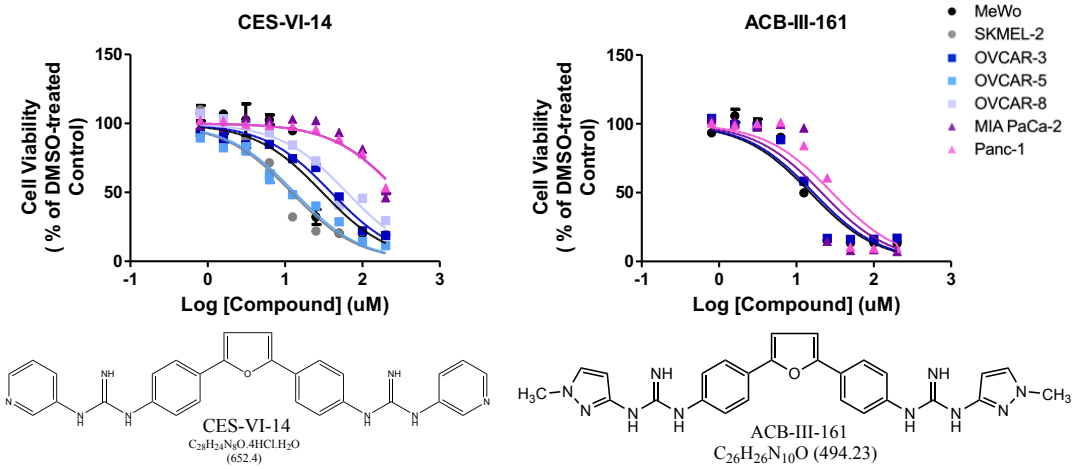

Figure 4.10. CES-VI-14 and ACB-III-161 cytotoxicity in various cell lines.

success in some melanoma and ovarian cancer cell lines as well with IC_{50} values between 30.31 to 62.84 µM. CES-VI-14 did show somewhat high cytotoxicity in SKMEL-2 (IC_{50}: 12.1 µM, 95%CI: 11.37 to 15.41) and OVCAR-5 (IC_{50}: 13.24 µM, 95%CI: 14.98 to 36.51) cells. Then, ACB-III-161 was tested, which is closely related to CES-VI-14 since it also had no functional groups at the R_2 position, but contained a methyl-pyrazole ring on the terminal ends at the R_1 position. Only MeWo, OVCAR-3, MIA PaCa-2 and Panc-1 cells were used for this to simplify the amount of cell lines types, and ACB-III-161 exhibited moderate cytotoxicity in all four. MeWo (IC_{50}: 15.11 µM, 95%CI: 10.78 to 21.17) and OVCAR-3 (IC_{50}: 16.59 µM, 95%CI: 12.30 to 22.37) had the greatest decrease in cell viability, closely followed by both MIA PaCa-2 (IC_{50}: 21.21 µM, 95%CI: 13.02 to 34.52) and Panc-1 (IC_{50}: 28.92 µM, 95%CI: 20.68 to 40.45). Since the R_1 position containing methyl-pyrazole ring improved cell viability in ACB-III-161, we then tested

two compounds more closely related to it, ACB-III-163 and ACB-III-175, both of which preserved the terminal methyl-pyrazole groups.

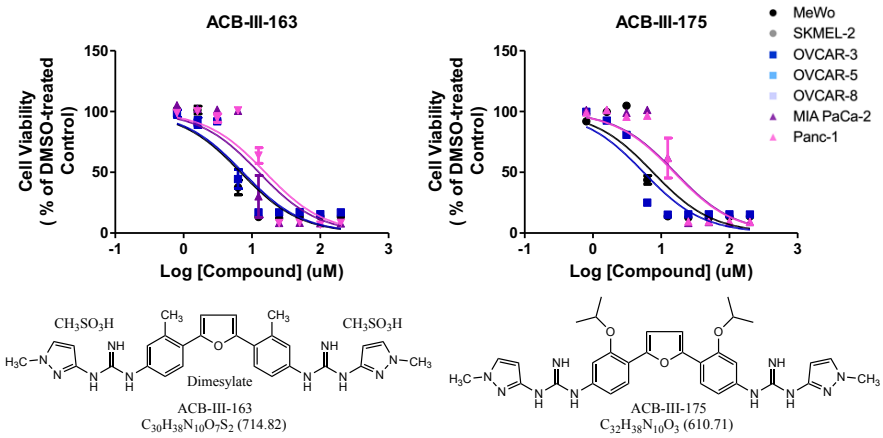

Figure 4.11. ACB-III-163 and ACB-III-175 cytotoxicity in various cell lines.

Both compounds also now contained functional groups at the R_2 position: ACB-III-163 with the addition of a methyl group and ACB-III-175 with the addition of the O-isopropyl group, similar to that observed in the prior set of DB-compounds. We investigated the cytotoxicity of these in the same four cell lies as ACB-III-161 to determine if changes in the functional groups at the R_2 position would improve cytotoxic effects. We found that both compounds were comparable in their ability to reduce cell viability. In fact, ACB-III-163 exhibited the lowest IC_{50} value for MIA PaCa-2 cells in the entire study (IC_{50}: 12.64 µM, 95%CI: 7.661 to 20.87) and one of the lowest for Panc-1 (IC_{50}: 15.63 µM, 95%CI: 10.36 to 23.60) and ACB-III-175 was similarly effective in MIA PaCa-2 (IC_{50}: 15.98 µM, 95%CI: 10.58 to 24.14) and Panc-1 (IC_{50}: 15.44 µM, 95%CI: 10.16 to 23.45) as well. MeWo responded similarly to both ACB-III-163 (IC_{50}: 6.829 µM, 95%CI: 4.643 to 10.05) and ACB-III-175 (IC_{50}: 7.586 µM, 95%CI: 5.040 to 11.42) as did OVCAR-3 in ACB-III-163 (IC_{50}: 7.362 µM, 95%CI: 5.290 to 10.25) and ACB-III-175 (IC_{50}: 5.531 µM, 95%CI: 3.921 to 7.802). We therefore concluded that the terminal methyl-pyrazole

groups were more influential in reducing cell viability in this set of guanidine-containing compounds, and that the functional groups we tested with variations at the R_2 were not of much relevance.

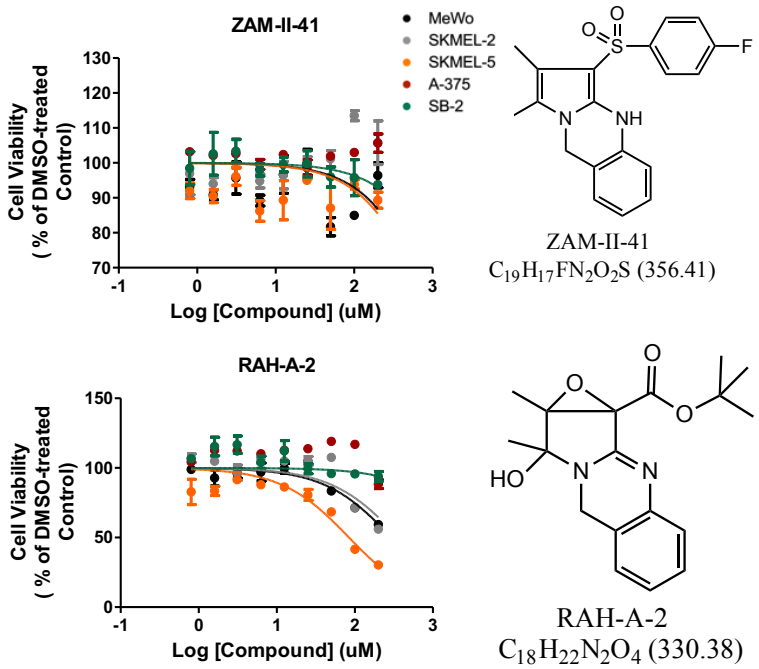

Figure 4.12. ZAM-II-41 and RAH-A-2 cytotoxicity in various cell lines.

Next, we tested ZAM-II-41 and RAH-A-2, which are compounds that both contain a unique dihydropyrrole-quinazoline structure, meaning that they share a backbone containing quinazoline rings or two attached benzene rings with nitrogen heteroatom and also an attached dihydropyrrole ring or a pentane ring sharing a nitrogen atom with the former benzene subpart. ZAM-II-41 is the simpler of the two compounds, with methyl groups stemming from the pyrazole ring, and a side chain containing a sulfonyl and fluorophenyl group. On the other hand, RAH-A-2 has a hydroxyl group and an epoxide group attached to the pyrazole ring, and a carboxylate and *tert*-butyl side chain. Both compounds were tested in five melanoma cell lines, and did not exhibit any notable changes in cell viability. ZAM-II-41 did not have any change in cell viability in

SKMEL-2 and A-375, and had minimal effects on MeWo, SKMEL-5 and SB-2 with IC_{50} values ranging from 1316 to 2639 µM. RAH-A-2 yielded similar results, with no response in A-375, and some response in SKMEL-5 (IC_{50}: 84.35 µM, 95%CI: 65.33 to 108.9) but little effect on cell viability on other cell lines with IC_{50} values ranging from 296.0 to 3184 µM.

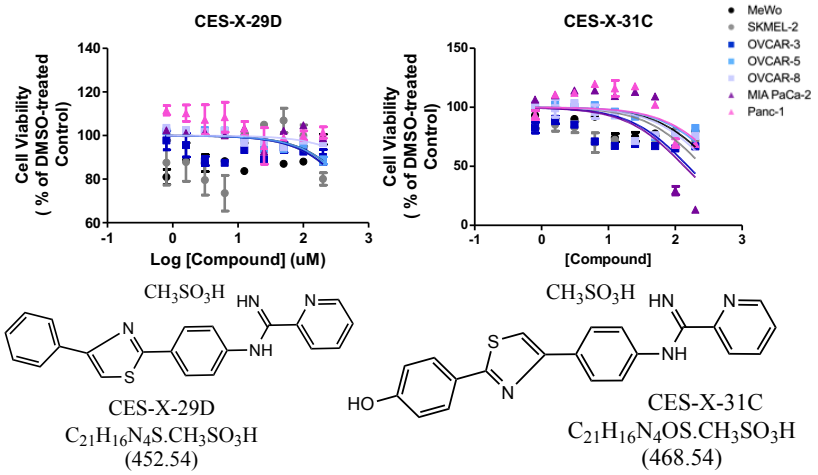

Figure 4.13. CES-X-29D and CES-X-31C cytotoxicity in various cell lines.

Another group of CES-compounds unrelated to CES-IX-38 and CES-IX-49 were tested in melanoma, ovarian and pancreatic cancer cell lines. First, we tested CES-X-12B in melanoma, which contains a thiazole ring, benzene rings, and an imidamide group attached to a pyridine ring. Results showed that this compound effectively reduced cell viability in SKMEL-2 (IC_{50}: 14.42 µM, 95%CI: 9.979 to 20.84), SKMEL-5 (IC_{50}: 13.81 µM, 95%CI: 10.42 to 18.30), A-375 (IC_{50}: 12.61 µM, 95%CI: 9.562 to 16.64) and SB-2 (IC_{50}: 8.883 µM, 95%CI: 5.925 to 13.32), but not in MeWo (IC_{50}: 382.1 µM). Then, we investigated CES-X-31C, which is very structurally similar to CES-X-12B, but contains a terminal hydroxyl group. Results in all cell lines showed that it did not have remarkable cytotoxicity in any cell line tested, with IC_{50} values ranging from 136.6 to 525.4 µM.

Finally, we looked at CES-X-29D, which was also similar to CES-X-12B, but had a flipped thiazole ring. This compound also had very little cytotoxicity in melanoma and ovarian cancer cell lines with an IC_{50} range of 1309 to 3921 μM, and no changes in cell viability whatsoever in pancreatic cancer cells.

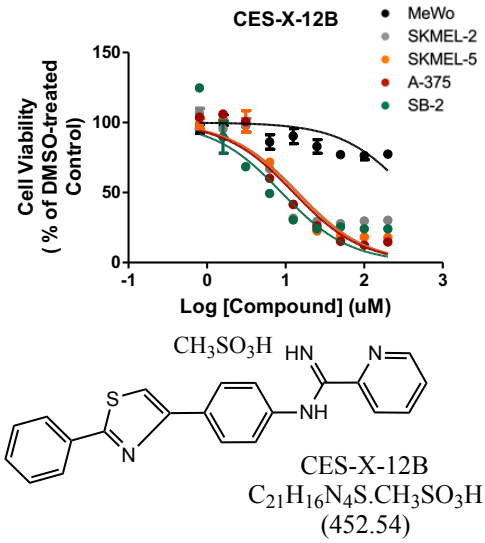

Figure 4.14. CES-X-12B cytotoxicity in various cell lines.

Our next group of 5 compounds also shared a similar backbone with a variable central R_1 group and variable R_2 terminal groups and were tested in 8 melanoma or primary melanocyte cell lines.

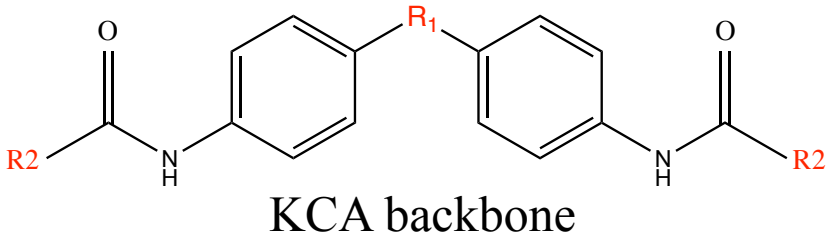

Figure 4.15. KCA backbone. A group of 5 compounds had this backbone structure containing carbonyl and amino group.

LSM-I-95 was investigated first, and contained a central oxide group at the R_1 position with terminal ethylpyrrolidine rings. It did not show high cytotoxic effects in any

cell line tested, with only SKMEL-5 and all SKMEL-2 (parental, LPAR3wr and 2aa-mutant) cell lines resulting in IC_{50} values under 100 µM (33.54 to 62.96 µM). All other cell lines exhibited IC_{50} values ranging from 146.3 to 574.8 µM. Next, we examined KCA-I-25 and KCA-I-15, which both contained a sulfonyl group at the R_1 position. However, KCA-I-25 had the same ethylpyrrolidine terminal group while KCA-I-15 had

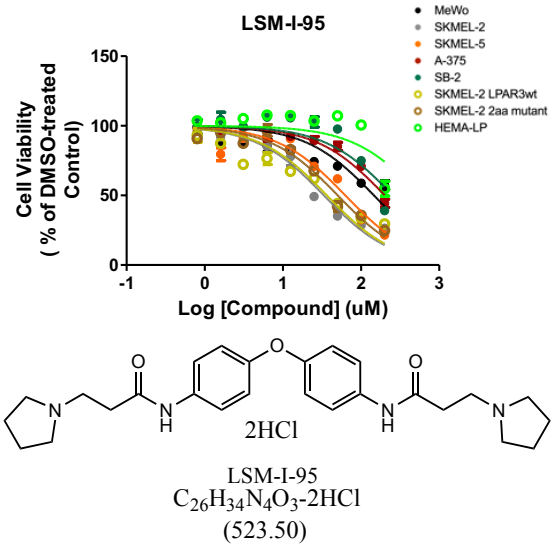

Figure 4.16. LSM-I-95 cytotoxicity in various cell lines.

a methylpyrrolidine terminal group. KCA-I-25 was similarly ineffective in all the cell lines as LSM-I-95, with IC_{50} values ranging from 70.59 to 630.1 µM. However, KCA-I-15 was more moderately cytotoxic in the 5 melanoma cell lines tested (MeWo, SKMEL-2, SKMEL-5, A-375 and SB-2) with IC_{50} values between 34.11 to 99.06 µM. Therefore, the addition of the central sulfonyl group to KCA-I-25 was ineffective at reducing cell viability, and so was shortening the terminal group pyrrolidine ring attachment.

We next examined KCA-I-27 and KCA-I-08, which both also contained the central sulfonyl group. KCA-I-27 had a terminal dimethyl amino group, and did not exhibit remarkable cytotoxicity in any cell line, with IC values ranging from 87.3 to

603.7 µM. KCA-I-08 had a terminal pyridine ring, and instead of the propanamide group leading to the terminal end, it contained the imidamide group previously seen in the DB-related compounds.

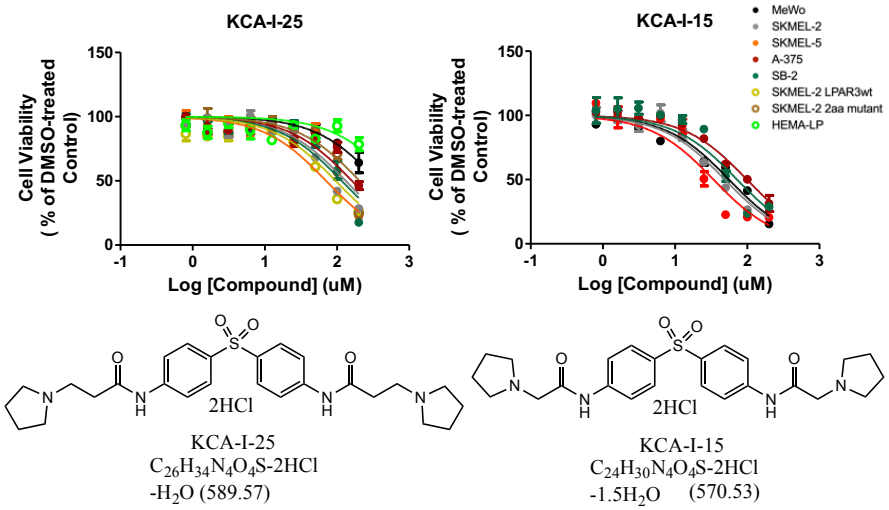

Figure 4.17. KCA-I-25 and KCA-I-15 cytotoxicity in various cell lines.

This change did not result in reduced cell viability, A-375 resulted in no change, whereas the other cell line IC_{50} values were between 260.9 to 1435 µM. In conclusion, this group of KCA compounds were not effective, even with various functional group changes, in reducing cell viability in melanoma and melanocyte cell lines.

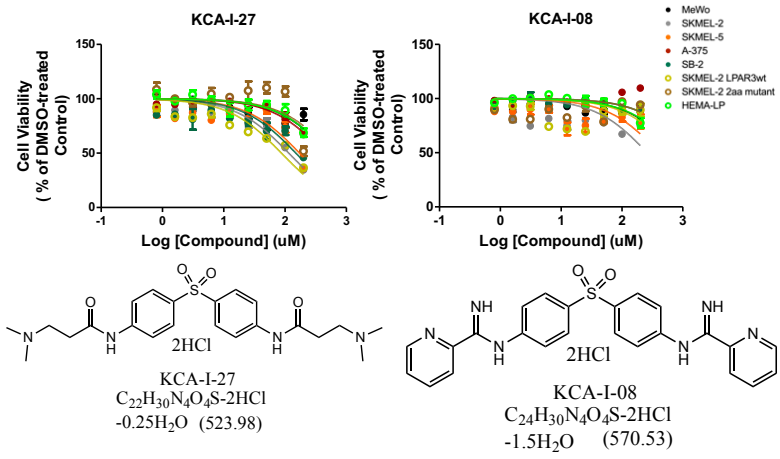

Figure 4.18. KCA-I-27 and KCA-I-08 cytotoxicity in various cell lines.

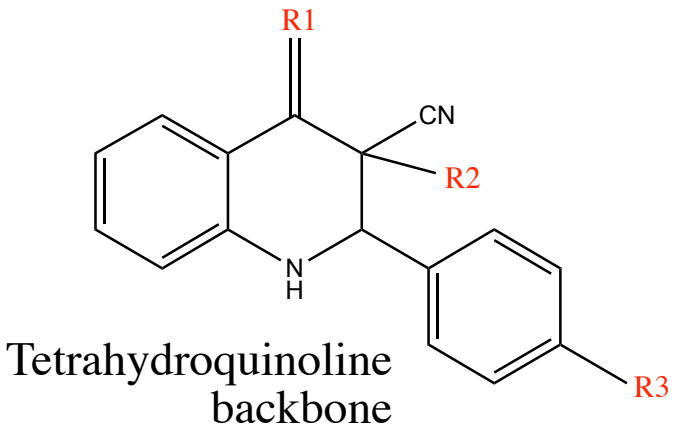

Figure 4.19. Tetrahydroquinoline backbone. A group of 6 compounds shared a similar backbone with a tetrahydroquinoline backbone attached to two benzene rings and variable functional group.

The final group of 6 compounds that had similar structures were tested only in melanoma cell lines, and contained a backbone of a tetrohydroquinoline structure with a branching benzene ring with three areas of variable groups. Functional groups at R_1, R_2, and R_3 positions were modified one at a time to determine if subsequent replacements were able to increase the cytotoxic effects in melanoma cells.

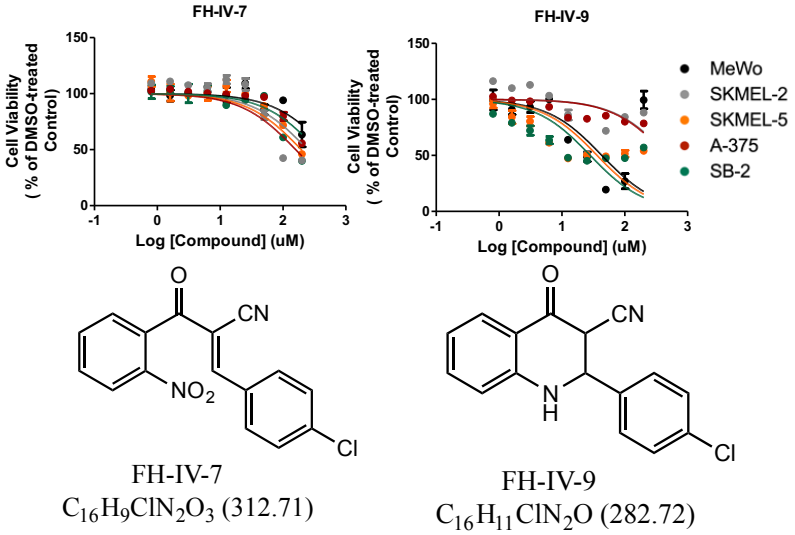

Figure 4.20. FH-IV-7 and FH-IV-9 cytotoxicity in various cell lines.

However, the first compound in this series, FH-IV-7, did not have a complete tetrohydroquinoline ring, but instead a nitrite in its place and was considered as a precursor to the backbone depicted above. The R_1 position contained a carbonyl group and R_3 a chlorine group, with no side chain at the R_2 position. FH-IV-7 did not show impressive cytotoxicity in any melanoma cell line, with IC_{50} values between 159.1 to 514 µM. Then, we tested FH-IV-9, which closed the nitrite group into a ring and therefore had the backbone tetrohydroquinoline backbone structure, making it structurally very similar to FH-IV-7. FH-IV-9 had much greater, but moderate, cytotoxic effect in MeWo (IC_{50}: 43.24 µM), SKMEL-5 (IC_{50}: 36.33 µM) and SB-2 (IC_{50}: 28.24 µM), but showed no improvement in SKMEL-2 (IC_{50}: 489.7 µM) and A-375 (IC_{50}: 468.6 µM).

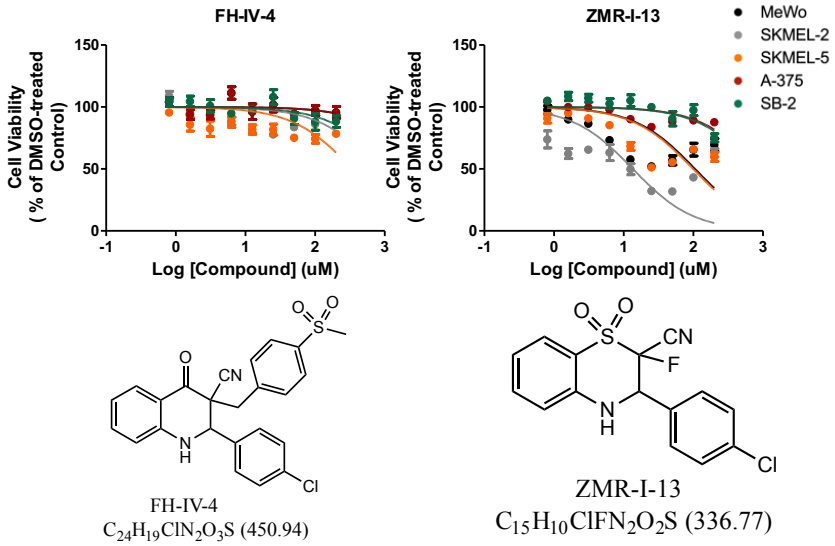

Figure 4.21. FH-IV-4 and ZMR-I-13 cytotoxicity in various cell lines.

To optimize and increase the moderate cytotoxicity observed in FH-IV-9, we then tested FH-IV-4, which was very similar to its precursor, but contained a methylsulfonyl-attached benzene ring at the R_2 position. This resulted in a much weaker cytotoxic effect in all cell lines, with IC_{50} values ranging from 343.3 to 3657 µM. We then tested another

variation of FH-IV-9 named ZMR-I-13, which contained a sulfonyl group instead of a carbonyl group on the tetrohydroquinoline structure, and a fluorine group at the R_2 position, while maintaining the R_3 chlorine. ZMR-I-13 had improved cytotoxicity compared to FH-IV-4, with the most notable effect in MeWo (IC_{50}: 13.55 µM, 95%CI: 7.125 to 25.76). Other cell lines had IC_{50} values between 99.11 to 901.9 µM, showing only somewhat moderate to little reduction in cell viability. Since the change to the R_1 sulfonyl group resulted in an impressive increase in cytotoxicity, especially in MeWo cells, we then tested two compounds that preserved this functional group.

RP-I-15 contains the same functional groups as ZMR-I-13 at the R_1 and R_3 positions, but the fluorine at R_2 was replaced with a benzene ring with an attached fluorine group, moving this atom further away from the backbone structure. Once again, this resulted in a reversal of cytotoxic effects, as A-375 cells exhibited no response to the

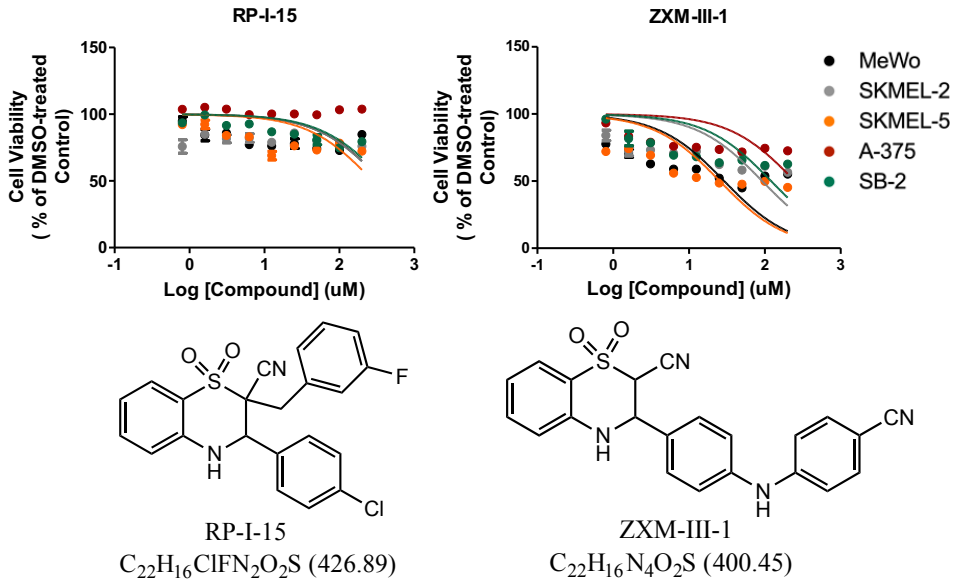

RP-I-15
$C_{22}H_{16}ClFN_2O_2S$ (426.89)

ZXM-III-1
$C_{22}H_{16}N_4O_2S$ (400.45)

Figure 4.22. RP-I-15 and ZXM-III-1 cytotoxicity in various cell lines.

compound, while others responded poorly with IC_{50} values between 280.1 and 412 µM. Finally, we tested ZXM-III-1, which maintained the R_1 sulfonyl group and had no

functional group at the R_2 position, but had a diphenylamino side chain with a cyanide group at the terminal end. Similar to FH-IV-9, ZXM-III-1 was able to effectively decrease cell viability in MeWo (IC_{50}: 29.17 µM, 95%CI: 15.79 to 53.89) and SKMEL-5 (IC_{50}: 25.5 µM, 95%CI: 14.61 to 44.52), albeit to only a moderate extent. SKMEL-2, A-375 and SB-2 did not show a remarkable decrease in viability, with IC_{50} values between 92.46 and 249.1 µM. Therefore, while none of the compounds with the tetrohydroquinoline backbone were particularly impressive overall, we did observe high cytotoxicity with ZMR-I-13 in MeWo, so this compound may be a future candidate for optimization.

The final four structures we tested in this study were not structurally similar to each other or any other group discussed previously. We first received CES-I-83 and WAB-I-81b for testing in melanoma cell lines. The structure of CES-I-83 contains fused

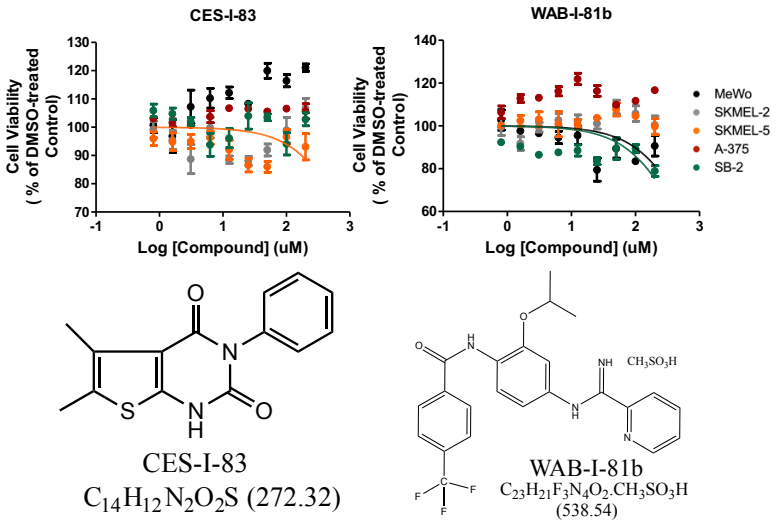

Figure 4.23. CES-I-83 and WAB-I-81b cytotoxicity in various cell lines.

theinopyrimidine and pyridine rings with an addition phenyl side chain stemming from the pyridine ring. This compound did not perform well in the melanoma cell lines tested, with all cell lines showing no change in cytotoxicity except SKMEL-5, which had an IC_{50}

value of 1560 µM. WAB-I-81b was a more complicated structure with a trifluoromethyl functional group, isopropoxy group, and imideamide group among other features. It also did not perform remarkably well in melanoma cells with only MeWo and SB-2 showing very little cytotoxicity at IC_{50} values of 874.1 and 609.7 µM respectively, while SKMEL-2, SKMEL-5 and A-375 were unaffected by treatment. Therefore, neither of the first two standalone compounds tested were particularly effective in melanoma cells.

The next two compounds were not structurally similar to any others in this study and tested in melanoma, ovarian and pancreatic cancer to address the issue that we were not possibly not looking beyond a specific model of cytotoxicity. First, we investigated ACB-III-172, which is related to the previously presented ACB compounds in the sense

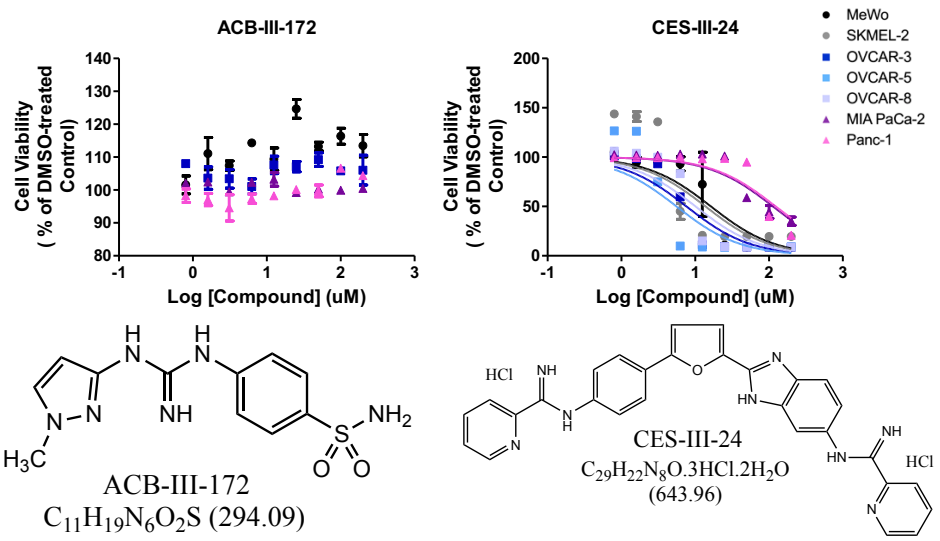

Figure 4.24. ACB-III-172 and CES-III-24 cytotoxicity in various cell lines.

that it is half the symmetrical structure as seen in the ACB family with the terminal methyl-pyrazole ring and guanidine group and then a sulfonamide group on the opposite terminal. However, this "half" version of the other ACB family did not result in any cytotoxic effect in all cell lines tested. Next, we examined CES-III-24, which is similar to

the CES-IX-38 and CES-IX-49 compounds in the sense that it has a furan ring and benzene ring on one half of the structure, but the right half has a benzoimidazole, with both terminal ends housing the imidamide-pyridine structure observed in CES and DB compounds previously in this study. CES-III-24 did not effectively reduce cell viability in pancreatic cancer cell lines (IC_{50} range: 113-1 to 123.4 μM), but performed surprisingly well in other cell lines. MeWo (IC_{50}: 16.34 μM, 95%CI: 9.497 to 28.12) and SKMEL-2 (IC_{50}: 13.79 μM, 95%CI: 5.967 to 31.86) exhibited slightly lower cytotoxic effects than OVCAR-3 (IC_{50}: 7.661 μM, 95%CI: 5.331 to 10.87), OVCAR-5 (IC_{50}: 5.584 μM, 95%CI: 2.931 to 10.64) and OVCAR-8 (IC_{50}: 10.12 μM, 95%CI: 6.502 to 15.74). Therefore, although it was essentially not as similar to other CES compounds as other variants were, CES-III-24 resulted in some impressive cytotoxic effects in melanoma and ovarian cancer cell lines.

In Vivo Tumor Inhibition Studies with Candidate Compounds

Due to the success of certain compounds in our *in vitro* studies, we decided to examine their ability to inhibit tumor growth in established xenografts. We established melanoma xenografts in athymic nude mice using MeWo cells, and allowed them to grow for approximately 3 weeks before commencing injections. We chose CES-IX-49 for this study, since it had an IC_{50} value of 11.73 μM in MeWo cells, a xenograft model that was previously established and optimized in our laboratory. Mice were dosed with a vehicle control, 5, 12.5 or 25 mg/kg of CES-IX-49 weekly. The 5 mg/kg dosing group received subcutaneous injections due to the widespread dissemination of CES-IX-49 through this route of administration, while the 12.5 and 25 mg/kg doses was administered intra-

tumorally to mitigate adverse events at such high doses. At approximately 70 days post tumor induction, mice were euthanized. Results show that tumor growth was significantly reduced in the group receiving 12.5 mg/kg CES-IX-49 (*p=0.0318). The highest dose group at 25 mg/kg did not have any inhibition in tumor growth, possibly due to the rapid growth of the tumors in this group earlier in the study. Mouse weights were also higher in this group, possibly due to the large sizes of the tumors. Adverse events observed with dosing were excessive rheum, shivering and disorientation immediately following dosing.

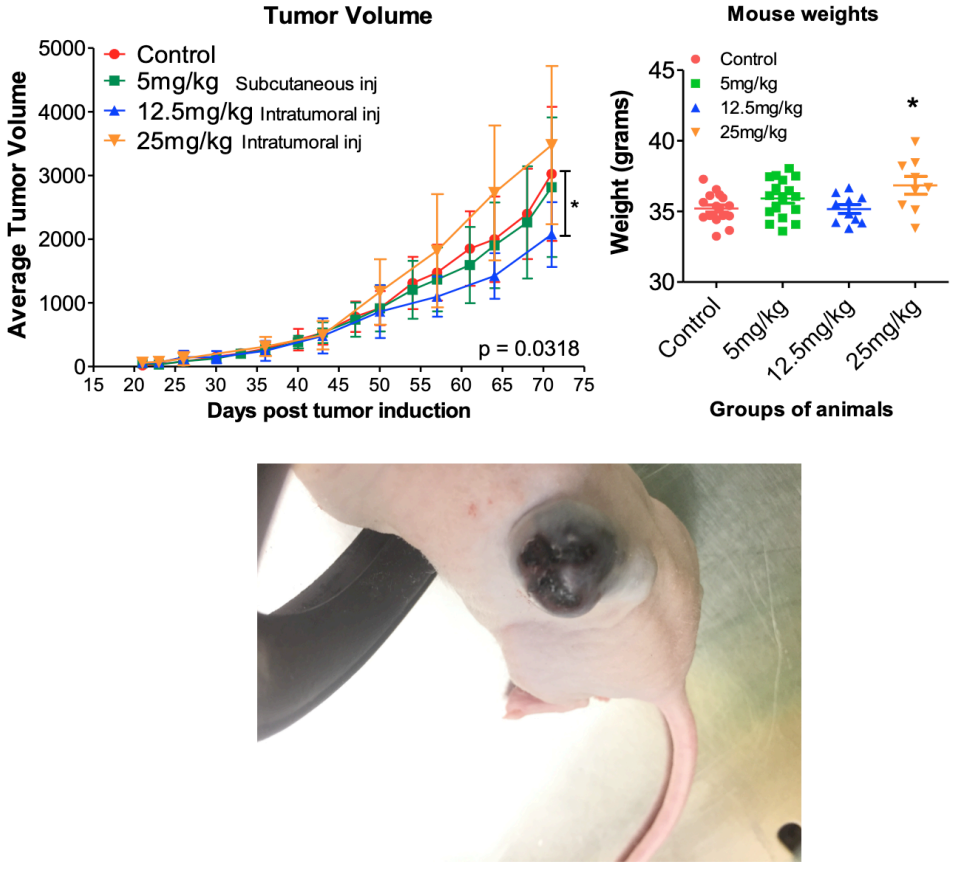

Figure 4.25. *In vivo* studies with a melanoma xenograft model to test the ability of CES-IX-49 to inhibit tumor growth. Over the course of 70 days post-injection of tumor, we were able to observe significant inhibition of tumor growth in the group dosed with 12.5 mg/kg of CES-IX-49. Mouse weights also remained healthy throughout the study. Tumors were injected at the back flank and were black in color due to the melanin.

Discussion

During the course of this study, we explored the cytotoxic effects of 34 compounds in 13 cell lines derived from melanoma, ovarian cancer and pancreatic cancer origins. Of the 34 compounds obtained, many could be segregated into groups based on structural similarity, allowing us to deduce more simply which functional group changes could be responsible for changes in cytotoxic activity. Several parent compounds, which represent the structure that subsequent compounds were derived from in a particular subset, have shown to have broad relevance as cytotoxic agents in the anti-microbial field against parasites such as the *Leishmania* or *Trypanosoma* species. Therefore, our results strived to show how modifications to the structure of compounds studied for their anti-parasitic activity could influence their capacity to reduce cell viability in cancer cells.

First, we explored the pentamidine-derived compound subset, which broadly included 14 compounds that were analogues of pentamidine derivatives or structural modifications of said analogues. The closest relative to pentamidine, CES-V-19, only had moderate cytotoxicity in melanoma cell lines MeWo and SKMEL-2. Of the next nine compounds that were analogues of the pentamidine derivative furamidine named DB766, CES-IX-49 showed remarkable cytotoxicity in all melanoma cell lines tested, but not as pronounced of an effect on ovarian or pancreatic cancer cell lines. Additionally, among five of the nine DB766-related compounds, which were also named with the DB-prefix, DB1856 had an even more pronounced reduction in cell viability in not only melanoma cell lines, but also ovarian cancer cell lines. With IC_{50} values ranging between 1.341 to 10.04 μM across the melanoma and ovarian cell lines, DB1856 treatment yielded the lowest observed μM IC_{50} concentrations in our study overall. Next, we explored another

set DB766 derivatives that contained a guanidine group in place of the imidamide group in their structures. All four compounds tested in this subset had moderate cytotoxic effect in select cell lines, with slightly better results in melanoma and ovarian cancer cell lines. Overall, ACB-III-163 had the lowest IC_{50} values ranging from 6.829 to 15. 63 μM across all cell lines.

The remaining 14 compounds tested in this study were derived from various parent structures, some of which are not well recognized in the literature, but have been grouped into subsets for the sake of consolidating preliminary structure-activity that may be distinguishable. Two compounds, ZAM-II-41 and RAH-A-2, that shared a dihydropyrrole-quinazoline backbone had little effect on melanoma cell lines, although their synthesis has been previously published and explored for possible anti-tumor activities. Further, among a group of three compounds sharing a complex multi-ring structure containing thiazole, benzene and pyridine rings, CES-X-29D and CES-X-31C showed little activity in melanoma, ovarian cancer or pancreatic cancer cells. However, upon further structural modifications, CES-X-12B within the same subset resulted in moderate cytotoxicity in melanoma cell lines. Next, a subset of KCA-variants, which contain a general backbone of a variable central group flanked by benzene rings and amide groups, were tested in a variety of melanoma cell lines, but overall resulted in moderate cytotoxicity at best, with the front runner compound being KCA-I-15. The next subset of six compounds shared a tetrahydroquinoline backbone, with variations in three possible terminal sites. All compounds exhibited little to moderate capacity in reducing cell viability in melanoma cell lines, with the most notable outcome being the effect of ZMR-I-13 in SKMEL-2 with an IC_{50} of 13.55 μM.

The final subset contained the four remaining compounds, which did not possess any structural similarity to other groups in this study, but did share some characteristics to other compounds tested prior. CES-I-83 and WAB-I-81b exhibited very little cytotoxicity, while ACB-III-172 resulted in no cytotoxicity in any cell line tested. However, CES-III-24, which is asymmetrical, but similar on one end of its structure to compounds derived from DB766, resulted in a notable reduction in cell viability in melanoma and ovarian cancer cell lines, but not in pancreatic cancer cells. IC_{50} values for this compound among melanoma and ovarian cancer ranged from 5.584 to 16.34 μM, which are comparable to other members of the DB-subset.

Due to its effectiveness in our *in vitro* studies, CES-IX-49 was further explored in a pilot *in vivo* study with MeWo tumor xenografts. Weekly CES-IX-49 treatment at 12.5 mg/kg in immune-deficient nude mice resulted in a significant inhibition of tumor growth, although the 25 mg/kg group resulted in the largest tumors of the study. This could be due to the insufficient dosing and frequency in this group that resulted in unrecoverable growth of the xenografts.

This study has several limitations that are essential to address. Firstly, not every compound we received was tested in all the 13 cell lines available to us. This is in part because we received the compounds periodically over a 30-month period depending on the *in vitro* results we obtained from the previous set of compounds. For example, in the DB-subset, we received DB1855 and DB1943 first, and then obtained DB1856 for testing. Further, we did not receive DB1931 or DB1908 until the results for DB1856 were deemed remarkable. Secondly, we did not explore further modifications in some subsets of compounds that were structurally similar when initial testing did not show notable

cytotoxicity. This was due to one of many reasons such as achieving a stable synthesis of modified compounds with high purity and the availability of enough compound required for testing across multiple cell lines. It is also possible that more modification of some of the compound subsets will be achieved in the future and provide us the opportunity to continue optimizing their cytotoxicity. A final limitation of this study is that, despite having tested two candidate compounds *in vivo*, we did not pursue them further to characterize their intracellular targets. Since DB1856 is derived from furamidine-analogs such as DB766 which have established activity as DNA minor groove binders, it is possible that is also a viable possibility for DB1856, and likely gives us a reliable starting point based on previous studies.

Future studies involving the 34 compounds tested here may include exploring more functional group modifications on the structures of compounds that could be optimized further to achieve nanomolar-range cytotoxicity, such as DB1856, which was at approximately 1 μM in MeWo and OVCAR-3 cells. Lower IC_{50} values would help boost the clinical relevancy of its successor and further explore it in *in vivo* studies in comparison with DB1856 itself. Additionally, we could perform a microarray to determine the targets of candidate compounds such as CES-IX-49 or DB1856, and any others that in future studies may have strong cytotoxic effects. This would allow us to look beyond the suggested targets in literature of these compounds and possibly find additional proteins or markers that would result in the compound having an additive cytotoxic effect. We could also pursue structurally modified versions of compounds that did not belong to any subset in this study such as CES-I-83, WAB-I-81b, ACB-III-172 and CES-III-24. Especially since CES-III-24 exhibited high cytotoxic effects comparable

to CES-IX-49 in melanoma and ovarian cancer cell lines, and it is possible that it's unique asymmetrical structure is responsible for this effect. Finally, once targets have been determined, we can also pursue combination treatments *in vitro* or *in vivo*. If we were to perform combination treatments in animals, we would have to thoroughly characterize adverse events of all compounds involved in a preliminary xenograft study to minimize side effects during the combination study, and ensure the mice suffer minimally.

Supplementary tables

*N/R = no response

Table II. IC_{50} values of compounds tested in melanoma cell lines (μM)

	SB-2	MeWo	A375	SK-MEL-5	SK-MEL2 parental	SK-MEL-2 LPA3wt	SK-MEL-2 2aa mutant	HEMA-LP
ACB-III-161		15.11						
ACB-III-163		6.829						
ACB-III-172		N/R*						
ACB-III-175		7.586						
CES-I-83	N/R*	N/R*	N/R*	1560	N/R*			
CES-II-50		N/R*			27.22			
CES-III-24		16.34			13.79			
CES-IV-16		N/R*			27.59			
CES-IX-38	6.41	347.80	19.12	64.07	8.48	10.55	21.82	18.03
CES-IX-49	2.71	11.73	10.39	4.43	2.87	6.72	6.75	6.16
CES-V-19		22.08			N/R*			
CES-VI-14		30.31			12.1			
CES-X-12B	8.83	382.1	12.61	13.81	14.42			
CES-X-29D		1515			260.4			
CES-X-31C		392.9			1309			
DB1855		N/R*			N/R*			
DB1856		1.341			1.877			
DB1908		17.4						
DB1931		12.61						
DB1943		3.118			5.766			
FH-IV-4	1199	21491	2044	343.80	827.00			

FH-IV-7	195.3	202.9	350.9	247.4	159.1			
FV-IV-9	28.24	32.22	468.6	36.33	489.7			
KCA-I-08	1435	869.5	N/R*	413.6	1645	5432	N/R*	900.6
KCA-I-15	72.23	55.93	99.06	34.11	49.81			
KCA-I-25	116.1	365.2	206	131.9	262.8	116	181	630.1
KCA-I-27	150.2	526.4	442.2	172.2	133.1	239.3	305	531
LSM-I-95	255.2	146.3	201.9	62.95	39.37	52.35	41.58	574.8
RAH-A-2	3184	296	N/R*	84.35	364.4			
RP-I-15	412	369.8	N/R*	280.1	368.5			
WAB-I-81b	N/R*	874.1	N/R*	609.7	N/R*			
ZAM-II-41	2639	1316	N/R*	1176	N/R*			
ZMR-I-13	823.10	106.10	901.90	99.11	13.55			
ZXM-III-1	121.1	85.39	249.1	25.5	92.46			

Table III. IC_{50} values of compounds tested in ovarian cancer cell lines (µM)

	OVCAR-3	**OVCAR-5**	**OVCAR-8**
ACB-III-161	16.59		
ACB-III-163	7.362		
ACB-III-172	N/R*		
ACB-III-175	5.531		
CES-I-83			
CES-II-50	1843	827.3	124.8
CES-III-24	7.611	5.584	10.12
CES-IV-16	1802	N/R*	1802
CES-IX-38			

CES-IX-49	15.23		
CES-V-19	75.65	387.4	75.65
CES-VI-14	39.36	13.24	62.84
CES-X-12B			
CES-X-29D	39.21	1500	3921
CES-X-31C	345.7	478.1	345.7
DB1855	408.7	1668	N/R*
DB1856	1.954	10.04	1.482
DB1908	13.78	23.39	10.92
DB1931	20.51	162.8	14.79
DB1943	9.74	28.6	30.35
FH-IV-4			
FH-IV-7			
FV-IV-9			
KCA-I-08			
KCA-I-15			
KCA-I-25			
KCA-I-27			
LSM-I-95			
RAH-A-2			
RP-I-15			
WAB-I-81b			
ZAM-II-41			
ZMR-I-13			
ZXM-III-1			

Table IV. IC_{50} values of compounds tested in pancreatic cancer cell lines (μM)

	MIA Paca-2	Panc-1
ACB-III-161	21.21	29.92
ACB-III-163	12.64	15.63
ACB-III-172	N/R*	N/R*
ACB-III-175	15.98	15.44
CES-I-83		
CES-II-50	N/R*	3298
CES-III-24	113.1	123.4
CES-IV-16	N/R*	639.2
CES-IX-38		
CES-IX-49	13.53	62.15
CES-V-19	21851	215.3
CES-VI-14	298	291.1
CES-X-12B		
CES-X-29D	N/R*	N/R*
CES-X-31C	136.6	525.4
DB1855	N/R*	327.4
DB1856	41	19.96
DB1908	25.61	47.78
DB1931	203.7	249.8
DB1943	49.42	13.19
FH-IV-4		
FH-IV-7		
FV-IV-9		
KCA-I-08		

KCA-I-15		
KCA-I-25		
KCA-I-27		
LSM-I-95		
RAH-A-2		
RP-I-15		
WAB-I-81b		
ZAM-II-41		
ZMR-I-13		
ZXM-III-1		

CHAPTER V

INVESTIGATING THE CYTOTOXIC EFFECTS OF NOVEL FURAMIDINE-RELATED COMPOUNDS IN MELANOMA, OVARIAN CANCER AND PANCREATIC CANCER

Sudeepti S. Kuppa, Wei Jia, and Mandi M. Murph

Under review at Journal of Infection and Chemotherapy

Abstract

Diamidine-related compounds such as pentamidine and furamidine have been extensively studied and used for their therapeutic efficacy in anti-parasitic and anti-fungal effects. DB766, a close relative of furamidine, has been shown to anti-infectious properties, but has also been investigated previously as a potential chemotherapeutic agent against Chagas disease. The objective of this study is to explore the cytotoxicity of four compounds derived from DB766, originally explored for their anti-microbial activity, in melanoma, ovarian and pancreatic cancer *in vitro* and with nude athymic mouse models of cancer *in vivo*. Based on a preliminary structure-activity relationship derived from terminal end groups of the four compounds, we uncovered one candidate that was best suited for a xenograft tumor model in athymic nude mice. DB1856 exhibited IC_{50} values in the ~1 μM range in MeWo (melanoma) and OVCAR-3 (ovarian cancer cells) upon 48 hours of treatment and contained a terminal pyrazole group that appears to be responsible for its ability to effectively reduce cell viability. *In vivo* experiments showed that while OVCAR-3 xenografts did not respond to DB1856, MeWo tumors exhibited significant (**$p<0.01$) tumor growth inhibition for up to 13 weeks of weekly treatment. Further tumor tissue analysis revealed the connection of DB1856 with several DNA damage and cell death proteins, indicating a possible mechanism of action. We posit that DB1856 might be the first furamidine-derivative to be cytotoxic in melanoma models *in vivo* and therefore could have relevancy as a small molecule treatment in this capacity, possibly enhancing cytotoxic compound options for melanoma.

Introduction

The goal of this study was to determine the preliminary structure-activity relationship of 34 potentially cytotoxic compounds in 13 cancer cell lines of melanoma, ovarian and pancreatic cancer origin. The structure of four of the 34 compounds share a similar backbone containing a furan ring flanked by benzene rings with 2-propoxy functional groups. However, the terminal functional groups differ between each compound to result in DB1855, DB1943, DB1931 and DB1856, and we have been able to determine the influence of these various functional groups related to cytotoxicity in cancer cells.

To understand the cytotoxic relevance of these four compounds on cancer cells, we explored their origin and therapeutic relevance in other fields. Diamidines, especially pentamidine, are compounds commonly utilized as anti-microbial agents against pneumonia, African trypanosomiasis, and other fungal or parasitic diseases (398-400). Moreover, diamidine compounds have the ability to target and inhibit epigenetic protein arginine methyl transferases (PRMTs), which are becoming increasingly relevant in cancer therapy (414). DB75, or furamidine, is a well-known aromatic diamidine which has shown both anti-parasitic activity, and some relevance to cytotoxic activity in cancer cells, as is characteristic of aromatic diamidines in previous studies (402, 414, 415). The four compounds in our study are derived from DB766 (2,5-Bis[4-amino-2-(2-propoxy)phenyl]furan) which belongs to a class of furamidine analogues known as arylimidamides (401, 416).

These compounds were originally synthesized as DNA minor groove binders, which have been extensively studied cancer biology and other fields as regulators of

global gene expression changes and inhibitors of chromosome condensation for mitosis (400, 404). DNA minor groove binders can be utilized against cancer cells in a similar fashion to chemotherapy, which also binds DNA (403). Furamidine, a cytotoxic agent in cancer cells, is also a DNA minor groove binder and has been shown to bind both nuclear and mitochondrial DNA (417). Further, it is a PRMT1 inhibitor and been shown to reverse epithelial-mesenchymal transition, a process employed by various cancer cell types to become more invasive (418, 419). In fact, DB766 itself has been studied as a chemotherapeutic agent effective in Chagas disease treatment (416).

Our results have shown that changes in terminal functional groups of these DB766 derivatives can directly impact cytotoxic activity in melanoma, ovarian cancer and pancreatic cancer cells. For example, replacing the thiazole-attached acetyl group on DB1931 with a methyl group to create DB1943 significantly reduced cell viability in melanoma and pancreatic cancer cell lines, some at low μM ranges. Through our testing, DB1856 was exhibited the greatest cytotoxic effects *in vitro* and was therefore tested in an ovarian cancer and melanoma xenograft mouse model. Results showed no effects in the ovarian cancer model, but we observed significant tumor growth inhibition in the melanoma model over the course of 13 weeks.

Further, we were able to perform reverse-phase protein array analysis on tumor tissue that was untreated and treated with DB1856 and found changes in protein expression that suggest that DB1856 may be a DNA-binding agent as suggested by its compound lineage. In conclusion, the compounds investigated in this study, all derived from furamidine analogs and directly related to DB766, may have significant therapeutic relevance in cancer and could possibly also be DNA binders. In particular, DB1856 is an

interesting small molecule with the potential to be further investigated for therapeutic relevance, especially in melanoma.

Materials and Methods

Cell Lines and Compounds

Cell lines for this study were obtained from ATCC (Manassas, VA, USA) and grown in the appropriate medium, such as RPMI or DMEM (Corning, Corning, NY, USA) supplemented with 10% fetal bovine serum (FBS) (Atlanta Biologicals, Flowery Branch, GA, USA) and Penicillin/Streptomycin (Thermo Fisher, Waltham, MA, USA) and placed in a humidified atmosphere of 5% CO_2 at 37ºC. Cell lines utilized were derived from pancreatic cancer (MIA PaCa-2 and Panc-1), ovarian cancer (OVCAR-3, OVCAR-5 and OVCAR-8) and melanoma (HEMA-LP, SB-2, MeWo, A-375, SK-Mel-5, SK-Mel-2, SK-Mel-2 LPAR3wt, SK-Mel-2 2aa mutant) origins. The latter two melanoma cells, SK-Mel-2 LPAR3wt and SK-Mel-2 2aa mutant, were generated from SK-Mel-2 parental cells in the laboratory as previously described (410). All cell lines were maintained below 15 passages for all *in vitro* experiments.

Compounds were synthesized from DB766 (furamidine analog) as previously described (401). Compounds were received in powder form from Augusta University and resuspended in dimethyl sulfoxide (DMSO) (Corning) to yield a 100 μM solution and stored at -20ºC in glass vials covered with aluminum foil to avoid light exposure. 34 compounds were tested in 13 cell lines and those with the highest efficacy determined by the lowest IC_{50} concentration were considered as candidates for *in vivo* studies. DB1856, the candidate compound in this study was evaluated for its physiochemical properties

using ChemDraw Professional (Perkin Elmer, Waltham, MA, USA) and MarvinSketch (ChemAxon, Budapest, Hungary).

***In vitro* treatment with compounds and cell viability assay**

Cell lines were plated in 96-well plates at a density of 4,000-7,000 cells per well (~50% confluency) depending on cell size. The following day, the cells were serum starved overnight with either RPMI or DMEM containing penicillin-streptomycin, but lacking FBS. This allows for all cells to be arrested in the G_1 cell cycle phase, which results in a more pronounced and accurate effect of subsequent treatment that is also unaffected by counteracting growth factors in the medium. Following serum starvation, cells were treated with varying concentrations of the compounds as follows, with 0.2% DMSO as the control condition: 0.8, 1.6, 3.1, 6.25, 12, 25, 50, 100, 200μM, to adhere to a log scale of treatment that would help us determine a dose response with a wide range of compound concentrations. Treated plates were placed back in the incubator at 5% CO_2 at 37ºC for 48 hours. Following the incubation, cells were treated with Cell Titer Blue Cell Viability Assay (Promega, Madison, WI, USA) for 4-6 hours. A change in color of the Cell Titer Blue solution from blue to pink indicates the presence of viable cells and their ability to metabolize Resazurin to Resorufin, a fluorescent dye. The SpectraMax M2 Plate Reader (Molecular Devices, Sunnyvale, CA, USA) was then used to detect florescence as a measurement of cell viability.

Absorbance values for compound-treated groups were compared to the DMSO-treated control group and cell viability was calculated as a percentage of control group cells using Microsoft Excel. Then, GraphPad Prism 7 was used to transform the values to

log-based compound response in cells, and a non-linear regression line was drawn to determine IC_{50} values for each compound treatment. Each compound was tested in triplicate to confirm accuracy of cytotoxic effects. Based on comprehensive *in* vitro compound testing, it was determined that DB1856 had the highest efficacy (lowest IC_{50}) compared to all other compounds tested and therefore chosen for further *in vivo* studies.

***In vivo* xenograft studies**

All animal work performed in this study was approved by the University of Georgia's Institutional Animal Care and Use Committee (IACUC). Animals for the xenograft study were ordered from Jackson Laboratories (Bar Harbor, ME, USA). The mouse (*Mus musculus*) strain selected was Nu/J or athymic nude mice. These mice have a defective thymus epithelium and therefore cannot produce T-cell responses and lack immunity, but have a partial B-cell response, creating an ideal environment for tumor xenograft growth. All mice were male and approximately 8 weeks old on the day of tumor induction.

To create tumor xenografts in mice, MeWo and OVCAR-3 cells were revived from liquid nitrogen storage and cultured in 10% RPMI with 10% fetal bovine serum (FBS) (Atlanta Biologicals) and Penicillin/Streptomycin (Thermo Fisher). Cells were grown in 15cm dishes and harvested and counted for injection. To embed the cells into the collagen matrix required for xenograft development, HyStem-C Hydrogel matrix was ordered (ESI Bio, Alameda, California) and the cell-hydrogel matrix was prepared per supplied protocol.

Animals receiving injections were segregated into cohorts of 5 per treatment

group and anesthetized using 2-4% isoflurane in a nose cone and allowed to naturally revive following injection and monitored for discomfort. For animals receiving MeWo injections, 1 million cells embedded in hydrogel were injected in the back flank subcutaneously, in a total volume of 125-150uL. For animals receiving OVCAR-3 injections, 5 million cells were embedded in hydrogel and injected intraperitoneally also in a total volume of 125-150uL. Mouse weights were recorded and animals were monitored over the next 2-3 weeks for tumor development at or near the injection site. Mice maintained a healthy 25-30g weight throughout the study.

Animal dosing and tumor growth

Tumor xenografts for MeWo (melanoma) OVCAR-3 (ovarian) tumors appeared around 14 days following injection of cells. Based on IC_{50} data from *in vitro* experiments, mice with MeWo tumors were dosed at 7.5mg/kg and those with OVCAR-3 tumors were dosed at 5mg/kg and 10mg/kg of DB1856 prepared in 5% DMSO and 95% sterile, UltraPure DNase/RNase-free Distilled Water (Invitrogen, Carlsbad, CA, USA). These concentrations were used based on the IC_{50} values for the compounds and the route of administration to minimize systemic adverse events but still expect a reduction in tumor growth. The mice in the control group receiving no compound were given a solution of 5% DMSO and 95% sterile, UltraPure DNase/RNase-free Distilled Water only.

Being a pilot *in vivo* study for DB1856, dosing adjustments were made as necessary as the study progressed. Being a pilot *in vivo* study for DB1856, dosing adjustments were made as necessary as the study progressed. Due to adverse events, the OVCAR-3 group receiving 10mg/kg of DB1856 were dosed only once per week and

reduced to 9mg/kg after the first week of treatment. Adverse events included injection site redness and swelling, and an injection site wound in certain mice. OVCAR-3 mice receiving both the 5mg/kg and 9mg/kg DB1856 dosing were euthanized 55 days after the tumor injection due to rapid metastatic disease spread.

MeWo mice receiving 7.5mg/kg of DB1856 were also dosed once per week and experienced similar adverse events as OVCAR-3 xenograft mice, such as injection site swelling, redness and wounds. The MeWo xenograft mice were euthanized 92 days following the tumor injection. Tumor sizes and mouse weights was measured twice a week to monitor changes and health of all mice. Serum, organs and tumors were collected and stored in liquid nitrogen upon necropsy for future RNA and protein analysis.

Investigators performing data analysis were not blinded to the groups or animals representing the treatment or control groups in order to ensure the treatment groups in mice were receiving adequate post-injection care. No data was omitted from the findings in this study.

Reverse phase protein array (RPPA) analysis of tumor tissue

Tumor tissue frozen in liquid nitrogen immediately after harvesting from animals. Melanoma tumor tissue, both untreated and treated with DB1856, was protein extracted using RIPA Lysis and Extraction Buffer containing Protease/Phosphatase Inhibitor Cocktail (100x) (Thermo Fisher) after homogenization using liquid nitrogen. Tissues in lysis buffer were shaken on ice for 30 min prior to sonication and centrifugation at 13,000 rpm for 10 minutes. Protein supernatant was collected and quantified using the Pierce BCA Protein Assay Kit (Thermo Fisher) as per manufacturer's instructions. Samples

were frozen and sent to MD Anderson Cancer Center's RPPA Core Facility for analysis. Received raw data was analyzed using GraphPad Prism 7 and Microsoft Excel for significant protein expression changes.

Statistics

In vitro data was statistically determined to be significant using the Students T-Test comparing the control, DMSO-treated group to each treated concentration. One-way ANOVA statistical test was used to analyze and determine significance of *in vivo* results involving change in mouse weight and tumor volume over time with a Bonferroni post-hoc test. A confidence interval of 95% with p-values under 0.05 were considered significant. GraphPad Prism 7 and Microsoft Excel were used for data calculations and determination of statistical significance.

Results and Discussion

For this study, we tested 34 compounds in 13 cancer cells of multiple origins to determine cytotoxic candidate compounds for *in vivo* studies that could successfully slow tumor growth. Upon encountering several structurally similar compounds with a common backbone, a furan ring flanked by benzene rings on both sides, with variations occurring on the benzene ring side chains, we then sought to investigate how changing functional groups on this general structure could affect cytotoxicity in cancer cells.

First, we tested DB1855 in melanoma, ovarian cancer, and pancreatic cancer cell lines, which has a pyrazine ring flanking both benzene rings on the backbone **(Fig. 5.1A)**. Results showed that DB1855 had little to no cytotoxic effects on any cancer cell line

(Fig. 5.1B, C, D). Next, we examined the effects of cells treated with DB1931, whose side chains stemming from benzene rings contain thiazole rings and terminal amide groups **(Fig. 5.2A)**. DB1931 treatment resulted in some reduction in cell viability for certain melanoma and ovarian cancer cells such as MeWo, OVCAR-3 and OVCAR-8 **(Fig. 5.2B, C)**. However, pancreatic cancer cell lines, Panc-1 and MIA PaCa-2, exhibited little to no reduction in cell viability except for when exposed to very high concentrations of DB1931 treatment **(Fig. 5.2D)**.

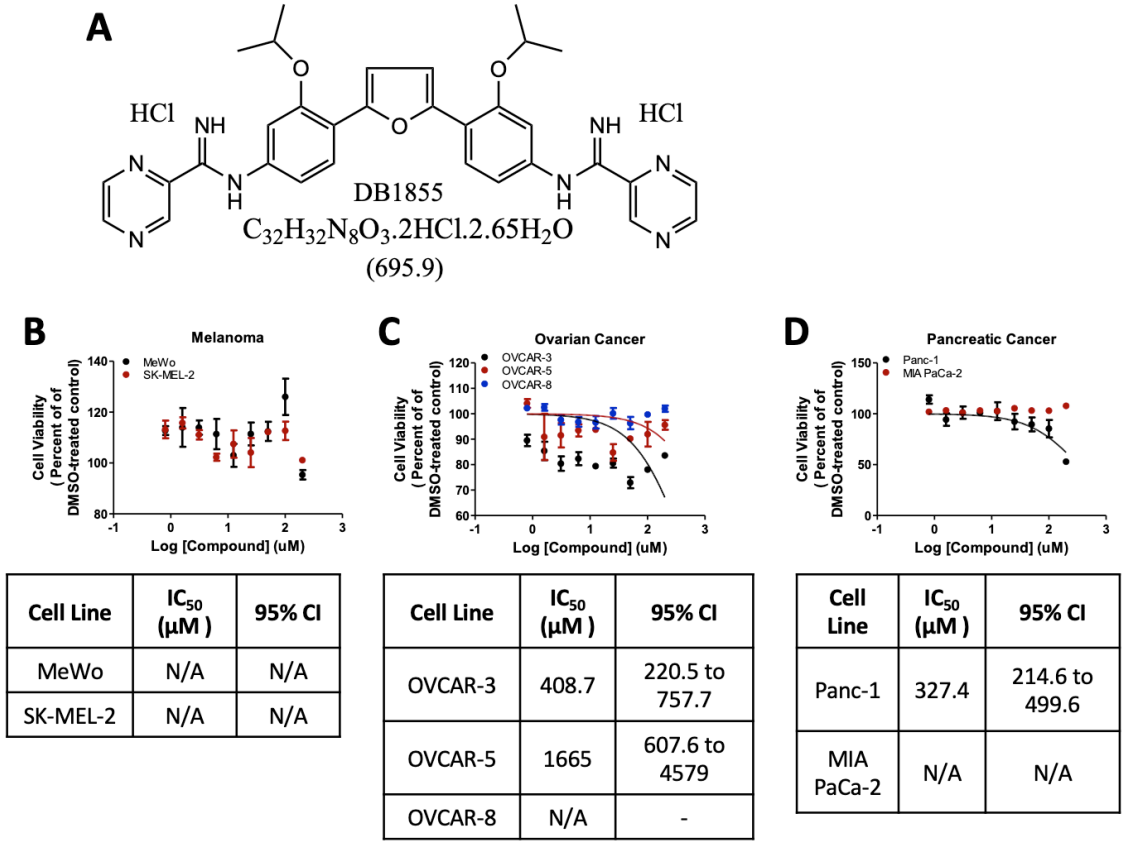

Cell Line	IC_{50} (μM)	95% CI
MeWo	N/A	N/A
SK-MEL-2	N/A	N/A

Cell Line	IC_{50} (μM)	95% CI
OVCAR-3	408.7	220.5 to 757.7
OVCAR-5	1665	607.6 to 4579
OVCAR-8	N/A	-

Cell Line	IC_{50} (μM)	95% CI
Panc-1	327.4	214.6 to 499.6
MIA PaCa-2	N/A	N/A

Figure 5.1. DB1855 cytotoxicity and structure. A) Melanoma cell lines MeWo and SK-MEL-2 exhibited no cytotoxicity upon 48 hours of DB1855 treatment. B) OVCAR-3 and OVCAR-5 showed minute cytotoxicity, while IC50 values for OVCAR-8 indicate there was no cell death with DB1855 treatment. C) Panc-1 and MIA PaCa-2 show little to no cytotoxicity with DB1855 treatment. D) Structure, molecular formula and molecular weight of DB1855.

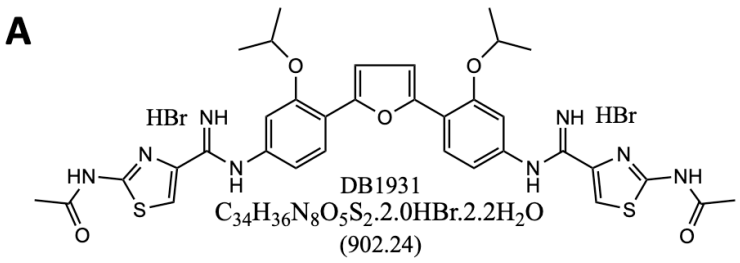

B

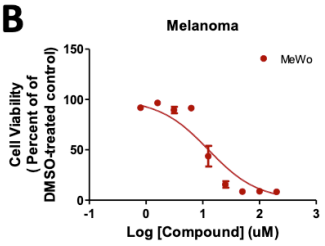

Cell Line	IC_{50} (µM)	95% CI
MeWo	12.61	9.126 to 17.42
SK-MEL-2		

C

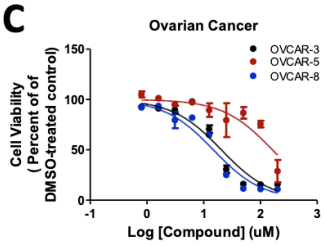

Cell Line	IC_{50} (µM)	95% CI
OVCAR-3	20.51	15.62 to 26.92
OVCAR-5	162.8	109.0 to 243.2
OVCAR-8	14.79	11.82 to 18.52

D

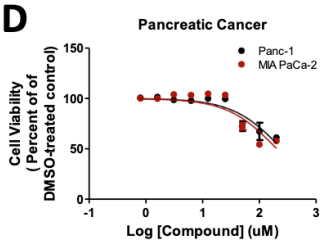

Cell Line	IC_{50} (µM)	95% CI
Panc-1	249.8	195.6 to 319.2
MIA PaCa-2	203.7	154.5 to 268.5

Figure 5.2. DB1931 cytotoxicity and structure. A) MeWo cells exhibited moderate cytotoxicity with DB1931 treatment for 48 hours, while SKMEL-2 cells did not have a notable reduction in cell viability. B) Cell death among ovarian cancer cell lines with DB1931 treatment was most pronounced in OVCAR-8 and OVCAR-3, respectively, followed by negligible effects in OVCAR-5 cells. C) Pancreatic cancer cell lines Panc-1 and MIA PaCa-2 exhibited little to no cell death with DB1931 treatment. D) Structure, molecular formula and molecular weight of DB1931.

We next investigated DB1943, which had a structure most similar to DB1931 with the only difference being the terminal methylamines **(Fig. 5.3A)**. This replacement from the DB1931 structure seemingly resulted in significantly higher cytotoxicity in melanoma cells and ovarian cancer cells with IC_{50} values ranging between 3 and 30 µM **(Fig. 5.3B, C)**. Pancreatic cancer cell lines also exhibited significantly higher cytotoxicity with DB1943 treatment, concluding that structural changes made from DB1931 resulted in overall less cell viability **(Fig. 5.3D)**.

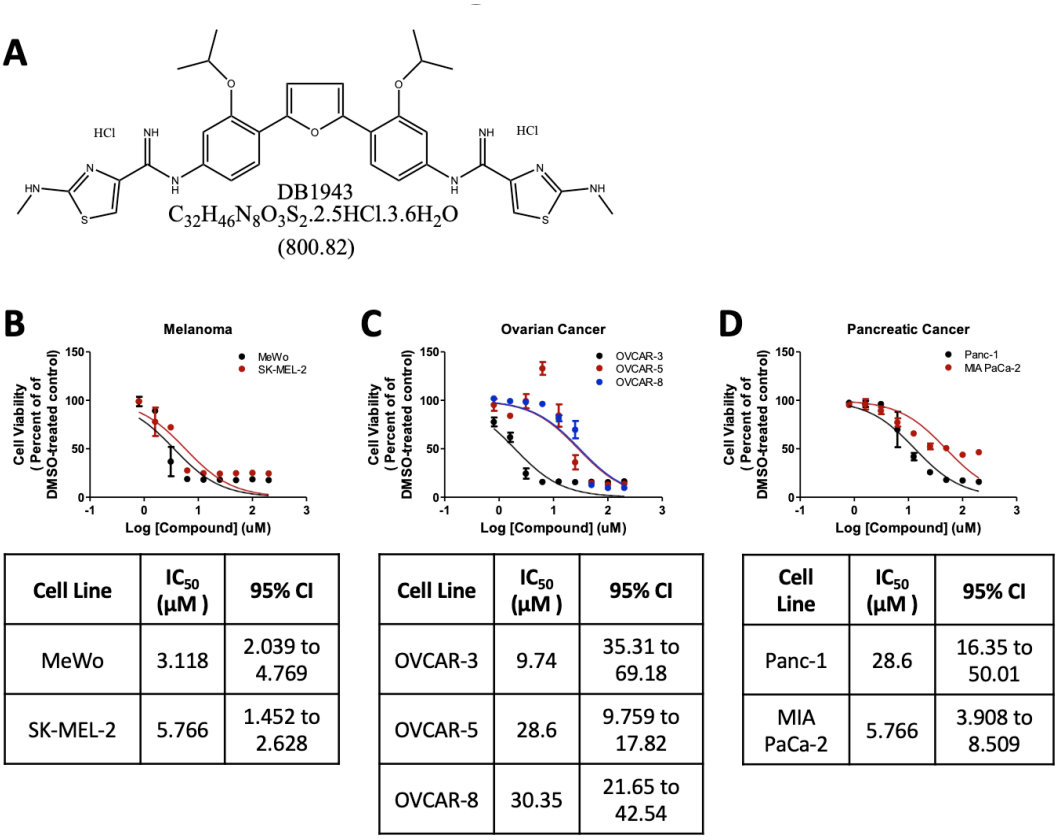

Cell Line	IC_{50} (μM)	95% CI
MeWo	3.118	2.039 to 4.769
SK-MEL-2	5.766	1.452 to 2.628

Cell Line	IC_{50} (μM)	95% CI
OVCAR-3	9.74	35.31 to 69.18
OVCAR-5	28.6	9.759 to 17.82
OVCAR-8	30.35	21.65 to 42.54

Cell Line	IC_{50} (μM)	95% CI
Panc-1	28.6	16.35 to 50.01
MIA PaCa-2	5.766	3.908 to 8.509

Figure 5.3. DB1943 cytotoxicity and structure. A) MeWo and SK-MEL-2 exhibit relatively high cytotoxicity when treated with DB1943. B) OVCAR-3 shows decent cytotoxic effects with DB1943 treatment, while OVCAR-5 and OVCAR-8 show little cell death. C) Among the pancreatic cancer cell lines, MIA PaCa-2 cells experience higher cytotoxicity compared to Panc-1, also depicted with the IC50 values. D) Structure, molecular formula and molecular weight of DB1943.

The structure of DB1856 compared to the other similar compounds in this study reveal that the terminal groups in the structure being pyrazole rings with a methyl group best corresponded to high cytotoxicity **(Fig. 5.4A)**. Among all the investigated compounds, DB1856 emerged as one of the most effective at reducing cell viability in both melanoma and ovarian cancer cell lines **(Fig. 5.4B, 4C)**. However, pancreatic cancer cell lines did not experience a great loss in cell viability upon treatment **(Fig. 5.4D)**.

Since DB1856 was deemed the most effective at reducing cell viability in both melanoma and ovarian cancer cells, we next developed a xenograft model with MeWo and OVCAR-3 tumor xenografts in nude mice in order to test the compound *in vivo*.

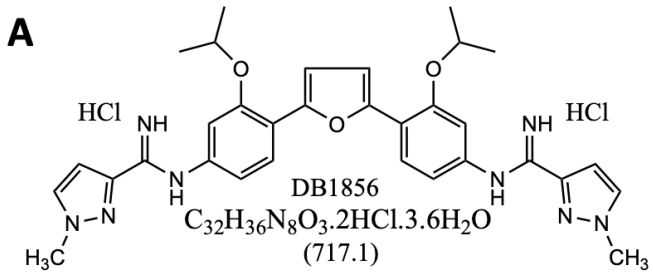

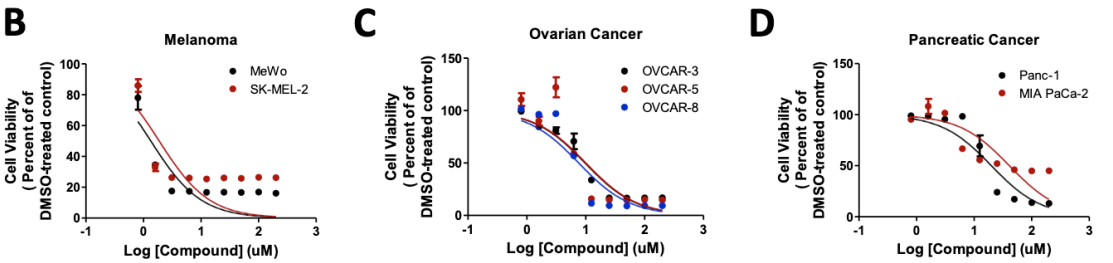

Cell Line	IC_{50} (µM)	95% CI
MeWo	1.341	0.9397 to 1.915
SK-MEL-2	1.877	1.148 to 3.069

Cell Line	IC_{50} (µM)	95% CI
OVCAR-3	1.954	7.757 to 12.23
OVCAR-5	10.04	5.998 to 16.81
OVCAR-8	1.482	5.276 to 10.95

Cell Line	IC_{50} (µM)	95% CI
Panc-1	19.96	14.51 to 27.45
MIA PaCa-2	41.00	27.24 to 61.71

Figure 5.4. DB1856 exhibits cytotoxic effects in melanoma and ovarian cancer. A) Exposure of MeWo and SK-MEL-2 to DB1856 compound for 48 hours results in high cytotoxicity. B) Effects of DB1856 in ovarian cancer is cell line dependent, with cytotoxic effects observed in OVCAR-3 and OVCAR-8, but not as prominently in OVCAR-5 as evidenced by a higher IC50 value. C) Pancreatic cancer cell lines Panc-1 and MIA PaCa-2 exhibit moderate cell death upon treatment with DB1856. D) Structure, molecular formula and molecular weight of DB1856.

Ovarian tumors were injected intraperitoneally into each mouse and resulted in rapid tumor growth after 40 days post-injection. DB1856 treatments, even at 9 mg/kg were not effective at slowing OVCAR-3 tumor growth compared to the vehicle-treated group **(Fig. 5.5A)**. The mice also were able to maintain their weight throughout the short

study, possibly attributable to the growing tumor sizes **(Fig. 5.5B)**. An image of a mouse with intraperitoneally injected OVCAR-3 tumors showed that the tumors had begun to slowly spread in the abdominal area, resulting in early termination of the study **(Fig. 5.5C)**. The lack of effectiveness of DB1856 in this model could be due to translation from *in vitro* to *in vivo*, since over 90% of compounds fail when translated from a pre-clinical to clinical model (420) and drug delivery issues are extremely common during translation.

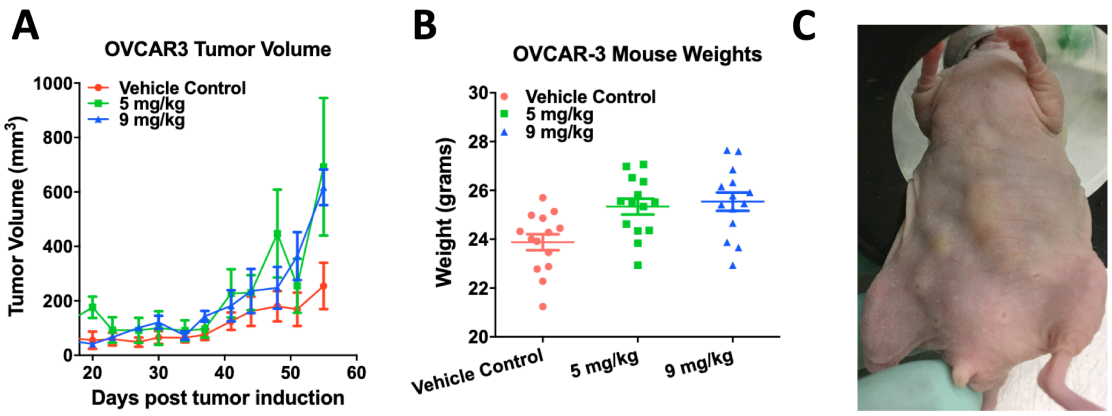

Figure 5.5. DB1856 treatments in in vivo ovarian tumor xenografts are not effectively translated. A) Growth of OVCAR-3 xenograft tumors in athymic nude mice was not successfully inhibited by DB1856 treatment at 5 mg/kg or 9 mg/kg of DB1856. Mice experienced rapid metastasis of injected tumors and health rapidly declined, resulting in termination of the study. B) Mice with OVCAR-3 xenograft tumors were able to maintain a healthy weight through the study despite tumor metastasis over time. Weight gain can partially be attributed to growing tumors in the mouse abdomens. C) Image of mouse with OVCAR-3 xenograft tumors embedded in the intraperitoneal cavity, with some metastatic spread in the abdominal region.

However, mice injected with MeWo cells to form melanoma tumor xenografts, showed significantly (*$p<0.001$) slower tumor growth with DB1856 treatment at 7.5 mg/kg over a period of 92 days post-injection **(Fig. 5.6A)**. The mouse weights in the DB1856-treated group were also significantly lower than the vehicle-treated group, possibly due to the latter having large tumor sizes by the end of the study **(Fig. 5.6B)**. A

large melanoma tumor on the back flank of a mouse in the vehicle-treated group suggests development of vasculature to support tumor growth **(Fig. 5.6C)**. In conclusion, DB1856 was the top candidate for *in vivo* studies and succeeded in inhibiting tumor growth in a melanoma xenograft model.

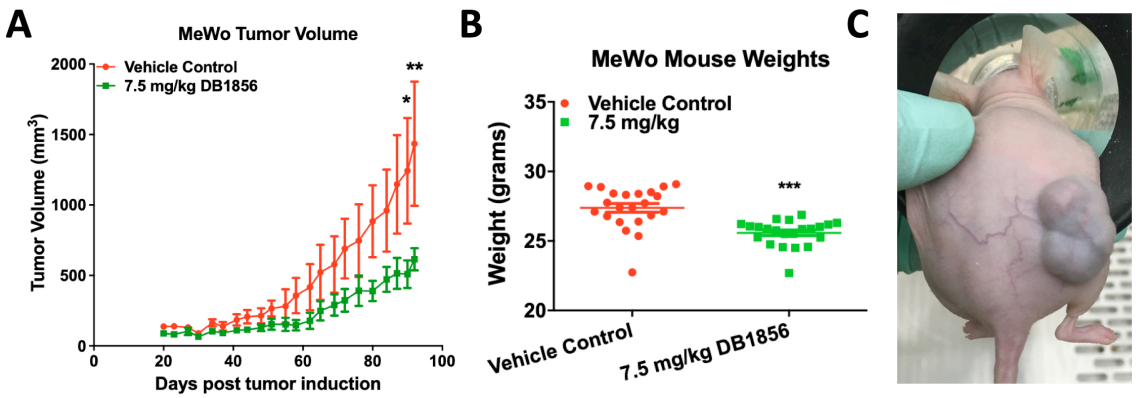

Figure 5.6. In vivo studies with melanoma xenografts showed a significant inhibition of tumor growth with DB1856 treatment. A) Treatment of MeWo melanoma xenograft tumors with 7.5 mg/kg DB1856 weekly resulted in significant inhibition of tumor growth (*p<0.01) by day 92 post-injection. B) Weights of mice undergoing treatment with 7.5 mg/kg DB1856 were significantly lower than those in the control group (***p<0.001), possibly due to tumor growth inhibition. C) Image of mouse in control, vehicle-treated group with large melanoma xenograft tumor on back right flank.

Protein analysis of melanoma tumor tissue treated showed that DB1856 treatment at 7.5 mg/kg resulted in a significant upregulation of ARID1A (**p<0.01) and DUSP4 (*p<0.05) protein compared to vehicle-treated tissue **(Fig. 5.7)**. ARID1A, a tumor suppressor, has previously been shown to bind DNA and initiate chromatin remodeling (421). Additionally, DUSP4 is a prominent oncoprotein responsible for increased cell survival and proliferation and induces autophagic cell death via inactivation of ERK (422). Both these proteins being upregulated suggests an increased potential for cell death, which was observed through tumor growth inhibition. Finally, beta-Catenin, also an oncogene implicated in multiple cancer types but especially melanoma, was

significantly decreased (*p<0.05) in DB1856-treated tissue, suggesting the reversal of its tumor promoting signaling **(Fig. 5.7)** (423).

Limitations of study are largely based on inability to pinpoint changes that are most effective at reducing cell viability. In other words, we could not explore exactly which part of each functional group was responsible for changes in cytotoxic effects. However, since we did not synthesize these compounds, this is difficult to overcome. Secondly, we were unable to explore the more extensive subset of compounds with the same furan and benzene ring backbone, partially attributed to the complexity of some structures that make it difficult stably synthesize them in large quantities, or access for our studies, and also due to our exploration of other diverse compounds that were not structurally similar to this subset.

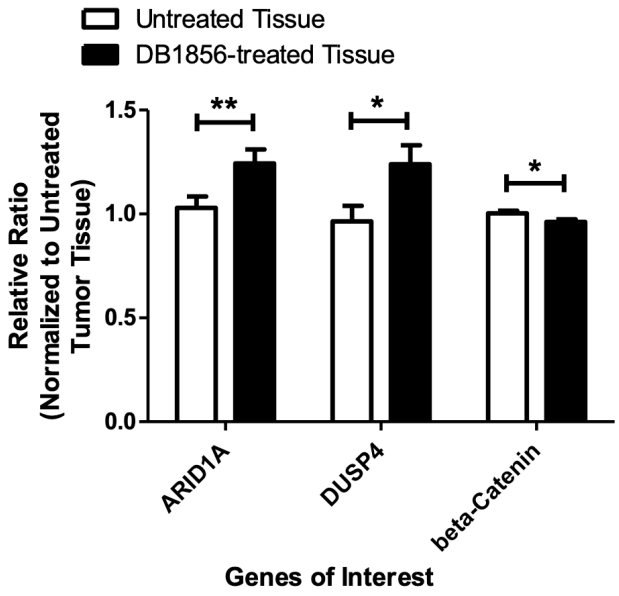

Figure 5.7. DB1856 treatment results in changes in DNA repair and oncogenic signaling in tumor tissue. ARID1A and DUSP4 are significantly increased (**p<0.01; p<0.05) in DB1856-treated tissue compared to vehicle-treated (untreated) tissue. Conversely beta-Catenin is reduced (p<0.05) in DB1856-treated tissue.

Future studies involving these compounds should involve deeper investigation of DB1856's intracellular targets, although preliminary tumor tissue analysis suggests its role in controlling protein expression possibly through DNA-binding. Defining pharmacokinetics will also add to DB1856's clinical relevancy. Preliminary physiochemical analysis has revealed that DB1856 has a LogP (lipophilicity) of 3.834, and pKa (acid dissociation constant) of 9.4, which suggest that it is largely hydrophobic with a preference for basic solutions. This correlates with its structure, which contains secondary amines and no terminal salt bridges to aid hydrophilic solvent interaction. Finally, further modifications to the furan and benzene ring backbone structure can help determine if functional groups outside of those explored in this study are more effective at reducing cell viability.

This study is significant for outlining the potential use of previously defined anti-microbial compounds in cancer, diversifying their utilization to other fields of research. The parallel of DB1856 with traditional chemotherapy and specifically anti-metabolites is exciting given their established relevance in cancer already. We believe that DB1856 has great potential as a promising candidate compound in cancer research, especially in melanoma.

CHAPTER VI

CONCLUSIONS AND FUTURE WORK

Summary and Limitations

The overarching goal of this research was to investigate autotaxin-induced miRNA changes and the subsequent downstream effects on cancer cell behavior. Since autotaxin is overexpressed in a variety of cancers with high-grade ovarian serous carcinoma being the most frequent alteration, a majority of our studies involving this enzyme were carried out with cell lines of ovarian cancer origin (345, 346). Other projects during this graduate tenure also involved discovering cytotoxic effects of organic compounds in cancer cell lines of various origins, and developing a novel method for miRNA delivery into cells that may enhance the opportunity for miRNA targeting in order to achieve desired inhibitory effects. Overall, my research has spanned a diverse array of techniques, research methodologies and creative pursuits, which have been important in perfecting the scientific method to develop a unique and impactful story.

The direct effects of autotaxin on miRNA expression *in vivo* was studied in Chapter I, where we utilized an autotaxin-transgenic mouse model that was previously utilized to study adipogenesis and thermogenesis (218). We aimed to investigate how our autotaxin transgenic mouse, under the alpha-1 antitrypsin promotor, could initiate signaling in the tumor and change miRNA expression that might indicate tumorigenesis or progression. As the transgenic mice reached 18-20 months of age, we observed the development of tumors of various origins, with mammary being the most common. Our

cohort was largely female, since the model was geared toward studying ovarian carcinoma, and due to the fact that we were unable to age the males due to aggressive behavior and extensive cage separations resulting in high care costs. Comparison of serum miRNA expression in healthy wildtype females, autotaxin transgenic females without tumors, and autotaxin transgenic females with tumors revealed distinct changes between the groups, indicating the possibility of a miRNA that could be used as liquid biopsy marker to indicate tumorigenesis. Close evaluation of the miRNA array revealed that miR-489-3p was increased with autotaxin overexpression, and further increased in the serum upon tumor development in mice with a variety of tumor types.

In vitro analysis using newly developed stable cell lines that overexpress functional autotaxin or its mutant form exhibited a similar phenomenon upon transfection with miR-489-3p, confirming its *in vivo* expression patterns. A miRNA database further revealed that miR-489-3p could target the oncogene MEK1, which we confirmed through *in vitro* protein samples and *in vivo* tissue analysis which revealed an inverse correlation between autotaxin and miR-489-3p expression. In other words, tumor tissue was producing elevated miR-489-3p in response to elevated autotaxin signaling, but exporting it into circulation as miRNA levels increased in the cells, thereby stunting its inhibitory effects on MEK1 and allowing the tumor cells to proliferate. Lastly, the cytotoxic effects of miR-489-3p were enhanced by addition of a PARP inhibitor to cells, which also synergized with the miRNA to further inhibit MEK1 expression and result in cell death.

Limitations for this study are related to the mouse model and miRNA array performed with serum samples. While successful animal models greatly increase the validity of any study and lend more significance to corresponding findings *in vitro*, all

whole system models come with a few limitations. A previous autotaxin mouse model with the transgene expressed under the MMTV promotor showed similar spontaneous tumor incidence, also with a majority of the tumors being of mammary origin. However, it is unclear where under the alpha-1 antitrypsin promotor this autotaxin transgene is inserted for our model. Therefore, variable expression between mice is possible, which could result in a variation in tumor incidence between the mice. This was observed during the aging process in our study, as approximately 70% of mice didn't develop tumors in their lifetime, but did exhibit excessive fat tissue, which is also attributable to autotaxin overexpression. Further, this study focused on ovarian carcinoma in female mice. Male mice and wildtype control mice were not aged like the transgenic female mice. The male transgenic mice exhibited aggressive behavior as they aged, especially when fed a lean-diet, which was found to be attributable to changes in energy metabolism with elevated autotaxin and a lean-diet (219). Wildtype mice were not aged since these were included as a result of a late-stage reviewer request during manuscript submission, and samples were used from healthy wildtype mice previously part of another study. Further related to mice, previous work in the lab investigated the involvement of adipogenesis and miR-30c-2-3p expression as a contributor to tumorigenesis. However, null- or multi-parous female mice with the autotaxin transgene did not significantly relate to their ability to exhibit miRNA changes in fat tissue that would promote tumorigenesis.

Another set of limitations in the autotaxin/MEK1/miR-489-3p study relates to the miRNA array performed to evaluate changes with autotaxin elevation and tumor development. First, since the array was a pre-developed kit assay, we were unable to determine the specific miRNAs of interest, and it is possible that even in the 750+

miRNAs in the array, there are crucial candidates of significance missing. Additionally, the array was supplied to be tested with mouse serum, thus not all miRNAs with significant changes in gene expression had a human homolog that could be clinically relevant and therefore had to be eliminated. Further, not all miRNAs that were relatable to human miRNAs were found in TarBase database which is used to find miRNA-target pairs by sequence similarity. This, only a portion of the total data is interpretable and relevant to humans. However, the one miRNA we did select as a candidate for future studies, miR-489-3p, has been studied across a variety of cancers and has been shown to target oncogenes beyond MEK1.

The development of antibody-labeled exosomes (Abi-exosomes) was the main focus of Chapter II, where we aimed to engineer a novel particle by inserting a fatty acid-anchored antibody attachment into human-derived exosomal membranes. Abi-exosomes construction was successfully confirmed using dynamic light scattering to measure particle size in solution. The complete particle can be electroporated with miRNA and delivered to cells, where they can target a surface marker that aids uptake into cells, thereby releasing the miRNA to exert an inhibitory effect on its target. Our data has shown that Abi-exosomes are capable of carrying 700,000-fold more miRNA with electroporation compared to transfection, and are also more effective at delivering miRNA to cells compared to plain exosomes electroporated with miRNA or miRNA transfection. Further optimization revealed greater miRNA stability and delivery efficiency with electroporation into fully constructed Abi-exosomes, and the ability to more effectively target cells with an antibody corresponding to an overexpressed target on the surface membrane. Finally, we validated miRNA functionality by confirming the

ability of miR-21-5p delivered in Abi-exosomes to MDA-MB-231 cells to inhibit its well-known target, PTEN, which is a prominent oncoprotein in a variety of cancers (385, 387). Development of this novel method has provided a unique avenue to expand on this idea to other cancer types or conditions outside the realm of cancer, as well as explore the opportunity to utilize this particle to expand its delivery efficiency with diverse cargo.

Since Abi-exosomes are a novel invention under patent consideration, the majority of limitations related to work involving this particle is related to optimization of its use. For example, Abi-exosomes can be constructed under 6 hours, and precipitated overnight for subsequent miRNA electroporation and delivery into cells, but storage at -80ºC after miRNA loading has proved unsuccessful for future use. It is possible that the miRNA may need to be electroporated after storage as the freeze-thaw cycle may disrupt its function, however, it is unclear whether the particle itself is unstable with long term cold storage. Further, exosomes are derived from cells that express CD44 on their surface, which might cause targeting issues if the antibody used to construct Abi-exosomes targeted a particle on the exosomal surface. However, this would be evident through dynamic light scattering since the particle would be much larger without insertion into the exosomal membrane. Fortunately, our calculations for the particle size was similar to the size expected and the CD44-Abi-exosomes were able to exhibit increased cell targeting and miRNA delivery efficiency, eliminating the possibility that the particle was incorrectly built.

Chapter III outlined the potentially cytotoxic effects of over 34 compounds that we tested in 16 cell lines of melanoma, ovarian cancer and pancreatic cancer origin with our goal being defining novel cytotoxic effects of some of these compounds *in vitro*. We

were able to divide the 34 compounds in various subsets based on their structure, with the largest subset consisting of 14 compounds derived from a furamidine analog known as DB766 (401). This compound and its derivatives, as well as its parent form, diamidine, has previously been evaluated for its anti-microbial effects and more specifically for its chemotherapeutic effects in Chagas disease, making it much more relevant to cancer treatment as well (416). Other compounds derived from DB766 were simply a result of reaction byproduct generation, and therefore were never investigated for their potential therapeutic purposes. While most tested candidates did not have remarkable cytotoxic effects in any of the cell lines, a few promising results from CES-IX-49 in melanoma resulted in *in vivo* testing using xenograft models in nude mice. Animals injected with melanoma cells showed significant tumor growth inhibition with CES-IX-49 dosed at 12.5mg/kg weekly, with adverse events being shivering and disorientation after the intra-tumoral injection and excessive rheum during treatment. CES-IX-49 has also previously been shown to cross the blood-brain barrier to reduce parasite load in mice, showing its therapeutic versatility across various fields of research (406).

There are a few limitations for this high throughput study that need to be addressed. First, expansion of cytotoxicity testing of all the 34 compounds to cell lines of more diverse origins may have resulted in some novel results worth pursuing. Since we are uncertain of the mechanism of action of the compounds tested, it is possible that they are cytotoxic in more cancers than we investigated here. Target identification of the most successful cytotoxic compounds would be a priority with expanded testing yielding promising results that can also be confirmed *in vivo*. It is also crucial that any high throughput assay be performed with numerous replications within each experiment to

ensure that the results obtained are accurate representations of the biology. Cytotoxic effects can also be evaluated through changes in morphology that can be observed with time-lapse live-cell imaging following treatment with the compound until up to 48 hours afterwards. Finally, future work can also involve developing strategic functional group modifications in collaboration with organic chemists to more consciously develop a successfully modified cytotoxic compound that can be characterized more accurately due to specific structural changes.

One of the compounds involved in the high throughput testing described in Chapter III named DB1856 was an excellent candidate for *in vivo* testing in a melanoma and ovarian cancer xenograft mouse model due to exhibiting the most impressive IC_{50} values *in vitro*. In Chapter IV, we narrowed in on the cytotoxic effects of DB1856 in MeWo and OVCAR-3 cells compared to other compounds, where DB1856 exhibited impressive IC_{50} values of 1.341 and 1.954 μM in the two cell lines, respectively. Compared to the other compounds, namely DB1855, DB1931, and DB1943 which had similar structures and were also derivations of DB766, it is possible that functional groups on DB1856 might be responsible for its effects in cancer cells. Treatment with 5mg/kg or 9mg/kg in ovarian xenograft models did now show any significant tumor inhibition, however, since the tumors quickly metastasized, resulting in termination of the study. However, MeWo tumors showed a significant inhibition in tumor growth up to day 92 after tumor induction. Further, preliminary analysis of the protein array performed with tumor tissue from the melanoma control and DB1856-treated groups exhibited some DNA-targeting abilities of DB1856. Since DB766, its parent compound, has been previously investigated for its role in DNA minor groove binding, results from our

protein array suggesting DB1856's DNA binding ability would corroborate this theory, however, our studies have not confirmed a specific target or mechanism of action yet.

Although DB1856 and its related compounds were derived from a known parent compound, DB766, that has been previously investigated for its DNA minor groove binding activity and anti-microbial effects, the specific functional groups that contribute to these qualities have not been defined. This was attempted in our studies through comparison of related compounds and their cytotoxic effects, but the specific region of each functional group and its ability to decrease cell viability was not explored in the scope of this work. It is possible that future endeavors involving target identification with DB1856 will help define the binding affinity and docking of the molecule onto its protein target or binding to DNA will shed some light on avenues to modify the structure to make it more effective.

Future Directions

Future directions stemming from the high throughput testing of 34 compounds in 16 cell lines of melanoma, ovarian cancer and pancreatic cancer origins should be mainly focused on defining multiple avenues: 1) finding the correct cell line model to accurately define cytotoxic effects of the compounds, 2) specifically manipulating functional groups to optimize anti-cancer activity of candidate compounds, 3) establishing an animal model from the selected cell lines that exhibit notable corresponding tumor growth inhibition, and 4) determining the molecular targets of successful candidate compounds. This is due to a limitation of the study where we may not have focused on the correct cell line models to showcase the cytotoxic, or even cytostatic or regulatory, effects of some

compounds. In other words, if a compound inhibits a specific protein most often upregulated in prostate cancer, evaluating targeting or binding ability in that model would be most beneficial. Second, candidate compounds such as CES-IX-49 and DB1856 require more comprehensive target determination studies to possibly optimize their effects in the future, possibly by making more purposeful changes to the molecular structure.

The future implications of the autotaxin-induced miR-489-3p and MEK1 elevation in tumor cells can reach far and wide. First, there is an abundance of work in cancer suggesting that cancer cells are fully capable of modulating the surrounding tumor microenvironment for their own survival benefit. This can occur through inducing inflammation but keeping the immune system suppressed to allow for cancer cell proliferation, sending growth factor signals to transform healthy cells in the microenvironment to adopt their malignant phenotype, and obtaining nutrients from nearby cells to decrease their energetics load. However, there has been a lack of studies suggesting that export of factors such as miRNA from cells can occur to remove an inhibitory molecule that threatens the survival of the cancer cell. Our results presented the concept that tumor tissue in autotaxin transgenic mice produces increased amounts of miR-489-3p and MEK1, but miR-489-3p is exported out of the cell into circulation. If it remained in the tumor cell, it would be able to target and suppress MEK1's proliferation capabilities, thereby possibly resulting in a more homeostatic or cytostatic phenotype. It seems as though the cancer cell cleverly avoids this possibility through miR-489-3p export, especially since increasing autotaxin levels also result in increased export of this miRNA while maintaining elevated MEK1 in the cells.

Other studies in hepatocellular carcinoma, osteosarcoma and its metastatic lesions, colorectal cancer, and breast cancer have also reported lower miR-489 levels in tumor tissue compared to normal tissue of the same organ, with direct correlation to increased proliferative and metastatic potential (358, 424-426). Further, two studies in breast and pancreatic cancer also outline how miR-489-3p directly targets a member of a MAPK pathway similar to our results, but is reduced in tumor tissue (359, 360). Therefore, although the export of miR-489-3p from cancer cells that decreases inhibition of oncogenes has been previously investigated in other cancers, perhaps it is valuable to explore whether cancer cells are deliberately exporting this miRNA for their survival benefit, or whether miR-489-3p is exported along with other cargo that is detrimental to the tumor microenvironment. It is fully possible that the increased levels of miR-489-3p are due to its transcription as a passenger along with a driver gene required for these tumor cells to proliferate and survive, but that is yet to be evaluated as well. Previous studies have shown that the miR-489 gene resides on chromosome 7, although neighboring genes have not yet been investigated except for miR-653 has been confirmed to be close to the miR-489 gene, which resides 10,000 bases away (427, 428). This aim would be valuable to understand the purpose behind miR-489-3p exportation from cells, especially if it is a deliberate process performed by cancer cells to preserve their oncogenic signaling processes.

The second future directions aim expands on miR-489-3p exportation out of cancer cells, and its subsequent potential effects on the tumor microenvironment. The surrounding microenvironment, particularly for ovarian cancer with ascites fluid, consists of various cell types, including immune cells, fibroblasts, an expansive vasculature

network and the addition of extracellular vesicles carrying cargo such as miRNA (429). Additionally, cancer cells are also capable of disseminating growth factor signals to surrounding cells to result in transformation, as is commonly seen in the conversion of normal fibroblasts to cancer associated fibroblasts. Export of miR-489-3p out of tumor cells may result in its uptake by players in the microenvironment. This would be particularly relevant for immune cells capable of mounting an anti-tumor response, and eventually lead to immunosuppression, as is often observed in ovarian cancer. To investigate this possibility, we could culture cells such as OVCAR-3 and its autotaxin-overexpression (ATXwt) and mutated counterparts (ATXmut) and transfect them with miR-489-3p to encourage export out of the cell as was observed in our previous work (216). Then we could use that tumor-conditioned medium to treat immune cells obtained from a human blood donor such as peripheral blood mononuclear cells (PBMCs) to assess downstream effects. This would help determine 1) through qRT-PCR if miR-489-3p is taken up by these cells, 2) where there are changes in downstream signaling of these cells based on their normal functional outcomes and 3) whether they have any notable reduction in cell viability, which would suggest an immunosuppressive effect by miR-489-3p inhibition of intracellular targets. To further explore immune and cancer cell cross-communication, a transwell assay can also be performed with miR-489-3p transfected cancer cells in the regular well and PBMCs in the transwell. This would allow for exchange of exosome-mediated signaling that could carry miR-489-3p to PBMCs and separate assessment of functional changes downstream in OVCAR-3 and PBMCs separately. Overall, these approaches would provide a starting point for assessing the

downstream effects miR-489-3p uptake in the tumor microenvironment, especially into immune cells.

Finally, as our studies showed, the majority of spontaneous tumors that formed in autotaxin transgenic mice were of mammary origin, and assessing the function of miR-489-3p in the context of breast cancer may also be valuable. It has been previously shown that miR-489-3p targets several prominent oncogenes in breast cancer cells such as AKT3, BCL2 and HER2 and is also responsible for inducing chemoresistance in Adriamycin-resistant MCF-7 cells (359, 430, 431). However, miR-489-3p might not be an ideal candidate to induce regulation, as studies involving breast cancer cells have shown treatment with MEK1 inhibitors can result in increased cell migration by compensatory signaling through the EGFR and ß-catenin pathways (432). On the other hand, our data showed some promise of miR-489-3p combined with PARP inhibitors synergistically causing cell death with additive MEK1 inhibition.

Future directions involving Abi-exosomes are remarkably exciting to pursue, especially since it is a novel development that may even be relevant in fields outside of cancer research. The first set of aims are framed to improve the customizable construction capabilities of Abi-exosomes. Our data has shown successful targeting of Abi-exosomes to cells overexpressing a surface marker targetable by the antibody used for particle construction, but has not outlined how Abi-exosomes can navigate or preferably target various cell types in culture or *in vivo* together. To address this, we can utilize two cell types one of which has higher expression of a targetable surface protein, and another which has basal levels of expression of the same protein in a transwell assay. Constructing Abi-exosomes with an antibody to target this particular surface marker and

adding it to cells separated by a transwell membrane will allow us to later deduce by qRT-PCR into which cells Abi-exosomes selectively delivered the miRNA. We can also take advantage of cells that overexpress multiple surface proteins, which is not uncommon for cancer cells, by constructing Abi-exosomes with multiple antibodies to more selectively target this cell type over other surrounding cells with lower or no expression of these markers. This may also help mitigate some off-target effects of Abi-exosomes in the presence of diverse cell types *in vivo* since it will more frequently and selectively target cells based on the antibodies used for construction. Secondly, Abi-exosome stability after construction has yet to be evaluated since our studies have found that storage of the particle after miRNA electroporation at -80ºC results in sub-optimal miRNA delivery into cells. It is possible that the freeze-thaw cycle results in miRNA leakage or degradation within the particle, and simply requires re-electroporation of miRNA into Abi-exosomes before delivery into cells.

Another facet of future work involving Abi-exosomes is focused on the cargo loaded into the particle, which thus far has only involved miRNA. To take full advantage miRNA electroporation in Abi-exosomes to cause cytotoxicity in target cells, the utilization of multiple miRNAs loaded into the particle must be considered. Delivery of a miRNA "cocktail" would provide the opportunity to target multiple oncogenes in cancer cells, possibly along the same pathway, such as MAPK, to fully shut down its proliferative signaling capacities. Secondly, efforts are currently underway in our laboratory to explore the electroporation of protein into Abi-exosomes by using fluorescent BSA and immunofluorescence to measure uptake into cells. This could be utilized to deliver fully constructed protein therapeutics to cells more efficiently using

Abi-exosomes, which can be especially relevant in diseases such as diabetes with insulin targeting to certain cell types, or can also be applicable to other conditions requiring inhibitory peptides, which are a new and emerging class of therapeutics. Small molecule electroporation into Abi-exosomes can also be explored for similar reasons since the targeting ability of Abi-exosomes can add to the inhibitor specificity.

Most importantly, Abi-exosomes may also be capable of carrying drugs that are already FDA-approved but require a new formulation to more specifically target cells and reduce off-target effects. This has previously been done with Nab-paclitaxel, which is an albumin nanoparticle packaged form of paclitaxel with the ability increased half-life circulation in blood (433). Liposomal doxorubicin has also been developed and approved by the FDA for use in several cancers as a means to improve dose-limiting cardiotoxicity associated with its non-liposomal formulation by increasing its half-life in blood (434, 435). These encapsulated therapies have been able to demonstrate increase circulation in blood, thereby removing the need for higher doses and lowering the incidence of high-grade adverse events. Abi-exosomes would be able to take a step further and not only increase circulation time due to the presence of the PEG(2000) fatty acid, but also possibly provide the ability to navigate various environments to only target and deliver its cargo to certain cell types. Adverse events are certainly possible with Abi-exosomes as translation from an *in vitro* system to mouse or human models presents challenges, but we hope that its targeting ability can be further refined in the future to best possibly avoid the worst off-target events.

Additionally, Abi-exosomes should not cause high immunogenic reactions that are common with artificial liposomal formulations, as the exosomes used for construction

are also human-derived. However, this would need to be explored further in a mouse model where immune reactions can be measure after treatment with an Abi-exosome formulation. Pharmacokinetic studies of Abi-exosome dissemination and excretion from a mammalian model are also necessary to assess before determining its safety and efficacy for treatment of any condition. For more personalized Abi-exosome formulations far in the future, it is also possible to match donor and recipient of Abi-exosomes by blood type, if the patient is unable to provide their exosomes for engineering. Overall, Abi-exosomes are a novel and highly versatile construction, which can be studied in diverse avenues to explore their therapeutic potential in cancer and beyond.

Overall, there are exciting and diverse avenues of research to pursue stemming from each of these projects outlined in the chapters. Testing of novel candidate compounds in diverse cell lines may uncover a new targeted inhibitor with unique regulatory properties for cancer types in need of effective non-chemotherapeutic options, while the exploration of miR-489-3p in the tumor microenvironment and beyond might shed light on its possible immunomodulatory role in cancer. Finally, Abi-exosomes may pave the way for a new formulation of therapeutics that are focused on specific cell targeting and improved patient care through reduced adverse events, making this an exciting future avenue of exploration.

REFERENCES

1. Lee RC, Feinbaum RL, Ambros V. The C. elegans heterochronic gene lin-4 encodes small RNAs with antisense complementarity to lin-14. Cell. 1993;75(5):843-54.

2. Ambros V, Horvitz HR. The lin-14 locus of Caenorhabditis elegans controls the time of expression of specific postembryonic developmental events. Genes Dev. 1987;1(4):398-414.

3. Arasu P, Wightman B, Ruvkun G. Temporal regulation of lin-14 by the antagonistic action of two other heterochronic genes, lin-4 and lin-28. Genes Dev. 1991;5(10):1825-33.

4. Reinhart BJ, Slack FJ, Basson M, Pasquinelli AE, Bettinger JC, Rougvie AE, et al. The 21-nucleotide let-7 RNA regulates developmental timing in Caenorhabditis elegans. Nature. 2000;403(6772):901-6.

5. Slack FJ, Basson M, Liu Z, Ambros V, Horvitz HR, Ruvkun G. The lin-41 RBCC gene acts in the C. elegans heterochronic pathway between the let-7 regulatory RNA and the LIN-29 transcription factor. Mol Cell. 2000;5(4):659-69.

6. Pasquinelli AE, Reinhart BJ, Slack F, Martindale MQ, Kuroda MI, Maller B, et al. Conservation of the sequence and temporal expression of let-7 heterochronic regulatory RNA. Nature. 2000;408(6808):86-9.

7. Rodriguez A, Griffiths-Jones S, Ashurst JL, Bradley A. Identification of mammalian microRNA host genes and transcription units. Genome Res. 2004;14(10A):1902-10.

8. Hammond SM. An overview of microRNAs. Adv Drug Deliv Rev. 2015;87:3-14.

9. Bartel DP. MicroRNAs: genomics, biogenesis, mechanism, and function. Cell. 2004;116(2):281-97.

10. Melamed Z, Levy A, Ashwal-Fluss R, Lev-Maor G, Mekahel K, Atias N, et al. Alternative splicing regulates biogenesis of miRNAs located across exon-intron junctions. Mol Cell. 2013;50(6):869-81.

11. Ying SY, Chang CP, Lin SL. Intron-mediated RNA interference, intronic microRNAs, and applications. Methods Mol Biol. 2010;629:205-37.

12. Cramer P. Structure and function of RNA polymerase II. Adv Protein Chem. 2004;67:1-42.

13. Goodfellow SJ, White RJ. Regulation of RNA polymerase III transcription during mammalian cell growth. Cell Cycle. 2007;6(19):2323-6.

14. Kim YK, Kim VN. Processing of intronic microRNAs. EMBO J. 2007;26(3):775-83.

15. Han J, Lee Y, Yeom KH, Kim YK, Jin H, Kim VN. The Drosha-DGCR8 complex in primary microRNA processing. Genes Dev. 2004;18(24):3016-27.

16. Lee Y, Ahn C, Han J, Choi H, Kim J, Yim J, et al. The nuclear RNase III Drosha initiates microRNA processing. Nature. 2003;425(6956):415-9.

17. Denli AM, Tops BB, Plasterk RH, Ketting RF, Hannon GJ. Processing of primary microRNAs by the Microprocessor complex. Nature. 2004;432(7014):231-5.

18. Han J, Pedersen JS, Kwon SC, Belair CD, Kim YK, Yeom KH, et al. Posttranscriptional crossregulation between Drosha and DGCR8. Cell. 2009;136(1):75-84.

19. Ruby JG, Jan CH, Bartel DP. Intronic microRNA precursors that bypass Drosha processing. Nature. 2007;448(7149):83-6.

20. Yi R, Qin Y, Macara IG, Cullen BR. Exportin-5 mediates the nuclear export of pre-microRNAs and short hairpin RNAs. Genes Dev. 2003;17(24):3011-6.

21. Bohnsack MT, Czaplinski K, Gorlich D. Exportin 5 is a RanGTP-dependent dsRNA-binding protein that mediates nuclear export of pre-miRNAs. RNA. 2004;10(2):185-91.

22. Chendrimada TP, Gregory RI, Kumaraswamy E, Norman J, Cooch N, Nishikura K, et al. TRBP recruits the Dicer complex to Ago2 for microRNA processing and gene silencing. Nature. 2005;436(7051):740-4.

23. Haase AD, Jaskiewicz L, Zhang H, Laine S, Sack R, Gatignol A, et al. TRBP, a regulator of cellular PKR and HIV-1 virus expression, interacts with Dicer and functions in RNA silencing. EMBO Rep. 2005;6(10):961-7.

24. Zhang H, Kolb FA, Brondani V, Billy E, Filipowicz W. Human Dicer preferentially cleaves dsRNAs at their termini without a requirement for ATP. EMBO J. 2002;21(21):5875-85.

25. Cifuentes D, Xue H, Taylor DW, Patnode H, Mishima Y, Cheloufi S, et al. A novel miRNA processing pathway independent of Dicer requires Argonaute2 catalytic activity. Science. 2010;328(5986):1694-8.

26. Diederichs S, Haber DA. Dual role for argonautes in microRNA processing and posttranscriptional regulation of microRNA expression. Cell. 2007;131(6):1097-108.

27. Rand TA, Petersen S, Du F, Wang X. Argonaute2 cleaves the anti-guide strand of siRNA during RISC activation. Cell. 2005;123(4):621-9.

28. Matranga C, Tomari Y, Shin C, Bartel DP, Zamore PD. Passenger-strand cleavage facilitates assembly of siRNA into Ago2-containing RNAi enzyme complexes. Cell. 2005;123(4):607-20.

29. Maniataki E, Mourelatos Z. A human, ATP-independent, RISC assembly machine fueled by pre-miRNA. Genes Dev. 2005;19(24):2979-90.

30. Winter J, Jung S, Keller S, Gregory RI, Diederichs S. Many roads to maturity: microRNA biogenesis pathways and their regulation. Nat Cell Biol. 2009;11(3):228-34.

31. Zeng Y, Cullen BR. RNA interference in human cells is restricted to the cytoplasm. RNA. 2002;8(7):855-60.

32. Jia W, Eneh JO, Ratnaparkhe S, Altman MK, Murph MM. MicroRNA-30c-2* expressed in ovarian cancer cells suppresses growth factor-induced cellular proliferation and downregulates the oncogene BCL9. Mol Cancer Res. 2011;9(12):1732-45.

33. Brennecke J, Stark A, Russell RB, Cohen SM. Principles of microRNA-target recognition. PLoS Biol. 2005;3(3):e85.

34. Saxena S, Jonsson ZO, Dutta A. Small RNAs with imperfect match to endogenous mRNA repress translation. Implications for off-target activity of small inhibitory RNA in mammalian cells. J Biol Chem. 2003;278(45):44312-9.

35. Doench JG, Sharp PA. Specificity of microRNA target selection in translational repression. Genes Dev. 2004;18(5):504-11.

36. Enright AJ, John B, Gaul U, Tuschl T, Sander C, Marks DS. MicroRNA targets in Drosophila. Genome Biol. 2003;5(1):R1.

37. Gregory RI, Chendrimada TP, Cooch N, Shiekhattar R. Human RISC couples microRNA biogenesis and posttranscriptional gene silencing. Cell. 2005;123(4):631-40.

38. Liu J, Carmell MA, Rivas FV, Marsden CG, Thomson JM, Song JJ, et al. Argonaute2 is the catalytic engine of mammalian RNAi. Science. 2004;305(5689):1437-41.

39. MacRae IJ, Ma E, Zhou M, Robinson CV, Doudna JA. In vitro reconstitution of the human RISC-loading complex. Proc Natl Acad Sci U S A. 2008;105(2):512-7.

40. Valencia-Sanchez MA, Liu J, Hannon GJ, Parker R. Control of translation and mRNA degradation by miRNAs and siRNAs. Genes Dev. 2006;20(5):515-24.

41. Parker R, Song H. The enzymes and control of eukaryotic mRNA turnover. Nat Struct Mol Biol. 2004;11(2):121-7.

42. Coller J, Parker R. Eukaryotic mRNA decapping. Annu Rev Biochem. 2004;73:861-90.

43. Brengues M, Teixeira D, Parker R. Movement of eukaryotic mRNAs between polysomes and cytoplasmic processing bodies. Science. 2005;310(5747):486-9.

44. Liu J, Valencia-Sanchez MA, Hannon GJ, Parker R. MicroRNA-dependent localization of targeted mRNAs to mammalian P-bodies. Nat Cell Biol. 2005;7(7):719-23.

45. Braun JE, Huntzinger E, Izaurralde E. The role of GW182 proteins in miRNA-mediated gene silencing. Adv Exp Med Biol. 2013;768:147-63.

46. Liu J, Rivas FV, Wohlschlegel J, Yates JR, 3rd, Parker R, Hannon GJ. A role for the P-body component GW182 in microRNA function. Nat Cell Biol. 2005;7(12):1261-6.

47. Bhattacharyya SN, Habermacher R, Martine U, Closs EI, Filipowicz W. Stress-induced reversal of microRNA repression and mRNA P-body localization in human cells. Cold Spring Harb Symp Quant Biol. 2006;71:513-21.

48. Hanahan D, Weinberg RA. Hallmarks of cancer: the next generation. Cell. 2011;144(5):646-74.

49. Macheret M, Halazonetis TD. DNA replication stress as a hallmark of cancer. Annu Rev Pathol. 2015;10:425-48.

50. Croce CM. Oncogenes and cancer. N Engl J Med. 2008;358(5):502-11.

51. Vicente-Duenas C, Romero-Camarero I, Cobaleda C, Sanchez-Garcia I. Function of oncogenes in cancer development: a changing paradigm. EMBO J. 2013;32(11):1502-13.

52. Joyce C, Kasi A. Cancer, Tumor-Suppressor Genes. StatPearls. Treasure Island (FL)2018.

53. Kastenhuber ER, Lowe SW. Putting p53 in Context. Cell. 2017;170(6):1062-78.

54. Shenouda SK, Alahari SK. MicroRNA function in cancer: oncogene or a tumor suppressor? Cancer Metastasis Rev. 2009;28(3-4):369-78.

55. Svoronos AA, Engelman DM, Slack FJ. OncomiR or Tumor Suppressor? The Duplicity of MicroRNAs in Cancer. Cancer Res. 2016;76(13):3666-70.

56. Jiang F, Liu T, He Y, Yan Q, Chen X, Wang H, et al. MiR-125b promotes proliferation and migration of type II endometrial carcinoma cells through targeting TP53INP1 tumor suppressor in vitro and in vivo. BMC Cancer. 2011;11:425.

57. Wang F, Yu D, Liu Z, Wang R, Xu Y, Cui H, et al. MiR-125b Functions as a Tumor Suppressor and Enhances Chemosensitivity to Cisplatin in Osteosarcoma. Technol Cancer Res Treat. 2016;15(6):NP105-NP12.

58. Lin S, Gregory RI. MicroRNA biogenesis pathways in cancer. Nat Rev Cancer. 2015;15(6):321-33.

59. Lee H, Han S, Kwon CS, Lee D. Biogenesis and regulation of the let-7 miRNAs and their functional implications. Protein Cell. 2016;7(2):100-13.

60. Pobezinsky LA, Wells AC. Let's fight cancer: let-7 is a tool to enhance antitumor immune responses. Future Oncol. 2018;14(12):1141-5.

61. He L, Thomson JM, Hemann MT, Hernando-Monge E, Mu D, Goodson S, et al. A microRNA polycistron as a potential human oncogene. Nature. 2005;435(7043):828-33.

62. Kumar P, Luo Y, Tudela C, Alexander JM, Mendelson CR. The c-Myc-regulated microRNA-17~92 (miR-17~92) and miR-106a~363 clusters target hCYP19A1 and hGCM1 to inhibit human trophoblast differentiation. Mol Cell Biol. 2013;33(9):1782-96.

63. Chan JA, Krichevsky AM, Kosik KS. MicroRNA-21 is an antiapoptotic factor in human glioblastoma cells. Cancer Res. 2005;65(14):6029-33.

64. Volinia S, Calin GA, Liu CG, Ambs S, Cimmino A, Petrocca F, et al. A microRNA expression signature of human solid tumors defines cancer gene targets. Proc Natl Acad Sci U S A. 2006;103(7):2257-61.

65. Rupaimoole R, Calin GA, Lopez-Berestein G, Sood AK. miRNA Deregulation in Cancer Cells and the Tumor Microenvironment. Cancer Discov. 2016;6(3):235-46.

66. Zhu S, Wu H, Wu F, Nie D, Sheng S, Mo YY. MicroRNA-21 targets tumor suppressor genes in invasion and metastasis. Cell Res. 2008;18(3):350-9.

67. Yan LX, Huang XF, Shao Q, Huang MY, Deng L, Wu QL, et al. MicroRNA miR-21 overexpression in human breast cancer is associated with advanced clinical stage, lymph node metastasis and patient poor prognosis. RNA. 2008;14(11):2348-60.

68. Frankel LB, Christoffersen NR, Jacobsen A, Lindow M, Krogh A, Lund AH. Programmed cell death 4 (PDCD4) is an important functional target of the microRNA miR-21 in breast cancer cells. J Biol Chem. 2008;283(2):1026-33.

69. Lu Z, Liu M, Stribinskis V, Klinge CM, Ramos KS, Colburn NH, et al. MicroRNA-21 promotes cell transformation by targeting the programmed cell death 4 gene. Oncogene. 2008;27(31):4373-9.

70. Sansal I, Sellers WR. The biology and clinical relevance of the PTEN tumor suppressor pathway. J Clin Oncol. 2004;22(14):2954-63.

71. Meng F, Henson R, Wehbe-Janek H, Ghoshal K, Jacob ST, Patel T. MicroRNA-21 regulates expression of the PTEN tumor suppressor gene in human hepatocellular cancer. Gastroenterology. 2007;133(2):647-58.

72. Peralta-Zaragoza O, Deas J, Meneses-Acosta A, De la OGF, Fernandez-Tilapa G, Gomez-Ceron C, et al. Relevance of miR-21 in regulation of tumor suppressor gene PTEN in human cervical cancer cells. BMC Cancer. 2016;16:215.

73. Wang P, Guan Q, Zhou D, Yu Z, Song Y, Qiu W. miR-21 Inhibitors Modulate Biological Functions of Gastric Cancer Cells via PTEN/PI3K/mTOR Pathway. DNA Cell Biol. 2018;37(1):38-45.

74. Wu Y, Song Y, Xiong Y, Wang X, Xu K, Han B, et al. MicroRNA-21 (Mir-21) Promotes Cell Growth and Invasion by Repressing Tumor Suppressor PTEN in Colorectal Cancer. Cell Physiol Biochem. 2017;43(3):945-58.

75. He C, Dong X, Zhai B, Jiang X, Dong D, Li B, et al. MiR-21 mediates sorafenib resistance of hepatocellular carcinoma cells by inhibiting autophagy via the PTEN/Akt pathway. Oncotarget. 2015;6(30):28867-81.

76. Wu ZH, Tao ZH, Zhang J, Li T, Ni C, Xie J, et al. MiRNA-21 induces epithelial to mesenchymal transition and gemcitabine resistance via the PTEN/AKT pathway in breast cancer. Tumour Biol. 2016;37(6):7245-54.

77. Mitra AK, Zillhardt M, Hua Y, Tiwari P, Murmann AE, Peter ME, et al. MicroRNAs reprogram normal fibroblasts into cancer-associated fibroblasts in ovarian cancer. Cancer Discov. 2012;2(12):1100-8.

78. Shiga K, Hara M, Nagasaki T, Sato T, Takahashi H, Takeyama H. Cancer-Associated Fibroblasts: Their Characteristics and Their Roles in Tumor Growth. Cancers (Basel). 2015;7(4):2443-58.

79. Tili E, Michaille JJ, Croce CM. MicroRNAs play a central role in molecular dysfunctions linking inflammation with cancer. Immunol Rev. 2013;253(1):167-84.

80. Tili E, Michaille JJ, Wernicke D, Alder H, Costinean S, Volinia S, et al. Mutator activity induced by microRNA-155 (miR-155) links inflammation and cancer. Proc Natl Acad Sci U S A. 2011;108(12):4908-13.

81. Hannafon BN, Ding WQ. Intercellular communication by exosome-derived microRNAs in cancer. Int J Mol Sci. 2013;14(7):14240-69.

82. Hessvik NP, Llorente A. Current knowledge on exosome biogenesis and release. Cell Mol Life Sci. 2018;75(2):193-208.

83. Wolf P. The nature and significance of platelet products in human plasma. Br J Haematol. 1967;13(3):269-88.

84. Harding C, Heuser J, Stahl P. Receptor-mediated endocytosis of transferrin and recycling of the transferrin receptor in rat reticulocytes. J Cell Biol. 1983;97(2):329-39.

85. Johnstone RM, Adam M, Hammond JR, Orr L, Turbide C. Vesicle formation during reticulocyte maturation. Association of plasma membrane activities with released vesicles (exosomes). J Biol Chem. 1987;262(19):9412-20.

86. Pan BT, Teng K, Wu C, Adam M, Johnstone RM. Electron microscopic evidence for externalization of the transferrin receptor in vesicular form in sheep reticulocytes. J Cell Biol. 1985;101(3):942-8.

87. Record M, Carayon K, Poirot M, Silvente-Poirot S. Exosomes as new vesicular lipid transporters involved in cell-cell communication and various pathophysiologies. Biochim Biophys Acta. 2014;1841(1):108-20.

88. Huotari J, Helenius A. Endosome maturation. EMBO J. 2011;30(17):3481-500.

89. Henne WM, Stenmark H, Emr SD. Molecular mechanisms of the membrane sculpting ESCRT pathway. Cold Spring Harb Perspect Biol. 2013;5(9).

90. Mobius W, Ohno-Iwashita Y, van Donselaar EG, Oorschot VM, Shimada Y, Fujimoto T, et al. Immunoelectron microscopic localization of cholesterol using biotinylated and non-cytolytic perfringolysin O. J Histochem Cytochem. 2002;50(1):43-55.

91. Wubbolts R, Leckie RS, Veenhuizen PT, Schwarzmann G, Mobius W, Hoernschemeyer J, et al. Proteomic and biochemical analyses of human B cell-derived exosomes. Potential implications for their function and multivesicular body formation. J Biol Chem. 2003;278(13):10963-72.

92. Raposo G, Stoorvogel W. Extracellular vesicles: exosomes, microvesicles, and friends. J Cell Biol. 2013;200(4):373-83.

93. Crescitelli R, Lasser C, Szabo TG, Kittel A, Eldh M, Dianzani I, et al. Distinct RNA profiles in subpopulations of extracellular vesicles: apoptotic bodies, microvesicles and exosomes. J Extracell Vesicles. 2013;2.

94. Schwarzenbach H. The clinical relevance of circulating, exosomal miRNAs as biomarkers for cancer. Expert Rev Mol Diagn. 2015;15(9):1159-69.

95. Clancy C, Joyce MR, Kerin MJ. The use of circulating microRNAs as diagnostic biomarkers in colorectal cancer. Cancer Biomark. 2015;15(2):103-13.

96. Hannafon BN, Trigoso YD, Calloway CL, Zhao YD, Lum DH, Welm AL, et al. Plasma exosome microRNAs are indicative of breast cancer. Breast Cancer Res. 2016;18(1):90.

97. Rabinowits G, Gercel-Taylor C, Day JM, Taylor DD, Kloecker GH. Exosomal microRNA: a diagnostic marker for lung cancer. Clin Lung Cancer. 2009;10(1):42-6.

98. Grange C, Tapparo M, Collino F, Vitillo L, Damasco C, Deregibus MC, et al. Microvesicles released from human renal cancer stem cells stimulate angiogenesis and formation of lung premetastatic niche. Cancer Res. 2011;71(15):5346-56.

99. Yang M, Chen J, Su F, Yu B, Su F, Lin L, et al. Microvesicles secreted by macrophages shuttle invasion-potentiating microRNAs into breast cancer cells. Mol Cancer. 2011;10:117.

100. Kumar S, Reddy PH. Are circulating microRNAs peripheral biomarkers for Alzheimer's disease? Biochim Biophys Acta. 2016;1862(9):1617-27.

101. Kumar S, Vijayan M, Bhatti JS, Reddy PH. MicroRNAs as Peripheral Biomarkers in Aging and Age-Related Diseases. Prog Mol Biol Transl Sci. 2017;146:47-94.

102. Mathivanan S, Simpson RJ. ExoCarta: A compendium of exosomal proteins and RNA. Proteomics. 2009;9(21):4997-5000.

103. Buschow SI, Liefhebber JM, Wubbolts R, Stoorvogel W. Exosomes contain ubiquitinated proteins. Blood Cells Mol Dis. 2005;35(3):398-403.

104. Cha DJ, Franklin JL, Dou Y, Liu Q, Higginbotham JN, Demory Beckler M, et al. KRAS-dependent sorting of miRNA to exosomes. Elife. 2015;4:e07197.

105. Lingwood D, Simons K. Lipid rafts as a membrane-organizing principle. Science. 2010;327(5961):46-50.

106. Schuler PJ, Saze Z, Hong CS, Muller L, Gillespie DG, Cheng D, et al. Human CD4+ CD39+ regulatory T cells produce adenosine upon co-expression of surface CD73 or contact with CD73+ exosomes or CD73+ cells. Clin Exp Immunol. 2014;177(2):531-43.

107. Wieckowski EU, Visus C, Szajnik M, Szczepanski MJ, Storkus WJ, Whiteside TL. Tumor-derived microvesicles promote regulatory T cell expansion and induce apoptosis in tumor-reactive activated CD8+ T lymphocytes. J Immunol. 2009;183(6):3720-30.

108. Gabrielsson S, Scheynius A. Exosomes in immunity and cancer--friends or foes? Semin Cancer Biol. 2014;28:1-2.

109. Whiteside TL. Tumor-Derived Exosomes and Their Role in Cancer Progression. Adv Clin Chem. 2016;74:103-41.

110. Zomer A, Maynard C, Verweij FJ, Kamermans A, Schafer R, Beerling E, et al. In Vivo imaging reveals extracellular vesicle-mediated phenocopying of metastatic behavior. Cell. 2015;161(5):1046-57.

111. Zhang L, Zhang S, Yao J, Lowery FJ, Zhang Q, Huang WC, et al. Microenvironment-induced PTEN loss by exosomal microRNA primes brain metastasis outgrowth. Nature. 2015;527(7576):100-4.

112. King HW, Michael MZ, Gleadle JM. Hypoxic enhancement of exosome release by breast cancer cells. BMC Cancer. 2012;12:421.

113. Park JE, Tan HS, Datta A, Lai RC, Zhang H, Meng W, et al. Hypoxic tumor cell modulates its microenvironment to enhance angiogenic and metastatic potential by secretion of proteins and exosomes. Mol Cell Proteomics. 2010;9(6):1085-99.

114. Peinado H, Aleckovic M, Lavotshkin S, Matei I, Costa-Silva B, Moreno-Bueno G, et al. Melanoma exosomes educate bone marrow progenitor cells toward a pro-metastatic phenotype through MET. Nat Med. 2012;18(6):883-91.

115. Ortiz A. Not all extracellular vesicles were created equal: clinical implications. Ann Transl Med. 2017;5(5):111.

116. Robbins PD, Dorronsoro A, Booker CN. Regulation of chronic inflammatory and immune processes by extracellular vesicles. J Clin Invest. 2016;126(4):1173-80.

117. Liu Q, Rojas-Canales DM, Divito SJ, Shufesky WJ, Stolz DB, Erdos G, et al. Donor dendritic cell-derived exosomes promote allograft-targeting immune response. J Clin Invest. 2016;126(8):2805-20.

118. Maybruck BT, Pfannenstiel LW, Diaz-Montero M, Gastman BR. Tumor-derived exosomes induce CD8(+) T cell suppressors. J Immunother Cancer. 2017;5(1):65.

119. Taylor DD, Gercel-Taylor C, Lyons KS, Stanson J, Whiteside TL. T-cell apoptosis and suppression of T-cell receptor/CD3-zeta by Fas ligand-containing membrane vesicles shed from ovarian tumors. Clin Cancer Res. 2003;9(14):5113-9.

120. Sharma S, Zuniga F, Rice GE, Perrin LC, Hooper JD, Salomon C. Tumor-derived exosomes in ovarian cancer - liquid biopsies for early detection and real-time monitoring of cancer progression. Oncotarget. 2017;8(61):104687-703.

121. Zheng H, Zhang L, Zhao Y, Yang D, Song F, Wen Y, et al. Plasma miRNAs as diagnostic and prognostic biomarkers for ovarian cancer. PLoS One. 2013;8(11):e77853.

122. Tengda L, Shuping L, Mingli G, Jie G, Yun L, Weiwei Z, et al. Serum exosomal microRNAs as potent circulating biomarkers for melanoma. Melanoma Res. 2018;28(4):295-303.

123. Malla B, Aebersold DM, Dal Pra A. Protocol for serum exosomal miRNAs analysis in prostate cancer patients treated with radiotherapy. J Transl Med. 2018;16(1):223.

124. Akinwunmi BO, Babic A, Vitonis AF, Cramer DW, Titus L, Tworoger SS, et al. Chronic Medical Conditions and CA125 Levels among Women without Ovarian Cancer. Cancer Epidemiol Biomarkers Prev. 2018;27(12):1483-90.

125. Wang PH, Huang YT, Ng KK, Chou HH, Lu HY, Ng SH, et al. Detecting recurrent ovarian cancer: revisit the values of whole-body CT and serum CA 125 levels. Acta Radiol. 2019:284185118822649.

126. Su YY, Sun L, Guo ZR, Li JC, Bai TT, Cai XX, et al. Upregulated expression of serum exosomal miR-375 and miR-1307 enhance the diagnostic power of CA125 for ovarian cancer. J Ovarian Res. 2019;12(1):6.

127. Tian Y, Li S, Song J, Ji T, Zhu M, Anderson GJ, et al. A doxorubicin delivery platform using engineered natural membrane vesicle exosomes for targeted tumor therapy. Biomaterials. 2014;35(7):2383-90.

128. Yang T, Martin P, Fogarty B, Brown A, Schurman K, Phipps R, et al. Exosome delivered anticancer drugs across the blood-brain barrier for brain cancer therapy in Danio rerio. Pharm Res. 2015;32(6):2003-14.

129. Yeo RW, Lai RC, Zhang B, Tan SS, Yin Y, Teh BJ, et al. Mesenchymal stem cell: an efficient mass producer of exosomes for drug delivery. Adv Drug Deliv Rev. 2013;65(3):336-41.

130. Sercombe L, Veerati T, Moheimani F, Wu SY, Sood AK, Hua S. Advances and Challenges of Liposome Assisted Drug Delivery. Front Pharmacol. 2015;6:286.

131. Chang TC, Shiah HS, Yang CH, Yeh KH, Cheng AL, Shen BN, et al. Phase I study of nanoliposomal irinotecan (PEP02) in advanced solid tumor patients. Cancer Chemother Pharmacol. 2015;75(3):579-86.

132. Wolfram J, Zhu M, Yang Y, Shen J, Gentile E, Paolino D, et al. Safety of Nanoparticles in Medicine. Curr Drug Targets. 2015;16(14):1671-81.

133. Raemdonck K, Braeckmans K, Demeester J, De Smedt SC. Merging the best of both worlds: hybrid lipid-enveloped matrix nanocomposites in drug delivery. Chem Soc Rev. 2014;43(1):444-72.

134. Turturici G, Tinnirello R, Sconzo G, Geraci F. Extracellular membrane vesicles as a mechanism of cell-to-cell communication: advantages and disadvantages. Am J Physiol Cell Physiol. 2014;306(7):C621-33.

135. Ha D, Yang N, Nadithe V. Exosomes as therapeutic drug carriers and delivery vehicles across biological membranes: current perspectives and future challenges. Acta Pharm Sin B. 2016;6(4):287-96.

136. Taylor DD, Shah S. Methods of isolating extracellular vesicles impact down-stream analyses of their cargoes. Methods. 2015;87:3-10.

137. Stefan C, Jansen S, Bollen M. NPP-type ectophosphodiesterases: unity in diversity. Trends Biochem Sci. 2005;30(10):542-50.

138. Chen M, O'Connor KL. Integrin alpha6beta4 promotes expression of autotaxin/ENPP2 autocrine motility factor in breast carcinoma cells. Oncogene. 2005;24(32):5125-30.

139. Kawagoe H, Stracke ML, Nakamura H, Sano K. Expression and transcriptional regulation of the PD-Ialpha/autotaxin gene in neuroblastoma. Cancer Res. 1997;57(12):2516-21.

140. Sioletic S, Czaplinski J, Hu L, Fletcher JA, Fletcher CD, Wagner AJ, et al. c-Jun promotes cell migration and drives expression of the motility factor ENPP2 in soft tissue sarcomas. J Pathol. 2014;234(2):190-202.

141. Benesch MG, Zhao YY, Curtis JM, McMullen TP, Brindley DN. Regulation of autotaxin expression and secretion by lysophosphatidate and sphingosine 1-phosphate. J Lipid Res. 2015;56(6):1134-44.

142. Jansen S, Stefan C, Creemers JW, Waelkens E, Van Eynde A, Stalmans W, et al. Proteolytic maturation and activation of autotaxin (NPP2), a secreted metastasis-enhancing lysophospholipase D. J Cell Sci. 2005;118(Pt 14):3081-9.

143. Tokumura A, Harada K, Fukuzawa K, Tsukatani H. Involvement of lysophospholipase D in the production of lysophosphatidic acid in rat plasma. Biochim Biophys Acta. 1986;875(1):31-8.

144. Tokumura A, Majima E, Kariya Y, Tominaga K, Kogure K, Yasuda K, et al. Identification of human plasma lysophospholipase D, a lysophosphatidic acid-producing enzyme, as autotaxin, a multifunctional phosphodiesterase. J Biol Chem. 2002;277(42):39436-42.

145. Stracke ML, Krutzsch HC, Unsworth EJ, Arestad A, Cioce V, Schiffmann E, et al. Identification, purification, and partial sequence analysis of autotaxin, a novel motility-stimulating protein. J Biol Chem. 1992;267(4):2524-9.

146. Murata J, Lee HY, Clair T, Krutzsch HC, Arestad AA, Sobel ME, et al. cDNA cloning of the human tumor motility-stimulating protein, autotaxin, reveals a homology with phosphodiesterases. J Biol Chem. 1994;269(48):30479-84.

147. Kawagoe H, Soma O, Goji J, Nishimura N, Narita M, Inazawa J, et al. Molecular cloning and chromosomal assignment of the human brain-type phosphodiesterase I/nucleotide pyrophosphatase gene (PDNP2). Genomics. 1995;30(2):380-4.

148. Lee HY, Murata J, Clair T, Polymeropoulos MH, Torres R, Manrow RE, et al. Cloning, chromosomal localization, and tissue expression of autotaxin from human teratocarcinoma cells. Biochem Biophys Res Commun. 1996;218(3):714-9.

149. Hashimoto T, Okudaira S, Igarashi K, Hama K, Yatomi Y, Aoki J. Identification and biochemical characterization of a novel autotaxin isoform, ATXdelta, with a four-amino acid deletion. J Biochem. 2012;151(1):89-97.

150. Narita M, Goji J, Nakamura H, Sano K. Molecular cloning, expression, and localization of a brain-specific phosphodiesterase I/nucleotide pyrophosphatase (PD-I alpha) from rat brain. J Biol Chem. 1994;269(45):28235-42.

151. Perrakis A, Moolenaar WH. Autotaxin: structure-function and signaling. J Lipid Res. 2014;55(6):1010-8.

152. Houben AJ, van Wijk XM, van Meeteren LA, van Zeijl L, van de Westerlo EM, Hausmann J, et al. The polybasic insertion in autotaxin alpha confers specific binding to heparin and cell surface heparan sulfate proteoglycans. J Biol Chem. 2013;288(1):510-9.

153. Ferry G, Tellier E, Try A, Gres S, Naime I, Simon MF, et al. Autotaxin is released from adipocytes, catalyzes lysophosphatidic acid synthesis, and activates preadipocyte proliferation. Up-regulated expression with adipocyte differentiation and obesity. J Biol Chem. 2003;278(20):18162-9.

154. Rancoule C, Dusaulcy R, Treguer K, Gres S, Attane C, Saulnier-Blache JS. Involvement of autotaxin/lysophosphatidic acid signaling in obesity and impaired glucose homeostasis. Biochimie. 2014;96:140-3.

155. Dusaulcy R, Rancoule C, Gres S, Wanecq E, Colom A, Guigne C, et al. Adipose-specific disruption of autotaxin enhances nutritional fattening and reduces plasma lysophosphatidic acid. J Lipid Res. 2011;52(6):1247-55.

156. Giganti A, Rodriguez M, Fould B, Moulharat N, Coge F, Chomarat P, et al. Murine and human autotaxin alpha, beta, and gamma isoforms: gene organization, tissue distribution, and biochemical characterization. J Biol Chem. 2008;283(12):7776-89.

157. Hausmann J, Perrakis A, Moolenaar WH. Structure-function relationships of autotaxin, a secreted lysophospholipase D. Adv Biol Regul. 2013;53(1):112-7.

158. Koike S, Keino-Masu K, Ohto T, Masu M. The N-terminal hydrophobic sequence of autotaxin (ENPP2) functions as a signal peptide. Genes Cells. 2006;11(2):133-42.

159. Hausmann J, Kamtekar S, Christodoulou E, Day JE, Wu T, Fulkerson Z, et al. Structural basis of substrate discrimination and integrin binding by autotaxin. Nat Struct Mol Biol. 2011;18(2):198-204.

160. Fulkerson Z, Wu T, Sunkara M, Kooi CV, Morris AJ, Smyth SS. Binding of autotaxin to integrins localizes lysophosphatidic acid production to platelets and mammalian cells. J Biol Chem. 2011;286(40):34654-63.

161. Vogt W. Pharamacologically active acidic phospholipids and glycolipids. Biochem Pharmacol. 1963;12:415-20.

162. Tigyi G, Miledi R. Lysophosphatidates bound to serum albumin activate membrane currents in Xenopus oocytes and neurite retraction in PC12 pheochromocytoma cells. J Biol Chem. 1992;267(30):21360-7.

163. Xu Y, Gaudette DC, Boynton JD, Frankel A, Fang XJ, Sharma A, et al. Characterization of an ovarian cancer activating factor in ascites from ovarian cancer patients. Clin Cancer Res. 1995;1(10):1223-32.

164. Lin ME, Herr DR, Chun J. Lysophosphatidic acid (LPA) receptors: signaling properties and disease relevance. Prostaglandins Other Lipid Mediat. 2010;91(3-4):130-8.

165. Takuwa Y, Takuwa N, Sugimoto N. The Edg family G protein-coupled receptors for lysophospholipids: their signaling properties and biological activities. J Biochem. 2002;131(6):767-71.

166. Umezu-Goto M, Kishi Y, Taira A, Hama K, Dohmae N, Takio K, et al. Autotaxin has lysophospholipase D activity leading to tumor cell growth and motility by lysophosphatidic acid production. J Cell Biol. 2002;158(2):227-33.

167. Bandoh K, Aoki J, Taira A, Tsujimoto M, Arai H, Inoue K. Lysophosphatidic acid (LPA) receptors of the EDG family are differentially activated by LPA species. Structure-activity relationship of cloned LPA receptors. FEBS Lett. 2000;478(1-2):159-65.

168. Hecht JH, Weiner JA, Post SR, Chun J. Ventricular zone gene-1 (vzg-1) encodes a lysophosphatidic acid receptor expressed in neurogenic regions of the developing cerebral cortex. J Cell Biol. 1996;135(4):1071-83.

169. An S, Dickens MA, Bleu T, Hallmark OG, Goetzl EJ. Molecular cloning of the human Edg2 protein and its identification as a functional cellular receptor for lysophosphatidic acid. Biochem Biophys Res Commun. 1997;231(3):619-22.

170. Bandoh K, Aoki J, Hosono H, Kobayashi S, Kobayashi T, Murakami-Murofushi K, et al. Molecular cloning and characterization of a novel human G-protein-coupled receptor, EDG7, for lysophosphatidic acid. J Biol Chem. 1999;274(39):27776-85.

171. Ishii S, Noguchi K, Yanagida K. Non-Edg family lysophosphatidic acid (LPA) receptors. Prostaglandins Other Lipid Mediat. 2009;89(3-4):57-65.

172. Noguchi K, Ishii S, Shimizu T. Identification of p2y9/GPR23 as a novel G protein-coupled receptor for lysophosphatidic acid, structurally distant from the Edg family. J Biol Chem. 2003;278(28):25600-6.

173. Lee M, Choi S, Hallden G, Yo SJ, Schichnes D, Aponte GW. P2Y5 is a G(alpha)i, G(alpha)12/13 G protein-coupled receptor activated by lysophosphatidic acid that reduces intestinal cell adhesion. Am J Physiol Gastrointest Liver Physiol. 2009;297(4):G641-54.

174. Pasternack SM, von Kugelgen I, Al Aboud K, Lee YA, Ruschendorf F, Voss K, et al. G protein-coupled receptor P2Y5 and its ligand LPA are involved in maintenance of human hair growth. Nat Genet. 2008;40(3):329-34.

175. Yanagida K, Masago K, Nakanishi H, Kihara Y, Hamano F, Tajima Y, et al. Identification and characterization of a novel lysophosphatidic acid receptor, p2y5/LPA6. J Biol Chem. 2009;284(26):17731-41.

176. Gerrard JM, Robinson P. Identification of the molecular species of lysophosphatidic acid produced when platelets are stimulated by thrombin. Biochim Biophys Acta. 1989;1001(3):282-5.

177. Baker DL, Desiderio DM, Miller DD, Tolley B, Tigyi GJ. Direct quantitative analysis of lysophosphatidic acid molecular species by stable isotope dilution electrospray ionization liquid chromatography-mass spectrometry. Anal Biochem. 2001;292(2):287-95.

178. Panupinthu N, Lee HY, Mills GB. Lysophosphatidic acid production and action: critical new players in breast cancer initiation and progression. Br J Cancer. 2010;102(6):941-6.

179. Ishii I, Contos JJ, Fukushima N, Chun J. Functional comparisons of the lysophosphatidic acid receptors, LP(A1)/VZG-1/EDG-2, LP(A2)/EDG-4, and LP(A3)/EDG-7 in neuronal cell lines using a retrovirus expression system. Mol Pharmacol. 2000;58(5):895-902.

180. Lai YJ, Chen CS, Lin WC, Lin FT. c-Src-mediated phosphorylation of TRIP6 regulates its function in lysophosphatidic acid-induced cell migration. Mol Cell Biol. 2005;25(14):5859-68.

181. Matas-Rico E, Garcia-Diaz B, Llebrez-Zayas P, Lopez-Barroso D, Santin L, Pedraza C, et al. Deletion of lysophosphatidic acid receptor LPA1 reduces neurogenesis in the mouse dentate gyrus. Mol Cell Neurosci. 2008;39(3):342-55.

182. Yung YC, Stoddard NC, Chun J. LPA receptor signaling: pharmacology, physiology, and pathophysiology. J Lipid Res. 2014;55(7):1192-214.

183. Inoue A, Arima N, Ishiguro J, Prestwich GD, Arai H, Aoki J. LPA-producing enzyme PA-PLA(1)alpha regulates hair follicle development by modulating EGFR signalling. EMBO J. 2011;30(20):4248-60.

184. Lee Z, Cheng CT, Zhang H, Subler MA, Wu J, Mukherjee A, et al. Role of LPA4/p2y9/GPR23 in negative regulation of cell motility. Mol Biol Cell. 2008;19(12):5435-45.

185. Ohuchi H, Hamada A, Matsuda H, Takagi A, Tanaka M, Aoki J, et al. Expression patterns of the lysophospholipid receptor genes during mouse early development. Dev Dyn. 2008;237(11):3280-94.

186. Hu YL, Tee MK, Goetzl EJ, Auersperg N, Mills GB, Ferrara N, et al. Lysophosphatidic acid induction of vascular endothelial growth factor expression in human ovarian cancer cells. J Natl Cancer Inst. 2001;93(10):762-8.

187. Tomsig JL, Snyder AH, Berdyshev EV, Skobeleva A, Mataya C, Natarajan V, et al. Lipid phosphate phosphohydrolase type 1 (LPP1) degrades extracellular lysophosphatidic acid in vivo. Biochem J. 2009;419(3):611-8.

188. Boucharaba A, Serre CM, Guglielmi J, Bordet JC, Clezardin P, Peyruchaud O. The type 1 lysophosphatidic acid receptor is a target for therapy in bone metastases. Proc Natl Acad Sci U S A. 2006;103(25):9643-8.

189. Okusa MD, Ye H, Huang L, Sigismund L, Macdonald T, Lynch KR. Selective blockade of lysophosphatidic acid LPA3 receptors reduces murine renal ischemia-reperfusion injury. Am J Physiol Renal Physiol. 2003;285(3):F565-74.

190. Palmer SM, Snyder L, Todd JL, Soule B, Christian R, Anstrom K, et al. Randomized, Double-Blind, Placebo-Controlled, Phase 2 Trial of BMS-986020, a Lysophosphatidic Acid Receptor Antagonist for the Treatment of Idiopathic Pulmonary Fibrosis. Chest. 2018;154(5):1061-9.

191. Allanore Y, Distler O, Jagerschmidt A, Illiano S, Ledein L, Boitier E, et al. Lysophosphatidic Acid Receptor 1 Antagonist SAR100842 for Patients With Diffuse Cutaneous Systemic Sclerosis: A Double-Blind, Randomized, Eight-Week Placebo-Controlled Study Followed by a Sixteen-Week Open-Label Extension Study. Arthritis Rheumatol. 2018;70(10):1634-43.

192. Tanaka M, Okudaira S, Kishi Y, Ohkawa R, Iseki S, Ota M, et al. Autotaxin stabilizes blood vessels and is required for embryonic vasculature by producing lysophosphatidic acid. J Biol Chem. 2006;281(35):25822-30.

193. Tabchy A, Tigyi G, Mills GB. Location, location, location: a crystal-clear view of autotaxin saturating LPA receptors. Nat Struct Mol Biol. 2011;18(2):117-8.

194. Ferry G, Giganti A, Coge F, Bertaux F, Thiam K, Boutin JA. Functional invalidation of the autotaxin gene by a single amino acid mutation in mouse is lethal. FEBS Lett. 2007;581(18):3572-8.

195. Federico L, Jeong KJ, Vellano CP, Mills GB. Autotaxin, a lysophospholipase D with pleomorphic effects in oncogenesis and cancer progression. J Lipid Res. 2016;57(1):25-35.

196. Xu A, Ahsanul Kabir Khan M, Chen F, Zhong Z, Chen HC, Song Y. Overexpression of autotaxin is associated with human renal cell carcinoma and bladder carcinoma and their progression. Med Oncol. 2016;33(11):131.

197. Cooper AB, Wu J, Lu D, Maluccio MA. Is autotaxin (ENPP2) the link between hepatitis C and hepatocellular cancer? J Gastrointest Surg. 2007;11(12):1628-34; discussion 34-5.

198. Kehlen A, Englert N, Seifert A, Klonisch T, Dralle H, Langner J, et al. Expression, regulation and function of autotaxin in thyroid carcinomas. Int J Cancer. 2004;109(6):833-8.

199. Yang Y, Mou L, Liu N, Tsao MS. Autotaxin expression in non-small-cell lung cancer. Am J Respir Cell Mol Biol. 1999;21(2):216-22.

200. Hoelzinger DB, Nakada M, Demuth T, Rosensteel T, Reavie LB, Berens ME. Autotaxin: a secreted autocrine/paracrine factor that promotes glioma invasion. J Neurooncol. 2008;86(3):297-309.

201. Popnikolov NK, Dalwadi BH, Thomas JD, Johannes GJ, Imagawa WT. Association of autotaxin and lysophosphatidic acid receptor 3 with aggressiveness of human breast carcinoma. Tumour Biol. 2012;33(6):2237-43.

202. Ptaszynska MM, Pendrak ML, Bandle RW, Stracke ML, Roberts DD. Positive feedback between vascular endothelial growth factor-A and autotaxin in ovarian cancer cells. Mol Cancer Res. 2008;6(3):352-63.

203. Tokumura A, Kume T, Fukuzawa K, Tahara M, Tasaka K, Aoki J, et al. Peritoneal fluids from patients with certain gynecologic tumor contain elevated levels of bioactive lysophospholipase D activity. Life Sci. 2007;80(18):1641-9.

204. Liu S, Umezu-Goto M, Murph M, Lu Y, Liu W, Zhang F, et al. Expression of autotaxin and lysophosphatidic acid receptors increases mammary tumorigenesis, invasion, and metastases. Cancer Cell. 2009;15(6):539-50.

205. Yang SY, Lee J, Park CG, Kim S, Hong S, Chung HC, et al. Expression of autotaxin (NPP-2) is closely linked to invasiveness of breast cancer cells. Clin Exp Metastasis. 2002;19(7):603-8.

206. Hanahan D, Weinberg RA. The hallmarks of cancer. Cell. 2000;100(1):57-70.

207. Colotta F, Allavena P, Sica A, Garlanda C, Mantovani A. Cancer-related inflammation, the seventh hallmark of cancer: links to genetic instability. Carcinogenesis. 2009;30(7):1073-81.

208. Brindley DN, Benesch MGK, Murph MM. Autotaxin – An Enzymatic Augmenter of Malignant Progression Linked to Inflammation. 2015.

209. Fang X, Yu S, Bast RC, Liu S, Xu HJ, Hu SX, et al. Mechanisms for lysophosphatidic acid-induced cytokine production in ovarian cancer cells. J Biol Chem. 2004;279(10):9653-61.

210. Liu S, Murph M, Panupinthu N, Mills GB. ATX-LPA receptor axis in inflammation and cancer. Cell Cycle. 2009;8(22):3695-701.

211. Bai Z, Cai L, Umemoto E, Takeda A, Tohya K, Komai Y, et al. Constitutive lymphocyte transmigration across the basal lamina of high endothelial venules is regulated by the autotaxin/lysophosphatidic acid axis. J Immunol. 2013;190(5):2036-48.

212. Knowlden S, Georas SN. The autotaxin-LPA axis emerges as a novel regulator of lymphocyte homing and inflammation. J Immunol. 2014;192(3):851-7.

213. Benesch MG, Tang X, Dewald J, Dong WF, Mackey JR, Hemmings DG, et al. Tumor-induced inflammation in mammary adipose tissue stimulates a vicious cycle of autotaxin expression and breast cancer progression. FASEB J. 2015;29(9):3990-4000.

214. Yu S, Murph MM, Lu Y, Liu S, Hall HS, Liu J, et al. Lysophosphatidic acid receptors determine tumorigenicity and aggressiveness of ovarian cancer cells. J Natl Cancer Inst. 2008;100(22):1630-42.

215. Andreasen C, Carbonetti NH. Pertussis toxin inhibits early chemokine production to delay neutrophil recruitment in response to Bordetella pertussis respiratory tract infection in mice. Infect Immun. 2008;76(11):5139-48.

216. Kuppa SS, Jia W, Liu S, Nguyen H, Smyth SS, Mills GB, et al. Autotaxin exacerbates tumor progression by enhancing MEK1 and overriding the function of miR-489-3p. Cancer Lett. 2018;432:84-92.

217. Pamuklar Z, Federico L, Liu S, Umezu-Goto M, Dong A, Panchatcharam M, et al. Autotaxin/lysopholipase D and lysophosphatidic acid regulate murine hemostasis and thrombosis. J Biol Chem. 2009;284(11):7385-94.

218. Federico L, Ren H, Mueller PA, Wu T, Liu S, Popovic J, et al. Autotaxin and its product lysophosphatidic acid suppress brown adipose differentiation and promote diet-induced obesity in mice. Mol Endocrinol. 2012;26(5):786-97.

219. Murph MM, Liu S, Jia W, Nguyen H, MacFarlane MA, Smyth SS, et al. Diet-regulated behavior: FVB/N mice fed a lean diet exhibit increased nocturnal bouts of aggression between littermates. Lab Anim. 2019:23677219834582.

220. Valdes-Rives SA, Gonzalez-Arenas A. Autotaxin-Lysophosphatidic Acid: From Inflammation to Cancer Development. Mediators Inflamm. 2017;2017:9173090.

221. Saunders LP, Ouellette A, Bandle R, Chang WC, Zhou H, Misra RN, et al. Identification of small-molecule inhibitors of autotaxin that inhibit melanoma cell migration and invasion. Mol Cancer Ther. 2008;7(10):3352-62.

222. Albers HM, van Meeteren LA, Egan DA, van Tilburg EW, Moolenaar WH, Ovaa H. Discovery and optimization of boronic acid based inhibitors of autotaxin. J Med Chem. 2010;53(13):4958-67.

223. Fells JI, Lee SC, Norman DD, Tsukahara R, Kirby JR, Nelson S, et al. Targeting the hydrophobic pocket of autotaxin with virtual screening of inhibitors identifies a common aromatic sulfonamide structural motif. FEBS J. 2014;281(4):1017-28.

224. Albers HM, Dong A, van Meeteren LA, Egan DA, Sunkara M, van Tilburg EW, et al. Boronic acid-based inhibitor of autotaxin reveals rapid turnover of LPA in the circulation. Proc Natl Acad Sci U S A. 2010;107(16):7257-62.

225. East JE, Kennedy AJ, Tomsig JL, De Leon AR, Lynch KR, Macdonald TL. Synthesis and structure-activity relationships of tyrosine-based inhibitors of autotaxin (ATX). Bioorg Med Chem Lett. 2010;20(23):7132-6.

226. Saga H, Ohhata A, Hayashi A, Katoh M, Maeda T, Mizuno H, et al. A novel highly potent autotaxin/ENPP2 inhibitor produces prolonged decreases in plasma lysophosphatidic acid formation in vivo and regulates urethral tension. PLoS One. 2014;9(4):e93230.

227. Benesch MG, Ko YM, Tang X, Dewald J, Lopez-Campistrous A, Zhao YY, et al. Autotaxin is an inflammatory mediator and therapeutic target in thyroid cancer. Endocr Relat Cancer. 2015;22(4):593-607.

228. Benesch MG, Tang X, Maeda T, Ohhata A, Zhao YY, Kok BP, et al. Inhibition of autotaxin delays breast tumor growth and lung metastasis in mice. FASEB J. 2014;28(6):2655-66.

229. Schleicher SM, Thotala DK, Linkous AG, Hu R, Leahy KM, Yazlovitskaya EM, et al. Autotaxin and LPA receptors represent potential molecular targets for the radiosensitization of murine glioma through effects on tumor vasculature. PLoS One. 2011;6(7):e22182.

230. Zhang H, Xu X, Gajewiak J, Tsukahara R, Fujiwara Y, Liu J, et al. Dual activity lysophosphatidic acid receptor pan-antagonist/autotaxin inhibitor reduces breast cancer cell migration in vitro and causes tumor regression in vivo. Cancer Res. 2009;69(13):5441-9.

231. Murph MM, Jiang GW, Altman MK, Jia W, Nguyen DT, Fambrough JM, et al. Vinyl sulfone analogs of lysophosphatidylcholine irreversibly inhibit autotaxin and prevent angiogenesis in melanoma. Bioorg Med Chem. 2015;23(17):5999-6013.

232. Bhave SR, Dadey DY, Karvas RM, Ferraro DJ, Kotipatruni RP, Jaboin JJ, et al. Autotaxin Inhibition with PF-8380 Enhances the Radiosensitivity of Human and Murine Glioblastoma Cell Lines. Front Oncol. 2013;3:236.

233. St-Coeur PD, Ferguson D, Morin P, Jr., Touaibia M. PF-8380 and closely related analogs: synthesis and structure-activity relationship towards autotaxin inhibition and glioma cell viability. Arch Pharm (Weinheim). 2013;346(2):91-7.

234. Desroy N, Housseman C, Bock X, Joncour A, Bienvenu N, Cherel L, et al. Discovery of 2-[[2-Ethyl-6-[4-[2-(3-hydroxyazetidin-1-yl)-2-oxoethyl]piperazin-1-yl]-8-methyli midazo[1,2-a]pyridin-3-yl]methylamino]-4-(4-fluorophenyl)thiazole-5-

carbonitrile (GLPG1690), a First-in-Class Autotaxin Inhibitor Undergoing Clinical Evaluation for the Treatment of Idiopathic Pulmonary Fibrosis. J Med Chem. 2017;60(9):3580-90.

235. Maher TM, van der Aar EM, Van de Steen O, Allamassey L, Desrivot J, Dupont S, et al. Safety, tolerability, pharmacokinetics, and pharmacodynamics of GLPG1690, a novel autotaxin inhibitor, to treat idiopathic pulmonary fibrosis (FLORA): a phase 2a randomised placebo-controlled trial. Lancet Respir Med. 2018;6(8):627-35.

236. Kawaguchi M, Okabe T, Okudaira S, Nishimasu H, Ishitani R, Kojima H, et al. Screening and X-ray crystal structure-based optimization of autotaxin (ENPP2) inhibitors, using a newly developed fluorescence probe. ACS Chem Biol. 2013;8(8):1713-21.

237. Norman DD, Ibezim A, Scott WE, White S, Parrill AL, Baker DL. Autotaxin inhibition: development and application of computational tools to identify site-selective lead compounds. Bioorg Med Chem. 2013;21(17):5548-60.

238. Siegel RL, Miller KD, Jemal A. Cancer statistics, 2019. CA: A Cancer Journal for Clinicians. 2019;69(1):7-34.

239. Society AC. Cancer Facts and Figures. 2019.

240. Rabbie R, Ferguson P, Molina-Aguilar C, Adams DJ, Robles-Espinoza CD. Melanoma subtypes: genomic profiles, prognostic molecular markers and therapeutic possibilities. J Pathol. 2019;247(5):539-51.

241. Cancer Genome Atlas N. Genomic Classification of Cutaneous Melanoma. Cell. 2015;161(7):1681-96.

242. Hayward NK, Wilmott JS, Waddell N, Johansson PA, Field MA, Nones K, et al. Whole-genome landscapes of major melanoma subtypes. Nature. 2017;545(7653):175-80.

243. Shain AH, Joseph NM, Yu R, Benhamida J, Liu S, Prow T, et al. Genomic and Transcriptomic Analysis Reveals Incremental Disruption of Key Signaling Pathways during Melanoma Evolution. Cancer Cell. 2018;34(1):45-55 e4.

244. Garraway LA, Widlund HR, Rubin MA, Getz G, Berger AJ, Ramaswamy S, et al. Integrative genomic analyses identify MITF as a lineage survival oncogene amplified in malignant melanoma. Nature. 2005;436(7047):117-22.

245. Network NCC. Cutaneous Melanoma. 2019.

246. Domingues B, Lopes JM, Soares P, Populo H. Melanoma treatment in review. Immunotargets Ther. 2018;7:35-49.

247. Austin E, Mamalis A, Ho D, Jagdeo J. Laser and light-based therapy for cutaneous and soft-tissue metastases of malignant melanoma: a systematic review. Arch Dermatol Res. 2017;309(4):229-42.

248. Wilson MA, Schuchter LM. Chemotherapy for Melanoma. Cancer Treat Res. 2016;167:209-29.

249. Kim C, Lee CW, Kovacic L, Shah A, Klasa R, Savage KJ. Long-term survival in patients with metastatic melanoma treated with DTIC or temozolomide. Oncologist. 2010;15(7):765-71.

250. Chapman PB, Hauschild A, Robert C, Haanen JB, Ascierto P, Larkin J, et al. Improved survival with vemurafenib in melanoma with BRAF V600E mutation. N Engl J Med. 2011;364(26):2507-16.

251. Ballantyne AD, Garnock-Jones KP. Dabrafenib: first global approval. Drugs. 2013;73(12):1367-76.

252. Rizos H, Menzies AM, Pupo GM, Carlino MS, Fung C, Hyman J, et al. BRAF inhibitor resistance mechanisms in metastatic melanoma: spectrum and clinical impact. Clin Cancer Res. 2014;20(7):1965-77.

253. Wright CJ, McCormack PL. Trametinib: first global approval. Drugs. 2013;73(11):1245-54.

254. Flaherty KT, Robert C, Hersey P, Nathan P, Garbe C, Milhem M, et al. Improved survival with MEK inhibition in BRAF-mutated melanoma. N Engl J Med. 2012;367(2):107-14.

255. Flaherty KT, Infante JR, Daud A, Gonzalez R, Kefford RF, Sosman J, et al. Combined BRAF and MEK inhibition in melanoma with BRAF V600 mutations. N Engl J Med. 2012;367(18):1694-703.

256. Hopkins AM, Van Dyk M, Rowland A, Sorich MJ. Effect of early adverse events on response and survival outcomes of advanced melanoma patients treated with vemurafenib or vemurafenib plus cobimetinib: A pooled analysis of clinical trial data. Pigment Cell Melanoma Res. 2019.

257. Grimaldi AM, Simeone E, Ascierto PA. Vemurafenib plus cobimetinib in the treatment of mutated metastatic melanoma: the CoBRIM trial. Melanoma Manag. 2015;2(3):209-15.

258. Gencler B, Gonul M. Cutaneous Side Effects of BRAF Inhibitors in Advanced Melanoma: Review of the Literature. Dermatol Res Pract. 2016;2016:5361569.

259. Kiyohara T, Nagano N, Miyamoto M, Shijimaya T, Nakamaru S, Makimura K, et al. BRAF-mutated, acral verrucous melanoma successfully treated by dabrafenib plus trametinib combination therapy. Clin Exp Dermatol. 2019.

260. Sun J, Zager JS, Eroglu Z. Encorafenib/binimetinib for the treatment of BRAF-mutant advanced, unresectable, or metastatic melanoma: design, development, and potential place in therapy. Onco Targets Ther. 2018;11:9081-9.

261. Dummer R, Ascierto PA, Gogas HJ, Arance A, Mandala M, Liszkay G, et al. Encorafenib plus binimetinib versus vemurafenib or encorafenib in patients with BRAF-mutant melanoma (COLUMBUS): a multicentre, open-label, randomised phase 3 trial. Lancet Oncol. 2018;19(5):603-15.

262. von Moos R, Seifert B, Simcock M, Goldinger SM, Gillessen S, Ochsenbein A, et al. First-line temozolomide combined with bevacizumab in metastatic melanoma: a multicentre phase II trial (SAKK 50/07). Ann Oncol. 2012;23(2):531-6.

263. Kim KJ, Li B, Winer J, Armanini M, Gillett N, Phillips HS, et al. Inhibition of vascular endothelial growth factor-induced angiogenesis suppresses tumour growth in vivo. Nature. 1993;362(6423):841-4.

264. Kazazi-Hyseni F, Beijnen JH, Schellens JH. Bevacizumab. Oncologist. 2010;15(8):819-25.

265. Guterres AN, Herlyn M, Villanueva J. Melanoma. 2018:1-10.

266. Lugowska I, Teterycz P, Rutkowski P. Immunotherapy of melanoma. Contemp Oncol (Pozn). 2018;22(1A):61-7.

267. Ives NJ, Suciu S, Eggermont AMM, Kirkwood J, Lorigan P, Markovic SN, et al. Adjuvant interferon-alpha for the treatment of high-risk melanoma: An individual patient data meta-analysis. Eur J Cancer. 2017;82:171-83.

268. Kirkwood JM, Ibrahim JG, Sosman JA, Sondak VK, Agarwala SS, Ernstoff MS, et al. High-dose interferon alfa-2b significantly prolongs relapse-free and overall survival compared with the GM2-KLH/QS-21 vaccine in patients with resected stage IIB-III melanoma: results of intergroup trial E1694/S9512/C509801. J Clin Oncol. 2001;19(9):2370-80.

269. Eggermont AM, Suciu S, Santinami M, Testori A, Kruit WH, Marsden J, et al. Adjuvant therapy with pegylated interferon alfa-2b versus observation alone in resected stage III melanoma: final results of EORTC 18991, a randomised phase III trial. Lancet. 2008;372(9633):117-26.

270. Cameron F, Whiteside G, Perry C. Ipilimumab: first global approval. Drugs. 2011;71(8):1093-104.

271. Rowshanravan B, Halliday N, Sansom DM. CTLA-4: a moving target in immunotherapy. Blood. 2018;131(1):58-67.

272. Tsai KK, Zarzoso I, Daud AI. PD-1 and PD-L1 antibodies for melanoma. Hum Vaccin Immunother. 2014;10(11):3111-6.

273. Xu-Monette ZY, Zhang M, Li J, Young KH. PD-1/PD-L1 Blockade: Have We Found the Key to Unleash the Antitumor Immune Response? Front Immunol. 2017;8:1597.

274. Raedler LA. Opdivo (Nivolumab): Second PD-1 Inhibitor Receives FDA Approval for Unresectable or Metastatic Melanoma. Am Health Drug Benefits. 2015;8(Spec Feature):180-3.

275. Ribas A, Puzanov I, Dummer R, Schadendorf D, Hamid O, Robert C, et al. Pembrolizumab versus investigator-choice chemotherapy for ipilimumab-refractory melanoma (KEYNOTE-002): a randomised, controlled, phase 2 trial. Lancet Oncol. 2015;16(8):908-18.

276. Larkin J, Chiarion-Sileni V, Gonzalez R, Grob JJ, Cowey CL, Lao CD, et al. Combined Nivolumab and Ipilimumab or Monotherapy in Untreated Melanoma. N Engl J Med. 2015;373(1):23-34.

277. Weber J, Mandala M, Del Vecchio M, Gogas HJ, Arance AM, Cowey CL, et al. Adjuvant Nivolumab versus Ipilimumab in Resected Stage III or IV Melanoma. N Engl J Med. 2017;377(19):1824-35.

278. Pol J, Kroemer G, Galluzzi L. First oncolytic virus approved for melanoma immunotherapy. Oncoimmunology. 2016;5(1):e1115641.

279. Russell SJ, Peng KW, Bell JC. Oncolytic virotherapy. Nat Biotechnol. 2012;30(7):658-70.

280. Morton DL, Eilber FR, Holmes EC, Hunt JS, Ketcham AS, Silverstein MJ, et al. BCG immunotherapy of malignant melanoma: summary of a seven-year experience. Ann Surg. 1974;180(4):635-43.

281. van Zeijl MC, van den Eertwegh AJ, Haanen JB, Wouters MW. (Neo)adjuvant systemic therapy for melanoma. Eur J Surg Oncol. 2017;43(3):534-43.

282. Banerjee S, Kaye SB. New strategies in the treatment of ovarian cancer: current clinical perspectives and future potential. Clin Cancer Res. 2013;19(5):961-8.

283. Kurman RJ, Shih Ie M. Molecular pathogenesis and extraovarian origin of epithelial ovarian cancer--shifting the paradigm. Hum Pathol. 2011;42(7):918-31.

284. Marquez RT, Baggerly KA, Patterson AP, Liu J, Broaddus R, Frumovitz M, et al. Patterns of gene expression in different histotypes of epithelial ovarian cancer correlate with those in normal fallopian tube, endometrium, and colon. Clin Cancer Res. 2005;11(17):6116-26.

285. Kurman RJ. Origin and molecular pathogenesis of ovarian high-grade serous carcinoma. Ann Oncol. 2013;24 Suppl 10:x16-21.

286. Ahmed AA, Etemadmoghadam D, Temple J, Lynch AG, Riad M, Sharma R, et al. Driver mutations in TP53 are ubiquitous in high grade serous carcinoma of the ovary. J Pathol. 2010;221(1):49-56.

287. Shih Ie M, Kurman RJ. Ovarian tumorigenesis: a proposed model based on morphological and molecular genetic analysis. Am J Pathol. 2004;164(5):1511-8.

288. Senturk E, Cohen S, Dottino PR, Martignetti JA. A critical re-appraisal of BRCA1 methylation studies in ovarian cancer. Gynecol Oncol. 2010;119(2):376-83.

289. Kindelberger DW, Lee Y, Miron A, Hirsch MS, Feltmate C, Medeiros F, et al. Intraepithelial carcinoma of the fimbria and pelvic serous carcinoma: Evidence for a causal relationship. Am J Surg Pathol. 2007;31(2):161-9.

290. Lee Y, Miron A, Drapkin R, Nucci MR, Medeiros F, Saleemuddin A, et al. A candidate precursor to serous carcinoma that originates in the distal fallopian tube. J Pathol. 2007;211(1):26-35.

291. Kurman RJ, Shih Ie M. The origin and pathogenesis of epithelial ovarian cancer: a proposed unifying theory. Am J Surg Pathol. 2010;34(3):433-43.

292. Medeiros F, Muto MG, Lee Y, Elvin JA, Callahan MJ, Feltmate C, et al. The tubal fimbria is a preferred site for early adenocarcinoma in women with familial ovarian cancer syndrome. Am J Surg Pathol. 2006;30(2):230-6.

293. Shaw PA, Rouzbahman M, Pizer ES, Pintilie M, Begley H. Candidate serous cancer precursors in fallopian tube epithelium of BRCA1/2 mutation carriers. Mod Pathol. 2009;22(9):1133-8.

294. Risch HA, Weiss NS, Lyon JL, Daling JR, Liff JM. Events of reproductive life and the incidence of epithelial ovarian cancer. Am J Epidemiol. 1983;117(2):128-39.

295. Society AC. Tests for Ovarian Cancer 2018 [

296. Network NCC. Ovarian Cancer. 2019.

297. Elias KM, Guo J, Bast RC, Jr. Early Detection of Ovarian Cancer. Hematol Oncol Clin North Am. 2018;32(6):903-14.

298. Buys SS, Partridge E, Greene MH, Prorok PC, Reding D, Riley TL, et al. Ovarian cancer screening in the Prostate, Lung, Colorectal and Ovarian (PLCO) cancer screening trial: findings from the initial screen of a randomized trial. Am J Obstet Gynecol. 2005;193(5):1630-9.

299. Pinsky PF, Yu K, Kramer BS, Black A, Buys SS, Partridge E, et al. Extended mortality results for ovarian cancer screening in the PLCO trial with median 15years follow-up. Gynecol Oncol. 2016;143(2):270-5.

300. Skates SJ. Ovarian cancer screening: development of the risk of ovarian cancer algorithm (ROCA) and ROCA screening trials. Int J Gynecol Cancer. 2012;22 Suppl 1:S24-6.

301. Skates SJ, Pauler DK, Jacobs IJ. Screening Based on the Risk of Cancer Calculation From Bayesian Hierarchical Changepoint and Mixture Models of Longitudinal Markers. Journal of the American Statistical Association. 2001;96(454):429-39.

302. Jacobs IJ, Menon U, Ryan A, Gentry-Maharaj A, Burnell M, Kalsi JK, et al. Ovarian cancer screening and mortality in the UK Collaborative Trial of Ovarian Cancer Screening (UKCTOCS): a randomised controlled trial. The Lancet. 2016;387(10022):945-56.

303. Rojas V, Hirshfield KM, Ganesan S, Rodriguez-Rodriguez L. Molecular Characterization of Epithelial Ovarian Cancer: Implications for Diagnosis and Treatment. Int J Mol Sci. 2016;17(12).

304. Vaughan S, Coward JI, Bast RC, Jr., Berchuck A, Berek JS, Brenton JD, et al. Rethinking ovarian cancer: recommendations for improving outcomes. Nat Rev Cancer. 2011;11(10):719-25.

305. Armstrong DK, Bundy B, Wenzel L, Huang HQ, Baergen R, Lele S, et al. Intraperitoneal cisplatin and paclitaxel in ovarian cancer. N Engl J Med. 2006;354(1):34-43.

306. van Meurs HS, Tajik P, Hof MH, Vergote I, Kenter GG, Mol BW, et al. Which patients benefit most from primary surgery or neoadjuvant chemotherapy in stage IIIC or

IV ovarian cancer? An exploratory analysis of the European Organisation for Research and Treatment of Cancer 55971 randomised trial. Eur J Cancer. 2013;49(15):3191-201.

307. du Bois A, Luck HJ, Meier W, Mobus V, Costa S, Richter B, et al. Carboplatin/paclitaxel versus cisplatin/paclitaxel as first-line chemotherapy in advanced ovarian cancer: an interim analysis of a randomized phase III trial of the Arbeitsgemeinschaft Gynakologische Onkologie Ovarian Cancer Study Group. Semin Oncol. 1997;24(5 Suppl 15):S15-44-S15-52.

308. van Warmerdam LJ, Huizing MT, Giaccone G, Postmus PE, ten Bokkel Huinink WW, van Zandwijk N, et al. Clinical pharmacology of carboplatin administered in combination with paclitaxel. Semin Oncol. 1997;24(1 Suppl 2):S2-97-S2-104.

309. Burger RA, Brady MF, Bookman MA, Fleming GF, Monk BJ, Huang H, et al. Incorporation of bevacizumab in the primary treatment of ovarian cancer. N Engl J Med. 2011;365(26):2473-83.

310. Monk BJ, Huang HQ, Burger RA, Mannel RS, Homesley HD, Fowler J, et al. Patient reported outcomes of a randomized, placebo-controlled trial of bevacizumab in the front-line treatment of ovarian cancer: a Gynecologic Oncology Group Study. Gynecol Oncol. 2013;128(3):573-8.

311. Minagawa Y, Kigawa J, Kanamori Y, Itamochi H, Terakawa N, Okada M, et al. Feasibility study comparing docetaxel-cisplatin versus docetaxel-carboplatin as first-line chemotherapy for ovarian cancer. Gynecol Oncol. 2006;101(3):495-8.

312. Pignata S, S CC, Du Bois A, Harter P, Heitz F. Treatment of recurrent ovarian cancer. Ann Oncol. 2017;28(suppl_8):viii51-viii6.

313. Friedlander M, Trimble E, Tinker A, Alberts D, Avall-Lundqvist E, Brady M, et al. Clinical trials in recurrent ovarian cancer. Int J Gynecol Cancer. 2011;21(4):771-5.

314. Gonzalez-Martin A, Gladieff L, Tholander B, Stroyakovsky D, Gore M, Scambia G, et al. Efficacy and safety results from OCTAVIA, a single-arm phase II study evaluating front-line bevacizumab, carboplatin and weekly paclitaxel for ovarian cancer. Eur J Cancer. 2013;49(18):3831-8.

315. Foley OW, Rauh-Hain JA, del Carmen MG. Recurrent epithelial ovarian cancer: an update on treatment. Oncology (Williston Park). 2013;27(4):288-94, 98.

316. Carden CP, Stewart A, Thavasu P, Kipps E, Pope L, Crespo M, et al. The association of PI3 kinase signaling and chemoresistance in advanced ovarian cancer. Mol Cancer Ther. 2012;11(7):1609-17.

317. Farley J, Brady WE, Vathipadiekal V, Lankes HA, Coleman R, Morgan MA, et al. Selumetinib in women with recurrent low-grade serous carcinoma of the ovary or peritoneum: an open-label, single-arm, phase 2 study. Lancet Oncol. 2013;14(2):134-40.

318. Yap TA, Sandhu SK, Carden CP, de Bono JS. Poly(ADP-ribose) polymerase (PARP) inhibitors: Exploiting a synthetic lethal strategy in the clinic. CA Cancer J Clin. 2011;61(1):31-49.

319. Deeks ED. Olaparib: first global approval. Drugs. 2015;75(2):231-40.

320. Ledermann J, Harter P, Gourley C, Friedlander M, Vergote I, Rustin G, et al. Olaparib maintenance therapy in patients with platinum-sensitive relapsed serous ovarian cancer: a preplanned retrospective analysis of outcomes by BRCA status in a randomised phase 2 trial. Lancet Oncol. 2014;15(8):852-61.

321. Matulonis UA, Penson RT, Domchek SM, Kaufman B, Shapira-Frommer R, Audeh MW, et al. Olaparib monotherapy in patients with advanced relapsed ovarian cancer and a germline BRCA1/2 mutation: a multistudy analysis of response rates and safety. Ann Oncol. 2016;27(6):1013-9.

322. Oza AM, Cibula D, Benzaquen AO, Poole C, Mathijssen RH, Sonke GS, et al. Olaparib combined with chemotherapy for recurrent platinum-sensitive ovarian cancer: a randomised phase 2 trial. Lancet Oncol. 2015;16(1):87-97.

323. Scott LJ. Niraparib: First Global Approval. Drugs. 2017;77(9):1029-34.

324. Mirza MR, Monk BJ, Herrstedt J, Oza AM, Mahner S, Redondo A, et al. Niraparib Maintenance Therapy in Platinum-Sensitive, Recurrent Ovarian Cancer. N Engl J Med. 2016;375(22):2154-64.

325. Oza AM, Matulonis UA, Malander S, Hudgens S, Sehouli J, Del Campo JM, et al. Quality of life in patients with recurrent ovarian cancer treated with niraparib versus placebo (ENGOT-OV16/NOVA): results from a double-blind, phase 3, randomised controlled trial. Lancet Oncol. 2018;19(8):1117-25.

326. Syed YY. Rucaparib: First Global Approval. Drugs. 2017;77(5):585-92.

327. Swisher EM, Lin KK, Oza AM, Scott CL, Giordano H, Sun J, et al. Rucaparib in relapsed, platinum-sensitive high-grade ovarian carcinoma (ARIEL2 Part 1): an international, multicentre, open-label, phase 2 trial. Lancet Oncol. 2017;18(1):75-87.

328. Cortez AJ, Tudrej P, Kujawa KA, Lisowska KM. Advances in ovarian cancer therapy. Cancer Chemother Pharmacol. 2018;81(1):17-38.

329. Aghajanian C, Blank SV, Goff BA, Judson PL, Teneriello MG, Husain A, et al. OCEANS: a randomized, double-blind, placebo-controlled phase III trial of

chemotherapy with or without bevacizumab in patients with platinum-sensitive recurrent epithelial ovarian, primary peritoneal, or fallopian tube cancer. J Clin Oncol. 2012;30(17):2039-45.

330. Bamias A, Gibbs E, Khoon Lee C, Davies L, Dimopoulos M, Zagouri F, et al. Bevacizumab with or after chemotherapy for platinum-resistant recurrent ovarian cancer: exploratory analyses of the AURELIA trial. Ann Oncol. 2017;28(8):1842-8.

331. Hu W, Lu C, Dong HH, Huang J, Shen DY, Stone RL, et al. Biological roles of the Delta family Notch ligand Dll4 in tumor and endothelial cells in ovarian cancer. Cancer Res. 2011;71(18):6030-9.

332. Lu C, Han HD, Mangala LS, Ali-Fehmi R, Newton CS, Ozbun L, et al. Regulation of tumor angiogenesis by EZH2. Cancer Cell. 2010;18(2):185-97.

333. Sato E, Olson SH, Ahn J, Bundy B, Nishikawa H, Qian F, et al. Intraepithelial CD8+ tumor-infiltrating lymphocytes and a high CD8+/regulatory T cell ratio are associated with favorable prognosis in ovarian cancer. Proc Natl Acad Sci U S A. 2005;102(51):18538-43.

334. Zhang L, Conejo-Garcia JR, Katsaros D, Gimotty PA, Massobrio M, Regnani G, et al. Intratumoral T cells, recurrence, and survival in epithelial ovarian cancer. N Engl J Med. 2003;348(3):203-13.

335. Chester C, Dorigo O, Berek JS, Kohrt H. Immunotherapeutic approaches to ovarian cancer treatment. J Immunother Cancer. 2015;3:7.

336. Coleman RL, Brady WE, McMeekin DS, Rose PG, Soper JT, Lentz SS, et al. A phase II evaluation of nanoparticle, albumin-bound (nab) paclitaxel in the treatment of

recurrent or persistent platinum-resistant ovarian, fallopian tube, or primary peritoneal cancer: a Gynecologic Oncology Group study. Gynecol Oncol. 2011;122(1):111-5.

337. Kaye SB, Lubinski J, Matulonis U, Ang JE, Gourley C, Karlan BY, et al. Phase II, open-label, randomized, multicenter study comparing the efficacy and safety of olaparib, a poly (ADP-ribose) polymerase inhibitor, and pegylated liposomal doxorubicin in patients with BRCA1 or BRCA2 mutations and recurrent ovarian cancer. J Clin Oncol. 2012;30(4):372-9.

338. Mahner S, Meier W, du Bois A, Brown C, Lorusso D, Dell'Anna T, et al. Carboplatin and pegylated liposomal doxorubicin versus carboplatin and paclitaxel in very platinum-sensitive ovarian cancer patients: results from a subset analysis of the CALYPSO phase III trial. Eur J Cancer. 2015;51(3):352-8.

339. Pujade-Lauraine E, Wagner U, Aavall-Lundqvist E, Gebski V, Heywood M, Vasey PA, et al. Pegylated liposomal Doxorubicin and Carboplatin compared with Paclitaxel and Carboplatin for patients with platinum-sensitive ovarian cancer in late relapse. J Clin Oncol. 2010;28(20):3323-9.

340. Siegel RL, Miller KD, Jemal A. Cancer Statistics, 2017. CA Cancer J Clin. 2017;67(1):7-30.

341. Tomasetti C, Vogelstein B. Cancer etiology. Variation in cancer risk among tissues can be explained by the number of stem cell divisions. Science. 2015;347(6217):78-81.

342. Brindley DN, Benesch MG, Murph MM. Autotaxin: An Enzymatic Augmenter of Malignant Progression Linked to Inflammation. In: Murph M, editor. Melanoma – Current Clinical Management and Future Therapeutics. 1: InTech; 2015. p. 426.

343. van Meeteren LA, Ruurs P, Stortelers C, Bouwman P, van Rooijen MA, Pradere JP, et al. Autotaxin, a secreted lysophospholipase D, is essential for blood vessel formation during development. Mol Cell Biol. 2006;26(13):5015-22.

344. Kishi Y, Okudaira S, Tanaka M, Hama K, Shida D, Kitayama J, et al. Autotaxin is overexpressed in glioblastoma multiforme and contributes to cell motility of glioblastoma by converting lysophosphatidylcholine to lysophosphatidic acid. J Biol Chem. 2006;281(25):17492-500.

345. Cerami E, Gao J, Dogrusoz U, Gross BE, Sumer SO, Aksoy BA, et al. The cBio cancer genomics portal: an open platform for exploring multidimensional cancer genomics data. Cancer Discov. 2012;2(5):401-4.

346. Gao J, Aksoy BA, Dogrusoz U, Dresdner G, Gross B, Sumer SO, et al. Integrative analysis of complex cancer genomics and clinical profiles using the cBioPortal. Sci Signal. 2013;6(269):pl1.

347. Kaffe E, Katsifa A, Xylourgidis N, Ninou I, Zannikou M, Harokopos V, et al. Hepatocyte autotaxin expression promotes liver fibrosis and cancer. Hepatology. 2017;65(4):1369-83.

348. Nam SW, Clair T, Kim YS, McMarlin A, Schiffmann E, Liotta LA, et al. Autotaxin (NPP-2), a metastasis-enhancing motogen, is an angiogenic factor. Cancer Res. 2001;61(18):6938-44.

349. Xu X, Prestwich GD. Inhibition of tumor growth and angiogenesis by a lysophosphatidic acid antagonist in an engineered three-dimensional lung cancer xenograft model. Cancer. 2010;116(7):1739-50.

350. Bast RC, Jr., Croce CM, Hait WN, Waun KH, Kufe DW, Piccart-Gebhart M, et al. Holland-Frei Cancer Medicine, 9th Edition. 9th ed: Wiley; 2017.

351. Cohen JD, Li L, Wang Y, Thoburn C, Afsari B, Danilova L, et al. Detection and localization of surgically resectable cancers with a multi-analyte blood test. Science. 2018;359(6378):926-30.

352. Londin E, Loher P, Telonis AG, Quann K, Clark P, Jing Y, et al. Analysis of 13 cell types reveals evidence for the expression of numerous novel primate- and tissue-specific microRNAs. Proc Natl Acad Sci U S A. 2015;112(10):E1106-15.

353. Calin GA, Croce CM. MicroRNA signatures in human cancers. Nat Rev Cancer. 2006;6(11):857-66.

354. Lu J, Getz G, Miska EA, Alvarez-Saavedra E, Lamb J, Peck D, et al. MicroRNA expression profiles classify human cancers. Nature. 2005;435(7043):834-8.

355. Mitchell PS, Parkin RK, Kroh EM, Fritz BR, Wyman SK, Pogosova-Agadjanyan EL, et al. Circulating microRNAs as stable blood-based markers for cancer detection. Proc Natl Acad Sci U S A. 2008;105(30):10513-8.

356. Murph MM, Liu W, Yu S, Lu Y, Hall H, Hennessy BT, et al. Lysophosphatidic acid-induced transcriptional profile represents serous epithelial ovarian carcinoma and worsened prognosis. PLoS One. 2009;4(5):e5583.

357. Eisen MB, Spellman PT, Brown PO, Botstein D. Cluster analysis and display of genome-wide expression patterns. Proc Natl Acad Sci U S A. 1998;95(25):14863-8.

358. Lin Y, Liu J, Huang Y, Liu D, Zhang G, Kan H. microRNA-489 Plays an Anti-Metastatic Role in Human Hepatocellular Carcinoma by Targeting Matrix Metalloproteinase-7. Transl Oncol. 2017;10(2):211-20.

359. Patel Y, Shah N, Lee JS, Markoutsa E, Jie C, Liu S, et al. A novel double-negative feedback loop between miR-489 and the HER2-SHP2-MAPK signaling axis regulates breast cancer cell proliferation and tumor growth. Oncotarget. 2016;7(14):18295-308.

360. Yuan P, He XH, Rong YF, Cao J, Li Y, Hu YP, et al. KRAS/NF-kappaB/YY1/miR-489 Signaling Axis Controls Pancreatic Cancer Metastasis. Cancer Res. 2017;77(1):100-11.

361. Baker DL, Fujiwara Y, Pigg KR, Tsukahara R, Kobayashi S, Murofushi H, et al. Carba analogs of cyclic phosphatidic acid are selective inhibitors of autotaxin and cancer cell invasion and metastasis. J Biol Chem. 2006;281(32):22786-93.

362. Nam SW, Clair T, Campo CK, Lee HY, Liotta LA, Stracke ML. Autotaxin (ATX), a potent tumor motogen, augments invasive and metastatic potential of ras-transformed cells. Oncogene. 2000;19(2):241-7.

363. Catuogno S, Cerchia L, Romano G, Pognonec P, Condorelli G, de Franciscis V. miR-34c may protect lung cancer cells from paclitaxel-induced apoptosis. Oncogene. 2013;32(3):341-51.

364. Maroof H, Islam F, Ariana A, Gopalan V, Lam AK. The roles of microRNA-34b-5p in angiogenesis of thyroid carcinoma. Endocrine. 2017.

365. Pan BT, Johnstone RM. Fate of the transferrin receptor during maturation of sheep reticulocytes in vitro: selective externalization of the receptor. Cell. 1983;33(3):967-78.

366. Iranifar E, Seresht BM, Momeni F, Fadaei E, Mehr MH, Ebrahimi Z, et al. Exosomes and microRNAs: New potential therapeutic candidates in Alzheimer disease therapy. J Cell Physiol. 2019;234(3):2296-305.

367. Di C, Zhang Q, Wang Y, Wang F, Chen Y, Gan L, et al. Exosomes as drug carriers for clinical application. Artif Cells Nanomed Biotechnol. 2018:1-7.

368. Das CK, Jena BC, Banerjee I, das S, Parekh A, Bhutia SK, et al. Exosome as a Novel Shuttle for Delivery of Therapeutics across Biological Barriers. Mol Pharm. 2018.

369. Kim MS, Haney MJ, Zhao Y, Mahajan V, Deygen I, Klyachko NL, et al. Development of exosome-encapsulated paclitaxel to overcome MDR in cancer cells. Nanomedicine. 2016;12(3):655-64.

370. Whiteside TL. Exosomes and tumor-mediated immune suppression. J Clin Invest. 2016;126(4):1216-23.

371. Shen M, Ren X. New insights into the biological impacts of immune cell-derived exosomes within the tumor environment. Cancer Lett. 2018;431:115-22.

372. Liang G, Kan S, Zhu Y, Feng S, Feng W, Gao S. Engineered exosome-mediated delivery of functionally active miR-26a and its enhanced suppression effect in HepG2 cells. Int J Nanomedicine. 2018;13:585-99.

373. Siegel RL, Miller KD, Jemal A. Cancer statistics, 2018. CA Cancer J Clin. 2018;68(1):7-30.

374. Anders CK, Carey LA. Biology, metastatic patterns, and treatment of patients with triple-negative breast cancer. Clin Breast Cancer. 2009;9 Suppl 2:S73-81.

375. Masuda H, Baggerly KA, Wang Y, Zhang Y, Gonzalez-Angulo AM, Meric-Bernstam F, et al. Differential response to neoadjuvant chemotherapy among 7 triple-negative breast cancer molecular subtypes. Clin Cancer Res. 2013;19(19):5533-40.

376. Cancer Genome Atlas N. Comprehensive molecular portraits of human breast tumours. Nature. 2012;490(7418):61-70.

377. Sil P, Wicklum H, Surell C, Rada B. Macrophage-derived IL-1beta enhances monosodium urate crystal-triggered NET formation. Inflamm Res. 2017;66(3):227-37.

378. Matsuzaki K, Murase O, Sugishita K, Yoneyama S, Akada K, Ueha M, et al. Optical characterization of liposomes by right angle light scattering and turbidity measurement. Biochim Biophys Acta. 2000;1467(1):219-26.

379. Nobbmann U, Connah M, Fish B, Varley P, Gee C, Mulot S, et al. Dynamic light scattering as a relative tool for assessing the molecular integrity and stability of monoclonal antibodies. Biotechnol Genet Eng Rev. 2007;24:117-28.

380. Ling K, Jiang H, Zhang Q. A colorimetric method for the molecular weight determination of polyethylene glycol using gold nanoparticles. Nanoscale Res Lett. 2013;8(1):538.

381. Li S, Xing D, Li J. Dynamic light scattering application to study protein interactions in electrolyte solutions. J Biol Phys. 2004;30(4):313-24.

382. Stetefeld J, McKenna SA, Patel TR. Dynamic light scattering: a practical guide and applications in biomedical sciences. Biophys Rev. 2016;8(4):409-27.

383. Lobba AR, Forni MF, Carreira AC, Sogayar MC. Differential expression of CD90 and CD14 stem cell markers in malignant breast cancer cell lines. Cytometry A. 2012;81(12):1084-91.

384. Cahall CF, Lilly JL, Hirschowitz EA, Berron BJ. A Quantitative Perspective on Surface Marker Selection for the Isolation of Functional Tumor Cells. Breast Cancer (Auckl). 2015;9(Suppl 1):1-11.

385. Dai X, Fang M, Li S, Yan Y, Zhong Y, Du B. miR-21 is involved in transforming growth factor beta1-induced chemoresistance and invasion by targeting PTEN in breast cancer. Oncol Lett. 2017;14(6):6929-36.

386. Senbanjo LT, Chellaiah MA. CD44: A Multifunctional Cell Surface Adhesion Receptor Is a Regulator of Progression and Metastasis of Cancer Cells. Front Cell Dev Biol. 2017;5:18.

387. Fragni M, Bonini SA, Bettinsoli P, Bodei S, Generali D, Bottini A, et al. The miR-21/PTEN/Akt signaling pathway is involved in the anti-tumoral effects of zoledronic acid in human breast cancer cell lines. Naunyn Schmiedebergs Arch Pharmacol. 2016;389(5):529-38.

388. Rupaimoole R, Slack FJ. MicroRNA therapeutics: towards a new era for the management of cancer and other diseases. Nat Rev Drug Discov. 2017;16(3):203-22.

389. Agostini M, Knight RA. miR-34: from bench to bedside. Oncotarget. 2014;5(4):872-81.

390. van der Ree MH, van der Meer AJ, van Nuenen AC, de Bruijne J, Ottosen S, Janssen HL, et al. Miravirsen dosing in chronic hepatitis C patients results in decreased microRNA-122 levels without affecting other microRNAs in plasma. Aliment Pharmacol Ther. 2016;43(1):102-13.

391. Baroni S, Romero-Cordoba S, Plantamura I, Dugo M, D'Ippolito E, Cataldo A, et al. Exosome-mediated delivery of miR-9 induces cancer-associated fibroblast-like properties in human breast fibroblasts. Cell Death Dis. 2016;7(7):e2312.

392. Lou G, Song X, Yang F, Wu S, Wang J, Chen Z, et al. Exosomes derived from miR-122-modified adipose tissue-derived MSCs increase chemosensitivity of hepatocellular carcinoma. J Hematol Oncol. 2015;8:122.

393. Fiskus W, Mitsiades N. B-Raf Inhibition in the Clinic: Present and Future. Annu Rev Med. 2016;67:29-43.

394. Ascierto PA, Kirkwood JM, Grob JJ, Simeone E, Grimaldi AM, Maio M, et al. The role of BRAF V600 mutation in melanoma. J Transl Med. 2012;10:85.

395. Lavoue V, Huchon C, Akladios C, Alfonsi P, Bakrin N, Ballester M, et al. [Management of epithelial ovarian cancer. Short text drafted from the French joint recommendations of FRANCOGYN, CNGOF, SFOG, GINECO-ARCAGY and endorsed by INCa]. Bull Cancer. 2019;106(4):354-70.

396. Diab M, Azmi A, Mohammad R, Philip PA. Pharmacotherapeutic strategies for treating pancreatic cancer: advances and challenges. Expert Opin Pharmacother. 2019;20(5):535-46.

397. Binju M, Padilla MA, Singomat T, Kaur P, Suryo Rahmanto Y, Cohen PA, et al. Mechanisms underlying acquired platinum resistance in high grade serous ovarian cancer - a mini review. Biochim Biophys Acta Gen Subj. 2019;1863(2):371-8.

398. Monk JP, Benfield P. Inhaled pentamidine. An overview of its pharmacological properties and a review of its therapeutic use in Pneumocystis carinii pneumonia. Drugs. 1990;39(5):741-56.

399. Paine MF, Wang MZ, Generaux CN, Boykin DW, Wilson WD, De Koning HP, et al. Diamidines for human African trypanosomiasis. Curr Opin Investig Drugs. 2010;11(8):876-83.

400. Wilson WD, Tanious FA, Mathis A, Tevis D, Hall JE, Boykin DW. Antiparasitic compounds that target DNA. Biochimie. 2008;90(7):999-1014.

401. Liu ZY, Wenzler T, Brun R, Zhu X, Boykin DW. Synthesis and antiparasitic activity of new bis-arylimidamides: DB766 analogs modified in the terminal groups. Eur J Med Chem. 2014;83:167-73.

402. Batista DG, Pacheco MG, Kumar A, Branowska D, Ismail MA, Hu L, et al. Biological, ultrastructural effect and subcellular localization of aromatic diamidines in Trypanosoma cruzi. Parasitology. 2010;137(2):251-9.

403. Cai X, Gray PJ, Jr., Von Hoff DD. DNA minor groove binders: back in the groove. Cancer Treat Rev. 2009;35(5):437-50.

404. Zihlif M C, D, Bernard S, Wakelin L. Effects of DNA Minor Groove Binding Agents on Global Gene Expression. Cancer Genomics and Proteomics. 2010;7.

405. Luo Y, Li W, Liao H. HMGA2 induces epithelial-to-mesenchymal transition in human hepatocellular carcinoma cells. Oncol Lett. 2013;5(4):1353-6.

406. Debache K, Guionaud C, Kropf C, Boykin D, Stephens CE, Hemphill A. Experimental treatment of Neospora caninum-infected mice with the arylimidamide DB750 and the thiazolide nitazoxanide. Exp Parasitol. 2011;129(2):95-100.

407. Sundararajan S, Badri T. Cancer, Metastatic Melanoma. StatPearls. Treasure Island (FL)2019.

408. Rosypal AC, Hall JE, Bakunova S, Patrick DA, Bakunov S, Stephens CE, et al. In vitro activity of dicationic compounds against a North American foxhound isolate of Leishmania infantum. Vet Parasitol. 2007;145(3-4):207-16.

409. Hawkins RA, Stephens CE. Aerobic epoxidation and hydroxylation of a pyrrolo[2,1-b]quinazoline under ambient conditions. Tetrahedron Letters. 2010;51(47):6129-31.

410. Jia W, Tran SK, Ruddick CA, Murph MM. The Src homology 3 binding domain is required for lysophosphatidic acid 3 receptor-mediated cellular viability in melanoma cells. Cancer Lett. 2015;356(2 Pt B):589-96.

411. Collar CJ, Zhu X, Werbovetz K, Boykin DW, Wilson WD. Molecular factors governing inhibition of arylimidamides against Leishmania: conservative computational modeling to improve chemotherapies. Bioorg Med Chem. 2011;19(15):4552-61.

412. Stephens CE, Tanious F, Kim S, Wilson WD, Schell WA, Perfect JR, et al. Diguanidino and "reversed" diamidino 2,5-diarylfurans as antimicrobial agents. J Med Chem. 2001;44(11):1741-8.

413. Suthiwangcharoen N, Pochini SM, Sweat DP, Stephens CE. An intramolecular N-arylation approach to 3-functionalized 4,9-dihydropyrrolo[2,1-b]quinazolines. Journal of Heterocyclic Chemistry. 2011;48(3):706-9.

414. Ame´lie Lansiaux FT, Zohar Mishal, Laurent Dassonneville, Arvind Kumar, Chad E. Stephens, Qiyue Hu,, W. David Wilson DWB, and Christian Bailly. Distribution of Furamidine Analogues in Tumor Cells: Targeting of the Nucleus or Mitochondria Depending on the Amidine Substitution. Cancer Research. 2002;62:7219-29.

415. Lanteri CA, Trumpower BL, Tidwell RR, Meshnick SR. DB75, a novel trypanocidal agent, disrupts mitochondrial function in Saccharomyces cerevisiae. Antimicrob Agents Chemother. 2004;48(10):3968-74.

416. Batista Dda G, Batista MM, de Oliveira GM, do Amaral PB, Lannes-Vieira J, Britto CC, et al. Arylimidamide DB766, a potential chemotherapeutic candidate for Chagas' disease treatment. Antimicrob Agents Chemother. 2010;54(7):2940-52.

417. Antony S, Marchand C, Stephen AG, Thibaut L, Agama KK, Fisher RJ, et al. Novel high-throughput electrochemiluminescent assay for identification of human tyrosyl-DNA phosphodiesterase (Tdp1) inhibitors and characterization of furamidine (NSC 305831) as an inhibitor of Tdp1. Nucleic Acids Res. 2007;35(13):4474-84.

418. Iderzorig T, Kellen J, Osude C, Singh S, Woodman JA, Garcia C, et al. Comparison of EMT mediated tyrosine kinase inhibitor resistance in NSCLC. Biochem Biophys Res Commun. 2018;496(2):770-7.

419. Yan L, Yan C, Qian K, Su H, Kofsky-Wofford SA, Lee WC, et al. Diamidine compounds for selective inhibition of protein arginine methyltransferase 1. J Med Chem. 2014;57(6):2611-22.

420. Mak IW, Evaniew N, Ghert M. Lost in translation: animal models and clinical trials in cancer treatment. Am J Transl Res. 2014;6(2):114-8.

421. Guo XQ, Zhang QX, Huang WR, Duan XL, Cai ZM. [Tumor suppressor role of chromatin-remodeling factor ARID1A]. Yi Chuan. 2013;35(3):255-61.

422. Li KC, Hua KT, Lin YS, Su CY, Ko JY, Hsiao M, et al. Inhibition of G9a induces DUSP4-dependent autophagic cell death in head and neck squamous cell carcinoma. Mol Cancer. 2014;13:172.

423. Xue G, Romano E, Massi D, Mandala M. Wnt/beta-catenin signaling in melanoma: Preclinical rationale and novel therapeutic insights. Cancer Treat Rev. 2016;49:1-12.

424. Chai P, Tian J, Zhao D, Zhang H, Cui J, Ding K, et al. GSE1 negative regulation by miR-489-5p promotes breast cancer cell proliferation and invasion. Biochem Biophys Res Commun. 2016;471(1):123-8.

425. Liu Q, Yang G, Qian Y. Loss of MicroRNA-489-3p promotes osteosarcoma metastasis by activating PAX3-MET pathway. Mol Carcinog. 2017;56(4):1312-21.

426. Tao Y, Han T, Zhang T, Ma C, Sun C. LncRNA CHRF-induced miR-489 loss promotes metastasis of colorectal cancer via TWIST1/EMT signaling pathway. Oncotarget. 2017;8(22):36410-22.

427. Landgraf P, Rusu M, Sheridan R, Sewer A, Iovino N, Aravin A, et al. A mammalian microRNA expression atlas based on small RNA library sequencing. Cell. 2007;129(7):1401-14.

428. Meunier J, Lemoine F, Soumillon M, Liechti A, Weier M, Guschanski K, et al. Birth and expression evolution of mammalian microRNA genes. Genome Res. 2013;23(1):34-45.

429. Wu T, Dai Y. Tumor microenvironment and therapeutic response. Cancer Lett. 2017;387:61-8.

430. Chen X, Wang YW, Xing AY, Xiang S, Shi DB, Liu L, et al. Suppression of SPIN1-mediated PI3K-Akt pathway by miR-489 increases chemosensitivity in breast cancer. J Pathol. 2016;239(4):459-72.

431. Jiang L, He D, Yang D, Chen Z, Pan Q, Mao A, et al. MiR-489 regulates chemoresistance in breast cancer via epithelial mesenchymal transition pathway. FEBS Lett. 2014;588(11):2009-15.

432. Zhao Y, Ge CC, Wang J, Wu XX, Li XM, Li W, et al. MEK inhibitor, PD98059, promotes breast cancer cell migration by inducing beta-catenin nuclear accumulation. Oncol Rep. 2017;38(5):3055-63.

433. Hoffman RM, Bouvet M. Nanoparticle albumin-bound-paclitaxel: a limited improvement under the current therapeutic paradigm of pancreatic cancer. Expert Opin Pharmacother. 2015;16(7):943-7.

434. Franco YL, Vaidya TR, Ait-Oudhia S. Anticancer and cardio-protective effects of liposomal doxorubicin in the treatment of breast cancer. Breast Cancer (Dove Med Press). 2018;10:131-41.

435. Sousa I, Rodrigues F, Prazeres H, Lima RT, Soares P. Liposomal therapies in oncology: does one size fit all? Cancer Chemother Pharmacol. 2018;82(5):741-55.